

Analytical and Simulation Studies in Complex Plasma Systems

Thesis submitted for the award of
Doctor of Philosophy (Science)

By
CHINMAY DAS

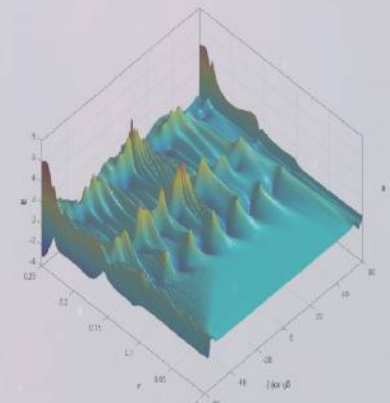
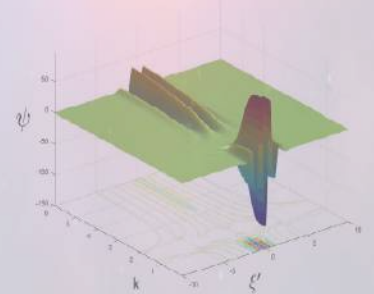
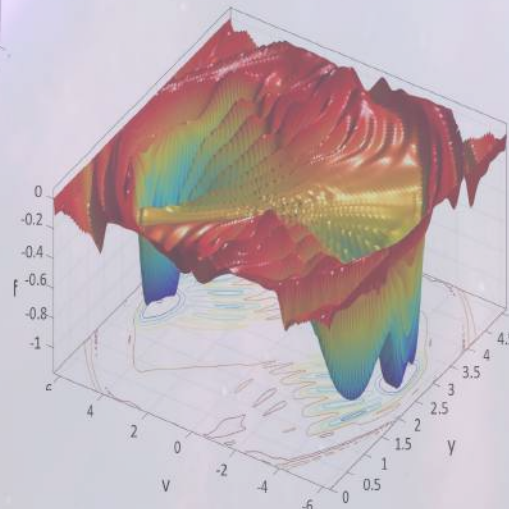
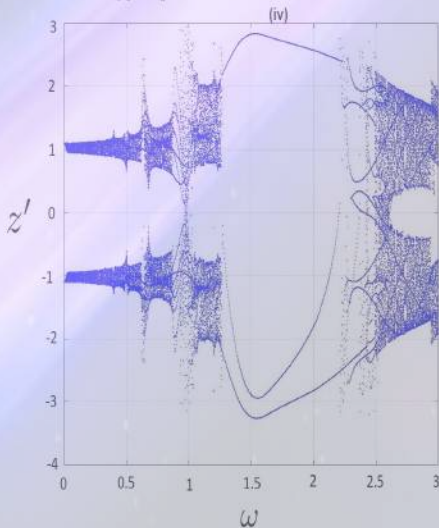
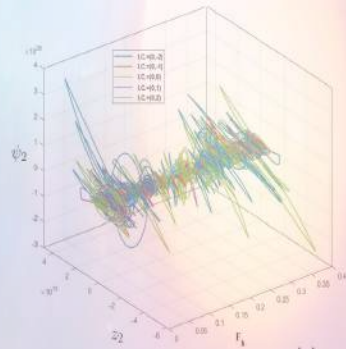
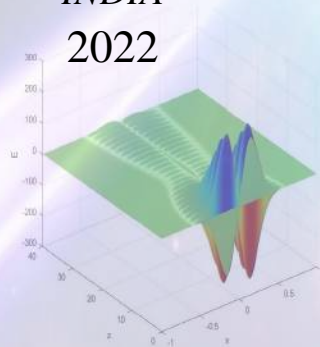
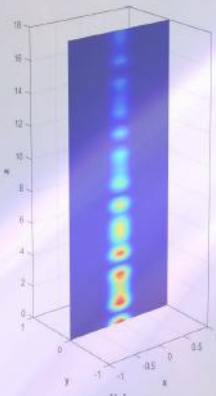
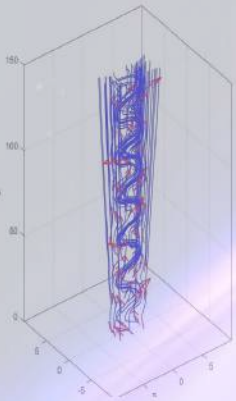
Index Number - 34/20/Phys./27

Department of Physics
Jadavpur University

Kolkata - 700032

West Bengal

INDIA
2022




$$\frac{\partial f}{\partial t} + \mathbf{p} \cdot \nabla_y f + F(y, t) \nabla_y f(y, \mathbf{p}, t) = 0$$

$$\left(\frac{\partial}{\partial t} + \mathbf{v}_e \cdot \nabla \right) \mathbf{E} = \frac{\mathbf{h} e \mathbf{v}_e}{\omega} + \left[\nabla \times \mathbf{B} - \mathbf{E} (\nabla \cdot \mathbf{v}_e) - \nabla \times (\mathbf{v}_e \times \mathbf{E}) + (\mathbf{E} \cdot \nabla) \mathbf{v}_e \right]$$

CERTIFICATE FROM THE SUPERVISORS

This is to certify that the thesis entitled "ANALYTICAL AND SIMULATION STUDIES IN COMPLEX PLASMA SYSTEMS" submitted by Sri. Chinmay Das who got his name registered on 12/10/2020 for the award of Ph.D. (Science) degree of Jadavpur University, is absolutely based upon his own work under the supervision of Prof. Basudev Ghosh and Dr. Swarniv Chandra and that neither this thesis nor any part of it has been submitted for either any degree / diploma or any other academic award anywhere before.


18/7/22

.....
Dr. Swarniv Chandra
Department of Physics,
Government General Degree College at
Kushmandi
Dakshin Dinajpur West Bengal, 733121,
INDIA

Assistant Professor of Physics
Govt. Gen. Degree College
at Kushmandi
Dist-Dakshin Dinajpur


18/7/22

.....
Prof. Basudev Ghosh
Department of Physics,
Jadavpur University,
Jadavpur, Kolkata West Bengal, 700032,
INDIA

Dr. Basudev Ghosh
Professor
Department of Physics
Jadavpur University
Kolkata-700032

ACKNOWLEDGMENT

This doctoral thesis overviews my research on **"Analytical and Simulation Studies in Complex Plasma Systems"**. I have carried out the whole work consolidated in this thesis in the Department of Physics, Jadavpur University, Kolkata-700032, India, under the supervision of Dr. Swarniv Chandra and Prof. Basudev Ghosh. They introduced me to this new and rapidly expanding field of plasma research.

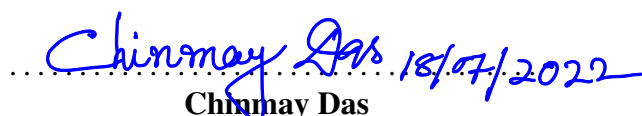
I am overwhelmed with humility and gratitude to those who have assisted me in putting these ideas far above the level of simplicity into something concrete.

I express my deepest gratitude to Dr. Swarniv Chandra for his inspiring guidance, profound knowledge, unwavering encouragement, mathematical ingenuity, and fatherly love, which helped him rise above my mentorship and become my friendly philosopher. I would also like to thank Prof. Basudev Ghosh for constantly motivating me and discovering new directions in my research.

I express my gratitude to the authorities of Jadavpur University for providing me with the library and other facilities in a pleasant teaching and learning environment. I would also like to thank Dr. Gouranga Biswas, Dr. Sourabh Banerjee, Prof. Alope Kumar Das and my other colleagues for supporting in my pursuit.

Finally, I would like to thank my parents, Sri. Madan Das and Smt. Arati Das for their blessings and moral support.

Above all, I must acknowledge the divine blessings of the Almighty.



Chinmay Das

Department of Physics,
Jadavpur University
Jadavpur, Kolkata, West Bengal, 700032,
INDIA

OATH

India is my country. All Indians are my brothers and sisters. I love my country and I am proud of its rich and varied heritage. I shall always strive to be worthy of it. I shall respect my parents, teachers, and elders; and treat everyone with courtesy. To my country and my people, I pledge my devotion. In their well-being and prosperity alone lies my happiness.

PUBLISHED PAPERS

Publications included in this thesis:

- [1] Das, C., Chandra, S., & Ghosh, B. (2020). "Amplitude modulation and soliton formation of an intense laser beam interacting with dense quantum plasma: Symbolic simulation analysis." *Contributions to Plasma Physics*, (2020), 60(8), e202000028. doi: 10.1002/ctpp.202000028
- [2] Das, C., Chandra, S. and Ghosh, B., "Nonlinear interaction of intense laser beam with dense plasma." *Plasma Physics and Controlled Fusion*, (2020), 63(1), p.015011. doi: 10.1088/1361-6587/abc732
- [3] Das, C., Chandra, S. and Ghosh, B., "Effects of exchange symmetry and quantum diffraction on amplitude-modulated electrostatic waves in quantum magnetoplasma." *Pramana*, (2021), 95(2), pp.1-16. doi: 10.1007/s12043-021-02108-x
- [4] Das, C., Chandra, S., Sharry and Chatterjee, P., "Semi-Lagrangian Method to Study Nonlinear Electrostatic Waves in Quantum Plasma," *IEEE Transactions on Plasma Science*, (2022), 50(6), pp. 1579-1584, doi: 10.1109/TPS.2022.3158965
- [5] Chandra, S., Das, C. and Sarkar, J., "Evolution of nonlinear stationary formations in a quantum plasma at finite temperature." *Zeitschrift für Naturforschung A*, (2021), 76(4), pp.329-347. doi: 10.1515/zna-2020-0328
- [6] Chandra, S., Kapoor, S., Nandi, D., Das, C. and Bhattacharjee, D., "Bifurcation Analysis of EAWs in Degenerate Astrophysical Plasma: Chaos and Multistability," *IEEE Transactions on Plasma Science*, (2022), 50(6), pp. 1495-1507, June 2022, doi: 10.1109/TPS.2022.3166694. doi: 10.1109/TPS.2022.3166694
- [7] Ghosh, A., Goswami, J., Chandra, S., Das, C., Arya, Y. and Chhibber, H., "Resonant interactions and chaotic excitation in nonlinear surface waves in dense plasma." *IEEE Transactions on Plasma Science*, (2022), 50(6), pp. 1524-1535, doi: 10.1109/TPS.2021.3109297
- [8] Goswami, J., Chandra, S., Das, C. and Sarkar, J., "Nonlinear Wave-Wave Interaction in Semiconductor Junction Diode." *IEEE Transactions on Plasma Science*, (2022), 50(6), pp. 1508-1517, doi: 10.1109/TPS.2021.3124454

- [9] Sarkar, J., Chandra, S., Dey, A., Das, C., Marick, A. and Chatterjee, P., "Forced KdV and Envelope Soliton in Magnetoplasma With Kappa Distributed Ions." *IEEE Transactions on Plasma Science*, (2022), 50(6), pp. 1565-1578, doi: 10.1109/TPS.2022.3140318

Publications not included in this thesis:

- [1] Chandra, S., Goswami, J., Sarkar, J. and Das, C., "Analytical and simulation studies of forced kdv solitary structures in a two-component plasma." *Journal of the Korean Physical Society*, (2020), 76(6), pp.469-478. doi: 10.3938/jkps.76.469
- [2] Chandra, S., Sarkar, J., Das, C. and Ghosh, B., "Self-interacting stationary formations in plasmas under externally controlled fields." *Plasma Physics Reports*, (2021), 47(3), pp.306-317. doi: 10.1134/S1063780X21030041
- [3] Sarkar, J., Chandra, S., Goswami, J., Das, C. and Ghosh, B., "Growth of RT instability at the accreting magnetospheric boundary of neutron stars.": *AIP Conference Proceedings* (2021), 2319(1) p. 030006. doi: 10.1063/5.0037017
- [4] Thakur,S., Das, C. and Chandra, S., "Stationary Structures in a Four Component Dense Magnetoplasma with Lateral Perturbations." *IEEE Transactions on Plasma Science*, (2022), 50(6), pp. 1545-1556, doi: 10.1109/TPS.2021.3133082
- [5] Sahoo, H., Das, C., Chandra, S., Ghosh, B., and Mondal, K.K., "Quantum and Relativistic Effects on the KdV and Envelope Solitons in Ion-Plasma Waves." *IEEE Transactions on Plasma Science*, (2021), 50(6), pp. 1610-1623, doi: 10.1109/TPS.2021.3120077
- [6] Dey, A., Chandra, S., Das, C., Mandal, S., and Das, T., "Rogue Wave Generation Through Nonlinear Self-Interaction of Electrostatic Waves in Dense Plasma." *IEEE Transactions on Plasma Science*, (2022), 50(6), pp. 1557-1564, doi: 10.1109/TPS.2022.3143001
- [7] Sarkar, S., Sett, A., Pramanick, S., Ghosh, T., Das, C. and Chandra, S., "Homotopy Study of Spherical Ion-Acoustic Waves in Relativistic Degenerate Galactic Plasma." *IEEE Transactions on Plasma Science*, (2022), 50(6), pp. 1477-1487, doi: 10.1109/TPS.2022.3146441
- [8] Chandra, S., Goswami, J., Sarkar, J., Das, C., Nandi, D., and Ghosh, B., "Formation of electron acoustic shock wave in inner magnetospheric plasma." *Indian Journal of Physics*, (2022), doi: 10.1007/s12648-021-02276-x

TABLE OF CONTENTS

Abstract	xi
Chapter 1: Introduction	1
1.1 Plasma Waves	1
1.2 Instabilities in Plasma waves	3
1.3 Plasma Modeling	4
1.4 Hydrodynamic Model	5
1.5 Analysis of Plasma Waves and Instability	5
1.5.1 Hydrodynamic Instabilities	6
1.6 Analytical Studies	8
1.6.1 Methods for Study of Non-linear Waves in Space Plasma	8
1.7 Computer Simulation	11
1.8 Motivation	12
Chapter 2: Amplitude modulation and soliton formation of an intense laser beam interacting with dense quantum plasma: symbolic simulation analysis	13
2.1 Introduction	13
2.2 Basic Formulations	15
2.3 Symbolic simulation	18
2.4 Result	20
2.5 Conclusion	25
Chapter 3: Nonlinear interaction of intense laser beam with dense plasma	27
3.1 Introduction	27

3.2	Basic formulation	28
3.3	Symbolic simulation	31
3.4	Result and discussion	33
3.5	Conclusion	37
Chapter 4: Effects of exchange symmetry and quantum diffraction on amplitude modulated electrostatic waves in quantum magnetoplasma		38
4.1	Introduction	38
4.2	Basic Equations	44
4.3	Linear and nonlinear analysis	46
4.4	Result and discussion	51
4.5	HAM study	59
4.6	Conclusion	60
Chapter 5: Semi-Lagrangian Method to Study Nonlinear Electrostatic Waves in Quantum Plasma		61
5.1	Introduction	61
5.2	Temperature anisotropy and Kinetic model	63
5.3	Basic Equations	65
5.4	Numerical Scheme	66
5.5	Results and Discussions	72
5.6	Applications	73
5.7	Conclusion and Summary	74
Chapter 6: Bifurcation Theory and Stability Analysis		75
6.1	Introduction	75
6.2	Quantum plasma at finite temperature	78
6.2.1	Derivation of KdV-Burger's equation	80
6.2.2	Amplitude Modulation and Nonlinear Schrodinger Equation	84

6.3	Bifurcation Analysis of EAWs in Degenerate Astrophysical Plasma: Chaos and Multistability	92
6.3.1	Derivation of KdV equation	95
6.3.2	Dynamical systems of Electron Acoustic Forced-KdV	96
6.3.3	Analytic derivation of NLSE	107
6.3.4	Dynamical Systems of Amplitude Modulated EAWs	109
6.3.5	Applications	111
6.4	Conclusion	111
Chapter 7: Resonant Interactions and Chaotic Excitation in Nonlinear Surface Waves in Dense Plasma		113
7.1	Introduction	113
7.2	Model Equations	115
7.3	Linear Theory	116
7.3.1	Linear Dispersion Characteristic	116
7.3.2	Linear Surface waves	117
7.3.3	Particle dynamics under one harmonic wave	119
7.3.4	Superposition of Waves and Lagrangian Chaos	125
7.4	Nonlinear Theory	127
7.4.1	Harmonics of Field Quantities: Generation and Evolution	127
7.4.2	Parametric Dependence of Field Quantities	129
7.5	Conclusions	134
Chapter 8: Nonlinear Wave-Wave Interaction in Semiconductor Junction Diode		135
8.1	Introduction	135
8.2	Basic Formulation	137
8.3	Derivation of Evolutionary Equations	140

8.3.1	Numerical Analysis of Solitary waves and Wave-wave Interactions	141
8.4	Simulation	144
8.4.1	Theory	144
8.4.2	Results	146
8.5	Summary	151
Chapter 9: Stationary Structures and Its Evolution		152
9.1	Introduction	152
9.2	Evolution of nonlinear stationary formations in a quantum plasma at finite temperature	155
9.2.1	Basic equation	157
9.2.2	Non-perturbative Analysis	158
9.2.3	Reductive Perturbation Method	162
9.3	Forced KdV and Envelope Soliton in Magnetoplasma with Kappa Distributed Ions	174
9.3.1	Basic Equations	175
9.3.2	Results of HASS Technique	176
9.3.3	Analytical Study	181
9.4	Conclusion	195
Chapter 10: Summary and Conclusion		196
Appendix A: Nonlinear interaction of intense laser beam with dense plasma		201
Appendix B: Effects of exchange symmetry and quantum diffraction on amplitude modulated electrostatic waves in quantum magnetoplasma		202
B.1	n=1, l=1 perturbation relations:	202
B.2	n=1, l=1 perturbation coefficients:	202
B.3	n=2, l=1 perturbation relations:	203

B.4	n=2, l=1 perturbation coefficients:	203
B.5	n=2, l=2 perturbation relations:	204
B.6	n=2, l=2 perturbation coefficients:	204
B.7	n=3, l=0 perturbation relations:	205
B.8	n=2, l=0 perturbation coefficients:	205
B.9	n=3, l=1 perturbation relations:	206
Appendix C: Resonant Interactions and Chaotic Excitation in Nonlinear Surface Waves in Dense Plasma		207
C.1	First Harmonic Quantities	207
C.2	Second Harmonic Quantities	208
Appendix D: Bifurcation Theory and Stability Analysis		210
References		249

ABSTRACT

In this dissertation a large volume of nonlinear wave phenomena in plasma has been studied. We have carried out investigations pertaining to different wave modes observed in plasma under different configuration. The applicability of such study ranges from laser plasma interaction, astrophysical plasma, magnetospheric plasma, semiconductor plasma etc. We have used analytical and simulation techniques to obtain the results. In the process we have designed some mathematical and simulation tools that will help the future researchers to investigate various other aspects of plasma physics. In the process we have studied KdV equation, Burgers equations, nonlinear Schrodinger equation and also came up with the modified versions. Amplitude modulation and the formation of envelope soliton in quantum plasma have been studied with reference to laser plasma interaction and is presented in chapters 2 and 3. The effects of quantum diffraction and exchange symmetry have been also studied in magnetoplasma, the findings are presented in chapter 4. A semi-Lagrangian method to study the nonlinear electrostatic waves in quantum plasma is presented in chapter 5. We have also studied the dynamical system analysis, bifurcation theory and stability analysis, Lyapunov exponent and chaotic scenario in various plasma configuration and all these are presented in chapter 6. Resonant interaction and it's contribution towards harmonic generation in surface plasma waves observed in vacuum-plasma interface has been studied and presented in chapter 7. The chapter 8 deals with the wave-wave interaction in a semiconductor plasma where we have used designed simulation codes. In chapter 9 the nonlinear evolution of stationary structures has been presented in details with limiting and boundary conditions. This is crucial for new researches in this field. Finally we have summarised our important findings and also pointed out the future prospect of these findings and the scope for application of the new technique developed in the present thesis.

CHAPTER 1

INTRODUCTION

Plasma is the most abundant state of known matter in the universe. It has been said that almost 99.9% of the matter in the universe is in the plasma state. This estimate may be inaccurate, but it is undeniably an important reason for studying plasma dynamics to better understand the various fields in our universe. Plasma physics is the study of ionized gases containing charged particles and fluids interacting with self-consistent electric and magnetic fields. It is a basic research topic with numerous applications, including space and astrophysics, controlled fusion [1, 2], accelerator physics [3, 4] and beam storage [5, 6]. Plasmas are found in stellar interiors and atmospheres, gaseous nebulae, and much of the interstellar medium. As soon as one leaves the earth's atmosphere, one enters our neighborhood and comes into contact with the plasma that makes up the solar wind and the Van Allen radiation belts. A lightning strike, the gentle glow of the Aurora Borealis, the conducting gas inside a fluorescent tube or neon sign, a slight degree of ionization in a rocket exhaust, etc., are common contacts with plasmas.

1.1 Plasma Waves

Plasma is an electrically conducting, quasi-neutral fluid. It comprises electrons and a single species of positive ions in the most straightforward instance. Still, it can also contain several ion species, including negative and positive ions and neutral particles. Waves in plasmas are due to the correlated motion of particles and the interplay of fields that propagate in a plasma medium. Plasma particles interact through electric and magnetic fields due to their electrical conductivity. This complex of particles and fields can support a wide range of wave events. A linear perturbation in space plasma can be reviewed as a linear combination of the Eigen wave modes derived from the space plasma's lin-

ear wave dispersion relations. There is no interaction between these Eigen wave modes under the linear superimposition assumption. As a result, the linear combination's coefficients should not change over time. Nonlinear plasma dynamics is used to explore the formation, evolution, propagation, and characteristics of the large amplitude quasi-stationary nonlinear waves, structures, or turbulence commonly observed in the plasmas and numerical simulations of space plasmas. The natural electric and magnetic field holds the plasma particles. The electric and magnetic fields will fluctuate over time due to motions within the plasma, and these variations will appear as plasma waves.

Plasma is rich in wave phenomena. We can find many important plasma properties by studying the waves in plasma. Some nonlinear phenomena, such as the formation of solitary waves and various forms of instability, involve waves of finite amplitude. Again, since 99.9% of matter is in the plasma state, studying plasma provides an idea of an astrophysical environment. For this reason, studying nonlinearity in plasma waves for cosmological applications [7, 8, 9, 10] has greatly interested many scientists. It has been observed that galactic plasmas [11] are multispecies plasmas with both positive and negative charges. The existence of plasma electron-positron-ion (e-p-i) is found in black holes, in the magnetospheric regions of neutron stars [12, 13, 14, 15], in the regions of aurorae, etc. The e-p-i plasmas are also generated in several laboratory environments [16, 17, 18]. Thus, during the last two decades, many authors have become interested in studying nonlinear waves and the e-p-i plasma phenomenon [19, 20, 21, 22, 23, 24, 16, 17].

The space from the upper ionosphere to the solar system contains a fully ionized gas of varied densities. Most of the ions are hydrogen, and the touch of helium and electrons produces an overall neutral plasma. Magnetized plasma waves are generated around magnetized planets (Mercury, Earth, Jupiter, Saturn, Neptune, Uranus) and propagate in the magnetosphere. Frequencies well below the ion cyclotron frequency have three possible wave modes. These are 'slow', 'fast', and 'Shear-Alfven modes'. Only high-speed and Shear-Alfven modes exist for low-energy plasmas (about 10 eV).

”Fast” mode allows energy to propagate diagonally to the surrounding magnetic field and disperse wave energy throughout the magnetosphere. It is a kind of magnetic force wave (blast). In shear mode, energy is guided along the ambient magnetic field. It is a transverse wave.

1.2 Instabilities in Plasma waves

The buoyant waves that travel across the tops of fluid bodies and crash upon boundaries all across the physical world are observed. The disturbances in the atmosphere that cause what is known as the weather are equally common, but they are not always recognized as waves. Wave phenomena are critical in the behavior of plasmas. According to plasma physics, waves in plasmas are a network of related particles and fields that move in a cyclically repeating pattern. A wide range of wave phenomena is supported by these complex interactions of particles and fields. According to plasma physics, waves in plasmas are a complex interaction of particles and fields that move in a cyclically repeating pattern.

The species that oscillates can be used to further categorize waves. The electron temperature in most plasmas of interest is either comparable with or higher than the ion temperature. This observation suggests that the electrons move much more quickly than the ions because of their much smaller mass. The rapid motion of the electrons determines the electron mode, but the ions can be assumed to be endlessly heavy and therefore stationary. The stability of the plasma is a crucial area in plasma physics. A plasma’s stability is typically only meaningfully examined when it has been determined that it is in equilibrium. If there are net forces that will accelerate any portion of the plasma, this is what ”equilibrium” investigates. If not, ”stability” determines whether a minor disturbance will increase, oscillate, or be dampened.

A plasma instability is a region in the frequency/wavelength domain where turbulence occurs due to changes in the characteristics of a plasma (e.g. temperature, den-

sity, electric fields, magnetic fields). Such turbulence has great implications in space based technology [25, 26], astrophysical [27] and laser base measurement [28]. Extreme manifestations of space plasma instability are space storms [29, 30]. Examples of complicated events involving quick disturbances and system reconfiguration on both the macroscopic and microscopic scales include the onset of a solar flare or the growth of a substorm. Plasma instabilities explains the importance of e-p-i plasma with relevance to various astrophysical applications like in pulsar atmosphere to laboratory experiments like tokamak.

1.3 Plasma Modeling

Plasmas behave like fluids and sometimes like a collection of individual particles—the basic approaches for plasma modeling are analytic and some times numerical simulations. There are a few primary kinds of plasma models: single particle, kinetic, fluid, hybrid kinetic/fluid, gyrokinetic, and a system of many particles. Among them, fluid and kinetic are two fundamental approaches.

The kinetic model is the most basic way to describe a plasma, yielding a distribution function $f(\vec{x}, \vec{v}, t)$ with independent variables \vec{x} and \vec{v} representing position and velocity, respectively. The electromagnetic fields are determined by the charges and currents specified by the distribution functions using Maxwell's equations. A kinetic description is obtained by solving the Boltzmann equation or, when an accurate description of long-range Coulomb interaction is required, by the Vlasov equation, which contains a self-consistent collective electromagnetic field, or by the Fokker-Planck equation, which contains approximations to derive manageable collision terms. The fluid description treats the large-scale properties of plasma involving mass, momentum, and energy transport [31, 32].

1.4 Hydrodynamic Model

Without taking into account microscopic events, we trace the mobility of small volume elements in the plasma in the hydrodynamic description. Average values are well-centered because there are enough particles in the volume to prevent fluctuations from significantly shifting the average values. In the same way, we assume that the average fields considered to be acting globally on this same volume element account for the effect of the electric and magnetic micro fields produced by the charged particles in the volume element on the macroscopic scale. Since the volume elements are so small, a detailed spatial description can be provided. In comparison to calculations from the kinetic theory, which are far more difficult to derive and interpret, the hydrodynamic model allows us to characterize all the physical occurrences in the plasma in a relatively comprehensive manner.

The charged particles in a plasma make up one (for example, the electrons, with the ions remaining at rest and forming a continuous background, providing an effective viscosity to the electron motion) or more fluids (that of the electrons and that of the ions). Each fluid's motion is characterized locally by an average velocity \vec{v} , the value of which is determined by incorporating the velocity distribution of the particles contained in the volume element under consideration. The motion of the charged particles generates the electromagnetic fields \vec{E} and \vec{B} (for which the average local value is retained (macroscopic fields), which are included in the equations of motion [33] in a self-consistent manner. Furthermore, collisions are included in the model, which alters the pre-determined motion defined by the superposition of the external and induced fields.

1.5 Analysis of Plasma Waves and Instability

Plasma stability is an important consideration in the study of plasma physics. When systems containing plasmas are in equilibrium, certain parts of the plasma can be per-

turbed by the small perturbations that act on them. The system's stability determines whether the perturbation grows, vibrates, or disappears. Plasma can often be treated as a fluid, and its stability is analyzed using hydrodynamics (HD) formulation. Since HD theory is the most straightforward representation of plasma, HD stability is necessary for stable devices used for fusion, especially magnetohydrodynamic (MHD) energy. However, there are other types of instability—velocity space instability in systems with magnetic mirrors and beams. Interesting things are observed due to stability effects. Field-reversed configuration was predicted to be unstable by MHD but was observed to be stable, probably due to kinetic effects.

Plasma instabilities are categorized into two general categories: (i) Hydrodynamic instabilities and (ii) Kinetic instabilities.

1.5.1 Hydrodynamic Instabilities

In fluid mechanics, hydrodynamic stability is the field of analyzing fluid flow stability and the onset of instability. The study of hydrodynamic stability aims to investigate whether a given flow is stable or unstable and, if so, how these instabilities cause turbulence. The theoretical and experimental foundations of hydrodynamic stability were laid primarily by Helmholtz, Kelvin, Rayleigh and Reynolds in the 19th century [34, 35, 36, 37, 38]. These foundations have provided many useful tools for studying hydrodynamic stability. These include Reynolds numbers, Euler equations, and Navier-Stokes equations. When studying flow stability, it is helpful to understand a more straightforward system. It is an incompressible, non-viscous fluid that can develop into more complex flows [38]. Since the 1980s, more computational methods have been used to model and analyze complex flows.

To distinguish between fluid flow states, consider how the fluid reacts to a disturbance in the initial state [39]. These disturbances will be related to the system's initial properties, such as velocity, pressure, and density. Stable flow, any infinitely slight variation considered a disturbance, will not affect the system's initial state and will eventually

die down in time [39]. For a fluid flow to be considered stable, it must be stable concerning every possible disturbance. This implies that no mode of disturbance exists for which it is unstable [38]. On the other hand, for an unstable flow, any fluctuation will have some noticeable effect on the system's state. This would then cause the disturbance to grow amplitude so that the system progressively departs from the initial state and never returns [39]. This means that there is at least one mode of disturbance concerning which the flow is unstable, and the disturbance will therefore distort the existing force equilibrium [40].

Reynolds number (R_e) is the critical tool used to determine the stability of a flow. A dimensionless number gives the ratio of inertial and viscous terms [41]. In a physical sense, this number is a ratio of the forces due to the fluid's momentum (inertial terms) and the forces arising from the relative motion of the different layers of a flowing fluid (viscous terms). The equation for this is [39]

$$R_e = \frac{\text{inertial}}{\text{viscous}} = \frac{\rho u^2}{\frac{\mu u}{L}} = \frac{\rho u L}{\mu} = \frac{u L}{\nu}$$

where ρ = density, \mathbf{u} = velocity of the fluid flow, μ = dynamic viscosity - measures the fluids resistance to shearing flows, L = characteristic length, ν = kinematic viscosity and $= \frac{\mu}{\rho}$ - measures ratio of dynamic viscosity to the density of the fluid.

The Reynolds number is useful because it can provide cut-off points for when the flow is stable or unstable, namely the Critical Reynolds number R_c . As it increases, the amplitude of a disturbance which could then lead to instability gets smaller [38]. It is agreed that fluid flows will be unstable at high Reynolds numbers. A High Reynolds number can be achieved in several ways, e.g., if μ is a small value or if ρ and u are high values [39]. This means that instabilities will arise almost immediately, and the flow will become unstable or turbulent [38].

1.6 Analytical Studies

A plasma system can be described by a set of nonlinear partial differential equations (PDEs). Computer simulation is a good way to model and test astrophysical processes. In this way, the experimental data is explained in terms of the physics of the model, and the computer model is improved compared to the experimental data. This cycle provides a better understanding of the predictability and level of application of the study. Design and program a series of simulations using astrophysical differential equations.

1.6.1 Methods for Study of Non-linear Waves in Space Plasma

Quasi-linear Approximation:

The quasi-linear approximation is useful for studying small but finite amplitude nonlinear waves. The quasi-linear approximation preserves the first and second-order terms in the Taylor expansion of the nonlinear equation. The quasi-linear approximation is often used to study nonlinear phenomena due to wave interactions. The quasi-linear approximation allows the study of nonlinear phenomena at many space and time scales. The quasi-linear approximation solution can be a time-independent structure over a long time interval but becomes a time-dependent structure over a short interval.

Pseudo Potential Method:

The pseudopotential method is often used to study solutions of nonlinear waves that are stable over time. The pseudopotential method can help us find analytical solutions to nonlinear equations with or without approximations of quasars. Unlike the standard approximation, there is no standard procedure for determining the pseudopotentials of fully nonlinear equations. Fortunately, the pseudopotential can be obtained in nonlinear plasma physics based on energy flux conservation. If we consider solutions of nonlinear one-dimensional plane waves ($\nabla = \hat{x} \frac{\partial}{\partial x}$) which propagate at a constant speed, then we can choose a moving frame such that the wave structure becomes stationary

(time-independent, i.e., $\frac{\partial}{\partial t} = 0$). Thus, the set of partial differential equations (PDEs) is reduced into a set of ordinary differential equations (ODEs). Since numerical methods for solving ordinary differential equations are well established, one can always obtain nonlinear-wave solutions by solving these ODEs numerically with different boundary conditions. One may need to examine numerical solutions for many different parameters and initial conditions to understand systematic changes in wave characteristics. So, it is difficult to get a full dependency on numerical solutions. However, suppose the nonlinear wave equations can be reduced to equations similar to the equations of motion. In that case, the so-called pseudopotential method can be used for exploratory analysis of the solution space. The pseudopotential method can be used to study electrostatic and electromagnetic waves in collision-free plasma.

Reductive Perturbation Method (RPM):

The perturbation theory results in an expression of the desired solution as a formal power series in a "small" parameter (called a perturbation series), quantifying the deviation from the equilibrium that can be solved exactly. The primary term in this entire series is the solution of the correctly solved problem. In contrast, the other words describe the deviation in the solution due to the deviation from the initial problem. Formally, we have for the approximation to the complete solution A , a series in the small parameter (here called " ϵ "), like the following:

$$A = A_0 + \epsilon^1 A_1 + \epsilon^2 A_2 + \dots$$

In this example, A_0 would be the known solution to the precisely solvable initial problem, and A_1, A_2, \dots represent the higher-order terms found iteratively by some systematic procedure. For small ϵ , higher-order terms in the series become successively smaller. Next, the reductive perturbation method is presented as a solution that allows us to reduce a general nonlinear hyperbolic system to a single, solvable nonlinear equation describing the far-field of the system. The reductive perturbation method applied to more general systems, including dispersion dissipation, shows that they can be reduced to the Burgers

equation or the Kortweg-de-Vries (KdV) equation for long waves. Additionally, it is demonstrated that the Schrodinger equation governs the far-field for the slow modulated propagation of plane waves with extremely small amplitudes and that, for small but finite amplitudes, the general wave system can be reduced to a nonlinear Schrodinger type equation, which we refer to as the general nonlinear Schrodinger equation.

Homotopy Perturbation Method:

The Homotopy perturbation method (HPM) is a semi-analytical method for solving linear and nonlinear differential equations. A system of coupled linear and nonlinear ordinary/partial differential equations can also be solved using this method. In mathematics, homotopy is a method of categorizing geometric regions by looking at the various kinds of routes that can be created in the region. If one of two paths can be constantly deformed into the other while keeping the end points stable and staying inside its defined region, the paths are said to be homotopic. The shaded zone in portion *A* of the figure 1.1 has a hole in it; while f and g are homotopic pathways, g' is not homotopic to f or g since it cannot be deformed into one of them without going through the hole and leaving the territory.

In more technical terms, homotopy entails creating a path by continuously mapping points in the range of 0 to 1 to points in the area, so that adjacent points on the interval also correspond to adjacent points on the path. The continuous homotopy map $h(x, t)$ is a function of two variables x and t that is equal to $f(x)$ when $t = 0$ and equal to $g(x)$ when $t = 1$. It associates with two acceptable paths, $f(x)$ and $g(x)$, and is a function of two variables. The graphic (figure 1.1) depicts the intuitive notion of a steady distortion as t increases from 0 to 1 without leaving the area. For instance, the homotopic function for pathways f and g in portion *A* of the figure is $h(x, t) = (1 - t)f(x) + tg(x)$; the points $f(x)$ and $g(x)$ are connected by a straight line segment, and $h(x, t)$ specifies a path connecting the same two endpoints for each fixed value of t .

The homotopic pathways beginning and ending at a single place are of particular

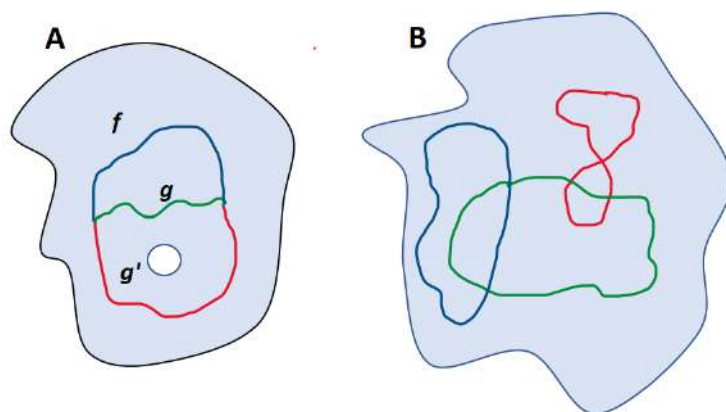


Figure 1.1: Homotopy

importance (see part B of the figure 1.1). A homotopy class is the collection of all such pathways that are homotopic to one another within a particular geometric region. The fundamental group of the region, whose structure differs depending on the type of area, can be used to represent the set of all such classes in algebra. In a region without holes, all closed pathways are homotopic, and there is only one element in the fundamental group. All pathways that go around the hole the same amount of times are homotopic in a region with a single hole. Similarly, we define a set of homotopy pathways and basic regions on a general manifold in three or more dimensions. In higher dimensions, one can also define higher dimensional homotopy groups.

In homotopy perturbation method or homotopy perturbation technique (HPT) first splits the differential equations into two parts (linear and nonlinear). Next, we construct the homotopy by considering the initial condition or initial approximation. Then, as the homotopy parameter goes from 0 to 1, the initial state goes to an exact or approximated analytic solution.

1.7 Computer Simulation

Computer simulation is a good way to model and test astrophysical processes. In this way, the experimental data is explained in terms of the physics of the model, and the

computer model is improved compared to the experimental data. This cycle provides a better understanding of the predictability and level of application of the study. Design and program a series of simulations using astrophysical differential equations. It has a wide range of uses in astrophysics. The hybrid simulation combines the electromagnetic equation with charged particle dynamics. This simulation shows the time evolution of particles and fields in the presence of two backpropagating ion beams. The magneto-hydrodynamic equation is a combination of the electromagnetic (Maxwell-Heaviside) equation and the fluid equation. In general, MHD equations are non-linear. An example of astrophysics is the modeling of Kelvin-Helmholtz instability. This happens when there are fluids of various densities with velocity shear at the interface. Examples include atmospheric wind shear, lakes (winds on the water), and magnetosphere boundaries. The simulation shows a computer model of the temporal evolution of the magnetosphere interface. By linearizing the MHD equation, one can simulate the propagation of Ultra-Low Frequency (ULF) waves in the magnetosphere.

1.8 Motivation

The motivation behind this doctoral work is to study the different nonlinear phenomenon using analytic and simulation tools. I have studied various wave modes, stabilities, wave interaction and stationary structure formations. Keeping in mind the limitations (both technical and computation system facility) we have been motivated to design new simulation techniques and employed certain topological methods to carry out our investigations. We have addressed problems in different fields like laser plasma interaction (LPI), semiconductor plasma, astrophysical plasma, ionospheric plasma etc. This thesis contains a variety of techniques and a plethora of applications of plasma physics. The subsequent chapters will elaborate the works accordingly.

CHAPTER 2

AMPLITUDE MODULATION AND SOLITON FORMATION OF AN INTENSE LASER BEAM INTERACTING WITH DENSE QUANTUM PLASMA: SYMBOLIC SIMULATION ANALYSIS

2.1 Introduction

In the field of fluid dynamics or nonlinear optics or plasma physics, modulational instability (MI) or amplitude modulation (AM) is an interesting phenomena whereby an initial periodic waveform undergo derivation which are reinforced by the nonlinearity present in the system, generating spectral sidebands which eventually breakup the waveform (initially uniform) into a train of pulses [42, 43, 44]. Initially discovered and modeled for periodic surface waves in 1967 [45], it was suggested that this mechanism is probably the cause of rogue waves [46, 47]. This modulational instability occurs when there is anomalous group velocity dispersion, where short wavelength (high energy) pulses travel fast (with higher group velocity) than the less energetic pulses. In nonlinear optics such phenomena is related with Kerr nonlinearity. This instability strongly depends on the frequency of perturbation. The growth of instability is therefore frequency dependent and an overall gain spectrum can be obtained analytically by starting with the nonlinear Schrodinger equations (NLSE). The nonlinear Schrodinger equation describe the evolution of the complex valued slowly varying wave envelope with space and time.

Plasma is a very complex system. Different order of non linearity and dispersion are seen to occur in plasma. As a result the complexity of the physical problem increases manifold. To deal with such orders of nonlinearity and incorporating others effects different approaches have been attempted. Among them the common ones are the fluid model and the particle model. In practice both methods have their limitations and ad-

vantages. Over the past few years these models have found widespread usage and we too will confine ourselves with the fluid picture. Plasma as we all knew is an extremely heated soup of charged particles which manifest collective phenomena and also conform to quasineutrality conditions. Dense matter in the plasma state manifest some additional effects [48, 49, 50, 51]. Firstly the pressure experienced by the plasma is due to the relativistic degeneracy [52, 53] accounting for particle speeds closes to the speed of light. Now it has been quiet interesting to study the effect of quantum mechanical tunneling or other quantum effects in dense plasmas. Pioneers like Shukla [54, 55, 56], Manfredi [57, 58], Hass [59, 60] have done tome of works on quantum plasma. Often they have used quantum hydrodynamic (QHD) model to deal with the quantum behaviour of plasma particles. After them Misra [61, 62], Sahoo [63], Ghosh [64], Chandra [65, 66, 67, 68], Brodin [69], Bonitz [70, 71], Singh [72, 73] and others authors have made use of the same hydrodynamics model to solve many problems. This model takes into consideration the quantum statistical effect through the equation of state and the quantum diffraction effect through the Bohm potential term. Many authors [74, 75] have made use of this QHD model with certain additions and alterations [76] depending upon the applicability of the model under different criteria. Since such a model includes terms in the momentum equation, this equation is crucial in plasma dynamics. The pressure of magnetic field introduce certain changes in the system. The inclusion of directionality, the propagation vector and the electromagnetic interaction modifies the electrostatic picture. Considering the plasma as a dielectric medium which shields the electromagnetic fields to modify it, a low power electromagnetic field can't cause much visible change. The electromagnetic radiation just reflects back for the interface. But with the advent of high power and ultra fast laser beams there has been changes in this picture. A survey of available literature [77, 78, 79, 80, 81] shows how plasma interacts with laser fed into it. In many electrostatic situations where the phase speed is less than speed of light, some wave particle resonant interaction occurs amounting to Lanbdau damping or something of similar nature.

Often the techniques or methods employed to solve the problems of this kind are either analytical or computational. Both have their limitations. In analytic approach there exists certain level of ingenuity but it can't be scaled up and we have to contain ourselves with few orders of approximations. The computational approach on the other hand suffers from technical constrains and a high end super computer is the basic prerequisite. In order to solve the issues of analytical solutions and computational technique we make use of elements of topology and continuous mapping and take an attempt to solve coupled partial differential equations (PDE). To our knowledge PDE has been solved in few cases by employing homotopy perturbation technique (HPT). But coupled PDE has not been solved by this method immense effort to solve our equations with symbolic notation and not numerical values. In essence our method is computer aided analytical method. The originality of the problem is inherent in the method employed here. In brief the chapter is organized in the following manner. In the second section we provide with the basic formulation with associated normalization. In the next section we make use of symbolic computation and obtained solution for different orders of homotopy parameter (p). Finally we check the convergence and discuss the results obtained and cross check the results this obtained with other previous findings (analytical or computational).

2.2 Basic Formulations

Here we consider that the pressure exerted by particle at such high densities follow the relativistic degeneracy pressure given by Chandrasekhar [52, 53]. Further we have considered a Gaussian distribution of density and beam profile in space. It is assumed to be irradiated with a intense laser beam with a radial Gaussian cross section given by [77]

$$\vec{\mathbf{E}} = \hat{x} E_0 e^{-\frac{r^2}{r_0^2}} e^{i(\mathbf{k}\cdot\mathbf{r}-\omega\cdot t)} + c.c. \quad (2.1)$$

Here, the quantities have usual meaning. Now assuming slow variation in laser beam amplitude and employing Maxwell's equations the magnetic field equation can be writ-

ten as

$$\vec{\mathbf{B}} \equiv \hat{y} \frac{kc}{\omega} E_0 e^{-\frac{r^2}{r_0^2}} e^{i(\mathbf{k}\cdot\mathbf{r}-\omega t)} + c.c. \quad (2.2)$$

We have assumed the electric field is coupled the initial unperturbed laser field and accordingly small perturbations due to the beam plasma interaction is given by [77]

$$\vec{\mathbf{E}} = \vec{\mathbf{E}}_0 + \vec{\mathbf{E}}_1$$

where E_0 and E_1 are corresponds to initial value of the laser beam and unstable perturbation ($|E_0| \gg |E_1|$) respectively. In this system we consider a dense plasma containing relativistically degenerate electrons and relatively inertial ionic background satisfy neutralizing criteria. The electrons are assumed to have a streaming along the direction of motion, such that the speed is close to the speed of light and hence experience relativistic effects. Now let an intense laser beam be introduce in the plasma. Here the laser is called intense because if it were weak electromagnetic beam then plasma would shield the electric field and behave as dielectric. Taking these factors into consideration the dynamic equations describing the laser plasma interaction is given by

$$\frac{\partial(\gamma\mathbf{n})}{\partial t} + \vec{\nabla} \cdot (\gamma\mathbf{n} \vec{\mathbf{v}}) = 0, \quad (2.3)$$

$$\frac{\partial(\gamma\vec{\mathbf{v}})}{\partial t} + \vec{\mathbf{v}} \cdot \vec{\nabla}(\gamma\vec{\mathbf{v}}) = -\frac{e}{m_0} \left(\vec{\mathbf{E}} + \frac{\vec{\mathbf{v}}}{c} \times \vec{\mathbf{B}} \right) - \frac{\vec{\nabla} \cdot \mathbf{P}}{m_0\mathbf{n}} + \frac{\hbar^2}{2m_0^2} \vec{\nabla} \cdot \left(\frac{\nabla^2 \sqrt{\mathbf{n}}}{\sqrt{\mathbf{n}}} \right), \quad (2.4)$$

$$\left(\frac{\partial}{\partial t} + \vec{\mathbf{v}} \cdot \vec{\nabla} \right) \vec{\mathbf{E}} = \frac{1}{\epsilon_0} \mathbf{J}. \quad (2.5)$$

Here the pressure is ultra relativistic in nature

$$\mathbf{P} = \frac{1}{8} \left(\frac{3}{\pi} \right)^{\frac{1}{3}} \hbar c (\mathbf{n})^{\frac{4}{3}}. \quad (2.6)$$

In equations (2.3) and (2.4) γ is the streaming factor as considered by many authors [82].

For ease of mathematical treatment we use normalization so as to obtain dimensionless differential equations. Therefore, using normalization scheme for field quantities $x \rightarrow x \frac{\omega_p}{v_{th}}$, $y \rightarrow y \frac{\omega_p}{v_{th}}$, $z \rightarrow z \frac{\omega_p}{v_{th}}$, $t \rightarrow \omega_p t$, $u \rightarrow \frac{u}{v_{th}}$, $v \rightarrow \frac{v}{v_{th}}$, $w \rightarrow \frac{w}{v_{th}}$, $E \rightarrow \frac{eE}{m_0 v_{th} \omega_p}$ and $n \rightarrow \frac{n}{n_0}$, where v_{th}, ω_p, m_0 and n_0 are the thermal velocity, plasma frequency, mass of electron and initial density of plasma, we obtained the differential equations in the normalized form and resolve into scalar components given by

$$\frac{\partial(\gamma n)}{\partial t} + \frac{\partial(\gamma n u)}{\partial x} + \frac{\partial(\gamma n v)}{\partial y} + \frac{\partial(\gamma n w)}{\partial z} = 0, \quad (2.7)$$

$$\begin{aligned} \frac{\partial(\gamma u)}{\partial t} + u \frac{\partial(\gamma u)}{\partial x} + v \frac{\partial(\gamma u)}{\partial y} + w \frac{\partial(\gamma u)}{\partial z} = -E + \frac{k}{\omega} E w - A_u \frac{\partial}{\partial x} \left(n^{\frac{1}{3}} \right) \\ + \frac{H^2}{2} \frac{\partial}{\partial x} \left(\frac{1}{\sqrt{n}} \left(\frac{\partial^2 \sqrt{n}}{\partial x^2} + \frac{\partial^2 \sqrt{n}}{\partial y^2} + \frac{\partial^2 \sqrt{n}}{\partial z^2} \right) \right), \end{aligned} \quad (2.8)$$

$$\begin{aligned} \frac{\partial(\gamma v)}{\partial t} + u \frac{\partial(\gamma v)}{\partial x} + v \frac{\partial(\gamma v)}{\partial y} + w \frac{\partial(\gamma v)}{\partial z} = -A_u \frac{\partial}{\partial y} \left(n^{\frac{1}{3}} \right) \\ + \frac{H^2}{2} \frac{\partial}{\partial y} \left(\frac{1}{\sqrt{n}} \left(\frac{\partial^2 \sqrt{n}}{\partial x^2} + \frac{\partial^2 \sqrt{n}}{\partial y^2} + \frac{\partial^2 \sqrt{n}}{\partial z^2} \right) \right), \end{aligned} \quad (2.9)$$

$$\begin{aligned} \frac{\partial(\gamma w)}{\partial t} + u \frac{\partial(\gamma w)}{\partial x} + v \frac{\partial(\gamma w)}{\partial y} + w \frac{\partial(\gamma w)}{\partial z} = -\frac{k}{\omega} E u - A_u \frac{\partial}{\partial z} \left(n^{\frac{1}{3}} \right) \\ + \frac{H^2}{2} \frac{\partial}{\partial z} \left(\frac{1}{\sqrt{n}} \left(\frac{\partial^2 \sqrt{n}}{\partial x^2} + \frac{\partial^2 \sqrt{n}}{\partial y^2} + \frac{\partial^2 \sqrt{n}}{\partial z^2} \right) \right), \end{aligned} \quad (2.10)$$

$$\frac{\partial E}{\partial t} + u \frac{\partial E}{\partial x} + v \frac{\partial E}{\partial y} + w \frac{\partial E}{\partial z} + n u = 0. \quad (2.11)$$

where $A_u = \frac{1}{2} \left(\frac{3}{\pi} \right)^{\frac{1}{3}} \frac{h}{m_0 v_{th}} n_0^{\frac{1}{3}}$, $H = \frac{\hbar \omega_p}{m_0 v_{th}^2}$. Now with such equations available for solutions (analytical or computational) we will proceed accordingly. As discussed in the later part of the introduction we will construct homotopy and obtain our solutions from it.

2.3 Symbolic simulation

In plasma physics nonlinear phenomena are of great importance. Therefore, analytical methods were initially tried such as perturbation with smallness parameters (often denoted by λ and ϵ). But in problems with strong nonlinearity, there is no smallness parameter at all and the approximate solutions obtained by reductive perturbation or multiple scale perturbations, in most of the cases are valid only for extremely small values of the smallness parameter finds limited application here. As long the system parameters are small such a perturbation method is okay. But an universality of the perturbation technique is not acceptable as there is no criteria on which the smallness parameter shall depend. So such an analytical method need to be verified experimentally or numerically. With the upgradation of different mathematical software and the scope to employ symbolic computations as in Matlab R2019, we attempted successfully to incorporate our extended homotopy perturbation technique to get desired results. Unlike numerical simulation where we feed into the problem numerical values, such that they evolve into solutions that approximately describes the physical problem, symbolic simulation makes use of mathematical functions that is is run in the program to give higher order analytical solution. This technique does not make numerical approximation and accurately provides simulation results of the functions initially fed into the problem. The average run time of the code is optimized so as to provide the solutions in a short period of time. With our modest hardware facilities of 8GB RAM and 2.2 GHz processor we could successfully make provisions for our symbolic simulation. In nutshell this technique is the computer aided analytical solution of partial differential equations with boundary conditions.

To brief the techniques let us consider the following non linear differential equation

$$\mathcal{A}(\bar{u}) - f(\bar{r}) = 0, \tag{2.12}$$

with boundary condition

$$\mathcal{B}(\bar{u}, \frac{\partial \bar{u}}{\partial n}) = 0, \quad r \in \Gamma. \quad (2.13)$$

Here $\mathcal{A}, \mathcal{B}, f(r)$ and Γ are a general differential operator, a boundary operator, an analytical function (which is previously known) and the boundary of the domain Ω . The operator \mathcal{A} can be divided into linear (\mathcal{L}) and non linear part (\mathcal{N}) such that

$$\mathcal{L}(\bar{u}) + \mathcal{N}(\bar{u}) - f(\bar{r}) = 0 \quad (2.14)$$

By employing basic homotopy principle, we construct the homotopy for this problem as:

$$\mathcal{H}(\bar{v}, p) \equiv (1 - p) [\mathcal{L}(\bar{v}) - \mathcal{L}(\bar{u}_0)] + p [\mathcal{A}(\bar{v}) - f(\bar{r})] = 0, \quad p \in [0, 1]. \quad (2.15)$$

or equivalently

$$\mathcal{H}(\bar{v}, p) \equiv \mathcal{L}(\bar{v}) - \mathcal{L}(\bar{u}_0) + p[\mathcal{N}(\bar{v}) - f(\bar{r})] = 0 \quad (2.16)$$

where \bar{u}_0 is initial assumption satisfying the boundary condition (2.13). As the homotopy parameter p changes from zero to unity the picture convolutes from $\bar{u}_0(r)$ to $\bar{v}(r)$ (exact or approximated analytic solution). In topology, this is called deformation and $\mathcal{L}(\bar{v}) - \mathcal{L}(\bar{u}_0)$, $\mathcal{A}(\bar{v}) - f(\bar{r})$ are said to be homotopic. According to the HPT, we can first use the embedding parameter p as a small parameter, and assume that the solutions of equation (2.16) can be written as a power series in p :

$$\bar{v} = p^0 \bar{v}^{(0)} + p \bar{v}^{(1)} + p^2 \bar{v}^{(2)} + \dots \quad (2.17)$$

To obtain solution of (2.16) we make use of equation (2.17) and expand $\mathcal{A}(\bar{u})$ by Taylor series in p and putting this expression in (2.16). Then equating the coefficient of like

powers of p , we obtain equation which are easily solvable. Setting $p = 1$, the results in the approximate solution of equation (2.16) takes the form

$$\bar{u} = \lim_{p \rightarrow 1} \bar{v} = \bar{v}^{(0)} + \bar{v}^{(1)} + \bar{v}^{(2)} + \dots \quad (2.18)$$

The convergence of the series (2.18) has been suggested by He [83, 84] requires :

1. The second derivative of $\mathcal{N}(\bar{v})$ with respect to v must be small because the parameter may be relatively large, i.e., $p \rightarrow 1$.
2. The norm of $\mathcal{L}^{-1} \frac{\partial \mathcal{N}}{\partial v}$ must be smaller than unity so that the series converges.

2.4 Result

In the following figures (2.1)-(2.2) we visualize the velocity streamlines and the velocity profile as well as electric field and density at different instances of time and for different initial density and laser wavelengths. From the figures, it appear that the laser can propagate within the plasma to some extent and gradually ceases to cause any perturbations. With decreasing wavelength the laser penetrates less and shows bifurcation (figure (2.3)). The streamline motions are intersecting in between. It shows clearly the trapping of electrons graphically. Since we are just making projections with our governing equations, there is hardly any difference from the kinetic theory. Laser wakefield accelerations can be easily understood from the figures. The streamlines show the lateral extent perpendicular to laser propagation where the particles are influenced. The interesting part of the figure is that the streamlines extend along propagation direction but the electric field of the laser is not up to that level. The density fluctuations too do not extend that far. A detailed study would reveal that there are electronic fluctuations, but they are many orders smaller. The density fluctuations are less prominent due to the shielding mechanism and the quasi-neutrality.

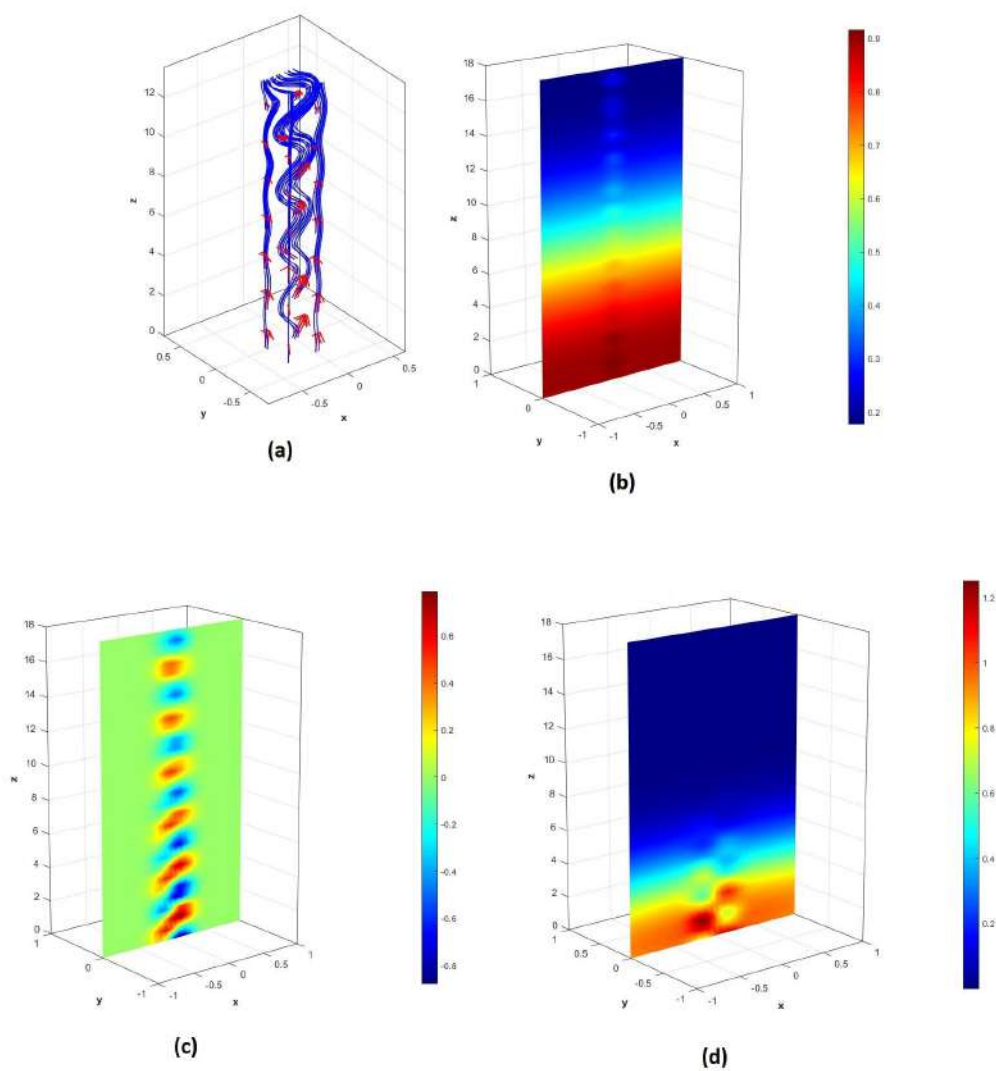


Figure 2.1: (a) Streamline, (b) velocity profile (c) electric field and (d) density slices at $t = 1fs$ for $n_0 = 10^{28}/m^3$, $\lambda = 10^{-8}m$, $T = 20 eV$

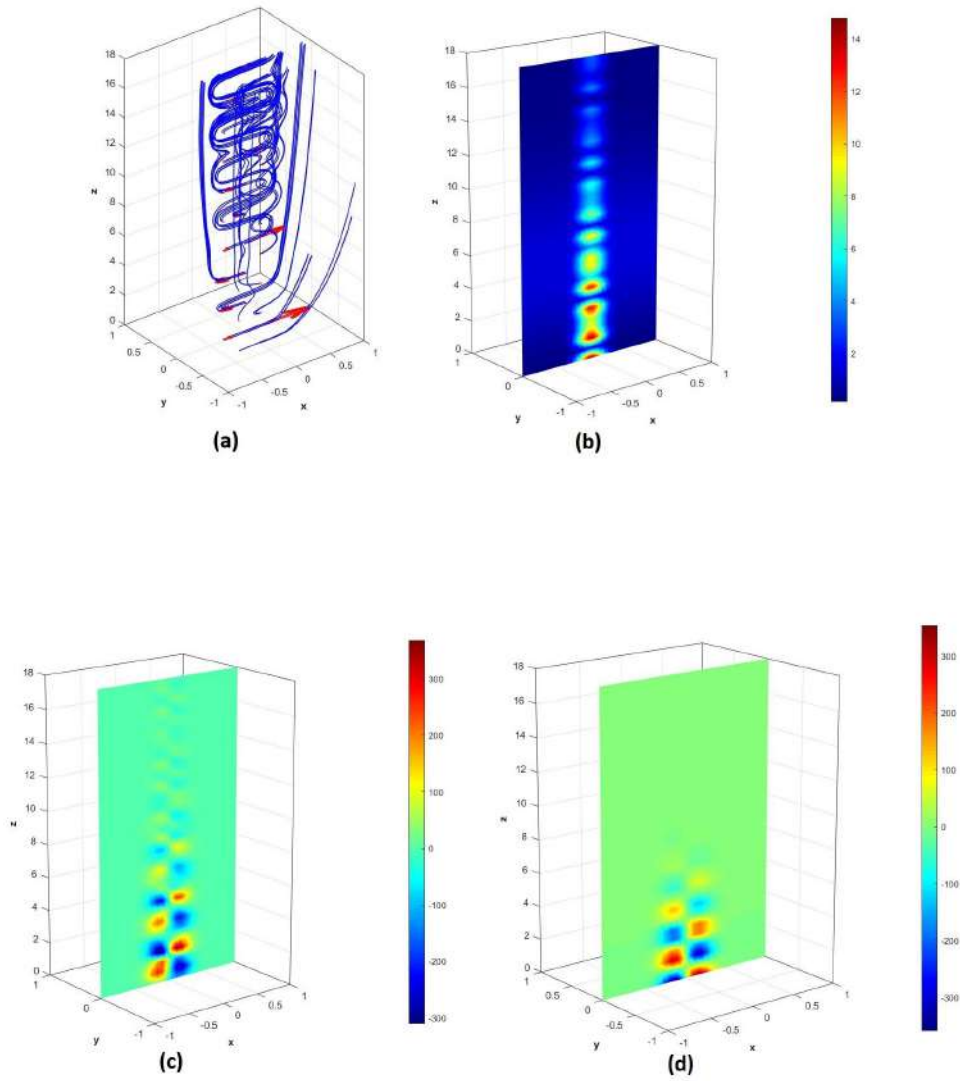


Figure 2.2: (a) Streamline, (b) velocity profile (c) electric field and (d) density slices at $t = 12fs$ for $n_0 = 10^{28}/m^3$, $\lambda = 10^{-8}m$, $T = 20 eV$

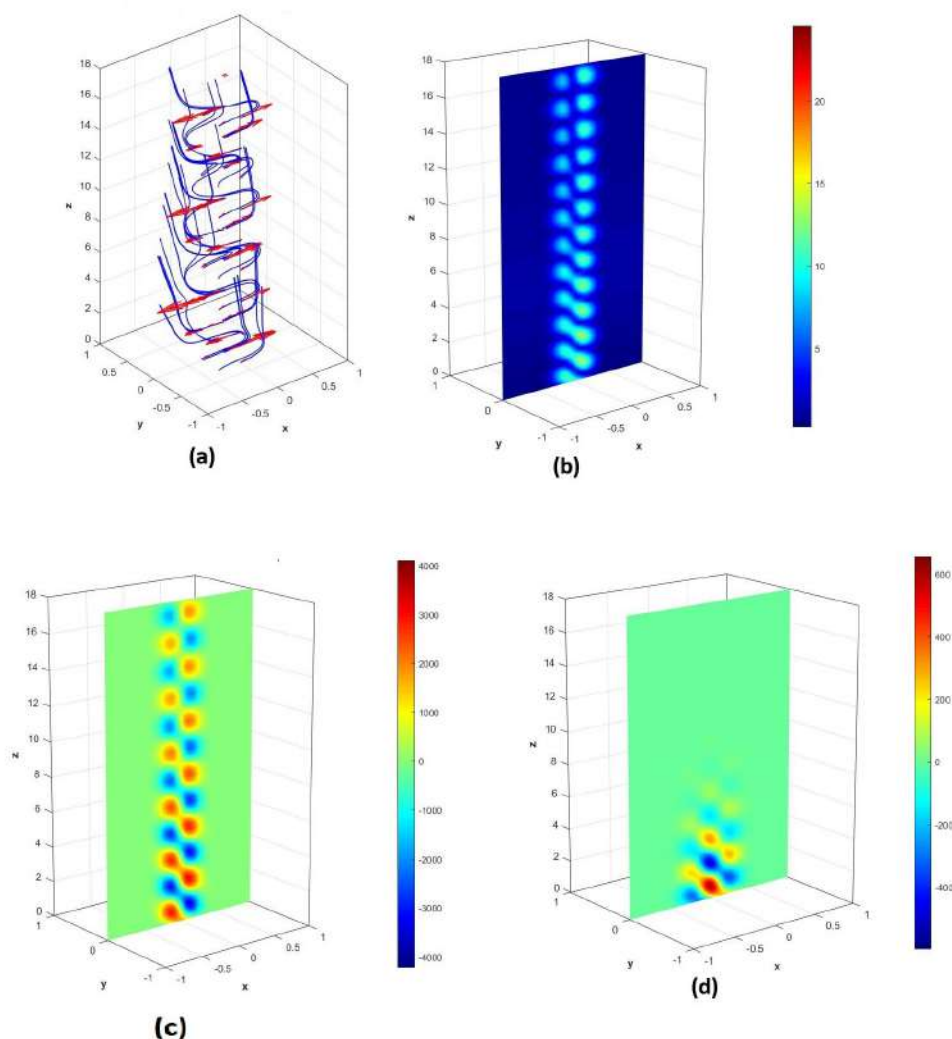


Figure 2.3: (a) Streamline, (b) velocity profile (c) electric field and (d) density slices at $t = 12 fs$ for $n_0 = 10^{28}/m^3$, $\lambda = 10^{-8}m$, $T = 30 eV$

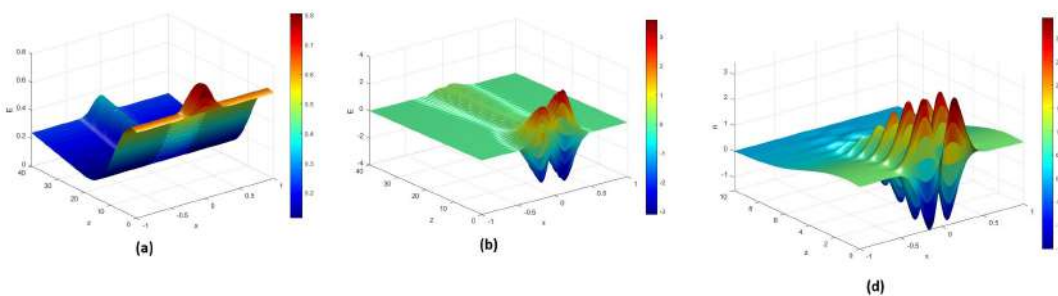


Figure 2.4: (a) Velocity (b) electric field and (c) density surface evolution on $x - z$ plane at $t = 8 fs$ for $n_0 = 10^{27}/m^3$, $\lambda = 10^{-8}m$, $T = 13 eV$

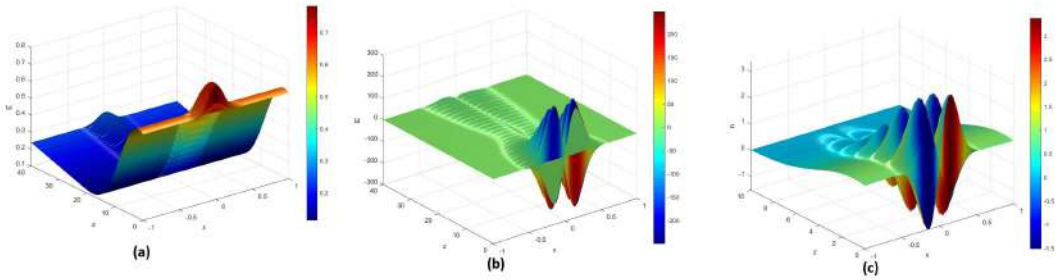


Figure 2.5: (a) Velocity (b) electric field and (c) density surface evolution on $x - z$ plane at $t = 8 fs$ for $n_0 = 10^{27}/m^3$, $\lambda = 10^{-10}m$, $T = 13 eV$

In figure (2.3) we see that after a certain level ($n_0 = 10^{28}/m^3$, $T = 30 eV$) the velocity profile bifurcates. The electric field also extends deep in the plasma and there is more oblique fluctuation in density. This is attributed to some kind of dispersion phenomena in which the velocity profile split up. Some kind of field particle resonant interaction might be occurring in the background. Such filamentations is reported in intense laser interacting with plasma [85, 86]. This can also produce instability producing zones of intense laser intensity. Such studies have been carried out by Young et al [87, 88], Schmitt [89] and Hercher [90].

In figures 2.1, 2.2 and 2.3 we find that the electric field, density and velocity profiles acquire certain modulation which cause to exits once the laser enters the plasma. The density profile takes the shape of humps and dips that corresponds to soliton or solitary structures. If given sufficient time to observe, such modulations will repeat and from the associated time scales we can claim that solitons with different temporalexent can be generate such a situation is often repeated by workers who study laser plasma interaction [91]. In a recent works by Song et al [91], it has been reported that optical solitons (bright) are found in optical fibre lsaers. They have gone a step formed and showed that breathers are generated and provided the nonlinear Schrodinger equation. Similar breathers solitons are also an outcome of our theoretical results (figure 2.4 & 2.5).

In this work figures 2.4 and 2.5 predicts envelop solitons formation. The electric field component shows initial modulations that originate and die out to reappear again with

diminished amplitude. Such a attention obvious as plasma is nonlinear media and the order of nonlinearity depends on the plasma density (via Debye shielding parameter). A number of experimental observations support our theoretical claim. Our Homotopy Assisted Symbolic Simulation (HASS) technique is newly developed by C. Das and S. Chandra is a step forwards this direction. Since it makes use of topological perturbations technique and to our knowledge no works has been done like this, we hope our method holds immense potential to predict possible plasma effects that would be helpful to design any future experiments. This can be also help full in potential studies on mode locking [92, 93, 94]. Solitons observed in optical domain is nano structures and graphene based system [95, 96, 97, 98] can be obtained theoretically by this technique (HASS). Energy exchange phenomena [99] is the crucial aspect here. Such an exchange occurs between electric field vectors and plasma particles and such an interactions becomes more meaningful when we go for higher laser and ultra dense plasmas. We store similar experiments works for future theoretical verification by our designed HASS technique.

2.5 Conclusion

To sum up, our symbolic simulation studies give a real picture of the physical problem and opens up the door to analytically solve physical problem by making use of symbolic computations. This technique far more superior than classical perturbations methods and also do not require super computing facilities to obtain the results. In short the novelty of such an advantageous analytical approach outnumber the pros of other techniques commonly used. The results obtained here suggests oblique instability in finite beam plasma system [100]. It can also provide a solution to transverse filamentations instability along a short fire ball bunch [101]. It also shows micro bunching of plasma particles along the direction of propagation of laser beam up to certain extent inside the plasma [102]. This kind of radiative compression triggers localized magnetic re-connection. Different PIC simulation studies suggest trapping of electrons amounting the thermal acceleration

[103]. Thus our HPT studies suggest that there is potential scope of symbolic simulation in studying complex phenomena in dense laser plasma interaction.

CHAPTER 3

NONLINEAR INTERACTION OF INTENSE LASER BEAM WITH DENSE PLASMA

3.1 Introduction

In recent year inertial confinement fusion [104, 105, 106] and plasma heating technologies [107, 108] are in the news due to the potential application in fusion technology. Often laser is fed into the system for such a purpose. When the intensity of laser beam exceeds $\approx 10^{22} \text{ W/m}^2$ the quiver velocity of the particles approaches the speed of light. Further when the density of plasma is very high such that the equation of the state takes into consideration the relativistic degeneracy factors [109, 65] the situation displays new happening and further more there can be additional effects like instability [110], harmonic production [111], vortices [112] etc. However, in laser plasma interactions the density is such that the consideration of relativistic degeneracy is not so meaningful. The pressure in such a system is thermal in nature. Therefore, in order to take into consideration such factors we frame our governing equations accordingly. We assume the plasma particles to form fluid species. Such streams display many wave phenomena and in most of these cases there are associated instabilities [113]. The instabilities are not always those which die out easily but can often grow into magnified proportion such that the whole system becomes unstable [114]. Plasma being a highly complex system shows different levels of nonlinearity [115, 116] such that these nonlinearities add up to give stationary structure as solitary entities that propagate through the plasma. Now there are also dispersive effects within the media that tries to straighter out the nonlinearities. However, at some point these two might balance each other, and a modulated wave envelope propagates in space and time. To start with the basic equations and thereby taking perturbative pathway is old technique. Such technique hold goods for small per-

turbations where approximation methods are justified, but these technique often lack the appropriateness and universality. Some authors [72, 117, 118, 119] have used multiple scale reductive perturbative techniques (RPT) that are limited to its applications and fails to address the problem properly. Washimi and Taniuti [120] used RPT to study plasma problem. Later Nishikawa et al [121], Ghosh et al [82], Chandra et al [67, 122], Shukla and others [123, 124] have treaded the same path to address the problem. But in the recent years He [83, 84] and others have made use of elements of topology and came up with the homotopy perturbation method (HPM) in which the nonlinear differential equations can be solve exactly (or approximated analytically) to obtain the final state after starting from initial considerations with proper boundary conditions. It is somehow related to mapping from the real space to an equivalent space where the convergence criteria is accounted for. A research group from Turkey [125] have used HPM to solve the Zakharov-Kuznetsov equation. Ma [126] have used of HPM for the Wu-Zhang equations in the fluid dynamics and come out with fascinating results. Moini [127] have used the same technique to solve the PDE. In this chapter we went a step further to make use of HPM to solve coupled PDE and obtained solution for different orders of the embedding (homotopy) parameter. The final results give very beautiful results and match with experimental outcomes [128]. The motivation behind such a work is to study the modulation phenomena and the stability criteria. The chapter is organized as below: in the next section we start with the basic dynamic equations governing the fluid motion of plasma particles. Within this section we make use of normalization schemes for simplification of the problem. In the third section we construct homotopy befitting the problem at hand and finally discuss the results to compare with works of other authors.

3.2 Basic formulation

We consider that at such high densities the pressure exerted by particles follow the thermal pressure given by

$$\mathbf{p}_e = \mathbf{n}_e k_B T \quad (3.1)$$

where k_B , T and \mathbf{n}_e are Boltzman constant, temperature and electron density.

Assuming the particles and laser profile follow the Gaussian pattern in transverse direction in space, the plasma is considered to be irradiated with intense laser beam given by [77]

$$\vec{\mathbf{E}} = \hat{x} E e^{i(kz - \omega t)} + c.c., \quad (3.2)$$

where E , k and ω are amplitude, wave number and frequency of the laser beam respectively. Now assuming the slow variation for laser beam amplitude ($|\frac{1}{\omega} \frac{\partial E}{\partial t}| \ll |E|$) and employing Faraday's law of Maxwell's equations the magnetic field is

$$\vec{\mathbf{B}} \equiv \hat{y} \frac{kc}{\omega} E e^{i(kz - \omega t)} + c.c., \quad (3.3)$$

where c is the velocity of light. The wave equation for the electric field of the laser beam that governs the propagation of laser beam is given by

$$\left(\nabla^2 - \frac{1}{c^2} \frac{\partial^2}{\partial t^2} \right) \vec{\mathbf{E}} = \frac{1}{\mu_0} \frac{\partial \vec{\mathbf{J}}}{\partial t}, \quad (3.4)$$

where $\vec{\mathbf{J}}$ is the plasma current density.

The electric field is assumed to be coupled with the initial perturbed laser as small perturbation due to beam plasma interaction $\vec{\mathbf{E}} = \vec{\mathbf{E}}_0 + \vec{\mathbf{E}}_1$, where E_0 and E_1 are correspond to initial value of the laser beam and unstable perturbation ($|E_0| \gg |E_1|$) respectively. The perturbed terms are incorporated in E_1 . As per RPT E_1 has different order terms of perturbation expressions, but here in HASS we some them up together and while employing it will expand series. Assuming the ions to be extremely heavy as compared to electrons providing the neutralizing background the fluid equations for

electrons are as follows [77, 129]

$$\frac{\partial \mathbf{n}_e}{\partial t} + \vec{\nabla} \cdot (\mathbf{n}_e \vec{\mathbf{V}}_e) = 0, \quad (3.5)$$

$$\left(\frac{\partial}{\partial t} + \vec{\mathbf{V}}_e \cdot \vec{\nabla} \right) \vec{\mathbf{V}}_e = -\frac{e}{m_e} \left(\vec{\mathbf{E}} + \frac{\vec{\mathbf{V}}_e}{c} \times \vec{\mathbf{B}} \right) - \frac{\vec{\nabla} \mathbf{P}_e}{m_e n_e}, \quad (3.6)$$

$$\left(\frac{\partial}{\partial t} + \vec{\mathbf{V}}_e \cdot \vec{\nabla} \right) \vec{\mathbf{E}} = \frac{n_e e \vec{\mathbf{V}}_e}{\epsilon_0} + \left[c \vec{\nabla} \times \vec{\mathbf{B}} - \vec{\mathbf{E}} (\vec{\nabla} \cdot \vec{\mathbf{V}}_e) - \vec{\nabla} \times (\vec{\mathbf{V}}_e \times \vec{\mathbf{E}}) + (\vec{\mathbf{E}} \cdot \vec{\nabla}) \vec{\mathbf{V}}_e \right] \quad (3.7)$$

Here, e & $\vec{\mathbf{V}}_e = (u_e, v_e, w_e)$ denotes charge and velocity of electron and we take thermal pressure which is given by Eqn. (3.1). The justification of ignoring ion motion is due to the fact that the electrons respond to the beam field easily and set into oscillations, whereas the ions being impartially heavy do not set into oscillation and can be justified to be forming a neutralizing background.

For simplicity of the problem we use the following normalization scheme $x \rightarrow x \frac{\omega_p}{v_{th}}$, $y \rightarrow y \frac{\omega_p}{v_{th}}$, $z \rightarrow z \frac{\omega_p}{v_{th}}$, $t \rightarrow \omega_p t$, $u_e \rightarrow \frac{u_e}{v_{th}}$, $v_e \rightarrow \frac{v_e}{v_{th}}$, $w_e \rightarrow \frac{w_e}{v_{th}}$, $E \rightarrow \frac{eE}{m_0 v_{th} \omega_p}$ and $n_e \rightarrow \frac{n_e}{n_0}$, where v_{th}, ω_p, m_e and n_0 are the thermal velocity, plasma frequency, mass of electron and initial density of plasma, and the dynamic equations in normalized scalar forms are given as

$$\frac{\partial n_e}{\partial t} + \frac{\partial(n_e u)}{\partial x} + \frac{\partial(n_e v_e)}{\partial y} + \frac{\partial(n_e w_e)}{\partial z} = 0 \quad (3.8)$$

$$\frac{\partial u_e}{\partial t} + u_e \frac{\partial u_e}{\partial x} + v_e \frac{\partial u_e}{\partial y} + w_e \frac{\partial u_e}{\partial z} = -E + \frac{k}{\omega} E w_e - \frac{1}{n_e} \frac{\partial n_e}{\partial x} \quad (3.9)$$

$$\frac{\partial v_e}{\partial t} + u_e \frac{\partial v_e}{\partial x} + v_e \frac{\partial v_e}{\partial y} + w_e \frac{\partial v_e}{\partial z} = -\frac{1}{n_e} \frac{\partial n_e}{\partial y} \quad (3.10)$$

$$\frac{\partial w_e}{\partial t} + u_e \frac{\partial w_e}{\partial x} + v_e \frac{\partial w_e}{\partial y} + w_e \frac{\partial w_e}{\partial z} = -\frac{k}{\omega} E u_e - \frac{1}{n_e} \frac{\partial n_e}{\partial z} \quad (3.11)$$

$$\frac{\partial E}{\partial t} + u_e \frac{\partial E}{\partial x} + v_e \frac{\partial E}{\partial y} + w_e \frac{\partial E}{\partial z} + n_e u_e = 0. \quad (3.12)$$

We have reduced Eqn.(3.7) into scalar form and simplified with additional considerations (i) ignoring magnetic fluctuations implying the balance between conduction current and displacement current. (ii) Further considering $\vec{\nabla} \times \vec{E} = 0$, i.e. assuming uniformity in electric field and restraining our work in studying the fluctuation in the z component, the simulation studies were carried out in the following section. The above set of coupled PDEs when solved properly will give the solution for the field quantities.

3.3 Symbolic simulation

In complex plasma physics where a lot of nonlinear phenomena exists, reductive perturbation technique or Fourier methods are employed for the analytical part. In such a case small scale perturbation are easily solvable with varied orders of approximations. Further, where numerical methods are employed, the problem suffers from other mathematical disadvantages. But for numerical simulation often a high end computing facility is required. With the advances of available software and the introduction of symbolic method in Matlab R2019 we could design a technique with our modest computer facility (8 GB RAM, 2.2 GHz processor) that incorporates the analytical functions and provides results in terms of such functions with the aid of computers. Introducing elements of topology we make use of homotopy perturbation method (HPM) to solve coupled PDE.

To brief the techniques- let us consider the following non linear differential equation

$$\mathcal{D}(\bar{\mathcal{U}}) - f(\bar{r}) = 0 \quad (3.13)$$

with boundary condition

$$\mathcal{B}(\bar{\mathcal{U}}, \frac{\partial \bar{\mathcal{U}}}{\partial n}) = 0, r \in \Gamma. \quad (3.14)$$

Here \mathcal{D} , \mathcal{B} , $f(r)$ and Γ are a general differential operator, a boundary operator, an analytical function (which is previously known) and the boundary of the domain Ω . The operator \mathcal{D} can be divided into linear (\mathcal{L}) and non linear part (\mathcal{N}) such that

$$\mathcal{L}(\bar{\mathcal{U}}) + \mathcal{N}(\bar{\mathcal{U}}) - f(\bar{r}) = 0 \quad (3.15)$$

By employing basic homotopy technique, we construct homotopy

$$\mathcal{H}(\bar{\mathcal{V}}, p) \equiv (1 - p) \left[\mathcal{L}(\bar{\mathcal{V}}) - \mathcal{L}(\bar{\mathcal{U}}_0) \right] + p \left[\mathcal{D}(\bar{\mathcal{V}}) - f(\bar{r}) \right] = 0, \quad p \in [0, 1]. \quad (3.16)$$

or equivalently

$$\mathcal{H}(\bar{\mathcal{V}}, p) \equiv \mathcal{L}(\bar{\mathcal{V}}) - \mathcal{L}(\bar{\mathcal{U}}_0) + p\mathcal{L}(\bar{\mathcal{U}}_0) + p \left[\mathcal{N}(\bar{\mathcal{V}}) - f(\bar{r}) \right] = 0 \quad (3.17)$$

where $\bar{\mathcal{U}}_0$ is initial assumption satisfying the boundary condition (3.14). As the homotopy parameter p changes from zero to unity the picture convolutes from $\bar{\mathcal{U}}_0(r)$ to $\bar{\mathcal{U}}(r)$ (exact or approximated analytic solution). In topology, this is called deformation and $\mathcal{L}(\bar{\mathcal{V}}) - \mathcal{L}(\bar{\mathcal{U}}_0)$, $\mathcal{D}(\bar{\mathcal{V}}) - f(\bar{r})$ are called homotopic. According to the HPM, we can first use the embedding parameter p as a small parameter, and assume that the solutions of

Eqn. (3.17) can be written as a power series in p :

$$\bar{\mathcal{V}} = p^0 \bar{\mathcal{V}}^{(0)} + p \bar{\mathcal{V}}^{(1)} + p^2 \bar{\mathcal{V}}^{(2)} + \dots \quad (3.18)$$

To obtain solution of Eqn. (3.17) we make use of Eqn. (3.18) and expand $\mathcal{D}(\bar{\mathcal{V}})$ by Taylor series in p and putting this expression in Eqn. (3.17). Then equating the coefficient of like powers of p , which are easily solvable (ref. Appendix chapter A). Setting $p = 1$, the results in the approximate solution of Eqn. (3.17) takes the form

$$\bar{\mathcal{U}} = \lim_{p \rightarrow 1} \bar{\mathcal{V}} = \bar{\mathcal{V}}^{(0)} + \bar{\mathcal{V}}^{(1)} + \bar{\mathcal{V}}^{(2)} + \dots \quad (3.19)$$

The convergence of the series (3.19) has been suggested by He [83, 84] requires :

1. The second derivative of $\mathcal{N}(\bar{\mathcal{V}})$ with respect to $\bar{\mathcal{V}}$ must be small because the parameter may be relatively large, i.e., $p \rightarrow 1$.
2. The norm of $\mathcal{L}^{-1} \frac{\partial \mathcal{N}}{\partial \bar{\mathcal{V}}}$ must be smaller than one so that the series converges.

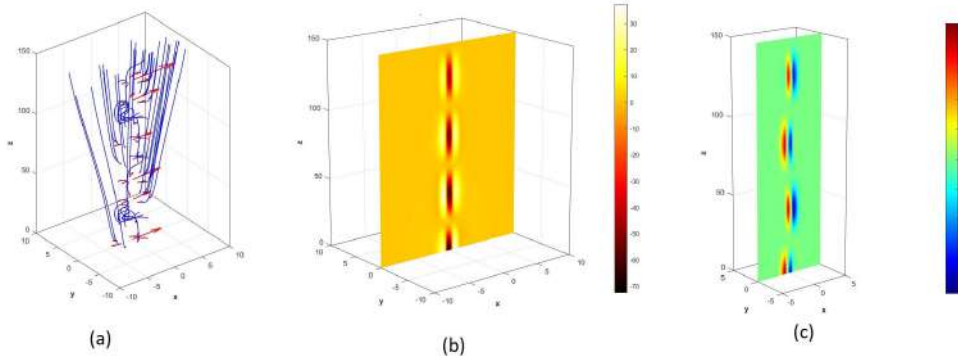


Figure 3.1: (a) Streamline and velocity profile (b) density slices and (c) electric field at $t = 45 fs$ for $n_0 = 10^{26}/m^3$, $\lambda = 10^{-7}m$, $T = 1 eV$

3.4 Result and discussion

In this section we will try to interpret the results based on the simulation results obtained by HASS method. In the figures mainly the velocity streamlines, the density volume

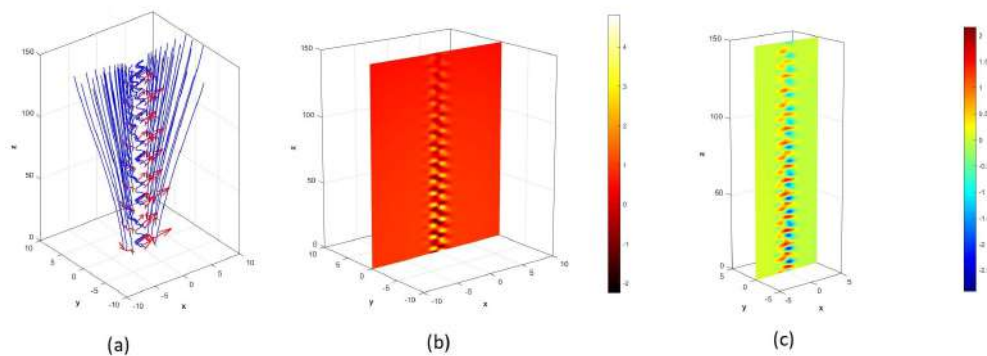


Figure 3.2: (a) Streamline and velocity profile (b) density slices and (c) electric field at $t = 50 fs$ for $n_0 = 10^{26}/m^3$, $\lambda = 10^{-8}m$, $T = 1 eV$

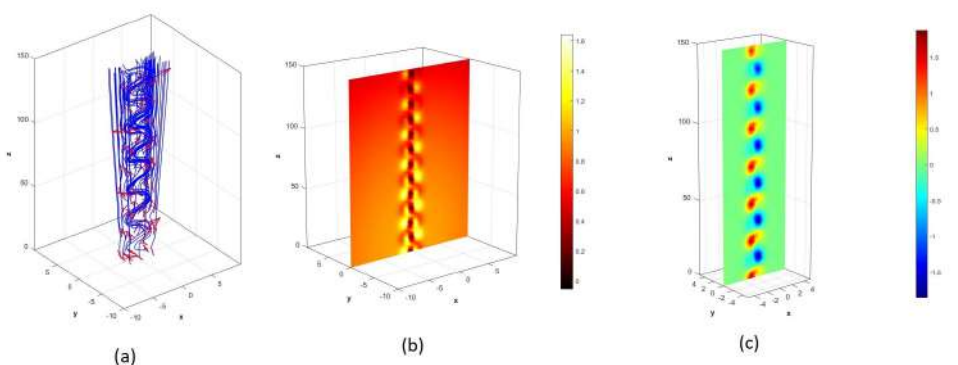


Figure 3.3: (a) Streamline and velocity profile (b) density slices and (c) electric field at $t = 90 fs$ for $n_0 = 10^{25}/m^3$, $\lambda = 10^{-7}m$, $T = 1.2 eV$

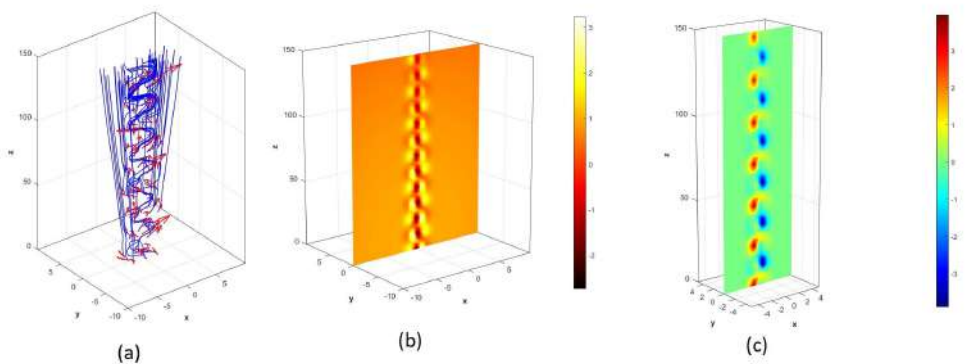


Figure 3.4: (a) Streamline and velocity profile (b) density slices and (c) electric field at $t = 120 fs$ for $n_0 = 10^{25}/m^3$, $\lambda = 10^{-7}m$, $T = 1.2 eV$

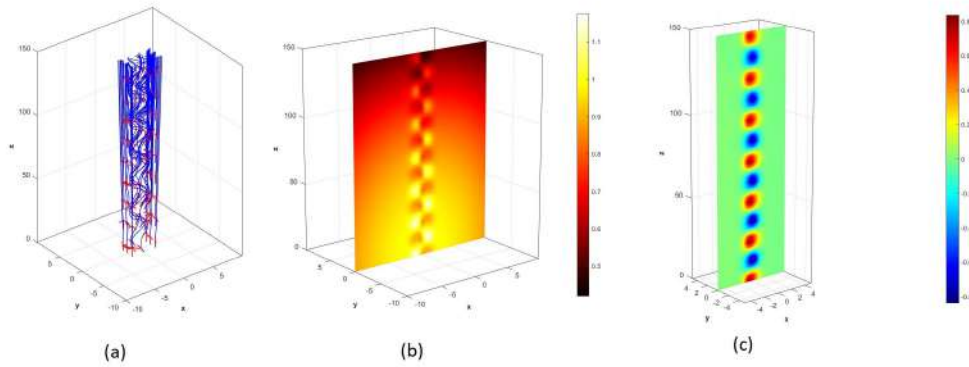


Figure 3.5: (a) Streamline and velocity profile (b) density slices and (c) electric field at $t = 50 fs$ for $n_0 = 10^{25}/m^3$, $\lambda = 10^{-7}m$, $T = 1.2 eV$

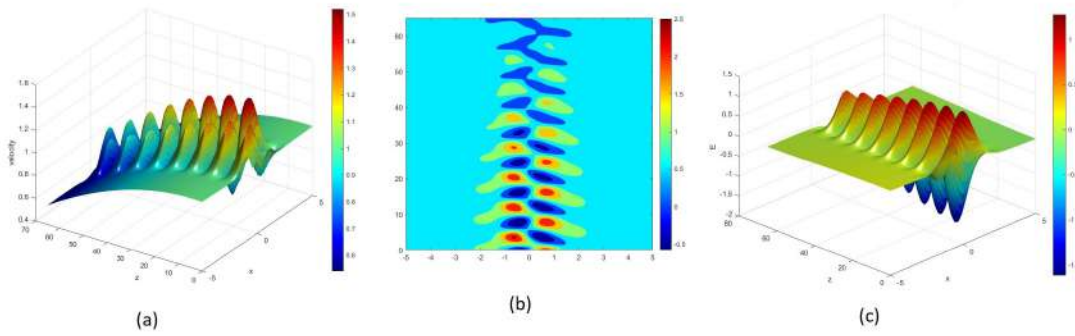


Figure 3.6: (a) velocity surface evolution (b) density contour (c) electric field surface evolution at $t = 400 fs$, $n_0 = 10^{24}/m^3$, $\lambda = 10^{-7}m$, $T = 1 eV$

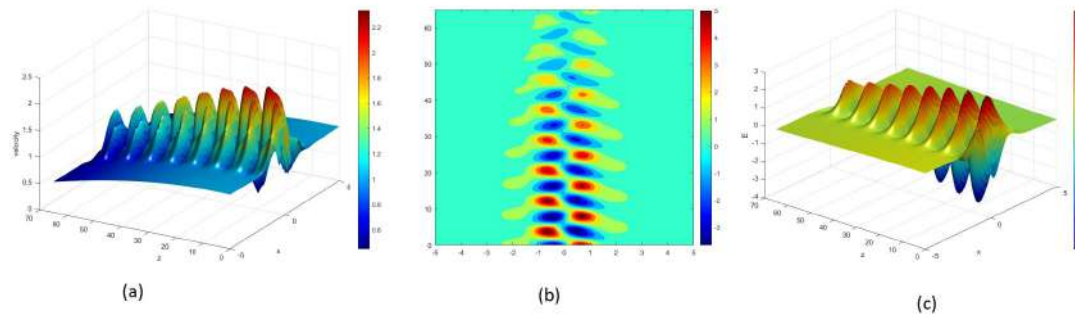


Figure 3.7: (a) velocity surface evolution (b) density contour (c) electric field surface evolution at $t = 520 fs$, $n_0 = 10^{24}/m^3$, $\lambda = 10^{-7}m$, $T = 1 eV$

slice and the electric field have been depicted. The results are observed at different instants and for different values of laser wavelength, plasma temperature and density.

Figure (3.1) shows that starting with an initial density of 10^{26} m^{-3} and plasma temperature of 1 eV with laser wavelength 10^{-7} m there appears a very small order response along the direction of laser propagation which may be said to be trapping of particles, majority particles diverge outward and this transverse widening is due to the initial response of the particles with the laser fields. The particles cannot respond fast to transport the input energy into the bulk of the plasma. The density volume slice (figure (3.1).(b)) support this claim as the transverse widening has not yet appeared. Likewise in figure (3.1.(c)), the electric field is not much modulated as we will find in the later figures. However, very soon, i.e. at 50 fs , [figure (3.2)] with same density and temperature, but with more energetic laser ($\lambda = 10^{-8} \text{ m}$) the initial modulation in velocity streamline become prominent. The particle density and the laser fields however shows more modulations and an enhanced widening. This is due to the reaction from the bulk of the plasma where energy localization appear and the transverse dispersion is reduced. The laser beam propagates more into the bulk but there are more frequent modulations as the frequency of the beam increases ten times.

Figure (3.3) shows the corresponding plots for lower density ($\approx 10^{25} \text{ m}^{-3}$) and slightly higher temperature $T = 1.2 \text{ eV}$. Here we find an appearance of spatial arrangement of density. Here the streamlines are less diverging implying the fact that at moderate plasma density and given enough time ($t = 90 \text{ fs}$) the bulk provides a transverse pressure so that the divergence is reduced. Given sufficient time (120 fs) in figure (3.4) the density volume slice have more prominent modulations. Accordingly the electric fields also acquire higher modulated values reflecting on the fact of particle localization in the bulk plasma. However we find an additional fact that there is an initial rarefaction in the density at the point where the laser is fed. Apparently it appears that the density at the input is reduced due to Coloumb repulsion that occurs when the particles interacts with the laser fields.

Figures (3.6) and (3.7) correspond to later instants of time $t = 400 \text{ fs}$ and $t = 520 \text{ fs}$. Other parameter like initial density is $10^{24}/\text{m}^3$, $\lambda = 10^{-7}\text{m}$ and $T = 1 \text{ eV}$. We find that the lateral broadening appears, though such a broadening lags with the propagating beam. The velocity of particles acquire a gradual decrease along the propagation direction (z-axis). Modulations however exists, but there is a gradual drop in the dc value. The profiles of the electric field confirm the fact that the momentum of particles influence the particle densities and thus alter the electric field of the laser beam inside the plasma.

We therefore observe that three factors determine the widening of laser beam and its propagation in the plasma, viz. the plasma density, the plasma temperature and the laser energy. All these parameters affect in a complex phenomena, mainly the energy of laser beam and the particle density. It is inferred that energy exchange and some kind of resonant interaction are play during the process.

3.5 Conclusion

To conclude we successfully introduce a symbolic simulation technique to study the amplitude modulation of electrostatic waves in dense plasma. The novelty of the work is in the technique and the correspondence of the results with earlier researchers [130, 131, 132, 133]. The employing of homotopy was suggested by He [83, 84] and apart from our previously published works [134], no work has been done to solve coupled PDE with HPM. We consider our work to be first of its kind where we have further gone a step ahead to make use of homotopy assisted symbolic simulation (HASS) technique and obtain the results. The best part of the work is the bypassing of mathematical approximation and overcoming the limitations of numerical methods. The results obtained here corresponds to some findings by other authors [135]. It matches with the temporal evolution reported by earlier work [135, 136, 137, 138, 139, 140].

CHAPTER 4
EFFECTS OF EXCHANGE SYMMETRY AND QUANTUM DIFFRACTION
ON AMPLITUDE MODULATED ELECTROSTATIC WAVES IN QUANTUM
MAGNETOPLASMA

4.1 Introduction

Degenerate matter is a highly dense state of matter are generally composed of Fermions which satisfy the Pauli Exclusion principle and therefore must occupy states of higher kinetic energy. Such degenerate matter in dense stellar environments include electrons, protons, neutrons etc. and is often found in astrophysical plasma and other dense stellar objects where gravitational pressure is so extreme that quantum mechanical effects are significantly important. In the evolutionary state of stars like white dwarfs and neutron stars, the thermal pressure is not enough to prevent gravitational collapse. Such degenerate matter is usually modeled as an ideal Fermi gas or some variants of it, an ensemble of non-interacting Fermions. In quantum physics, the exclusion criteria prevents identical Fermions to occupy same quantum states. From statistical physics we know that lowest energy levels are filled up even at non-zero temperature. Such a full degeneracy amounts to pressure which is non-zero even at absolute zero temperature [141, 142, 143]. Increasing the density (which can be done by either adding more particles or reducing the volume) forces the particles into higher quantum state . In such a situation, a compression force is required which gets manifested by a resisting pressure . This kind of degeneracy pressure does not depend upon temperature but on the density and keeps the dense stars in equilibrium. Degenerate matter with Fermions (whose energy become more than the rest mass energy) acquire velocities close to the speed of light, and are known to experience relativistic degeneracy. Noted scientists like A. Eddington [144, 145, 146, 147], Norton [148], Smith [149], R. Fowler [48, 49, 50, 51] , A. Milne

[150, 151, 152, 153], Koester [154], S. Chandrasekhar [155, 52, 156, 157, 53] have done celebrated works on the concept and properties of degenerate matter in stellar bodies. It was due to the pioneering works of S. Chandrasekhar on relativistic degenerate stellar mass and the associated pressure that we are able to study different phenomena in stellar entities.

With reference to the previous works on stellar evolution we know that if plasma is cooled and the pressure on it increased simultaneously, it will not be possible to compress the plasma any further due to the constraint in Pauli exclusion principle. In such a highly compressed state, there is no extra space for any particle and therefore its location is defined with certainty. Now if the uncertainty in location is almost absent, then according to Heisenberg uncertainty principle there will be extreme high level of momentum uncertainty. When such a situation is attained, the high uncertainty in momentum allows the particle to attain high kinetic energies, or in other words the particles move very fast. So it can be concluded that when a system is compressed to confine the particles into a very small volume, a tremendous force is required to control its momentum. Unlike a classical situation where the pressure is proportional to the temperature by the Clapeyron equation, here in the degenerate matter the pressure is given by Chandrasekhar [53] as:

$$P_e = (\pi m_e^4 c^5 / 3h^3) \left[R_e (2R_e^2 - 3) \sqrt{1 + R_e^2} + 3 \sinh^{-1} R_e \right] \quad (4.1)$$

where $R_e = p_{Fe}/m_e c = [3h^3 n_e / 8\pi m_e^3 c^3]$ Now under limiting conditions, for plasma with weak relativistic degeneracy the pressure is given by

$$P_e = \frac{1}{20} \left(\frac{3}{\pi} \right)^{\frac{2}{3}} \frac{h^2}{m_e} (n_e)^{\frac{5}{3}}, \quad (\text{for } R_e \rightarrow 0) \quad (4.2)$$

and for plasma with ultra relativistic degeneracy the pressure is given by

$$P_e = \frac{1}{8} \left(\frac{3}{\pi} \right)^{\frac{1}{3}} h c (n_e)^{\frac{4}{3}}, \quad (\text{for } R_e \rightarrow \infty) \quad (4.3)$$

In the former case (Eqn.(4.2)) the plasma can be treated as an ideal Fermi gas to a great extent; whereas in the latter situation (Eqn. (4.3)) (where the density is very high) the particles are forced into quantum states with relativistic energies and the pressure goes accordingly. Although every dense matter experiences both thermal and relativistic pressure, it has been noted that in commonly encountered gases thermal pressure dominates over the relativistic degeneracy pressure, and the latter may be ignored. However, degenerate matter though have thermal pressure at such high densities, the relativistic degeneracy pressure dominates primarily. In an ordinary Fermi gas, electrons occupy the majority of energy levels and electron degeneracy is observed. In the core of stars, once hydrogen forming stops, the mass is due to the positively charged carbon and helium nuclei, floating in a sea of electrons. Such matter do not obey ordinary gas laws. White dwarfs are not luminous because they produce energy, rather they radiate off the huge energy stored in them. When such matter is very closely packed, the particles position themselves right up against its neighbor and the degenerate gas behave similar to a solid in such cases. Therefore, the kinetic energies are quite high and the rate of collision is quite low. Under such situation the degenerate matter (here electrons) can travel great distances at velocities approaching the speed of light. Unlike common matter where temperature becomes an external manifestation of the kinetic energy, in a relativistically degenerate matter , the pressure only depend on the speed of degenerate particles. Interestingly adding heat does not increase the statistical speed of electrons, because they are stuck in fully occupied quantum energy levels. However, the masses of an object with electron degeneracy has an upper limit known as the Chandrasekhar limit [53], beyond which the degeneracy pressure can not prevent the collapse of the object. Celestial bodies below this limit (1.44 solar mass) are the white dwarfs and above which it is either a neutron star (supported partially by neutron degeneracy pressure) or a black hole.

In physics and particularly plasma physics, the exchange interaction or exchange correlation is a quantum mechanical effect that occurs between identical particles (here

Fermions). Though such an interaction term may be a part of the equation of motion or force, it is not a force in real sense as it lacks a force carrier. However, such effect is due to the exchange symmetry of wave function of identical particles. Both Fermions and Bosons experience such exchange interaction. In case of particles obeying the Fermi-Dirac statistics such interactions is sometimes called Pauli repulsion, due to the associated exclusion principle. Now the effect of this exchange interaction is manifold. When the wave function of quantum particles overlap, due to this exchange interaction the expectation value of distance may increase (for Fermions) or decrease (for Bosons). It is also responsible for ferromagnetism. However there is no classical analogue to this phenomenon. In case of plasma which contain Fermionic particles the exchange interaction may be electron-electron repulsive interaction, electron-proton attractive interaction and proton-proton repulsive interaction. The exchange interaction is a direct consequence of the symmetry of the wave functions. Such exchange interaction are also observed in solid as well as in the presence of magnetic field. In these cases the spin of the particles are crucial in determining the effects. In magnetized plasma's therefore the exchange interactions are more important. The coulomb exchange interaction is a function of the dielectric constant, density and effective mass of the plasma particles. As discussed previously space plasma (especially those in the case of neutron star, white dwarfs and other celestial objects) have very high density and the temperature is very low (ultra cold). In such a domain quantum effects come into play. There are intense magnetic field in and around these astrophysical objects. Therefore the plasma particles (Fermions majority) experience exchange interaction. The high density therefore causes a number of quantum phenomena, viz. relativistic degeneracy, exchange interaction as well as the quantum diffraction effect (through the Bohm potential term).

In space plasma, large number of wave phenomena of various origin has been observed. Some of them are the electron-acoustic (EA) waves, ion-acoustic (IA) waves, dust-acoustic (DA) waves which are lowfrequency waves whereas there are electron plasma waves, Langmuir wave, shocks, as well as in instabilities and vortices therein.

Various space plasma phenomenon which are constantly reported by numerous space agencies and observatories therefore require a solid theoretical explanation. Studies in space plasma nowadays have incorporated the quantum domain and the latest model is the quantum hydrodynamic (QHD) model developed by Haas [59, 60], Manfredi [57, 58], Shukla [54, 55, 56] and others [122, 134]. Researchers have included correction terms will proper justification in the dynamic equations. The pressure in the momentum equation include quantum terms as well as classical ones. A. Pavel [158] have included the exchange interaction term in the quantum hydrodynamic model. Initial researchers like Kuznetsov [159] Kuz'menkov [160], Fedoseev [161, 162], Kuz'menkov [160], Faddeev [163], Sulem et al. [164] and others have developed many particle quantum hydrodynamic (MPQHD) model to analyze different phenomena. In the nonlinear paradigm one of the interesting description is the envelop soliton [a nonlinearly modulated envelope wave packet]. Apart from the extended quasiperiodic solutions, the (integrable) nonlinear Schrodinger equation (NLSE) provides stationary profile envelop solitons which are localized structure bearing the from of an envelop excitation that is localize in space. It confines within itself modulated localized electrostatic carrier wave oscillations [164, 165]. Localized envelope solitary structure has been observed by space missions and observatories. Such structures may be either a bright type in which a pulse shaped, slowly oscillatory localised structure forms with gradually vanishing boundaries originating from the modulation of the initial waves; or it may be a negative pulse shaped localized disturbance like a propagating electron potential dip etc. If the potential is zero it is a dark soliton, whereas if it is finite yet has low compare to the other density/potential values, it is called a gray type. A harmonic (linear) wave evolves into a nonlinear multi soliton structure by the modulation instability (MI). Initially the nonlinear effect is first manifested as simple superposition of linear harmonic oscillation of the carrying wave, and then over time evolves from the weak perturbations until finally the wave collapse. There may be intermittent structures in the from of solitary structure in the electrostatic waves where the non-linearity generated is balanced by any kind of

group dispersive mechanism. In plasmas modulational instability has been studied by numerous authors. In recent years Shukla [54, 55, 56], Misra [61, 62], Bhowmik [166], Goswami [118, 167], Sarkar [168, 169], Singh [72, 73], Paul [117], Ghosh [82, 64], Sahoo [63], Chandra [66, 67, 68, 65], and others have studied the MI and solitary waves in quantum plasmas.

A survey of the available literature shows that modulation instability in an electron acoustic wave including electron-exchange correction and relativistic degeneracy in a magnetized quantum plasma has not been investigated so far. The motivation of the present chapter is to study the amplitude modulation of the electron acoustic waves with quantum diffraction effect (Bohm potential), Relativistic degeneracy pressure, electron exchange interaction taking all at a time. This work is important because studies on quantum plasma often do not include the exchange symmetry term. Further when such plasma have wave phenomenon within it (as here we have electron acoustic wave) due to non-linear effect as well as dispersive phenomena, the wave amplitude undergoes modulation and forms envelope soliton. The instability of such modulation and the growth on different parameters are of prime interest both theoretically as well as experimentally. The amplitude modulated waves often give rise to certain instabilities that are signature of the plasma. A proper understanding of the phenomena may also help to predict any new happening that might be crucial to the space plasma investigations of this day and the future.

In this chapter we considered a two component electron-ion plasma with relativistic degeneracy pressure, exchange interaction potential, quantum diffraction effect as well as the presence of magnetic field. The chapter organized in the following manner: in §4.2 we come up with the set of basic dynamic equations. We use reductive perturbation technique (RPT) and Fourier method to derive the linear dispersion relation relating frequency (ω) with wave number (k) as well as the group velocity of the wave (C_g) that will contribute to the formation and provides envelop soliton. In §4.3 we derive the non-linear Schrodinger equation which provides the key to amplitude modulation and

the instability therein. We discuss the result and the dependence on various parameters through the graphs in §4.4. To support our explanation, we study the dynamical properties of the amplitude modulated electrostatic waves (§4.4). In §4.5, we carry out a study based on homotopy perturbation and analyse the evolution of the potential function with space and time. Finally, in §4.6 we conclude with a note on the outcome of our finding and a brief overview of our future investigations.

4.2 Basic Equations

We consider a two component dense quantum plasma containing inertia-less electrons and inertial ions. We consider the streaming motion of the plasma particles. Due to its low inertia the electron attain high velocity due to the relativistic degeneracy which can be close to the speed of light there by introducing a relativistic factor γ_e for the velocity and density in the electron equations. The basic sets of dynamic equations governing the particle motion are given as the set of continuity Eqns. (4.4),(4.5) for electrons and ions as well as momentum Eqns. (4.6),(4.7) for these two species.

$$\frac{\partial(\gamma_e \mathbf{n}_e)}{\partial t} + \vec{\nabla} \cdot (\gamma_e \mathbf{n}_e \vec{\mathbf{v}}_e) = 0 \quad (4.4)$$

$$\frac{\partial \mathbf{n}_i}{\partial t} + \vec{\nabla} \cdot (\mathbf{n}_i \vec{\mathbf{v}}_i) = 0 \quad (4.5)$$

$$\mathbf{0} = \frac{e}{m_e} \left[\vec{\nabla} \varphi + \frac{1}{c} \vec{\mathbf{v}}_e \times \vec{\mathbf{B}} \right] - \frac{\vec{\nabla} \mathbf{p}_e}{m_e \mathbf{n}_e} + \frac{1}{m_e} \vec{\nabla} U_{xce} + \frac{\hbar^2}{2m_e^2 \gamma_e} \vec{\nabla} \left(\frac{\nabla^2 \sqrt{\mathbf{n}_e}}{\sqrt{\mathbf{n}_e}} \right) \quad (4.6)$$

$$\frac{\partial \vec{\mathbf{v}}_i}{\partial t} + (\vec{\mathbf{v}}_i \cdot \vec{\nabla}) \vec{\mathbf{v}}_i = -\frac{e}{m_i} \vec{\nabla} \varphi - \frac{\vec{\nabla} \mathbf{p}_i}{m_i \mathbf{n}_i} \quad (4.7)$$

$$\nabla^2 \varphi = \frac{e}{\epsilon_0} (\mathbf{n}_e - \mathbf{n}_i) \quad (4.8)$$

where $\varphi, n_j, \vec{v}_j, m_j, p_j, c, U_{xce}$ are the electrostatic potential, number density, velocity, mass, pressure, velocity of light in vacuum and interaction exchange potential for the j th species namely $j = i$ (ion), e (electron). The exchange correlation potential for electrons is given by [170]

$$U_{xce} = -0.985 \frac{e^2}{\epsilon_L} n_e^{\frac{1}{3}} \left[1 + \frac{0.034}{n_e^{\frac{1}{3}} \alpha_B^*} \ln \left(1 + 18.37 n_e^{\frac{1}{3}} \alpha_B^* \right) \right] \quad (4.9)$$

where ϵ_L is the effective dielectric constant, n_{0e} is the equilibrium densities of the electron species and $\alpha_B^* = \frac{\epsilon_L \hbar^2}{m_e^* e^2}$ is the Bohr radius.

For simplicity Eqn. (4.9) we can be written as

$$U_{xce} = -1.6 \frac{e^2}{\epsilon_L} n_e^{\frac{1}{3}} + 5.65 \frac{\hbar^2}{m_e} n_e^{\frac{2}{3}} \quad (4.10)$$

since $1.837 n_e^{\frac{1}{3}} \alpha_B^* \ll 1$.

Here we taking ultra relativistic degeneracy pressure for electron and fermi pressure for ion are given by

$$p_e = \frac{1}{8} \left(\frac{3}{\pi} \right)^{\frac{1}{3}} \hbar c n_e^{\frac{4}{3}} \quad (4.11)$$

$$p_i = \frac{E_{Fi}}{3n_{i0}} n_i^3 \quad (4.12)$$

We now normalize the quantities by $x \rightarrow \frac{\omega_{pi}}{C_s} x, t \rightarrow \omega_{pi} t, \varphi \rightarrow \frac{e\varphi}{E_{Fi}}, n_j \rightarrow \frac{n_j}{n_{i0}}, v_j \rightarrow \frac{v_j}{C_s}$, here subscript '0' denotes at equilibrium state for the j th species. For simplicity we reduce our three dimensional equation into an one-dimensional problem and the set of scalar fluid equations are

$$\frac{\partial (\gamma_e n_e)}{\partial t} + \frac{\partial (\gamma_e n_e v_e)}{\partial x} = 0 \quad (4.13)$$

$$\frac{\partial n_i}{\partial t} + \frac{\partial (n_i v_i)}{\partial x} = 0 \quad (4.14)$$

$$0 = \frac{\partial \varphi}{\partial x} + \frac{v_{e\perp}}{\rho_s} - \lambda_1 n_e^{-\frac{2}{3}} \frac{\partial n_e}{\partial x} + \lambda_2 n_e^{-\frac{1}{3}} \frac{\partial n_e}{\partial x} + \frac{H^2}{2\gamma_e} \frac{\partial}{\partial x} \left(\frac{1}{\sqrt{n_e}} \frac{\partial^2 \sqrt{n_e}}{\partial x^2} \right) \quad (4.15)$$

$$\frac{\partial v_i}{\partial t} + v_i \frac{\partial v_i}{\partial x} = -\frac{\partial \varphi}{\partial x} - n_i \frac{\partial n_i}{\partial x} \quad (4.16)$$

and

$$\frac{\partial^2 \varphi}{\partial x^2} = (n_e - n_i). \quad (4.17)$$

where $E_{Fi} = \frac{\hbar^2}{2m_i} (3\pi^2 n_0)^{\frac{2}{3}}$ is the ion Fermi energy, $v_{e\perp}$ is velocity of the electron along y-axis, $\omega_{pi} = \sqrt{\frac{e^2 Z^2 n_0}{m_i \epsilon_0}}$, (Z atomic number) is the ion plasma frequency, $C_s = \sqrt{\frac{E_{Fi}}{m_i}}$ is the quantum ion acoustic speed, $\omega_{pe} = \sqrt{\frac{e^2 n_0}{m_e \epsilon_0}}$ is the electron plasma frequency, $\omega_{ci} = \frac{eB_0}{m_i c}$, $H = \frac{\hbar \omega_{pi}}{C_s \sqrt{m_e E_{Fi}}}$, $\rho_s = \frac{c E_{Fi} \omega_{pi}}{e B_0 C_s}$, $A_e = \frac{1}{8 E_{Fi}} \left(\frac{3}{\pi}\right)^{\frac{1}{3}} \hbar c$, $\lambda_1 = \frac{4}{3} A_e + \frac{1.6 e^2 n_0^{\frac{1}{3}}}{3 \epsilon_L E_{Fi}}$ and $\lambda_2 = \frac{3.77 \hbar^2 n_0^{\frac{2}{3}}}{m_e E_{Fi}}$. Here density of plasma $\approx 10^{28} - 10^{32}$ per m^3 , temperature T few Kelvin and H denotes quantum diffraction parameter which is the ratio of energy associated with single plasmon to the ion Fermi energy. The magnetic fields help in constraining the motion in the direction of the field and therefore help us to study the fluctuations along and perpendicular to the field.

4.3 Linear and nonlinear analysis

Derivation of the Linear Dispersion relation::

Let us consider that both the electrons and ions respond to the varying part of the field quantities. Starting with a linear approximation for the electronic interactions, the ions participate and it tries to restore the disturbances created. The field quantities $n_e, n_i, v_e, v_{e\perp}, v_i$ & φ constitute the five components $U_i^{(n)}(\xi, \tau)$ of a dynamical state

vector U .

$$U_l = U_l^{(0)} + \sum_{n=1}^{\infty} \epsilon^n \sum_{l=-\infty}^{\infty} U_l^{(n)}(\xi, \tau) \exp[il(kx - \omega t)] \quad (4.18)$$

here k is wave number and ω is frequency and ϵ is a small parameter, with subjected to the reality condition $U_{-l}^{(n)} = U_l^{(n)*}$ (here * denote complex conjugate), where

$$U_l^{(0)} = \begin{pmatrix} 1 \\ 1 \\ u_0 \\ 0 \\ 0 \end{pmatrix} \quad (4.19)$$

We expand U near equilibrium state as

$$\begin{aligned} n_e &= 1 + \sum_{n=1}^{\infty} \epsilon^n \sum_{l=-\infty}^{\infty} n_{e,l}^{(n)}(\xi, \tau) \exp[il(kx - \omega t)], \\ n_i &= 1 + \sum_{n=1}^{\infty} \epsilon^n \sum_{l=-\infty}^{\infty} n_{i,l}^{(n)}(\xi, \tau) \exp[il(kx - \omega t)], \\ v_e &= u_0 + \sum_{n=1}^{\infty} \epsilon^n \sum_{l=-\infty}^{\infty} v_{e,l}^{(n)}(\xi, \tau) \exp[il(kx - \omega t)], \\ v_{e\perp} &= \sum_{n=1}^{\infty} \epsilon^n \sum_{l=-\infty}^{\infty} v_{e\perp,l}^{(n)}(\xi, \tau) \exp[il(kx - \omega t)], \\ v_i &= \sum_{n=1}^{\infty} \epsilon^n \sum_{l=-\infty}^{\infty} v_{i,l}^{(n)}(\xi, \tau) \exp[il(kx - \omega t)], \\ \varphi &= \sum_{n=1}^{\infty} \epsilon^n \sum_{l=-\infty}^{\infty} \varphi_l^{(n)}(\xi, \tau) \exp[il(kx - \omega t)]. \end{aligned} \quad (4.20)$$

Such an method involving about the different harmonics is known as the Fourier technique. We assume that $u_l^{(0)}$ and $u_l^{(n)}$ are slowly varying with time (t) and position (x), i.e. they are function of a set of new stretched variable ξ and τ given by $\xi = \epsilon(x - C_g t)$ and $\tau = \epsilon^2 t$.

Here the smallness parameter ϵ helps us to identify the various harmonic and ordered terms in the perturbation analysis, and C_g is the normalized group velocity.

Applying this above expansion (4.20) to the Eqns. (4.13)-(4.17) and equating both sides the coefficients of ordered harmonic i.e. $\exp[i(kx - \omega t)]$, $\exp[2i(kx - \omega t)]$ and the terms independent of $(kx - \omega t)$ (i.e. zeroth harmonic) and neglecting 2nd & higher order perturbation of perpendicular velocity of electron, we identify each groups of equations as set-I, set-II, and set-III respectively. To solve this sets of equations(I, II, III) we introduce the following perturbation for field variables .

$$\psi = \psi^{(1)} + \epsilon\psi^{(1)} + \epsilon^2\psi^{(2)} + \dots \quad (4.21)$$

Solving the lowest order ϵ (i.e. n=1) equations for $l = 1$, we get from equations (4.13) - (4.17) as

$$n_{e,1}^{(1)} = A_{11}\varphi_1^{(1)}, \quad n_{i,1}^{(1)} = B_{11}\varphi_1^{(1)}, \quad v_{e,1}^{(1)} = C_{11}\varphi_1^{(1)}, \quad v_{i,1}^{(1)} = D_{11}\varphi_1^{(1)}, \quad (4.22)$$

where he coefficients $A_{11}, B_{11}, C_{11}, D_{11}$ are given in Appendix §B.1. Solving this above relations for the five field quantities we get the linear dispersion relation as

$$\omega^2 = \frac{3k^2 + k^2(1 + k^2) \left(\lambda_1 - 2\lambda_2 + \frac{H^2 k^2}{4\gamma_3} \right)}{3 + k^2 \left(\lambda_1 - 2\lambda_2 + \frac{H^2 k^2}{4\gamma_3} \right)} \quad (4.23)$$

where $\gamma_1 = \frac{u_0}{2c^2}$, $\gamma_2 = 1 - \frac{u_0^2}{2c^2}$, $\gamma_3 = 1 + \frac{3u_0^2}{2c^2}$, using approximate expansion.

It describes the quantum mechanical counter part of the classical electron plasma wave dispersion relations with correlation terms arising from relativistic degeneracy, electron exchange interaction and quantum diffraction parameter. The value of H is quite important as it distinguishes a quantum phenomena from it classical counterpart (for $H > 1$, it is quantum and $H < 1$ it is semi classical regime). Eqn. (4.23) boils down to the linear dispersion relation is the classical case with slight modifications. In the regime with

higher wavelength values, i.e. lower wavenumber (k), the higher order terms in k may be neglected. Further in classical plasma there are no exchange correlation effects and quantum diffraction terms. So with reference to Eqn. (4.23) we put $\lambda_1 = \lambda_2 = H = 0$ and ignoring higher terms in k we get $\omega^2 = k^2$ which has the usual sound speed form. So we can easily comment the correspondence between quantum and classical picture.

Derivation of Nonlinear Schrodinger equation::

Going to the next higher order terms we obtain the group velocity term as

$$C_g = \frac{d\omega}{dk} \quad (4.24)$$

The first harmonic quantities in the second order perturbation relations i.e. for $n = 2, l = 1$ (given Appendix §B.3), we can write the field quantities in terms of $\frac{\partial \varphi_1^{(1)}}{\partial \xi}$ as

$$\begin{aligned} n_{e,1}^{(2)} &= iA_{21} \frac{\partial \varphi_1^{(1)}}{\partial \xi}, & n_{i,1}^{(2)} &= iB_{21} \frac{\partial \varphi_1^{(1)}}{\partial \xi}, \\ v_{e,1}^{(2)} &= iC_{21} \frac{\partial \varphi_1^{(1)}}{\partial \xi}, & v_{i,1}^{(2)} &= iD_{21} \frac{\partial \varphi_1^{(1)}}{\partial \xi}, \\ \varphi_1^{(2)} &= iE_{21} \frac{\partial \varphi_1^{(1)}}{\partial \xi}, \end{aligned} \quad (4.25)$$

The coefficients A_{21}'' , B_{21}'' , C_{21}'' & D_{21}'' are given in Appendix §B.4. From here we get the expression for group velocity as

$$\begin{aligned} C_g &= \frac{\omega}{k} + \frac{2(\omega - k)}{k^2} \left((\omega + k) \right. \\ &\quad \left. - \frac{\omega}{k} \cdot \frac{12\gamma_3(\omega^2 - k^2) + (k^4 + k^2 - \omega^2 k^2)(\gamma_3(-6 + 2\lambda_1 - 4\lambda_2) + 9H^2 k^2)}{\gamma_3(4\lambda_1 - 8\lambda_2) + 3H^2 k^2} \right) \end{aligned} \quad (4.26)$$

which is in the extended form.

Further collecting coefficients for $n=2$, and $l=2$, we get the second order terms in second

order harmonics as

$$\begin{aligned} n_{e,2}^{(2)} &= A_{22} \left(\varphi_1^{(1)} \right)^2, \quad n_{i,2}^{(2)} = B_{22} \left(\varphi_1^{(1)} \right)^2, \\ v_{e,2}^{(2)} &= C_{22} \left(\varphi_1^{(1)} \right)^2, \quad v_{i,2}^{(2)} = D_{22} \left(\varphi_1^{(1)} \right)^2, \\ \varphi_2^{(2)} &= E_{22} \left(\varphi_1^{(1)} \right)^2. \end{aligned} \quad (4.27)$$

where A_{22} , B_{22} , C_{22} & D_{22} are given in Appendix §B.6. It is found that from the field quantities from second order zeroth harmonic we can not determine the field quantities completely, we need to go 3rd order ($n = 3$) zeroth harmonic ($l = 0$), by doing so that we obtained

$$\begin{aligned} n_{e,0}^{(2)} &= A_{20} \left| \varphi_1^{(1)} \right|^2, \quad n_{i,0}^{(2)} = B_{20} \left| \varphi_1^{(1)} \right|^2, \\ v_{e,0}^{(2)} &= C_{20} \left| \varphi_1^{(1)} \right|^2, \\ v_{i,0}^{(2)} &= D_{20} \left| \varphi_1^{(1)} \right|^2, \quad \text{and} \quad \varphi_0^{(2)} = E_{20} \left| \varphi_1^{(1)} \right|^2 \end{aligned} \quad (4.28)$$

where A_{20} , B_{20} , C_{20} , D_{20} & E_{20} are given in Appendix §B.8.

Equating the coefficient of ϵ on all terms obtained for 3rd order ($n=3$) for first harmonic ($l=1$) and imposing compatibility condition we obtained the desire non-linear Schrodinger equation as

$$i \frac{\partial \varphi}{\partial \tau} + P \frac{\partial^2 \varphi}{\partial \xi^2} + Q \left| \varphi \right|^2 \varphi = 0 \quad (4.29)$$

Here $\varphi_1^{(1)} = \varphi$ and the group dispersion coefficient (P) and nonlinear coefficient (Q) are given by $P = \frac{q_1}{r}$ and $Q = \frac{q_2}{r}$, where

$$\begin{aligned} q_1 &= \frac{(W + 1)}{(k^2 - \omega^2)} (D_{21}(\omega - kC_g) + B_{21}(k - \omega C_g) + kE_{21}) \\ &+ 2kW E_{21} - \frac{2(k\gamma_3 + W)}{k(4\lambda_1\gamma_3 - 8\lambda_2\gamma_3 + 3H^2k^2)} ((2\lambda_1 - 4\lambda_2 + 9H^2k^2)A_{21} - H^2k^2A_{11} - 6\gamma_3E_{21}), \end{aligned}$$

$$q_2 = \frac{k(W-1)}{(k^2-\omega^2)} (kD_{22}D_{11} + kD_{20}D_{11} + \omega B_{11}D_{20} + 2\omega B_{11}D_{22} + \omega B_{20}D_{11}) + W(E_{20} + E_{22}),$$

$$r = \frac{(W+1)(kD_{11} + \omega B_{11})}{\omega^2 - k^2},$$

$$W = \frac{12\gamma_3(\omega^2 - k^2) - k(4\lambda_1\gamma_3 - 8\lambda_2\gamma_3 + 3H^2k^2)}{k(4\lambda_1\gamma_3 - 8\lambda_2\gamma_3 + 3H^2k^2)(1 - k^2(\omega^2 - k^2)) + 12\gamma_3(\omega^2 - k^2)}. \quad (4.30)$$

We can obtain the solution of NLSE (4.29) in form as given below [169]

$$\phi = \sqrt{\left(\frac{\beta}{P} + \alpha^2\right) \frac{P}{Q}} \cdot \operatorname{sech} \left[\left\{ \sqrt{\frac{\beta}{P} + \alpha^2} \right\} (\xi - 2\alpha P\tau) \right] \exp\{i(\alpha\xi + \beta\tau)\} \quad (4.31)$$

where α and β are real number.

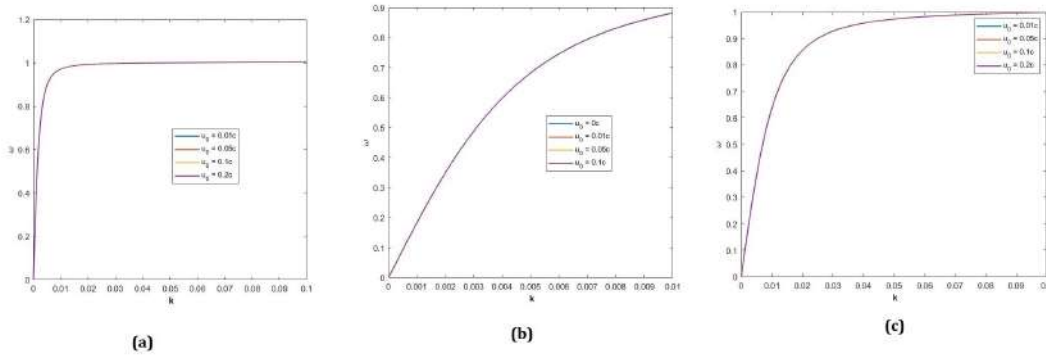


Figure 4.1: Linear dispersion characteristics (ω vs k) plot for different values of u_0 with $B_0 = 100T$ (a) $n_0 = 10^{28}/m^3$ (b) $n_0 = 10^{30}/m^3$ and (c) $n_0 = 10^{32}/m^3$

4.4 Result and discussion

Numerical plots of analytical results::

In this section we analyze graphically the linear dispersion relation and the nonlinear Schrodinger equation with different numerical values of the plasma parameters. Depending upon the normalization criteria our reduced quantities have specific range of values and accordingly our numerical plots are obtained. In figure 4.1, we plot the linear dispersion graphs for different density of plasma particles. We observe that as the

Chapter 4. Effects of exchange symmetry and quantum diffraction on amplitude modulated electrostatic waves in quantum magnetoplasma

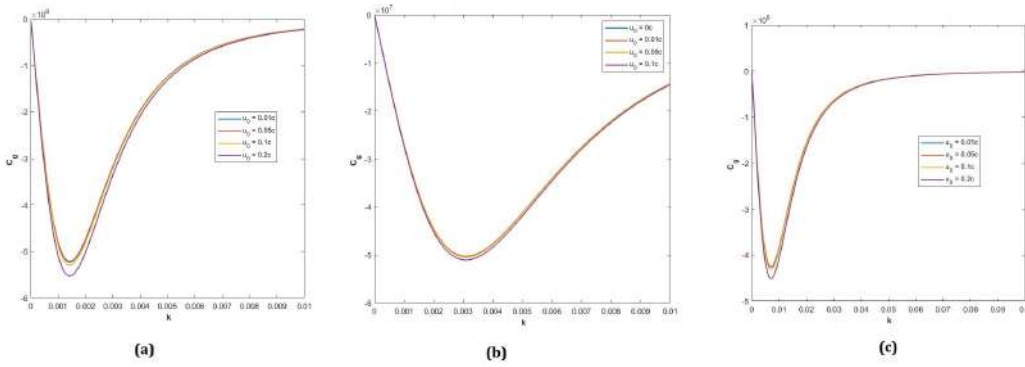


Figure 4.2: Group velocity (C_g) vs k plot for different values of u_0 with $B_0 = 100T$ (a) $n_0 = 10^{28}/m^3$ (b) $n_0 = 10^{30}/m^3$ and (c) $n_0 = 10^{32}/m^3$

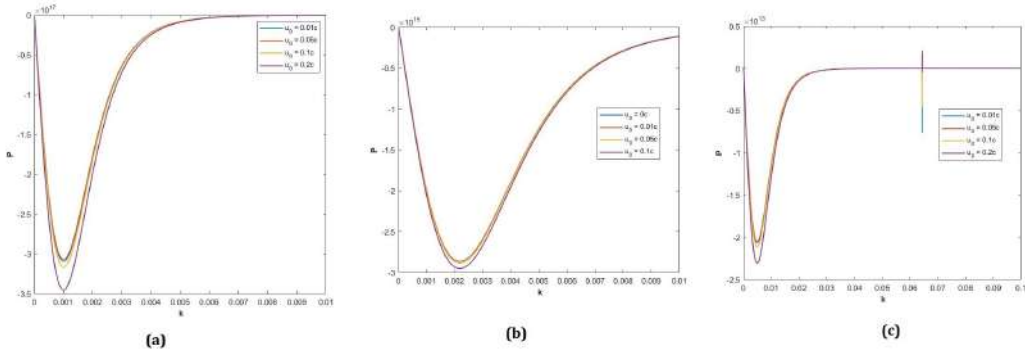


Figure 4.3: Dispersive coefficient (P) vs k plot for different values of u_0 with $B_0 = 100T$ (a) $n_0 = 10^{28}/m^3$ (b) $n_0 = 10^{30}/m^3$ and (c) $n_0 = 10^{32}/m^3$

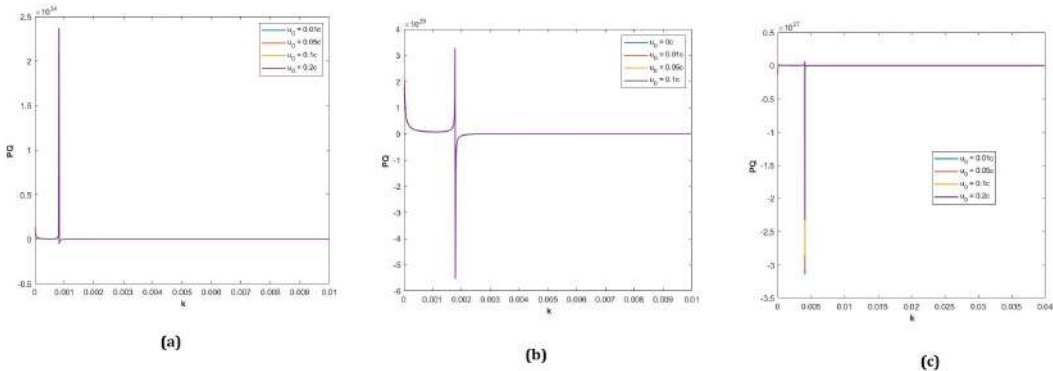


Figure 4.4: Stability domain (PQ) vs k plot for different values of u_0 with $B_0 = 100T$ (a) $n_0 = 10^{28}/m^3$ (b) $n_0 = 10^{30}/m^3$ and (c) $n_0 = 10^{32}/m^3$

density increases the slope of the dispersion characteristics reduces slightly. However, there is not much change due to streaming velocity (u_0). The figures (4.1)a, (4.1)b and

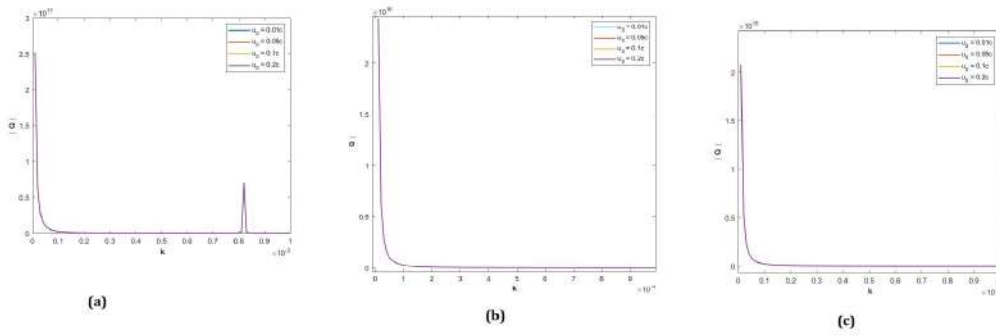


Figure 4.5: Growth rate ($|Q|$) vs k plot for different values of u_0 with $B_0 = 100T$ (a) $n_0 = 10^{28}/m^3$ (b) $n_0 = 10^{30}/m^3$ and (c) $n_0 = 10^{32}/m^3$

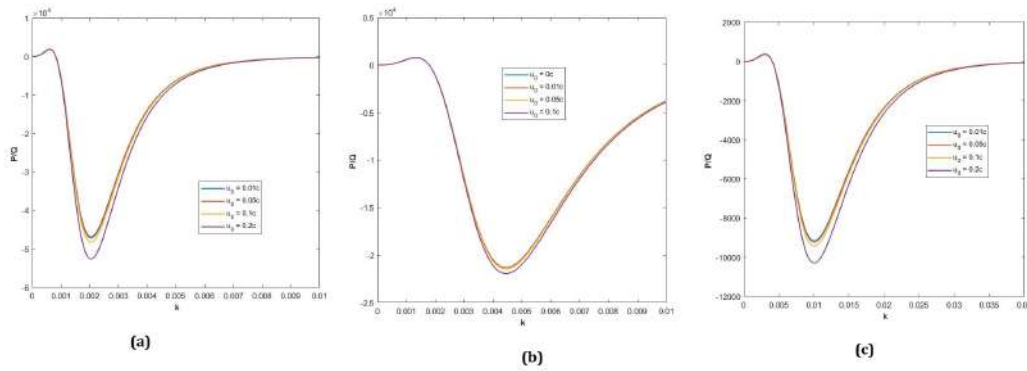


Figure 4.6: Wavenumber corresponding to maximum growth rate of instability ($\frac{P}{Q}$) vs k plot for different values of u_0 with $B_0 = 100T$ (a) $n_0 = 10^{28}/m^3$ (b) $n_0 = 10^{30}/m^3$ and (c) $n_0 = 10^{32}/m^3$

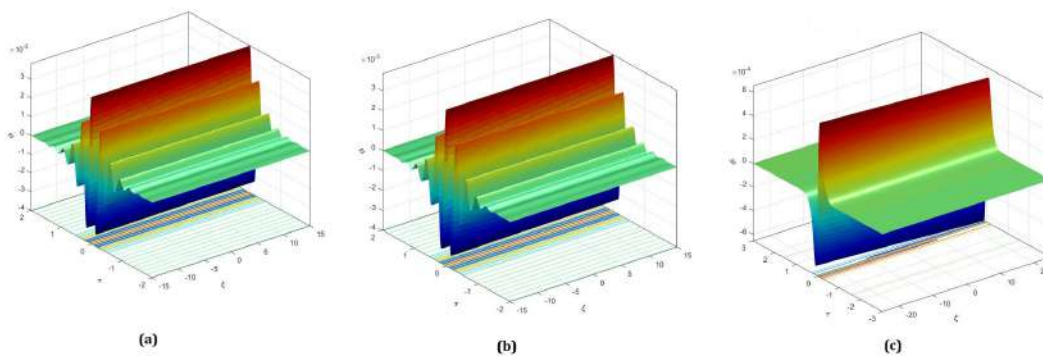


Figure 4.7: Spatio-temporal evolution of stable modulated waveform (a) $\alpha = 0.01, \beta = 20, n_0 = 10^{28}/m^3$ (b) $\alpha = 0.01, \beta = 20, n_0 = 10^{30}/m^3$ (c) $\alpha = 0.0052, \beta = 20, n_0 = 10^{32}/m^3$

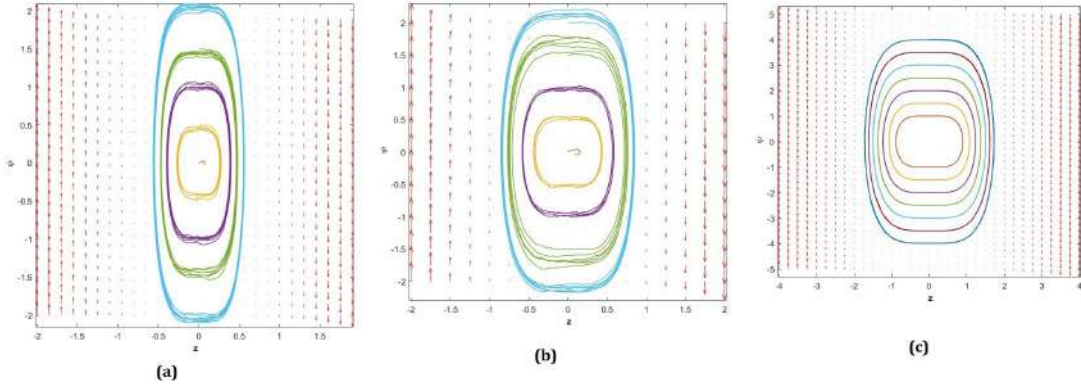


Figure 4.8: Phase space plot for (a) $n_0 = 10^{28}$ (b) $n_0 = 10^{30}$ (c) $n_0 = 10^{32}$ with $k = 0.2$, $u_0 = 0.01c$, $B_0 = 100T$

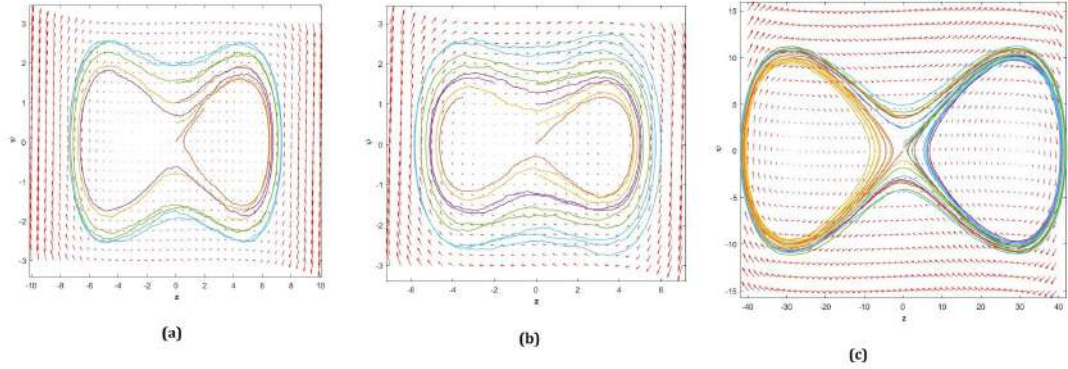


Figure 4.9: Phase space plot for (a) $n_0 = 10^{28}$, $k = 0.01$ (b) $n_0 = 10^{30}$ (c) $n_0 = 10^{32}$, $k = 0.01$ with $u_0 = 0.1c$, $B_0 = 100T$

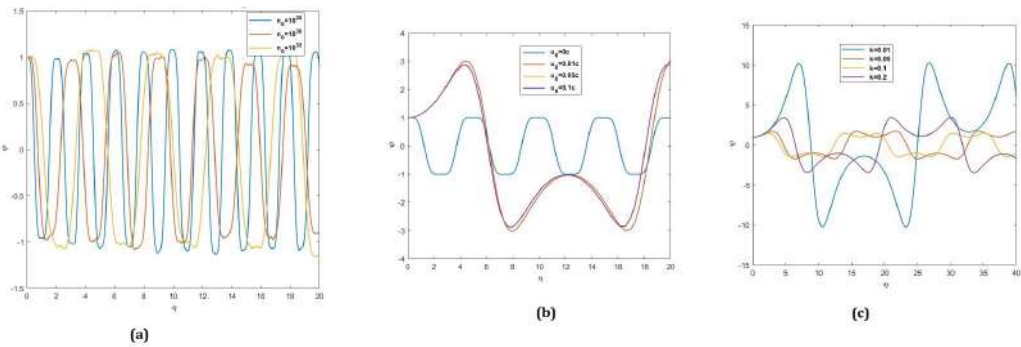


Figure 4.10: Superperiodic propagating waves ψ vs η plot for (a) different n_0 (*per* m^3) $k = 0.2$, $u_0 = 0.01c$, $B_0 = 100T$ (b) different u_0 with $n_0 = 10^{30}/m^3$, $k = 0.2$, $u_0 = 0.1c$, $B_0 = 100T$ and (c) different k with $n_0 = 10^{32}/m^3$, $u_0 = 0.01c$, $B_0 = 100T$

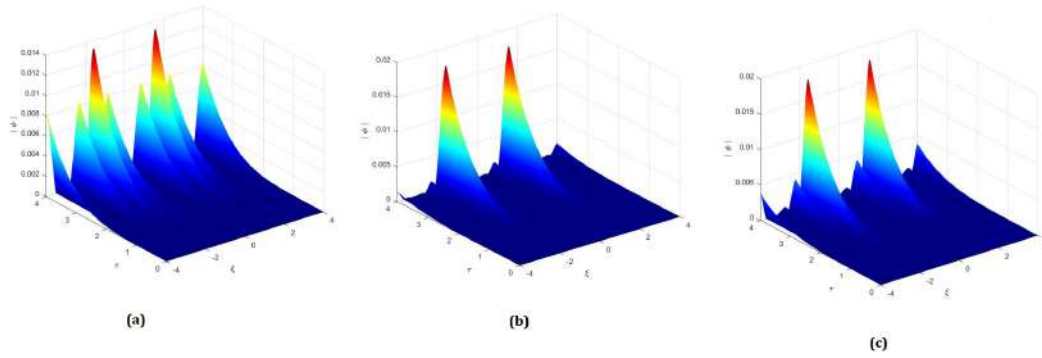


Figure 4.11: Spatial and temporal variation of amplitude of the potential ϕ for (a) $k = 0.1$ (b) $k = 0.3$ (c) $k = 0.5$ with $n_0 = 10^{30}$, $u_0 = 0.01c$, $B_0 = 100T$

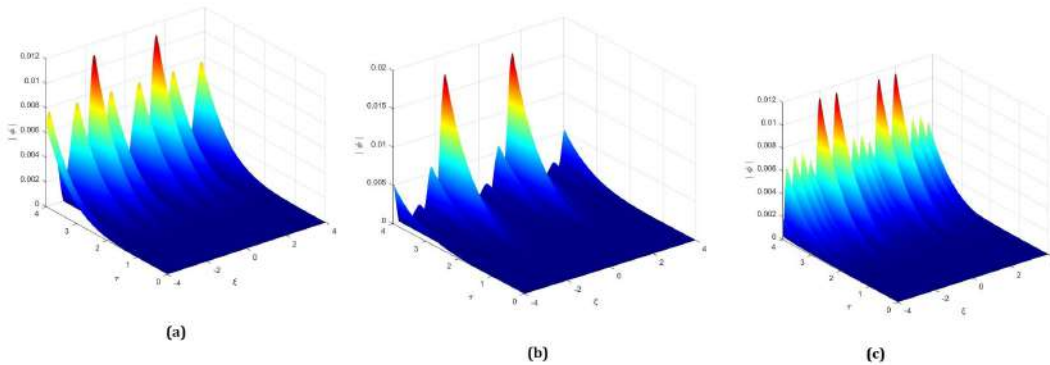


Figure 4.12: Spatial and temporal variation of amplitude of the potential ϕ for (a) $k = 0.1$ (b) $k = 0.3$ (c) $k = 0.5$ with $n_0 = 10^{32}$, $u_0 = 0.01c$, $B_0 = 100T$

(4.1)c corresponds to normalised frequency vs normalised wavenumber plot with equilibrium density ranging from $10^{28}/m^3$ to $10^{32}/m^3$. The magnetic field is taken 100T as per stellar environment data. In figure 4.2 group velocity is plotted as a function of wavenumber. We find that there is a dip in the value and the group velocity altogether have a negative value. This negative value signifies that compared to the initial wave velocity, the wave group is left more and more behind the waveframe. The more phase lagging happens at some specific values of wavenumber. This might be due to the fact that at certain values of wavenumber the particles are trapped in their positions and cannot move forward. Two possible explanation to this phenomenon are (i) either the particles cannot respond quickly and take up momentum from the wave field; or (ii) they have al-

ready tunneled out from the place of action of the force. With reference to the nonlinear Schrodinger equation [169] and from the expression of nonlinear and dispersive coefficients, we can claim that the dispersive effects increase and then decrease [figure4.3]. However, for moderate values of wave number there is a discontinuity. This is due to the fact that the different wave modes constituting the wave packet do not behave in similar manner with the media. This is due to the high level of nonlinearity inherent in plasma. It is observe that with increasing streaming velocity the dispersive effects are more pronounced. The amplitude modulation of this electron acoustic wave is described by nonlinear Schrodinger equation (NLSE) (4.29). It is known from the literature that an initially uniform wave function grows spatially modulated one which is energetically favorable. This causes the waves to be modulationally unstable. From the theory of NLSE and its application in plasma physics we come to learn that the sign of the product of the nonlinear coefficient (Q) and group dispersion coefficient (P) defines the region of stability or instability. With reference to Eqns. (4.29); The $PQ >, < 0$ value is crucial due to the fact that with reference to the nonlinear Schrodinger equation we may claim that the nonlinear effective potential is negative a possible bound state may be obtained such that the modulation is stable in nature. The product PQ in Eqn. (4.29) where both nonlinear and disperssive terms are are on the left hand side necessitates it to be negative to correspond to a stable mode. The positive values corresponds to instability. Such an instability found to be dependent on the nonlinear factors and this nonlinearity is propotional to the absolute value of the nonlinear coefficient (Q). The plot growth rate is therefore plotted through $|Q|$. If $PQ < 0$ then wave function modulationally stable, where as if $PQ > 0$, it is unstable. The relative strength of group dispersion and nonlinearity is measured by a quantity $\frac{P}{Q}$. The growth rate of the modulational instability depends on the wave number of the initial wave train. It(growth rate) attains a maximum value of $g_m = |Q| \varphi^2$ corresponding to the wave number $k_m = |\frac{Q}{P}| \varphi_0$ of the modulation. With reference to various parameter we now discuss on the stability/instability domain (represented by sign of PQ) and the growth rates (represented by $|Q|$) and the

wave number ($k_m = | \frac{Q}{P} |$) of modulation. To find the wavenumber (k_m) corresponding to maximum growth rate we differentiate the equation and after some basic algebraic calculation obtain that this value of wave number corresponds to maximum instability is propotional to P/Q .

Since the sign of PQ the determine the stability domain with reference to (figure 4.4) we can say that at very large wavelengths (low wave number) the modulated wavepacket is stable and then it becomes unstable. However, the stability regions shift towards higher wavenumber with increasing density suggesting that as density increases the modulated wave behave as a single entity over small wavelength region. Probably it is more compact and the level of nonlinearity is more and dispersive effects are less significant. The subsequent growth rate of modulational instability is depicted in figure 4.5. The growth rate is found to decrease with increasing wavenumber. However, streaming motion have no visible effect in influencing the growth rate. The wavenumber (k_m) corresponding to the maximum growth rate of instability however is located nearby to the to that which shows pronounced dispersive effects (figure 4.6). Figure (4.7) shows stable amplitude modulated envelop solitons for different plasma parameters. This suggests that once a degree of modulation reached, it becomes impossible to overlook dispersive effects and then the waveform becomes unstable and the modulation begins to change. If given enough time the modulation can split into a number of small wavepackets or individual waves. The intricate behaviour is better understood from the dynamical properties of the amplitude modulated waves in the next subsection.

Dynamical properties::

In order to investigate the dynamical properties of amplitude modulated electrostatic waves in this problem, we consider transformation $\eta = l\xi - V\tau$ and $\phi(\eta) = \psi(\eta)exp(i\delta\eta)$, the NLSE then transforms into

$$\frac{d^2\psi}{d\eta^2} = \left(\delta^2 - \frac{1}{Pl^2} \delta V \right) \psi + \frac{Q}{Pl^2} \psi^3 \quad (4.32)$$

Eqn. (4.32) can be expanded in the dynamical system as

$$\begin{aligned} \frac{\partial \psi}{\partial \eta} &= z \\ \frac{\partial z}{\partial \eta} &= P'\psi + Q'\psi^3 \end{aligned} \quad (4.33)$$

where $P' = \left(\delta^2 - \frac{1}{Pl^2} \delta V \right)$; $Q' = \frac{Q}{Pl^2}$. This system will be conservative if the corresponding field is solenoidal, i.e. $\vec{\nabla} \cdot \vec{F} = 0$, where

$\vec{F} = (z, P'\psi + Q'\psi^3)$. Hence the system is a planar one with Hamiltonian given by $\mathcal{H}' = \frac{z^2}{2} - \frac{P'\psi^2}{2} + \frac{Q'\psi^4}{4}$. Since the phase trajectories defined by equation (4.33) determine all the electrostatic modes we study the possibility of function and according to figure 4.8 it is clear that there is no critical points (other than (0,0)). However, there appears to be an attractor that is the source of the conservative field (F). We can easily see that the phase trajectory changes its slope and spreads more in the z axis and shrinks in this ψ -axis. It implies that as density increases there are more possible momentum eigenstates available for the system and position eigenstates are less accessible. This is a direct consequence of quantum mechanics. Interestingly here we find that the streaming velocity has some prominent effect in determining the phase trajectory. However at large wave approximation there are kinking suggesting the strength of hidden accelerator (4.9). In figure 4.10 a series of superperiodic waves are plotted with different quantities as the tuning parameters. Plasma density as well as streaming velocity decreases the superperiodicity. The wave number (k) on the other hand increases the superperiodicity. These studies second our findings of the perturbative analysis.

4.5 HAM study

To solve Eqn. (4.29) we make use homotopy analysis method (HAM) [134, 171] and study the evolution of amplitude modulated solitary structure. To brief the techniques- let us consider the following non linear differential equation

$$\mathcal{D}(\bar{\mathcal{U}}) - f(\bar{r}) = 0 \quad (4.34)$$

with boundary condition

$$\mathcal{B}(\bar{\mathcal{U}}, \frac{\partial \bar{\mathcal{U}}}{\partial n}) = 0, \quad r \in \Gamma. \quad (4.35)$$

Here \mathcal{D} , \mathcal{B} , $f(r)$ and Γ are a general differential operator, a boundary operator, an analytical function (which is previously known) and the boundary of the domain Ω respectively.

The operator \mathcal{D} can be divided into linear (\mathcal{L}) and non linear part (\mathcal{N}) such that

$$\mathcal{L}(\bar{\mathcal{U}}) + \mathcal{N}(\bar{\mathcal{U}}) - f(\bar{r}) = 0 \quad (4.36)$$

Now employing basic homotopy technique, we construct homotopy as

$$\begin{aligned} \mathcal{H}(\bar{\mathcal{V}}, p) \equiv (1 - p) \left[\mathcal{L}(\bar{\mathcal{V}}) - \mathcal{L}(\bar{\mathcal{U}}_0) \right] + p \left[\mathcal{D}(\bar{\mathcal{V}}) - f(\bar{r}) \right] = 0, \\ p \in [0, 1]. \end{aligned} \quad (4.37)$$

or equivalently

$$\mathcal{H}(\bar{\mathcal{V}}, p) \equiv \mathcal{L}(\bar{\mathcal{V}}) - \mathcal{L}(\bar{\mathcal{U}}_0) + p\mathcal{L}(\bar{\mathcal{U}}_0) + p \left[\mathcal{N}(\bar{\mathcal{V}}) - f(\bar{r}) \right] = 0 \quad (4.38)$$

where $\bar{\mathcal{U}}_0$ is initial assumption satisfying the boundary condition (4.35). As the embedding (homotopy) parameter p changes from zero to unity the picture convolutes from

$\bar{\mathcal{U}}_0(r)$ to $\bar{\mathcal{U}}(r)$ (exact or approximated analytic solution).

We now discuss the results obtained from HAM starting with a sinusoidal potential. Due to self interaction and associated non-linearity the wave evolution represented by the nonlinear Schrodinger equation slowly gets a spatial modulation (figure- 4.11 4.12) as shown. The density and the wavenumber are the tuning parameter here. If given enough time the modulation thus created grows over time (figure- 4.11 4.12). Such a wave is thus modulationally unstable as the amplitude increases. It is to be noted that we have chosen the value of k in such a way so as to allow amplitude modulation to take visible shape. This region is depicted by the sandwiched region of instability in $\frac{P}{Q}$ vs k plots. The modulation is found to occur in the form of an envelope solitary structure. This is relatable with previous studies on amplitude modulation in plasma waves.

4.6 Conclusion

We have studied here the effects of exchange correlation, the streaming motion as well as the quantum diffraction on the nonlinear evolution of modulated electron plasma waves. We have used the standard Fourier technique to derive the nonlinear Schrodinger equation. The NLSE describe the nonlinear evolution of envelop soliton and the associated modulational instability and it growth rate. We have shown how the wave's instability depends on various parameters and in which domain of wave number. To understand the physical situation we included a section on the dynamical properties of amplitude modulated electrostatic waves. The analysis of dynamical system supports the findings of the perturbative analysis. Furthermore we have employed a section based on homotopy perturbation technique and analyzed the growth of instability. Our findings match in both approaches and this second techniques holds promise in analyzing complex plasma phenomena.

CHAPTER 5

SEMI-LAGRANGIAN METHOD TO STUDY NONLINEAR ELECTROSTATIC WAVES IN QUANTUM PLASMA

5.1 Introduction

In the physical realm, the low temperature and high particle density delimits the quantum effects in plasma [172, 58] where the de Broglie wavelength overlaps over each other that's giving rise to Quantum effects as per the exclusion principle [56]. A number of works on highly dense and low temperature plasma, popularly termed as "Quantum plasmas" have been carried out by many authors [173]. Many wave modes like ion acoustic waves (IAWs) [174, 175, 117, 168] electron acoustic waves (EAWs) [67, 169, 176], electron plasma waves (EPWs) [64, 82], Dust Acoustic Waves (DAWs) [63, 177] etc. have been studied in quantum plasma. Studies on shocks and double layers in such plasma have been carried out [178, 179]. In all these works the often used model is the quantum hydrodynamic model [180]. Such a plasma have applications from laboratory to space [181, 182]. Originally developed by Haas [172], Shukla [183], Manfredi [58], Marklund [184], it was further studied by Misra [185] Ghosh [180] Chandra [66, 122] and others [186]. Many different types of nonlinear effects [187, 73] are observed in quantum plasma [188, 167, 72]. A number of approaches have been summarised in the review paper by Shukla [56]. Recently, chaos study in plasma have gained prominence [189, 190] and holds promises to understand the microscopic mechanisms in the plasma system.

The degeneracy in such Fermionic plasma have been dealt with a relativistic degeneracy [65, 68] or quantum degeneracy [64, 82]. The electron distribution function [191] plays an important role in determining the generation of different wave modes in which the dispersion characteristics, the thermodynamic processes as well as any form of inho-

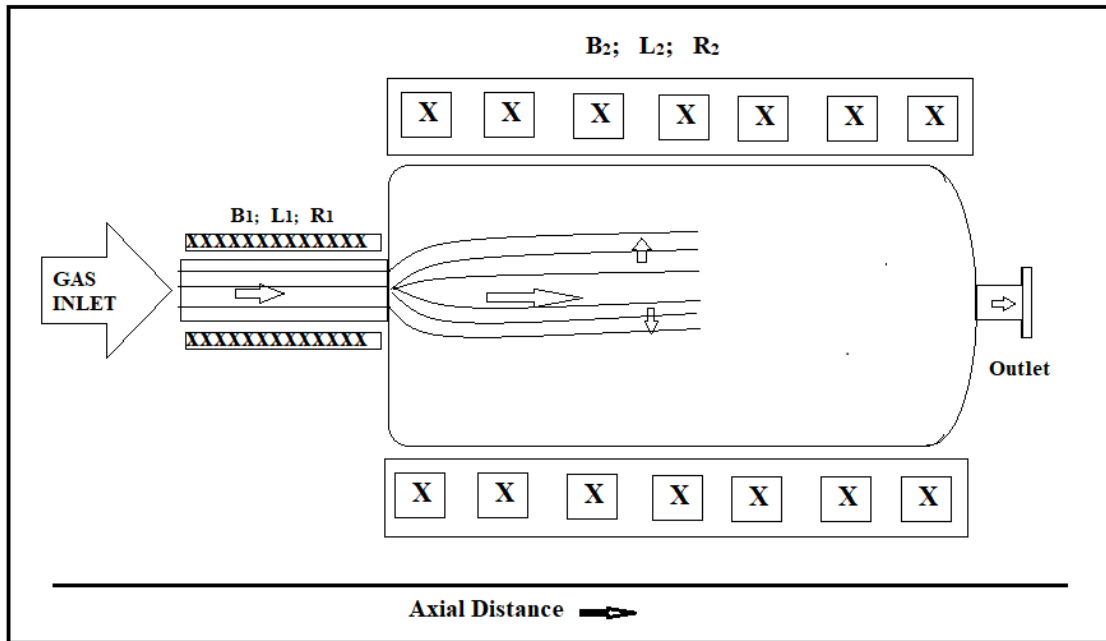


Figure 5.1: Schematic depiction of the experimental setup for generating temperature anisotropy. Adopted from Beatty et. al. [192]. Here $B_1, L_1 \& R_1$ are the magnetic field, length and radius respectively of the input plasma channel. And $B_2, L_2 \& R_2$ are the magnetic field, length and radius respectively of the plasma chamber where the anisotropy originates.

mogeneity or anisotropy is dependent on the distribution function. Such an anisotropy was recently reported by Beatty *et.al.* [192]. A schematic depiction of the experiment is given in figure (5.1). The Kinetic models for Plasma systems are crucial in the study of linear velocity space instabilities but are not so effective in providing information on micro density and collective Thomson scattering. The mathematical prescription of kinetic models is the Vlasov–Maxwell (VM) equation [193]. The requirement for the VM formulation is the particle distribution function. The motivation behind this work is to study the evolution of macroscopic quantities in a dense plasma with temperature anisotropy. In the fluid picture the moments of such a distribution function under equilibrium conditions will give the quantum hydrodynamic (QHD) model with one dimensional temperature anisotropy [191]. Recent works can be found in the following works [194, 195, 196, 197, 198, 199, 200]

5.2 Temperature anisotropy and Kinetic model

In the present work we consider a collisionless plasma in which plane longitudinal waves propagate leading to an adiabatic compression along the propagation direction, thus creating heating and temperature anisotropy in one direction. The ratio between the proton temperature perpendicular (T_{\perp}) and parallel (T_{\parallel}) to the background magnetic field is called temperature anisotropy. With slight deviation from the classical Vlasov picture, here from the Wigner equation, the phase fluid incompressibility is violated by way of quantum tunneling that is a phenomena observed in a dense quantum plasma. Such model was put forward by Eliasson and Shukla [191] and later worked upon by Chandra [67], Akbari [201] and others [171, 202, 134]. The numerical resolution of the Kinetic Vlasov equation has been studied by some authors in the particle-in-cell framework [203]. In this method the description of the temporal evolution of the equation through self consistent fields and finite number of particle is utilised along with the usage of a grid for resolution. Another method makes use of computation of distribution function for one time step in the backward direction in the grid and uses a standard interpolation technique [204, 35, 205]. This process couples the Eulerian and Lagrangian framework and the Vlasov equation (and equations derived from it) is obtained [206]. In this work we employ the distribution function presented by Eliasson and Shukla [191, 207] and later extensively studied by others [67, 208] is given by:

$$f(y, \vec{v}, t) = \frac{-\frac{n_0}{Li_{3/2}(-e^{\beta\mu})} \left(\frac{\beta m}{2\pi}\right)^{3/2}}{e^{\left\{\left(\frac{\beta m}{2}\right)[(v_y - v_{y,ex})^2 \eta + v_x^2 + v_z^2] - \beta\mu\right\}} + 1}, \quad (5.1)$$

where n_0 is the equilibrium electron density, $Li_{\alpha}(\xi)$ is the poly-logarithm function, $v_{y,ex}(y, t)$ is the average velocity of the particles in the propagation direction, m is the mass of the electron, μ is the chemical potential, $\beta = \frac{1}{k_B T_{e0}}$, k_B is the Boltzmann constant, T_{e0} is the background temperature and $\eta(y, t) = T_{e0}/T_{y,ex}(y, t)$ is the one-dimensional temperature anisotropy of the distribution function. Different proton

temperatures perpendicular and parallel to the magnetic field can cause waves in an electron-proton plasma. If $T_{\perp} > T_{\parallel}$, the plasma could be unstable to both proton cyclotron (PC) and mirror modes (MM) waves, which have been identified in the Venusian environment [209]. Temperature and temperature anisotropy's observations in the solar wind and magnetosheath are especially important because they reveal how heating happens at a collisionless shock and how the solar wind is produced. [210].

The electron temperature anisotropy is controlled by fluctuations produced by electromagnetic kinetic instabilities, according to kinetic plasma theory and simulations [211]. Many macroscopic parameters that describe the solar wind, such as particle temperature anisotropy or electron heat flow, are always measured with values that are constrained by the onset of kinetic instabilities, according to the argument. The general argument is that when the flow expands, it causes a distortion in the distribution function, which manifests as an increase in temperature anisotropy [211, 212, 213]. Plasma kinetic theory from microscopic interactions and motions of its constituents, describes and predicts the state of plasma. Plasma kinetics is the study of continua in velocity space and the link between velocity and forces [214, 202, 215, 216]. To provide accurate propagation and damping, the complete kinetic effects of finite temperature electrons must be kept in the parallel contributions to the dielectric tensor [217]. In the high-temperature limit, we retain the nonlinear fluid equations for a dense hot plasma and in the low-temperature limit, we retain the correct fluid equations for a fully degenerate plasma [191]. We use the Maxwell's equations and subsequently obtained the time evolution of the distribution function, the density and energy profiles by using the semi-Lagrangian method.

5.3 Basic Equations

The general form of Vlasov equation is given by

$$\frac{\partial f}{\partial t} + \mathbf{p} \cdot \nabla_y f + F(\mathbf{y}, t) \nabla_p f(\mathbf{y}, \mathbf{p}, t) = 0 \quad (5.2)$$

Such an equation when coupled with Maxwell equations form the Vlasov-Maxwell equations. In case of electrostatic waves in unmagnetised plasmas, Maxwell's equations include only the Poisson equation

$$\nabla_y \cdot \mathbf{E}(\mathbf{y}, t) = \int_{-\infty}^{+\infty} f(\mathbf{y}, \mathbf{p}, t) d\mathbf{p} - N_0 \quad (5.3)$$

Here we normalized time by the inverse of the plasma frequency: ω_p , velocity by thermal speed (and therefore momentum p to mv_{thermal}), and space by Debye length. $F(y, t)$ is a generalized force term, \mathbf{E} in the electrostatic case. We present the 1D electrostatic case for which the Vlasov equation simplifies to : [218]

$$\frac{\partial f}{\partial t} + v \frac{\partial f}{\partial y} + E(y, t) \frac{\partial f}{\partial v} = 0 \quad (5.4)$$

and

$$\frac{\partial E}{\partial y} = 1 - \int_{-\infty}^{\infty} f(y, v, t) dv \quad (5.5)$$

with initial condition $f(y, v, t = 0) = f_0(y, v)$. In the next sections we present the numerical scheme and the algorithm for this simulation study.

5.4 Numerical Scheme

Time Splitting: :

In this semi-Lagrangian method [219, 205] the Vlasov equation (5.4) can be recast in the following form:

$$\frac{\partial f}{\partial t} + \mathbf{U}(\mathbf{Y}, t) \cdot \nabla_{\mathbf{Y}} f = 0 \quad (5.6)$$

where \mathbf{Y} denotes the phase space coordinates (here $\mathbf{Y} = (y, p_y)$) and \mathbf{U} is a solenoidal vector field containing two components in the 1D case. Since \mathbf{U} is solenoidal (i.e. divergence-free), Eq. (5.6) can be formulated in a conservative form

$$\frac{\partial f}{\partial t} + \nabla_{\mathbf{Y}}(\mathbf{U}(\mathbf{Y}, t)f) = 0 \quad (5.7)$$

Splitting \mathbf{Y} into two components \mathbf{Y}_1 and \mathbf{Y}_2 , Eq. (5.7) can then be written as:

$$\frac{\partial f}{\partial t} + \nabla_{\mathbf{Y}_1}(\mathbf{U}_1(\mathbf{Y}_1, \mathbf{Y}_2, t)f) + \nabla_{\mathbf{Y}_2}(\mathbf{U}_2(\mathbf{Y}_1, \mathbf{Y}_2, t)f) = 0 \quad (5.8)$$

Further, it is well known [205] that solving separately

$$\begin{aligned} \frac{\partial f}{\partial t} + \nabla_{\mathbf{Y}_1}(\mathbf{U}_1(\mathbf{Y}_1, \mathbf{Y}_2, t)f) &= 0 \\ \frac{\partial f}{\partial t} + \nabla_{\mathbf{Y}_2}(\mathbf{U}_2(\mathbf{Y}_1, \mathbf{Y}_2, t)f) &= 0 \end{aligned} \quad (5.9)$$

keeps up to 2^{nd} order accuracy for the whole equation (5.6) by flipping the solutions. It should be noted that while this semi-Lagrangian scheme does not solve the Vlasov's equation in its conservative form, it does so in the advective version, allowing for the use of the backward characteristic approach. Subsequently, we get [219]

$$\frac{\partial f}{\partial t} + \mathbf{U}_1 \cdot \nabla_{\mathbf{Y}_1} f = 0 \quad (5.10)$$

$$\frac{\partial f}{\partial t} + \mathbf{U}_2 \cdot \nabla_{\mathbf{Y}_2} f = 0 \quad (5.11)$$

if and only if

$$\begin{aligned} \nabla_{\mathbf{Y}_1} \mathbf{U}_1(\mathbf{Y}_1, \mathbf{Y}_2, t) &= 0 \\ \nabla_{\mathbf{Y}_2} \mathbf{U}_2(\mathbf{Y}_1, \mathbf{Y}_2, t) &= 0 \end{aligned} \quad (5.12)$$

Semi-Lagrangian method::

In the semi-Lagrangian method we can introduce the solutions of the dynamical system i.e. the characteristics of (5.6)

$$\frac{d\mathbf{Y}}{dt} = \mathbf{U}(\mathbf{Y}(t), t) \quad (5.13)$$

Let us denote by $\mathbf{Y}(t; \mathbf{Y}, t_1)$ the solution at an instant t whose value is \mathbf{Y} at time t_1 .

Taking $\mathbf{Y}(t)$ a solution of Eq. (5.12), we have

$$\begin{aligned} \frac{d}{dt}(f(\mathbf{Y}(t), t)) &= \frac{\partial f}{\partial t} + \frac{d\mathbf{Y}}{dt} \cdot \nabla_{\mathbf{y}} f \\ &= \frac{\partial f}{\partial t} + \mathbf{U}(\mathbf{Y}(t), t) \cdot \nabla_{\mathbf{Y}} f = 0 \end{aligned} \quad (5.14)$$

which means that f is constant along the characteristics. This can also be written as

$$f(\mathbf{Y}(t; \mathbf{Y}, t_1), t) = f(\mathbf{Y}(t_1; \mathbf{Y}, t_1), t_1) = f(\mathbf{Y}, t_1) \quad (5.15)$$

for any times t and t_1 and phase-space coordinate \mathbf{y} . This property will be employed to solve such a discrete problem by Semi-Lagrangian method (SLM). By introducing a finite set of mesh points $(\mathbf{Y}_m)_{m=1, \dots, N}$ which is (or not) equally spaced we solve this discrete problem. Then, with a given value of f at the mesh points at any given time

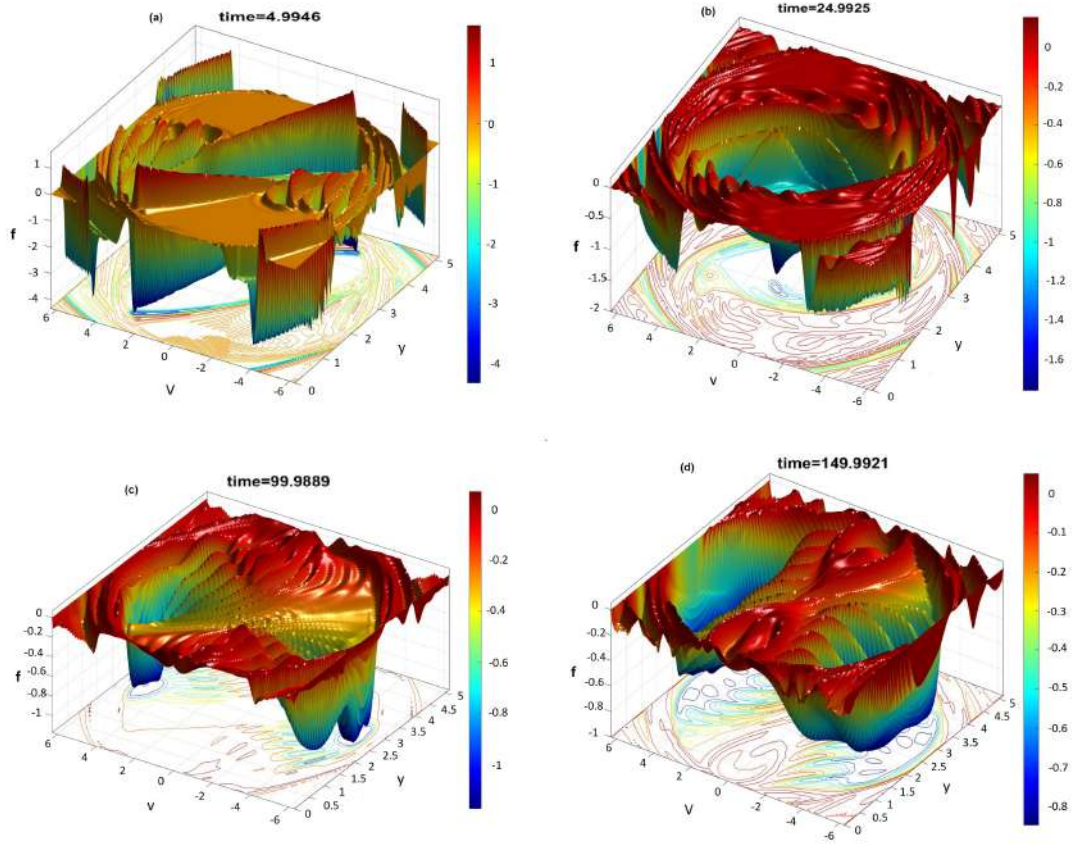


Figure 5.2: Evolution of distribution function in phase-space for different normalized runtime t . (a) $t=4.9946$; (b) $t=24.9925$; (c) $t=99.9889$ and (d) $t=149.9921$

step, we obtain the new value \mathbf{Y}_m at mesh point.

$$f(\mathbf{Y}_m, t_n + \Delta t) = f(\mathbf{Y}(t_n - \Delta t; \mathbf{Y}_m, t_n + \Delta t), t_n - \Delta t) \quad (5.16)$$

For each mesh point \mathbf{Y}_m , the distribution function (f) is computed in two steps which are

1. To find the starting point of the characteristic which is ending at \mathbf{Y}_m ,
i.e. $\mathbf{Y}(t_n - \Delta t; \mathbf{Y}_m, t_n + \Delta t)$.
2. Followed by the computation of $f(\mathbf{Y}(t_n - \Delta t; \mathbf{Y}_m, t_n + \Delta t), t_n - \Delta t)$ by spline interpolation, since f is known only at mesh points at the instant $t_n - \Delta t$.

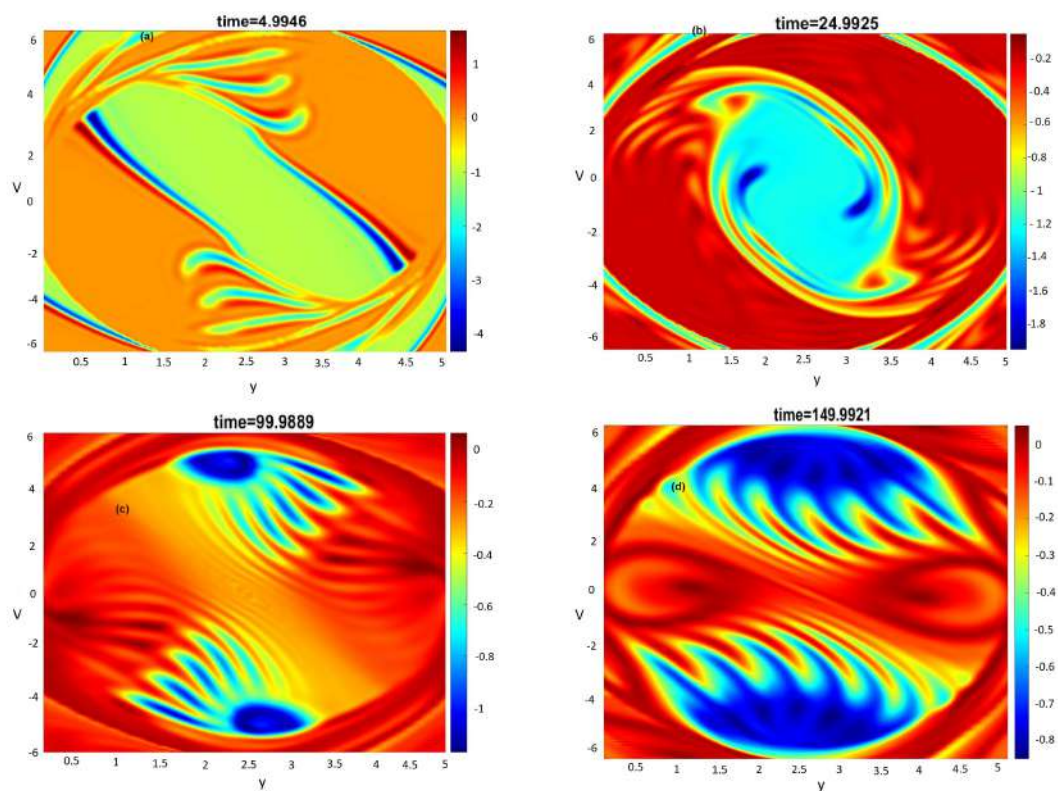


Figure 5.3: y - v contour plots for different normalized runtime t . (a) $t=4.9946$; (b) $t=24.9925$; (c) $t=99.9889$ and (d) $t=149.9921$

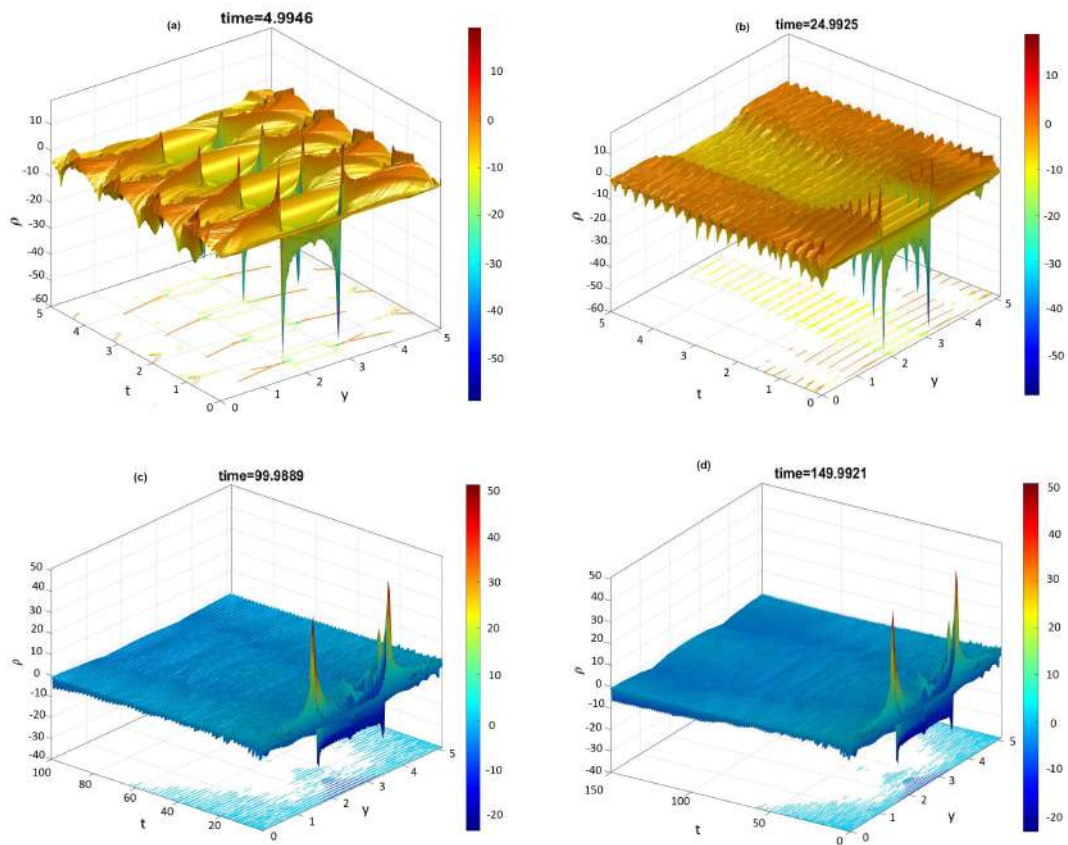


Figure 5.4: Evolution of normalized particle density (n) for different normalized runtime t . (a) $t=4.9946$; (b) $t=24.9925$; (c) $t=99.9889$ and (d) $t=149.9921$

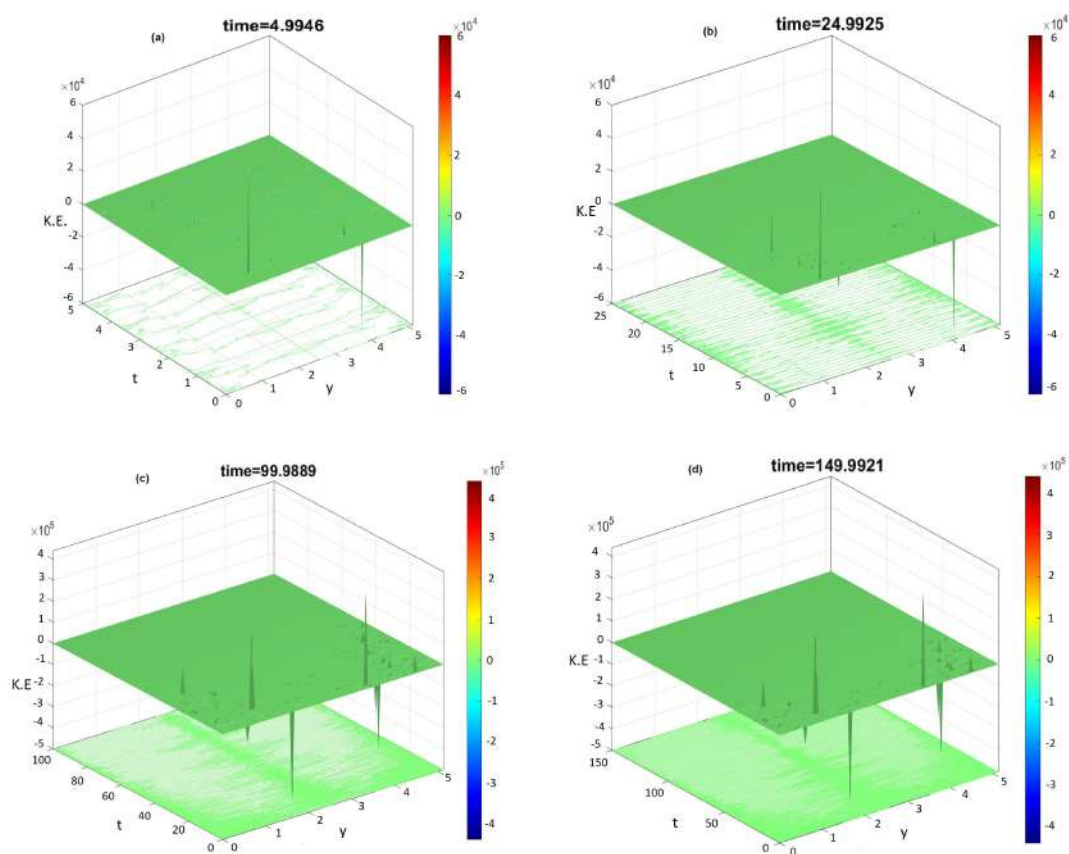


Figure 5.5: Distribution of kinetic energy (normalized) for different normalized runtime t . (a) $t=4.9946$; (b) $t=24.9925$; (c) $t=99.9889$ and (d) $t=149.9921$

Algorithm::

To solve the Vlasov–Poisson system Eqns. (5.4) & (5.5) numerically we using the time splitting scheme from time step t_n to t_{n+1} which involved here four steps :

1. We perform a half time–step shift along the y -direction $f^*(y, v) = f^n(y - v\Delta t/2, v)$
2. We compute the electric field at time $t_{n+1/2}$ by substituting f^* in the Poisson’s equation (5.5)
3. Perform a shift along the v -direction $f^{**}(y, v) = f^*(y, v - E(y, t_{n+1/2}) \Delta t)$
4. Perform a second halftime step shift along the y -axis $f^{n+1}(y, v) = f^{**}(y - v\Delta t/2, v)$.

Note, here electric field is the electrostatic one and it is normalized.

5.5 Results and Discussions

From the above sections we obtain the ”Semi-Lagrangian Vlasov Code” (SLVC) for the finite temperature quantum plasma with one dimensional temperature anisotropy. The gradual evolution of the distribution function in the phase space and subsequently the density and energy profiles reflect on the properties of the system and its evolution in time. In figure (5.2) we have shown the gradual evolution of the Eliasson–Shukla distribution function at different instants of time. From the figure (5.2)(a-d) it is found that there are regions of higher and lower values suggesting the formation of electron holes in the phase space. Such a pocket gradually evolves over time with tails of distribution minima suggesting the opposite velocity i.e. reflection of the phase fluid. Such a phenomenon is a direct outcome of the violation of the incompressibility of phase fluid in contrast to its classical counterpart. The temperature anisotropy causes particle trapping in the phase diagram. This is relatable due to the fact that adiabatic compression

causes electron localisation of particles which are clearly depicted in subsequent figures. From figure (5.3), it is clearly understood that there are multiple dips of the distribution function shaped as wings in the phase plots. These dips have pockets of higher electron concentrations and also regions of scarcity. These blue coloured regions corresponding to the reflected stream generated from thermal anisotropy. An animation file of the same can be found here ([link](#))

Based on the distribution function (DF), the physically measurable quantities like density and energy distributions are also studied with time. The density of particles which arise from the zeroth moment of the DF in velocity space and the energy is obtained from the second moment respectively. From figure (5.4) it becomes clear there exists density fluctuations which die out exponentially with time as well as with distance towards the boundary. There are gradual yet finite variations at the origin which appears after some time has elapsed (5.4) (c,d). This appears to be the Kelvin- Helmholtz instability as suggested by some authors in their work [35]. These small scale motions are a result of small scale turbulence that traces its origin to the temperature anisotropy in equation (5.1), as discussed in the previous sections. In the fluid picture, this would have correspondence with an increased value of the Reynold's number. These mixing regions periodically move away and a second order mixing region again appears at the centre of the phase space. Such a process suggests an excess and void of kinetic energy [figure (5.5)] in the configuration space implying both repulsive and attractive forces in action. Neighboring phase fluid layers induces a velocity shear thus trying to homogenise the temperature anisotropy.

5.6 Applications

Our work describes how a stellar wind evolves and is one of the more sophisticated scenarios that's been created to account for the various solar wind features that have been observed [220]. Weibel instability could be explained through anisotropic plasma [221]

and hence it could explain phenomena in astrophysical plasma like gamma ray burst and shock formation in supernovae remnants. Temperature anisotropy is also helpful in studying the plasma environment in the Venusian atmosphere. Also this method can be helpful in generating a magnetic field in laboratory plasma [222, 223, 224], especially within the setting of laser-plasma interaction [225]. Our work is applicable to study tokamaks and this is just one of the issues of fusion reactors that could be undergone through this model.

5.7 Conclusion and Summary

In this chapter, we employed the semi-Lagrangian method for the kinetic Vlasov equation corresponding to a Fermi distribution in dense plasma with 1D temperature anisotropy and discussed the numerical simplifications that can be further used in some other models, in which a time-splitting prescription can be applied. In brief, the full method applicable for any form of Vlasov type equations can be carried out with the guiding-centre Vlasov–Poisson model. It overcomes the limitations where it could not be solved accurately using such splitting method but possible in the advective form. The numerical results thus obtained are very satisfying. We used MATLAB R2019 module library and by assembling it we were enabled to treat many complex problems occurring in plasma physics through the SLVC. To a positive note that this methodology does not depend upon the use of regular grids. Rather, we use a set of lines (not necessarily equally spaced) in each direction to employ spline interpolation.

CHAPTER 6

BIFURCATION THEORY AND STABILITY ANALYSIS

6.1 Introduction

To analyze a physical plasma system, one must first apply a qualitative analytical method. One needs to look at the plasma system components, such as the plasma source itself and its diagnostic tools, to see how these components interact to provide results that explain the operation of the plasma system. For example, immersing a basic electrical diagnostic instrument, such as a Langmuir probe, in a thermally generated plasma source and measuring characteristic plasma parameters forms a plasma system. When the probe bias is applied to the probe chip, plasma charge currents are collected between the two polarities of the probe bias. The resulting so-called IV curve is similar to the logistic curve previously proposed by Verhulst [226]. Verhulst's logistic model curves show how the population grows compared to the available resources and form modern chaos theory's basis. This letter qualitatively discusses plasma charges' population growth (or depletion) and their maintenance in plasma systems. This is done without any additional assumptions about the physical composition of the plasma charge itself. In addition, the results here require a change in the approach of interpreting Langmuir probe trace data, which used only exponential fit to model plasma charge-current vs. probe bias data. This allows us to implement a better model for analyzing the behavior of different plasma systems.

Bifurcation theory and stability analysis are very useful tools for qualitatively and quantitatively studying the behavior of complex systems without explicitly determining the solutions of the governing equations for various initial and boundary conditions. This chapter is complementary to the corresponding mathematical theories. It conveys the basic idea of bifurcation theory and stability analysis. Here we chapter provide the

vocabulary to classify the equilibria and common branches commonly encountered in applications. This shows the application of theory for studying equilibrium criteria in plasma system. It also briefly describes some aspects related to stationary structures, wave modes, parametric influence, geometry of the system etc. It focuses on ordinary differential equations (ODEs), an important block for studying branching and stability. This chapter also describes how ODE research is generalized in the case of partial differential equations (PDEs).

A close field of research often studied in this regard is Chaos theory. Chaos is an interdisciplinary scientific theory, an area of mathematics susceptible to initial conditions and the basis of dynamical systems that were once thought to exhibit completely random disorder and irregular states. It focuses on patterns and deterministic laws. Chaos theory believes that the apparent randomness of chaotic and complex systems are the underlying patterns, interconnections, persistent feedback loops, iterations, self-similarities, fractals, and self-organization [227]. The butterfly effect, the basic principle of chaos, explains how small changes in one state of a deterministic nonlinear system lead to significant differences in later states (i.e., subtle to the initial conditions) [228]. The metaphor for this behavior is that a butterfly flapping its wings in Vrindavan can cause cyclone in Bay of Bengal.

Slight differences in initial conditions, such as those due to measurements or rounding errors in numerical computation, can yield widely diverging outcomes for such dynamical systems, rendering long-term prediction of their behavior impossible [229]. This can happen even though these systems are deterministic, meaning that their future behavior follows a unique evolution [230] and is entirely determined by their initial conditions, with no random elements involved. In other words, the deterministic nature of these systems does not make them predictable [231]. This behavior is known as deterministic chaos or simply chaos.

Lyapunov Exponent: In this context another quantity is important often termed as Lyapunov Exponent. In mathematics, the Lyapunov exponent of a dynamical system or

the characteristic Lyapunov exponent is a quantity that characterizes the separation of orbits near infinity. Quantitatively, the two orbitals diverge in phase space at the initial separation vector $\delta\mathbf{Z}_0$ diverge (provided that the divergence can be treated within the linearized approximation) at a rate given by

$$\|\delta\mathbf{Z}(t)\| \approx e^{\lambda t} |\delta\mathbf{Z}_0|,$$

where λ is the Lyapunov exponent. Separation rate may vary depending on the direction of the initial separation vector. Therefore, there is a spectrum of Lyapunov exponents—a number equal to the number of dimensions in topological space. It is customary to call the largest (maximal) Lyapunov exponent (LLE) to define the concept of predictability of dynamic systems. A positive LLE is usually considered to indicate that the system is chaotic (if other conditions are met, such as the compactness of the topological space). Note that any initial separation vector usually contains several components in the direction associated with the LLE, and because of the exponential growth rate, the effects of other indices are canceled over time. The index is named after Alexander Lyapunov. It has important application in plasma Physics. The Lyapunov exponent was investigated numerically and analytically for various plasma states by many authors in the recent years [232, 233, 234, 235]. A three-dimensional particle code that calculates the Coulomb force between individual particles is used to study the instantaneous expansion rate of nearby orbitals in topological space. It can be seen that the Lyapunov exponent has various dependencies on the Coulomb coupling constant, corresponding to dilute plasma, liquid plasma, and solid plasma. An analytical model has also been developed to show the relationship between the Lyapunov exponent and the dielectric response function [236]. This model shows that the Lyapunov exponent of the dilute plasma is on the order of the plasma frequency, which is consistent with the simulation results. In dilute plasmas, large fluctuations in the instantaneous expansion rate have been shown to be caused by close encounters that break force symmetry and lead to orbital instability.

This chapter is organized in the following way. In Section §6.2 we introduce quan-

tum plasma at finite temperature and the basic governing equations. Then we derive KdV-Burger equation in Subsection §6.2.1 and its dynamical properties. With higher degree of nonlinearity amplitude modulation is studied in Subsection §6.2.2 and the subsequent Subsection §6.2.2 provides a treatise on the chaotic study. In Section §6.3, we study bifurcation analysis of electron acoustic waves (EAWs) in degenerate astrophysical plasma with its basic governing equations. In the Subsection §6.3.1, we brief on the derivational part of KdV equation. Then dynamical characteristics of EAWS are studied in unperturbed (in §6.3.2) and perturbed system (in §6.3.2) and subsequently in Subsection §6.3.3, non-linear Schrodinger equation (NLSE) is derived. In the Subsection §6.3.4 we obtain the dynamical system equations and discuss the results in Section §6.4 with superperiodic solutions and phase plots.

6.2 Quantum plasma at finite temperature

Quantum effects in plasma have been studied by quantum hydrodynamic (QHD) model [60, 237]. It requires high density and extremely low temperature in order to display quantum statistical and quantum diffraction effects. However Shukla and Eliasson [56, 191] obtained nonlinear electron fluid equation for a quantum plasma with arbitrary electron degeneracy. The applicability of quantum effects in a finite temperature plasma showing quantum statistical and diffraction effects at a temperature not approaching absolute zero considered the temperature anisotropy have been the guiding motivation. Elliason and Shukla presented the model and have been used by Akbari et al [201] in later years. According to this model which is based on 3D equilibrium state in which nonlinear plane plasma wave propagate. Assuming 3D Fermi-Dirac equilibrium state for spin-1/2 particles, the particle density given by

$$\begin{aligned}
 n_0 &= \frac{1}{2\pi^2} \left(\frac{2m}{\hbar^2} \right) \int_0^\infty \frac{E^{1/2} dE}{e^{\beta(E-\mu)} + 1} \\
 &= \frac{1}{2\pi\beta^{1/2}} \left(\frac{2m}{\hbar^2} \right) \Gamma\left(\frac{3}{2}\right) Li_{3/2}(e^{\beta\mu}), \tag{6.1}
 \end{aligned}$$

(where $\beta = \frac{1}{k_B T_{Fh}}$ and μ is chemical potential) and taking different order of moment of distribution function the dynamical equations are obtained and are given as:

$$\frac{\partial}{\partial t}(n_h) + \frac{\partial}{\partial x}(n_h u_h) = 0 \quad (6.2)$$

$$\frac{\partial}{\partial t}(n_c) + \frac{\partial}{\partial x}(n_c u_c) = 0 \quad (6.3)$$

$$[\lambda] \left(\frac{\partial}{\partial t} + u_h \frac{\partial}{\partial x} \right) u_h = \frac{\partial}{\partial x} \phi - F_h \left(\frac{\partial}{\partial x} n_h \right) + \frac{H^2}{2} \frac{\partial}{\partial x} \left[\frac{1}{\sqrt{n_h}} \frac{\partial^2}{\partial x^2} \sqrt{n_h} \right] + \eta_h \frac{\partial^2 u_h}{\partial x^2} \quad (6.4)$$

$$\left(\frac{\partial}{\partial t} + u_c \frac{\partial}{\partial x} \right) u_c = \frac{\partial \phi}{\partial x} - F_c \frac{\partial n_c}{\partial x} + \frac{H^2}{2} \frac{\partial}{\partial x} \left[\frac{1}{\sqrt{n_c}} \frac{\partial^2}{\partial x^2} \sqrt{n_c} \right] + \eta_c \frac{\partial^2 u_c}{\partial x^2} \quad (6.5)$$

$$\frac{\partial^2 \phi}{\partial x^2} = (n_c + \frac{n_h}{\delta} - n_i \frac{\delta_1}{\delta}) \quad (6.6)$$

The value of $\lambda = 1, 0$ is due to the fact whether or not we want to study the inertia effects of hot electrons. Here we used the normalization scheme as $\bar{n}_j \rightarrow \frac{n_j}{n_{j0}}$, $\bar{u}_j \rightarrow \frac{u_j}{C_{sh}}$, $\bar{x} \rightarrow \frac{x \omega_c}{C_{sh}}$, $\bar{t} \rightarrow \omega_c t$, $\bar{\phi} \rightarrow \frac{e \phi}{k_B T_{Fh}}$, where the subscript j is used to denote hot (h), cold (c) electrons and ion (i), u_j, n_j ($j = c, h$) are the velocity, density, $F_h = \left(\frac{n_{h0}}{n_0} \right)^{\frac{1}{3}} \frac{m_e c^2}{6 k_B T_{Fh}}$, $F_c = (\delta)^{\frac{2}{3}} \frac{m_e c^2}{2 k_B T_{Fh}}$, $\delta = \frac{n_{c0}}{n_{h0}}$, $\delta_1 = \frac{n_{i0}}{n_{h0}}$ (subscript 0 stand for equilibrium state) and $H = \frac{\hbar \omega_c}{2 k_B T_{Fh}}$, $\omega_c = \sqrt{\frac{n_{c0} e^2}{\epsilon_0 m_e}}$ is the cold electron plasma frequency, $C_{sh} = \sqrt{\frac{2 k_B T_{Fh}}{m_e}}$ is the hot electron acoustic speed and T_{Fh} is the hot electron Fermi temperature respectively.

6.2.1 Derivation of KdV-Burger's equation

As done in previous works [68] perturbation expansion of the field quantities have been made. We take ϕ as the amplitude of the electric potential field, χ and τ are the stretched variables corresponding to x and t respectively [68] where $\chi = \varepsilon^{1/2}(x - Mt)$ and $\tau = \varepsilon^{3/2}t$. Accordingly the perturbation series is given by:

$$\begin{bmatrix} n_h \\ n_c \\ u_h \\ u_c \\ \phi \end{bmatrix} = \begin{bmatrix} 1 \\ 1 \\ u_0 \\ u_0 \\ \phi_0 \end{bmatrix} + \varepsilon \begin{bmatrix} n_h^{(1)} \\ n_c^{(1)} \\ u_h^{(1)} \\ u_c^{(1)} \\ \phi^{(1)} \end{bmatrix} + \varepsilon^2 \begin{bmatrix} n_h^{(2)} \\ n_c^{(2)} \\ u_h^{(2)} \\ u_c^{(2)} \\ \phi^{(2)} \end{bmatrix} + \dots \quad (6.7)$$

and the viscosity factor is $\eta_{h,c} = \varepsilon^{1/2}\eta_{h,c}^{(0)}$. Using the standard procedure and equating terms of same power in ε we finally obtain the KdV Burger's equation given by

$$\frac{\partial \phi}{\partial \tau} + A\phi \frac{\partial \phi}{\partial \chi} + B \frac{\partial^3 \phi}{\partial \chi^3} - C \frac{\partial^2 \phi}{\partial \chi^2} = 0 \quad (6.8)$$

where

$$A = \frac{\frac{2(M-u_0)^2}{(F_c-(M-u_0)^2)^3} + \frac{\frac{(M-u_0)^2}{(F_h-(M-u_0)^2)^2} + \frac{(M-u_0)^2}{(F_h-(M-u_0)^2)^2}}{\delta(F_h-(M-u_0)^2)}}{\frac{2(M-u_0)}{(F_c-(M-u_0)^2)^2} + \frac{\frac{M-u_0}{F_h-(M-u_0)^2} + \frac{(M-u_0)}{F_h-(M-u_0)^2}}{\delta(F_h-(M-u_0)^2)}}$$

$$B = -\frac{H^2 \left(\frac{1}{(F_c-(M-u_0)^2)^2} + \frac{1}{\delta(F_h-(M-u_0)^2)(F_h-(M-u_0)^2)} \right)}{4 \frac{\frac{2(M-u_0)}{(F_c-(M-u_0)^2)^2} + \frac{\frac{M-u_0}{F_h-(M-u_0)^2} + \frac{(M-u_0)}{F_h-(M-u_0)^2}}{\delta(F_h-(M-u_0)^2)}}} - 1$$

$$C = \frac{\frac{\eta_c^{(0)}(M-u_0)}{(F_c-(M-u_0)^2)^2} + \frac{\eta_h^{(0)}(M-u_0)}{\delta(F_h-(M-u_0)^2)(F_h-(M-u_0)^2)}}{\frac{2(M-u_0)}{(F_c-(M-u_0)^2)^2} + \frac{\frac{M-u_0}{F_h-(M-u_0)^2} + \frac{(M-u_0)}{F_h-(M-u_0)^2}}{\delta(F_h-(M-u_0)^2)}}$$

Dynamical Properties of Unperturbed EASWs:

To study the dynamical properties of steady state electron acoustic stationary wave structures (EASWs) we start with a traveling wave solution and using the KdV equation as the evolutionary system the progressive waves and the corresponding phase portraits are shown below. For this we use the transformation: $\eta_1 = l\chi - M\tau$, $\phi(\chi, \tau) = \psi_1(\eta_1)$ with the usual boundary conditions as $\eta_1 \rightarrow \pm\infty$, $\psi, \frac{\partial\psi}{\partial\eta_1}, \frac{\partial^2\psi}{\partial\eta_1^2} \rightarrow 0$ where M is the velocity of the wave frame. By using this transformation and upon integration of the KdV equations twice with respect to η_1 we obtain the set of equations corresponding to dynamical system as:

$$\frac{\partial^2\psi_1}{\partial\eta_1^2} = \frac{M}{Bl} \frac{\partial\psi_1}{\partial\eta_1} - \frac{C}{Bl^3}\psi_1 + \frac{A}{2Bl^2}\psi_1^2 \quad (6.9)$$

Now the Eqn. (6.9) can be transform in to dynamical system of the form

$$\begin{aligned} \frac{\partial\psi_1}{\partial\eta_1} &= z_1 \\ \frac{\partial z_1}{\partial\eta_1} &= \frac{C}{Bl}z_1 + \frac{M}{Bl^3}\psi_1 - \frac{A}{2Bl^2}\psi_1^2 \end{aligned} \quad (6.10)$$

The system will be conservative if the divergence of the field is zero i.e. $\vec{\nabla} \cdot \vec{F} = 0$, where $\vec{F} = (z_1, \frac{C}{Bl}z_1 + \frac{M}{Bl^3}\psi_1 - \frac{A}{2Bl^2}\psi_1^2)$. Accordingly the Hamiltonian is given by:

$$\mathcal{H} = \frac{z_1^2}{2} - \frac{C}{2Bl}z_1^2 - \frac{M}{2Bl^3}\psi_1^2 + \frac{A}{6Bl^2}\psi_1^3 \quad (6.11)$$

Since the phase plots describes all equations of EAWs we plan to study the dynamical properties of the system through the parametric phase portraits for different parameters and initial conditions.

Figure (6.1) shows the super periodic EAWs for different values of quantum diffraction parameter (H), streaming velocity (u_0) and Mach number (M). Here δ (cold and hot electron equilibrium density ratio) is 0.5. It is claim that as H increases the waves

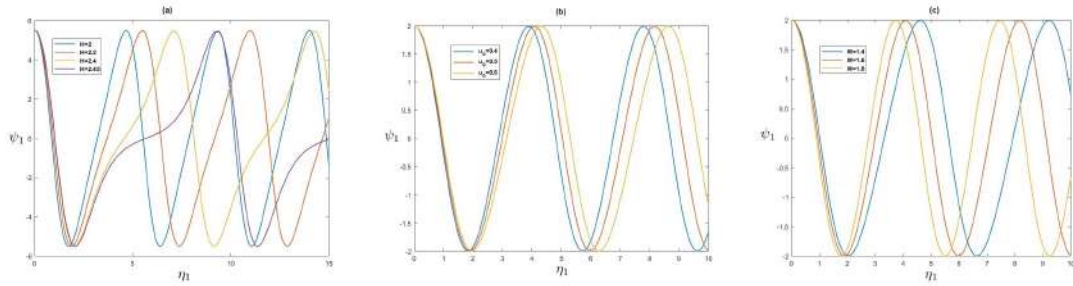


Figure 6.1: Effect of parameters on the superperiodic solutions (a) quantum diffraction (H), (b) Streaming motion (u_0) and (c) waveframe speed (M). Other parameters are $\eta_{h,c} = 1.5, \delta = 0.5, F_h = 1.4, F_c = 0.48$.

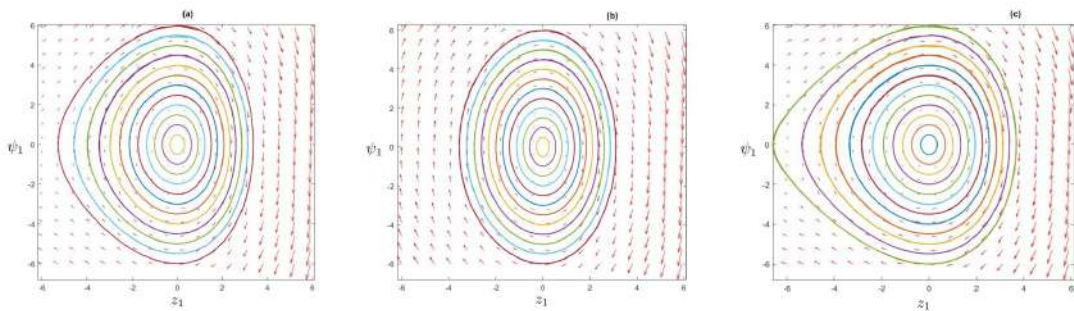


Figure 6.2: Phase portraits for different parameters in various combinations (a) $M = 1.6, H = 2$, (b) $M = 2, H = 2$ and (c) $M = 1.6, H = 2.2$. Other parameters are $u_0 = 0.5, \delta = 0.5, \eta_{h,c} = 1.5, F_h = 1.4, F_c = 0.48$.

undergo a phase shift and it clear that the phases corresponding to $H=2.45$ superposes on the second harmonic corresponding to $H=2$. It is noted for the first time that the quantum diffraction contributes to the phase apart from the amplitude of the wave ϕ . The contribution of the streaming velocity u_0 is similar to the effect of H but it is less effective when compared to H . The reason behind this may be due to the fact that streaming motion affects small nonlinearity which introduces a positive phase difference. On the contrary the wave-frame speed (reflected through the Mach number) acts contrary to the quantum diffraction and streaming. The wave frame speed which adds up a negative phase factor is somehow uncorrelated and not in consonance with nonlinear effects. In other words it compounds to increasing dispersive effects thus making the phases lag behind. Also it can be interpreted like this, the quantum diffraction parameter (H) which related to the plasmonic energy and inversely to the thermal energy. Shows that with higher values of H the periodicity decreases. (i.e. the energy associated with the propagating wave is less.)

From the phase diagrams we show the dependence of quantum diffraction and Mach number for different instances of time. From figure 6.2 we see that the phase trajectories become distorted as time grows by. The vector directions show a nonuniform force field thus supporting our claims in the previous sections on non-perturbative and perturbative investigations. Further from figure 6.2(a–b) it is clear that wave-frame velocity does not allow the distortion in phase trajectories and incorporates dispersive elements in the system. The same was evident from 6.1. Hence ϕ , η_1 and χ are state variables. From Eqn. (6.10) it is clear that the system has no equilibrium points (other than 0,0) thereby suggesting the probability of hidden attractor(s) on the left side of the diagram. From figures (6.2 a,b and c) it is clear that there are hidden attractor(s) that limits the momenta spectra slightly. From these figures we see that the motion is not chaotic.

6.2.2 Amplitude Modulation and Nonlinear Schrodinger Equation

The degree of nonlinearity amounts to the formation of modulated stationary structures. Such a nonlinearity may be due to external or internal perturbations of some kind. The system in the unperturbed case if acted upon by some external perturbations or some sort of nonlinear interactions originating within the system amounts to some disturbances, the dynamical equations undergo some modifications. Accordingly the KdV-B solitary wave evolves into amplitude modulated envelope solitary structures.

Perturbed System:

The evolutionary equation was obtained by adding a forcing term to the KdV-Burger's equation (6.8) and is given by:

$$\frac{\partial \phi}{\partial \tau} + A\phi \frac{\partial \phi}{\partial \chi} + B \frac{\partial^3 \phi}{\partial \chi^3} - C \frac{\partial^2 \phi}{\partial \chi^2} = f_0 \exp[i\omega' \tau] \quad (6.12)$$

Where f_0 and ω' are the magnitude and frequency of such perturbations. Such an alteration reflects in the dynamical system equation and the transformed set of equations are given below. To study the formation and properties of the envelop solitons we have to convert the KdV-B equation into nonlinear Schrodinger equation (NLSE). Using Fourier's method (Multiple scale perturbation technique) for a generalised dynamical state vector U with $\xi_1 = \varepsilon(\chi - c\tau)$, $\theta = \varepsilon^3\tau$, here c is the wave speed of the fundamental disturbance.

$$U_l = U_l^{(0)} + \sum_{n=1}^{\infty} \varepsilon^n \sum_{l=-\infty}^{\infty} U_l^{(n)}(\xi_1, \tau) \exp[il(k\chi - \omega\tau)] \quad (6.13)$$

and obtaining ordered equations for various harmonics [188] the NLSE is given as:

$$i \frac{\partial \varphi}{\partial \theta} + P \frac{\partial^2 \varphi}{\partial \xi_1^2} + Q |\varphi|^2 \varphi = 0 \quad (6.14)$$

Here P and Q are dispersive and nonlinear coefficients given by:

$$P = -(3Bk - iC); Q = \left[A^2k \left(\frac{1}{(6Bk^2 - i4kC)} - \frac{1}{3Bk^2} \right) \right] \quad (6.15)$$

Dynamical Properties of Nonlinear Schrodinger Equation:

It is important to study the dynamical properties of the nonlinear Schrodinger equation. So we have considered the following transformation $\eta_2 = l\xi_1 - V\tau$ and $\varphi(\eta_2) = \psi_2(\eta_2)\exp(i\Delta\eta_2)$, the NLSE (6.14) then transforms into

$$\frac{d^2\psi_2}{d\eta_2^2} = \left(\delta^2 - \frac{1}{Pl^2}\Delta V \right) \psi_2 + \frac{Q}{Pl^2}\psi_2^3 \quad (6.16)$$

Equation ((6.16)) can be expanded in the dynamical system as

$$\begin{aligned} \frac{\partial\psi_2}{\partial\eta_2} &= z_2 \\ \frac{\partial z_2}{\partial\eta_2} &= P'\psi_2 + Q'\psi_2^3 \end{aligned} \quad (6.17)$$

Here

$P' = \Delta^2 - \frac{1}{Pl^2}\Delta V$, $Q' = -\frac{Q}{Pl^2}$ This system will be conservative if the corresponding field is solenoidal, i.e. $\vec{\nabla} \cdot \vec{F} = 0$, where

$\vec{F} = (z_2, P'\psi_2 + Q'\psi_2^3)$. Hence the system is a planar one with Hamiltonian given by $\mathcal{H}' = \frac{z_2^2}{2} - \frac{P'\psi_2^2}{2} - \frac{Q'\psi_2^4}{4}$. Since the phase trajectories defined by equation (6.17), we study the system in details by introducing the parametric phase portraits (P3) of the amplitude modulated envelope solitons.

Chaotic Signature of Amplitude Modulated Structures:

The chaotic signature is important in studying the stability of amplitude modulated solitary structures. We have made use of particular system specific transformations and used our newly developed 'Parametric Phase Portrait Code (P3code)' to study the dependence

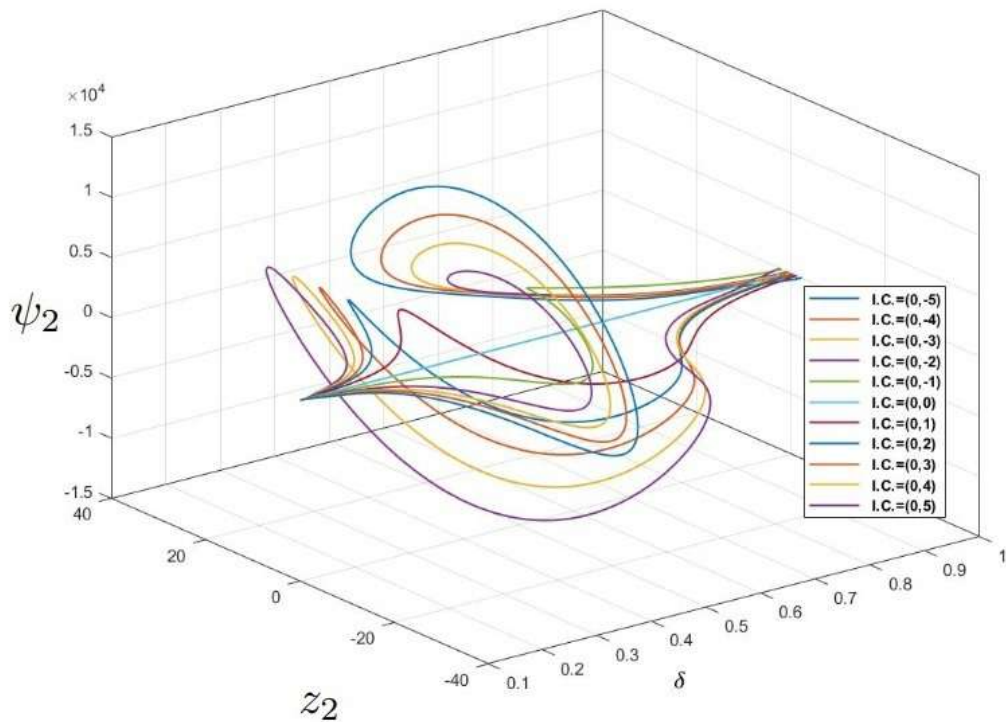
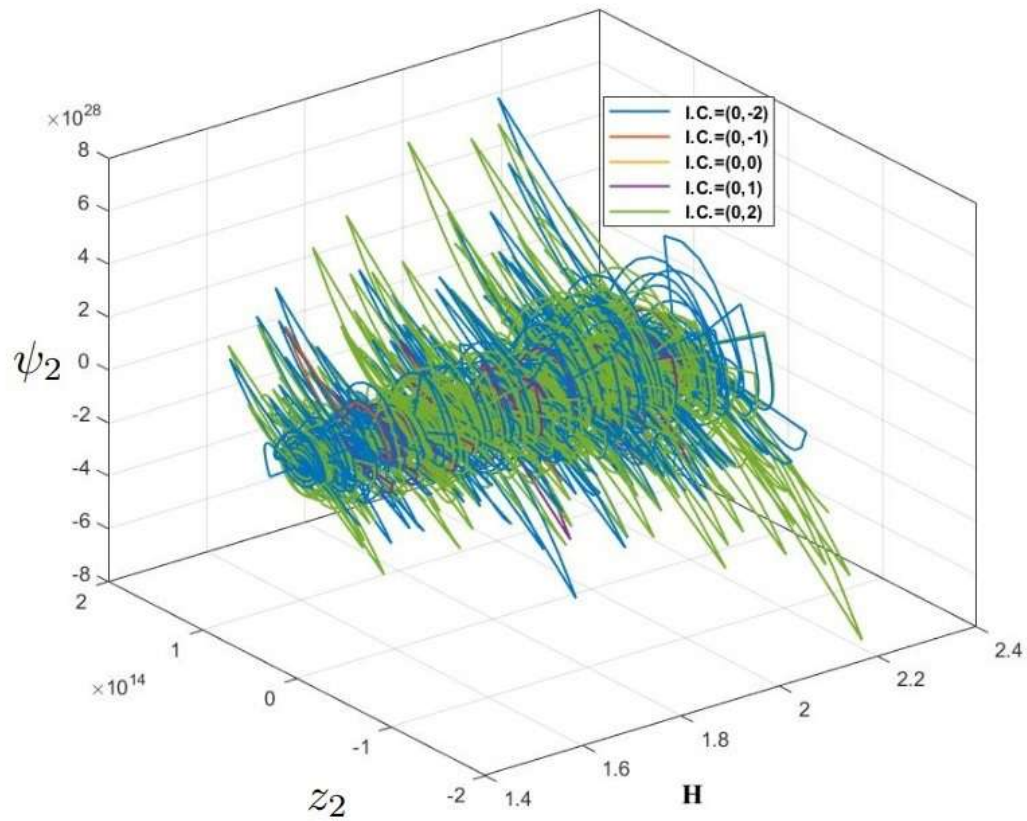


Figure 6.3: Parametric phase portraits for different (a) normalised quantum diffraction parameter (H) and (b) normalised equilibrium density ratio of cold-to-hot electrons (δ). Other parameters are $\eta_h = 0.4, \eta_c = 0.4, V = 1.6, k = 0.2, u_0 = 0.5, F_h = 0.05$ & $F_c = 0.0004$.

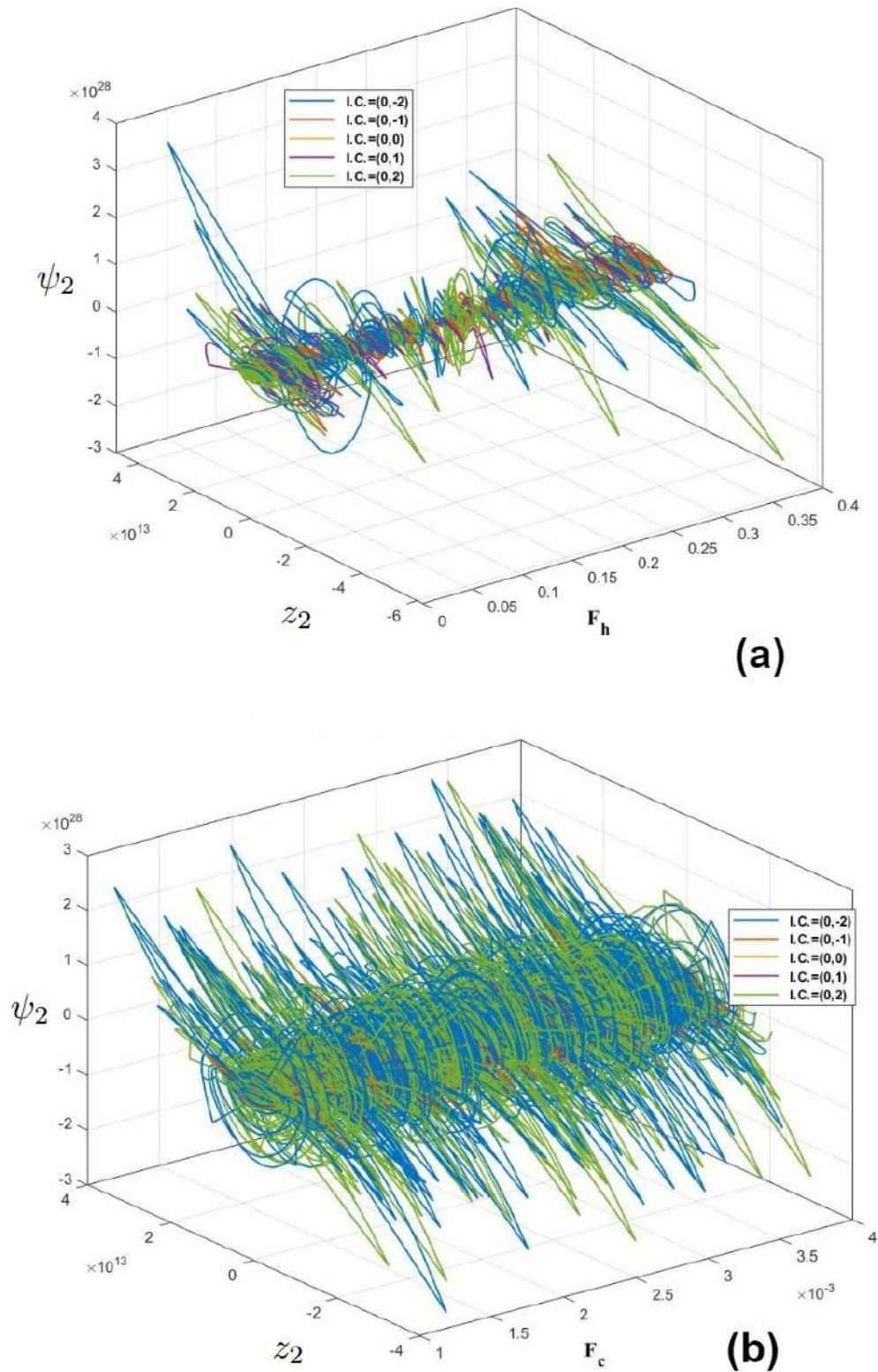
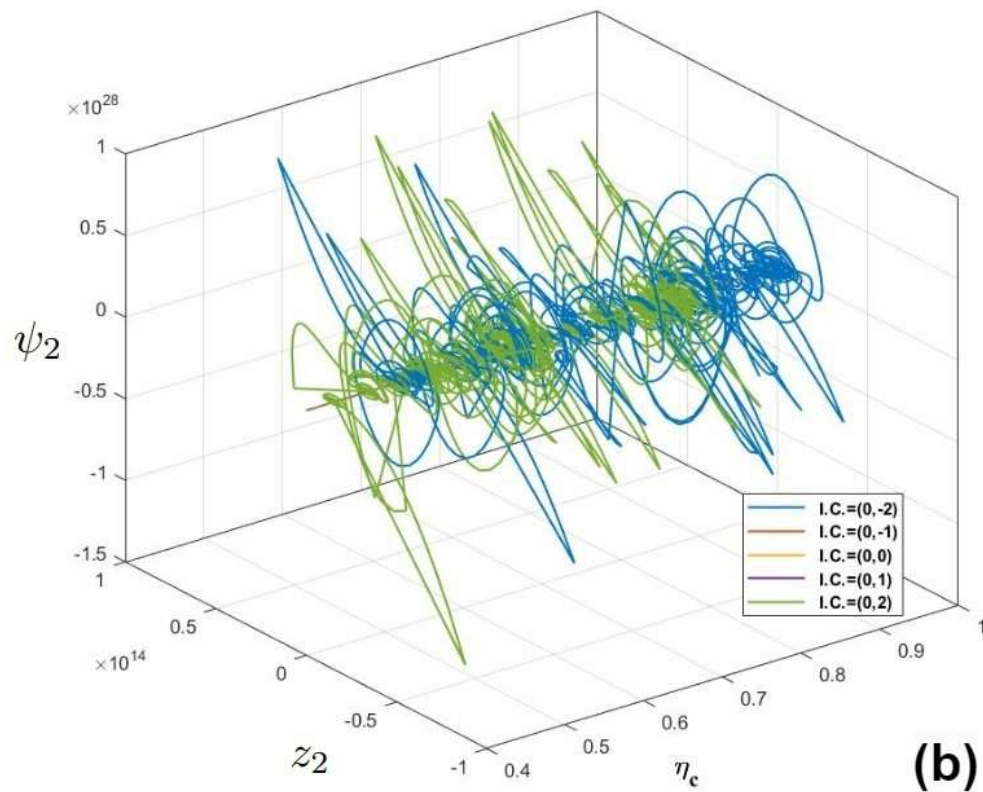
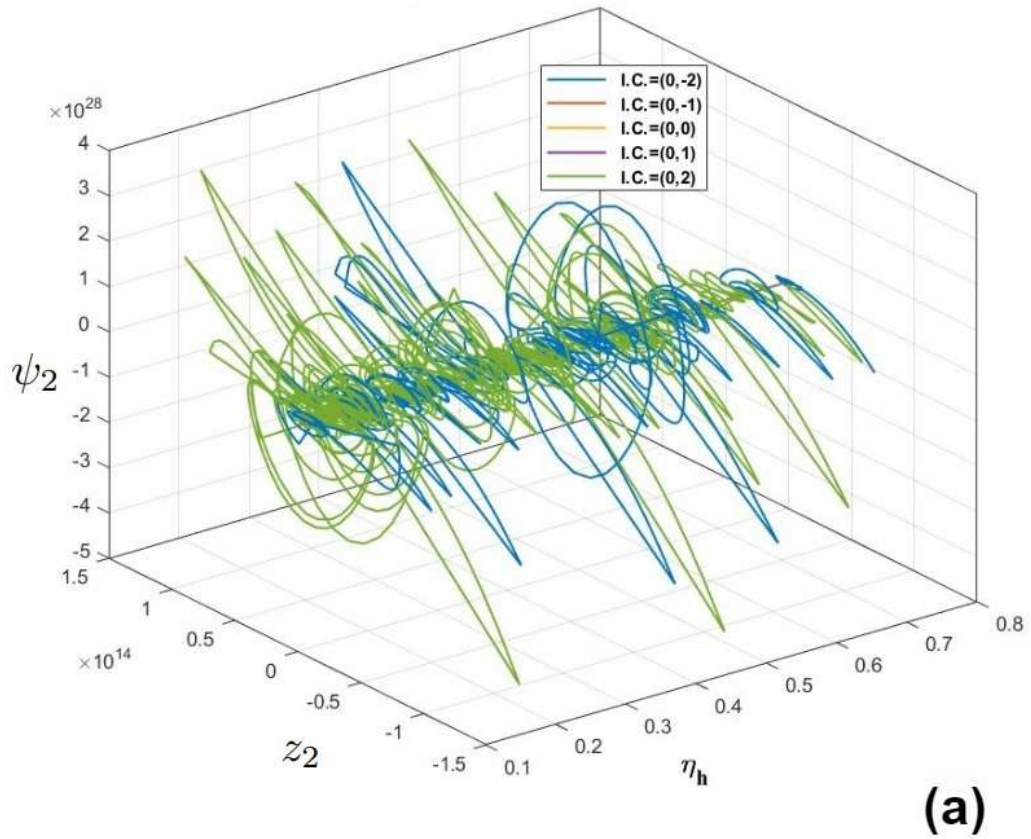


Figure 6.4: Parametric phase portraits for different (a) normalised hot electron degeneracy parameter (F_h) and (b) normalised cold electron degeneracy parameter (F_c). Other parameters are $\eta_h = 0.4, \eta_c = 0.4, V = 1.6, k = 0.2, u_0 = 0.5, H = 2\delta = 0.3$.



88
 Figure 6.5: Parametric phase portraits for different (a) normalised hot electron viscosity parameter (η_h) and (b) normalised cold electron viscosity parameter (η_c). Other parameters are $H = 2, \delta = 0.3, V = 1.6, k = 0.2, u_0 = 0.5, F_h = 0.05 \& F_c = 0.0004$.

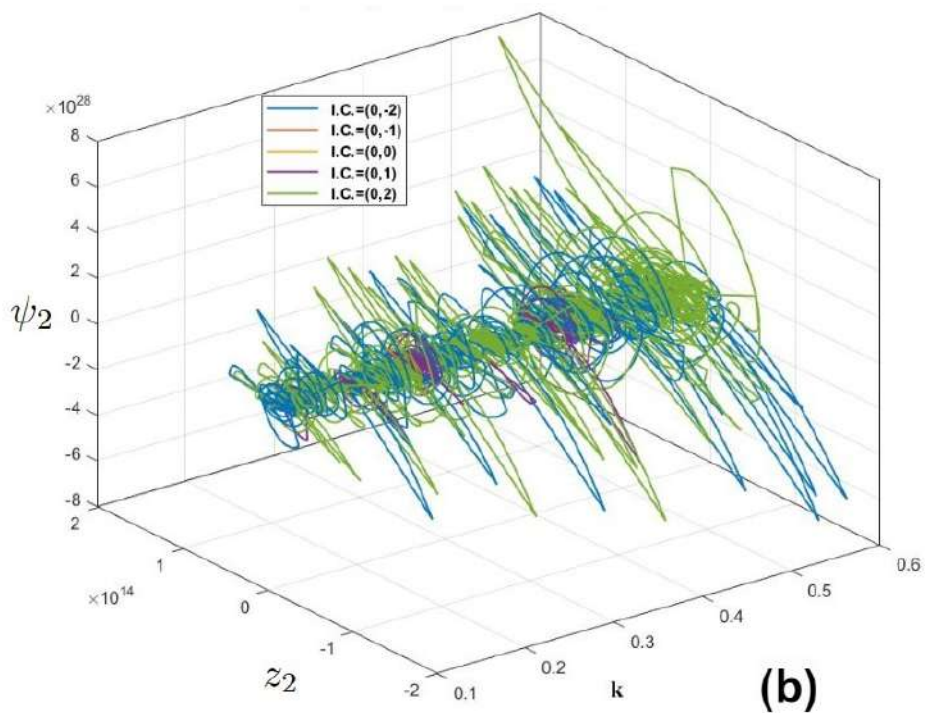
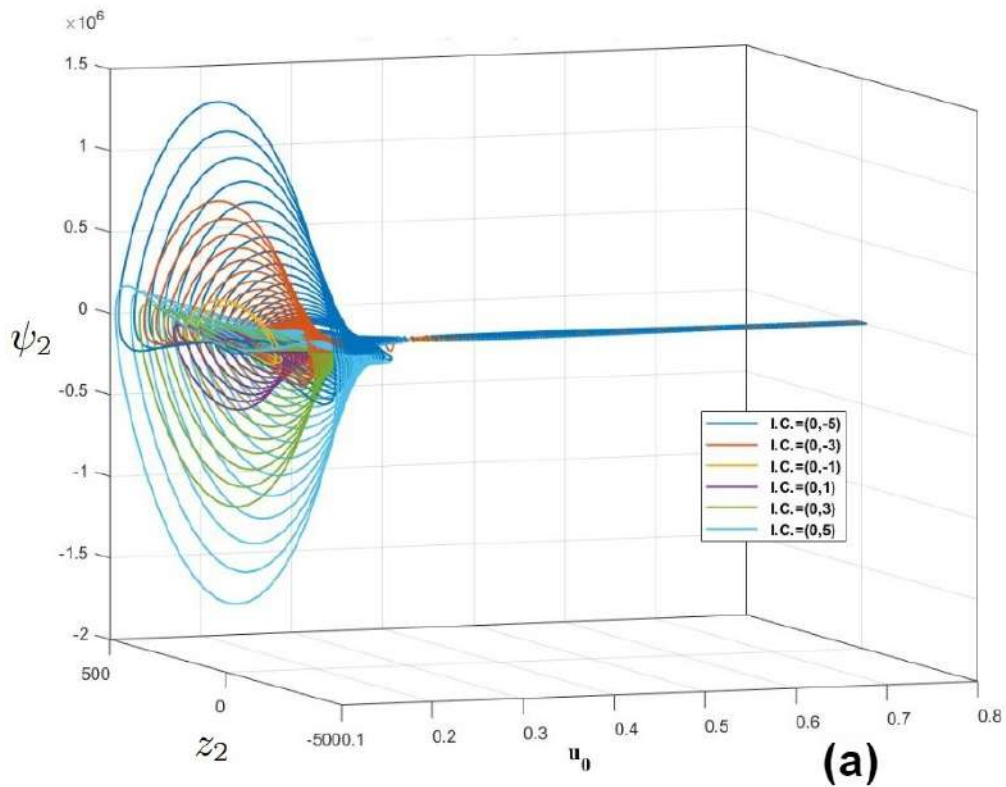


Figure 6.6: Parametric phase portraits for different (a) normalised streaming parameter (u_0) and (b) normalised wavenumber (k) of fundamental wave. Other parameters are $\eta_h = 0.4, \eta_c = 0.4, V = 1.6, H = 2, \delta = 0.3, F_h = 0.05$ & $F_c = 0.0004$.

of phase trajectories on various system parameters and a variety of initial conditions $(z_2, \frac{\partial z}{\partial \eta_2})_{\eta_2=0}$. The figures (6.3, 6.4, 6.5 and 6.6) show the influence of various parameters on the chaotic states of envelop solitons in phase portraits. The parametric range was taken where such stationary structures assumed significant variations. It is found from figure (6.3) that as the quantum diffraction parameter increases from $H=1.4$ to 2.4 (6.3 a), the phase portraits corresponding to Initial conditions, $IC=0,2$ & $0,-2$) becomes more chaotic. Such a system is relatable to the fact that higher the value of H , higher is the possibility of occurrence of quantum tunneling, which means that more electrons are free to execute randomised motion although the system started with an initially compact particle ensemble. The sudden reversal of phase trajectories in (ψ_2, z) plane which occurs at higher values of phase co-ordinates corresponding to higher H values reflect on the fact that reflections from the system boundaries. It is interesting to note that the phase reversals do not occur in the same path but follows a close-by yet separate trajectory. This type of quantum chaotic hysteresis is due to the fact that at such high densities, the states available to the system while moving in the forward direction is not available during the backward traversal in phase space, i.e. it has been occupied by segment of the system with different initial condition or those which have evolved in time. The information regarding such an occupied state is however missing with the present mathematical/theoretical formulation and may be termed as information loss. The dependence on hot-to-cold electron equilibrium density ratio (δ) is shown in figure (6.3 b). It is seen that the system takes different sets of trajectories [clockwise or anticlockwise w.r.t. δ axis] for unstable and stable initial conditions. The positive or negative values of $\frac{\partial z}{\partial \eta}$ corresponding to the stability domains. However, higher the stability/instability the more chaotic (or spread out) phase trajectories are opted. It reflects on the fact that the motion converges for extreme low or high values of δ . The chaotic motions corresponding to intermediate values of $\delta = 0.4 \rightarrow 0.6$ suggests that there is an exchange of energy among the hot and cold electron species, or in other words the hot electron because cold species by giving up randomness and acquiring less mobility and vice versa.

Figures (6.4a,b) shows the P3 plots for different values of degeneracy parameters of hot and cold electrons (F_h, F_c). It is to be noted that for a regular change of F_h value the already mobile hot electrons does not make the system more chaotic as it implies the less availability of states for randomised system. However, there are instances of sudden bursts of randomness which are statistical fluctuations and therefore less probable. However a shift in F_c takes the system to a more chaotic state and a quantum chaotic hysteresis is more pronounced. The restoring force which was to be contributed mainly by the hot electron species when shared by cold species, the initially inertial subsystem gains additional momentum and the state becomes more chaotic. In a nutshell the degeneracy parameters do not include orders of randomness to such a dense system. Figure (6.5) shows the effects of hot and cold electron viscosity parameters. Both these parameters retain the ordered system more or less around the initial point. There are limited signature of hysteresis and sometimes there are large scale fluctuations in a conservative system. The momenta in these states respond to those of a resonant state and thus there are almost circular/elliptical loops in the phase planes. The last P3 plot (6.6) correspond to variations of streaming motion (u_0) and initial disturbance's wavenumber (k). Here two interesting pictures are obtained. Firstly, if there is more streaming in the system the chaotic nature ceases manifold. This is due to the fact that the high longitudinal momenta within the wave makes the system less available a chaotic state, the initial disturbance is transported to the plasma wave and the randomised states are not available to the system. If the streaming is low there are almost circular phase trajectories (6.6 a) implying that both position and momentum undergo changes in the process. But as streaming increases the phase curves squeeze in ψ_2 axis and the variation is in the z-axis, i.e.; they are more localised with only degree of freedom being limited to the momenta axis. This is a beautiful finding as it implies that the motion is longitudinal only (the motion which is to and fro in nature) . A tilted view of figure (6.6a) will show a mode along the u_0 axis which suggests that at certain value of u_0 the motion almost ceases and the plasma system is like a dense compact matter. With reference to (6.6-b) it is

clear that as the fundamental wave becomes more energetic (high k) the system becomes chaotic with the additional energy fed to the system. To sum up these chaotic analysis provides with a number of additional information regarding such a dense system.

6.3 Bifurcation Analysis of EAWs in Degenerate Astrophysical Plasma: Chaos and Multistability

In space and astrophysical plasma, nonlinear ion-acoustic waves (IAWs) which are low frequency waves can exhibit chaotic dynamics, which have importance in telecommunication [238, 208]. Bifurcations of nonlinear travelling wave solutions in such plasmas were reported using dynamical systems theory [239]. By reducing the non-linear equation to a Hamiltonian system with electrostatic potential and applying the bifurcation theory of dynamical systems, various solitonic and quasiperiodic wave characteristics for ion-acoustic waves have been examined [240, 241, 199, 200]. In this section we have studied the effect of small perturbations on the system and have discussed the results with the help of phase portraits. In series of experiments on different properties of electron acoustic waves by F. Anderegg et.al [242], the experimental setup was as shown in figure 6.7. The trap is depicted in figure 6.7 as a series of hollow conducting cylinders held in ultrahigh vacuum. A mild "rotating wall" electric field applied to the sectored electrode keeps the plasma in a stable state for days. The revolving wall is turned off 100 milliseconds before each wave measurement and then turned back on 200 milliseconds later. Laser induced fluorescence (LIF) photons are gathered by optics perpendicular to the trap axis by a diagnostic laser beam parallel to the magnetic field close to the trap axis. The diagnosed volume is the intersection of the laser beam and the detection optics' viewing volume. And through this experiment they studied how the waves can be excited throughout a wide continuum of frequencies at moderate and great amplitude [242].

In an un-magnetized three-component degenerate dense plasma [177] with two groups

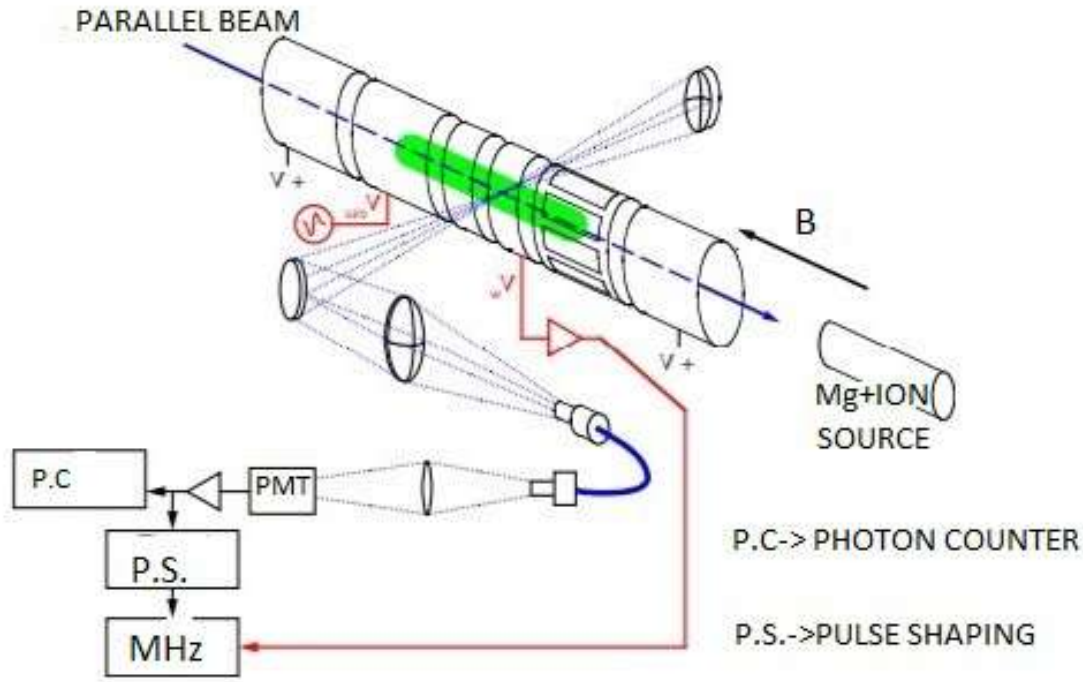


Figure 6.7: Experimental setup with coherent photon detection, adopted from F. Anderegg et.al [242]

of relativistic electrons at statistically different temperatures and stationary cold ions producing a uniform neutralising background, the propagation of electron-acoustic waves is examined. The quantum hydrodynamic (QHD) model equations that describe the behaviour of electron plasma waves in the model under consideration are given by [243, 180]

$$\frac{\partial (n_j)}{\partial t} + \vec{\nabla} \cdot (n_j \vec{u}_j) = 0 \quad (6.18)$$

$$\frac{\partial (\vec{u}_j)}{\partial t} + (\vec{u}_j \cdot \vec{\nabla}) (\vec{u}_j) = \frac{1}{m_e} \left[e \vec{\nabla} \phi - \frac{1}{n_j} \vec{\nabla} P_j + \frac{\hbar^2}{2m_e} \vec{\nabla} \left[\frac{\nabla^2 \sqrt{n_j}}{\sqrt{n_j}} \right] \right] \quad (6.19)$$

$$\nabla^2 \phi = 4\pi e (n_{ec} + n_{eh} - Z_i n_i) \quad (6.20)$$

The normalization scheme used is carried out as done by earlier researchers [171, 182] $x \rightarrow x\omega_c/c_{sh}$, $t \rightarrow t\omega_c$, $\phi \rightarrow e\phi/2k_B T_{Fh}$, $n_j \rightarrow n_j/n_{j0}$, $n_i \rightarrow n_i/n_{i0}$, $u_j \rightarrow u_j/c_{sh}$.

Here $\omega_{ec} = \sqrt{4\pi n_{ec0} e^2 / m_e}$ and $c_{sh} = \sqrt{2k_B T_{Feh} / m_e}$ and the set of normalized equations obtained are:

$$\frac{\partial (n_j)}{\partial t} + \frac{\partial (n_j u_j)}{\partial x} = 0 \quad (6.21)$$

$$\left(\frac{\partial}{\partial t} + u_j \frac{\partial}{\partial x} \right) u_j = \frac{\partial \phi}{\partial x} - F_j \frac{\partial n_j}{\partial x} + \frac{H^2}{2} \frac{\partial}{\partial x} \left[\frac{1}{\sqrt{n_j}} \frac{\partial^2 \sqrt{n_j}}{\partial x^2} \right] \quad (6.22)$$

$$\frac{\partial^2 \phi}{\partial x^2} = \left(n_{ec} + \frac{n_{eh}}{\delta} - n_i \frac{\delta_1}{\delta} \right) \quad (6.23)$$

where, $F_j = (\chi_e/3) \left(R_{j0}^2 / \sqrt{1 + R_{j0}^2} \right)$ is the term arising from relativistic pressure in weakly relativistic case, whereas for ultra relativistic case $F_j = \chi_e R_{j0} / 3$ where $\chi_e = m_e c^2 / 2k_B T_{Feh}$; $H = \hbar \omega_{ec} / 2k_B T_{Feh}$ is a non-dimensional quantum diffraction parameter, $\delta = n_{e0} / n_{h0}$ and $\delta_i = Z n_{i0} / n_{h0}$, T_{Feh} is the Fermi temperature of hot electrons and suffix $j=eh, ec$ stand for hot and cold electron species. In fully degenerate and relativistic configurations, the electron degeneracy pressure can be represented as follows :

$$P_j = (\pi m_e^4 c^5 / 3h^3) \left[R_j (2R_j^2 - 3) \sqrt{1 + R_j^2} + 3 \sinh^{-1} R \right] \quad (6.24)$$

where,

$$R_j = p_{Fj} / m_e c = [3h^3 n_j / 8\pi m_e^3 c^3]^{1/3} = R_{j0} n_j^{1/3} \quad (6.25)$$

in which $R_{j0} = (n_{j0} / n_0)^{1/3}$ with $n_0 = 8\pi m_e^3 c^3 / 3h^3$, 'c' being the speed of light in vacuum. p_{Fj} is the electron Fermi relativistic momentum [212, 173]. Therefore, the relativity pressure in ultra relativistic case is given by

$$P_j = \frac{1}{8} \left(\frac{3}{\pi} \right)^{1/3} h c n_j^{4/3} \quad (6.26)$$

It's worth remembering that electron number density, not electron temperature, determines the degenerate electron pressure.

6.3.1 Derivation of KdV equation

To investigate the non-linear behaviour of electron acoustic waves, we use inertia-less hot ultra relativistic electrons, inertial cold electrons and stationary ions. The heated electrons are thought to be the only cause of the pressure effect [188]. Using standard stretching variables of space and time [195, 244],

$$\xi' = \varepsilon^{1/2} (x - V_0 t) \quad \text{and} \quad \tau_1 = \varepsilon^{3/2} t \quad (6.27)$$

and perturbation expansion

$$\begin{bmatrix} n_j \\ u_j \\ \phi \end{bmatrix} = \begin{bmatrix} 1 \\ 0 \\ 0 \end{bmatrix} + \varepsilon \begin{bmatrix} n_j^{(1)} \\ u_j^{(1)} \\ \phi^{(1)} \end{bmatrix} + \varepsilon^2 \begin{bmatrix} n_j^{(2)} \\ u_j^{(2)} \\ \phi^{(2)} \end{bmatrix} + \dots \quad (6.28)$$

the KdV equation obtained is [245, 179]:

$$\frac{\partial \phi}{\partial \tau_1} + A' \phi \frac{\partial \phi}{\partial \xi'} + B' \frac{\partial^3 \phi}{\partial \xi'^3} = 0 \quad (6.29)$$

where,

$$A' = -\frac{3}{2V_0} = -\frac{3}{2\sqrt{\delta\chi_e R_{eh0}/3}},$$

$$B' = \frac{V_0^4 - (1+\delta)H^2/4}{2V_0} = \frac{(\delta\chi_e R_{eh0}/3)^2 - (1+\delta)H^2/4}{2\sqrt{\delta\chi_e R_{eh0}/3}}$$

We know the standard solution is given by [63]

$$\phi = \phi_m \operatorname{sech} h^2 \left(\frac{\eta'}{\Delta} \right) \quad (6.30)$$

where $\eta' = \xi' - M_1 \tau_1$ the amplitude ϕ_m and width Δ of the soliton are given by: $\phi_m =$

$$3\frac{M_1}{A'} \text{ and } \Delta = \sqrt{\frac{4B'}{M_1}}$$

A balance between dispersive and non-linear processes creates the single wave structure. The feature of such a solitary wave structure is determined by the relative strength of these two influences, which is in harmony with our previous studies [122].

6.3.2 Dynamical systems of Electron Acoustic Forced-KdV

Unperturbed system:

To obtain the dynamical system based on KdV equation, we now study a traveling wave solution. For this, we use the transformation $\eta' = \xi' - M_1\tau_1$ with the usual boundary conditions as $\eta' \rightarrow \pm\infty, \psi' \rightarrow 0, \frac{\partial\psi'}{\partial\eta'} \rightarrow 0, \frac{\partial^2\psi'}{\partial\eta'^2} \rightarrow 0$ where M_1 is the velocity of the wave frame. Using this transformation and integrating the KdV equations twice with respect to η' we obtain.

$$\frac{\partial^2\psi'}{\partial\eta'^2} = P_1\psi' - Q_1\psi'^2 \quad (6.31)$$

$$\text{where } P_1 = \frac{M_1}{B'} = \frac{M_1\sqrt{\delta\chi_e R_{eh0}/3}}{(\delta\chi_e R_{eh0}/3)^2 - (1+\delta)H^2/4}$$

$$, Q_1 = \frac{A'}{2B'} = \frac{3}{2((\delta\chi_e R_{eh0}/3)^2 - (1+\delta)H^2/4)},$$

Now the Eqn. (6.31) can be transformed into dynamical system of the form

$$\frac{\partial\psi'}{\partial\eta'} = z' \quad (6.32)$$

$$\frac{\partial z'}{\partial\eta'} = P_1\psi' - Q_1\psi'^2 \quad (6.33)$$

The system will be conservative if the divergence of the field is zero i.e. $\vec{\nabla} \cdot \vec{F}' = 0$, where $\vec{F}' = (z', P_1\psi' - Q_1\psi'^2)$. Hence, the Hamiltonian of the system is given by:

$$H'(\psi', z') = \frac{z'^2}{2} - \frac{P_1\psi'^2}{2} + \frac{Q_1\psi'^4}{4} \quad (6.34)$$

Since the phase plots describes all equations of EAWs with different initial conditions,

we plan to study the bifurcation of phase trajectories for different parameters and initial conditions. When a tiny smooth change to a system's parameter values (the bifurcation parameters) generates an abrupt 'qualitative' or topological change in its behaviour, it is termed as bifurcation [246, 247, 178].

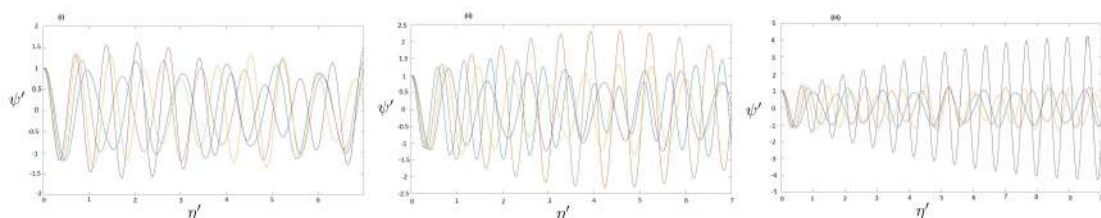


Figure 6.8: Supernonlinear wave solution corresponding to dynamical system for Forced KdV equation (i) with different values of parameter $R_{eh0} = 4$ (Blue), 6(Pink), 8(Orange), 9(Purple) with value of other parameters $H=2.2, \chi_e=0.8, f_0=1, \omega=10$ (ii) with different values of parameter $H= 1.8$ (Blue), 2(Pink), 2.2(Orange), 2.4(Purple) with value of other parameters $\chi_e=0.8, R_{eh0}=8, f_0=1, \omega = 10$ (iii) with different values of parameter $\delta= 0.1$ (Blue), 0.2(Pink), 0.3(Orange), 0.4(Purple) with value of other parameters $H=2.2, \chi_e=0.8, R_{eh0}=8, f_0=1, \omega=10$

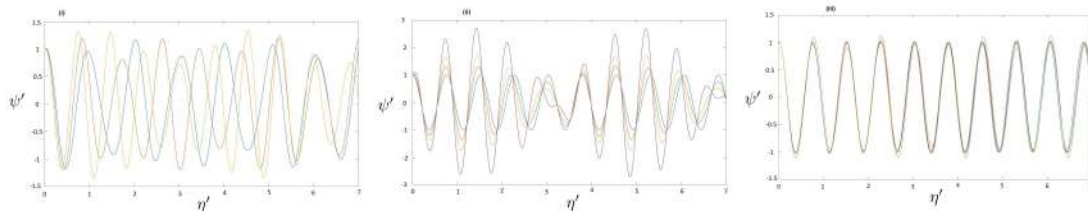


Figure 6.9: Supernonlinear wave solution corresponding to dynamical system for Forced KdV equation (i) with different values of parameter $\chi_e = 0.4$ (Blue), 0.6(Pink), 0.8(Orange) with value of other parameters $H = 2.2, \chi_e = 0.8, R_{eh0} = 8, f_0 = 1, \omega = 10$ (ii)with different values of parameter $f_0 = 0$ (Blue), 1(Pink), 2(Orange), 4(Purple) with value of other parameters $H = 2.2, \chi_e = 0.8, R_{eh0} = 8, \omega = 10$ (iii)with different values of parameter $\omega = 0$ (Blue), 0.5(Pink), 1(Orange), 2(purple), 3(Dark Blue) with value of other parameters $H = 2.2, \chi_e = 0.8, R_{eh0} = 8, f_0 = 1$.

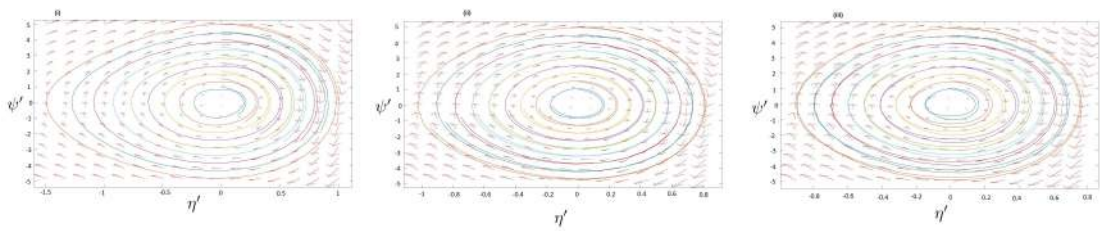


Figure 6.10: Phase portrait of Forced KdV for different values of (i) $R_{eh0}=6$, (ii) $R_{eh0}=9$, (iii) $R_{eh0}=10$ for different parameters $H=2.2$, $\chi_e=0.8$, $f_0=1$, $\omega = 10$

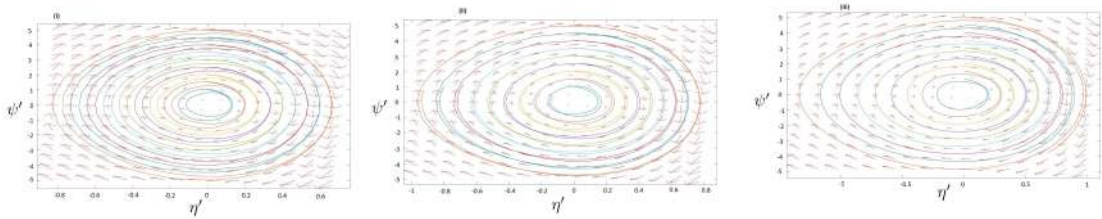


Figure 6.11: Phase portrait of Forced KdV for different values of (i) $H=1.8$, (ii) $H=2$, (iii) $H=2.4$ for different parameters $\chi_e=0.8$, $R_{eh0}=8$, $f_0=1$, $\omega = 10$

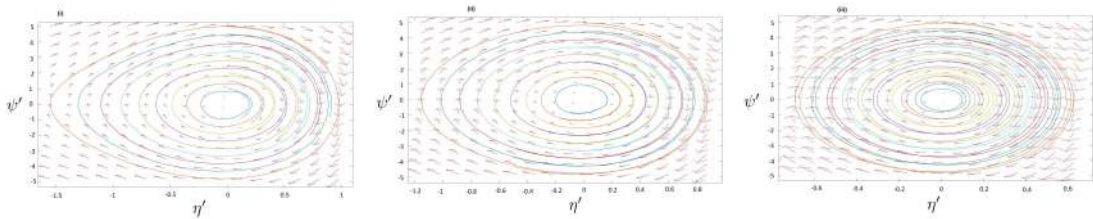


Figure 6.12: Phase portrait of Forced KdV for different values of (i) $\delta=0.1$, (ii) $\delta=0.2$, (iii) $\delta=0.3$ for different parameters $H=2.2$, $\chi_e=0.8$, $R_{eh0}=8$, $f_0=1$, $\omega = 10$

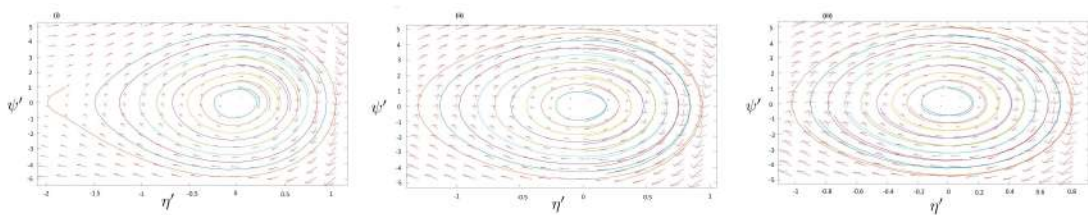


Figure 6.13: Phase portrait of Forced KdV for different values of (i) $\chi_e=0.5$, (ii) $\chi_e=0.7$, (iii) $\chi_e=0.9$ for different parameters $H=2.2$, $R_{eh0}=8$, $f_0=1$, $\omega = 10$

Perturbed system:

The effects of external force on a system are of great interest. Various kind of external forces may have various effects. In this study, the external force provided is $f_0 \cos(\omega_1 \eta')$

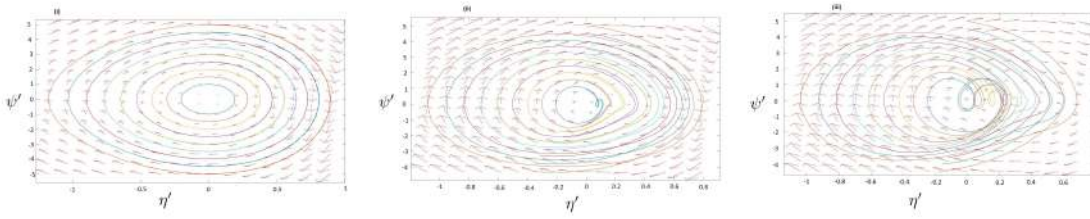


Figure 6.14: Phase portrait of Forced KdV for different values of (i) $f_0=0$ (ii) $f_0=5$, (iii) $f_0=10$ for different parameters $H=2.2, \chi_e=0.8, R_{eh0}=8, f_0=1, \omega = 10$

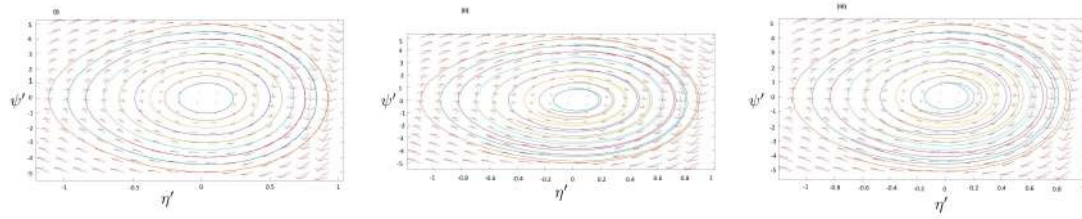


Figure 6.15: Phase portrait of Forced KdV for different values of (i) $\omega=0$, (ii) $\omega=2$, (iii) $\omega=3$ for different parameters $\chi_e=0.8, R_{eh0}=8, f_0=1$

[239]. Hence, we get

$$\frac{\partial z'}{\partial \eta'} = P_1 \psi - Q_1 \psi'^3 + f_0 \cos(\omega_1 \eta') \quad (6.35)$$

$$\frac{\partial \psi'}{\partial \eta'} = z'$$

The external perturbation is η' dependent, f_0 is the strength of the perturbation and ω_1 is the compounding frequency. Figure (6.8) shows how the increase in the value of R_{eh0} leads to increase in frequency and amplitude of the structure leading to increased dispersive effects and giving rise to some kind of an envelope wave [169, 248]. The increase in the value of quantum diffraction parameter (H) which is related to plasmonic energy leads to fluctuation and amplitude variation. The value of δ (cold to hot electron equilibrium number density ratio) upto $\delta=0.3$ gives stable modes with no much fluctuations but further increase leads to unstable modes with increasing amplitude. In figure 6.9 is the strongly coupled system in which the increase in χ_e (inversly proportional to thermal energy) leads to increase in Debye length (λ_D) giving rise to region of electric field that is the sphere of influence in the system. The increasing strength of perturbation

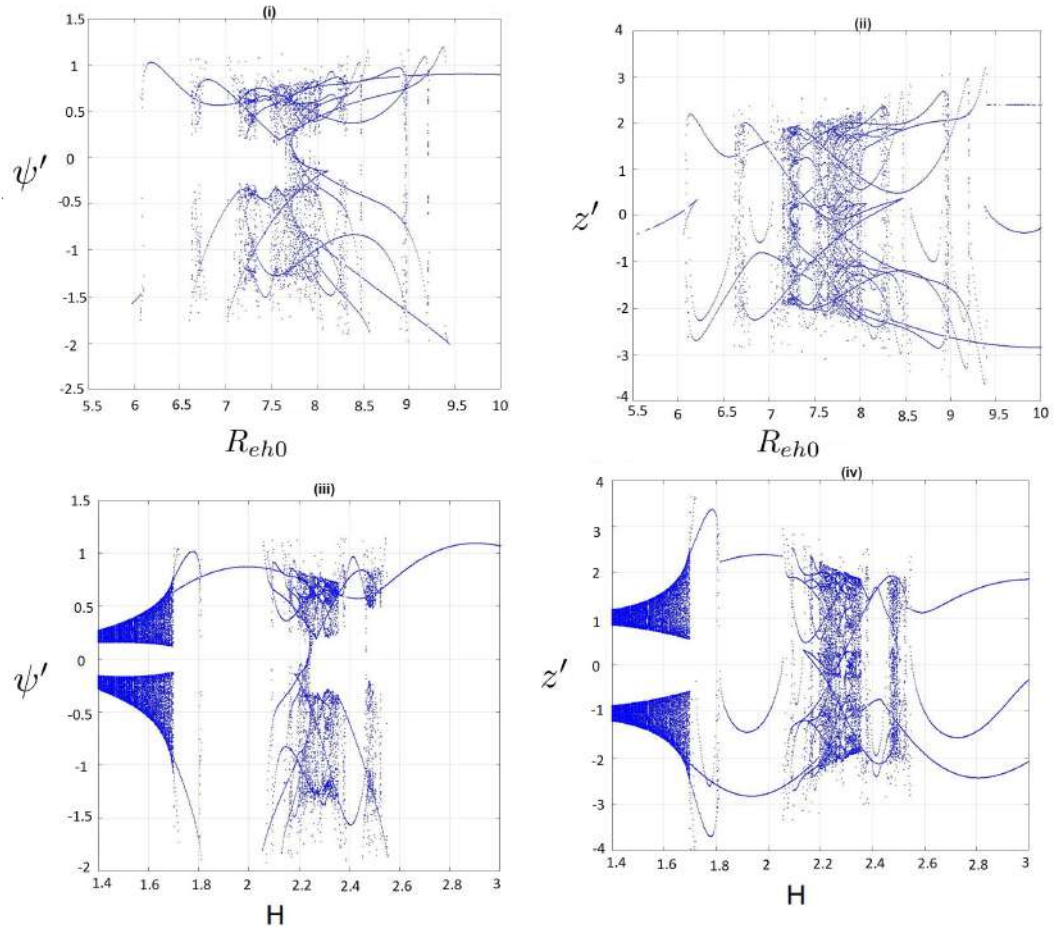


Figure 6.16: Bifurcation plots for ψ' and z for Forced KdV with variation in R_{eh0} and H for value of different parameters $\chi_e=0.8$, $f_0=0.8$, $\omega=2.5$

(f_0) increases the amplitude of the structure leaving the spatial frequency approximately unchanged and the compounding frequency does not affect the structures as the plasma is highly dense. Equation (6.35) compared to non autonomous system, can be related to corresponding autonomous system defined through the condition

$$\frac{\partial \xi'}{\partial \eta'} = 1 \quad (6.36)$$

Hence ψ' , η' and ξ' are state variables. From Eqn. (6.36), it is clear that the system has no equilibrium points, thereby suggesting the probability of hidden attractors. In figure 6.10, different initial conditions are having almost closed loop. Because of the external

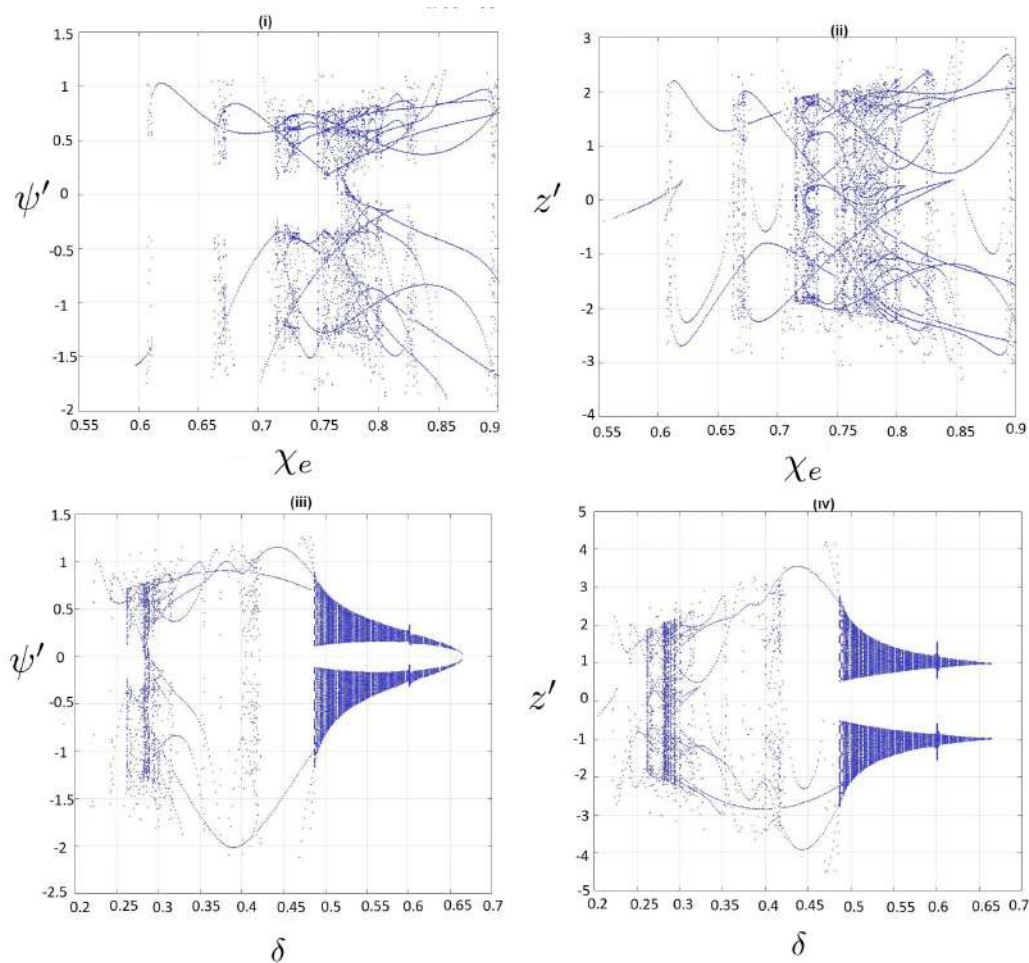


Figure 6.17: Bifurcation plots for ψ' and z for Forced KdV with variation in χ_e and δ for value of different parameters $H=2.2$, $R_{eh0}=8$, $f_0=0.8$, $\omega=2.5$

force provided, the phase portrait is tending to double the period in loop. It is because with increase in value of R_{eh0} , the external perturbation applied has ability to increase the frequency and hence provide extra energy to the system. Such a fluctuation in initial path could be studied through Lyapunov exponent [249]. To study such chaotic motions in detail [190, 189], the use of Lyapunov exponents is an effective tool as it characterizes the rate of separation of infinitesimally close trajectories. As z is directly proportional to electric field, we are getting two different values of electric field for same value of ψ' in figure 6.11, leading to degeneracy which is due to the non-linear mechanism in high energy plasma. The lesser value of δ leads to lesser inertia but as the value of δ rises, period-doubling bifurcation comes into play.

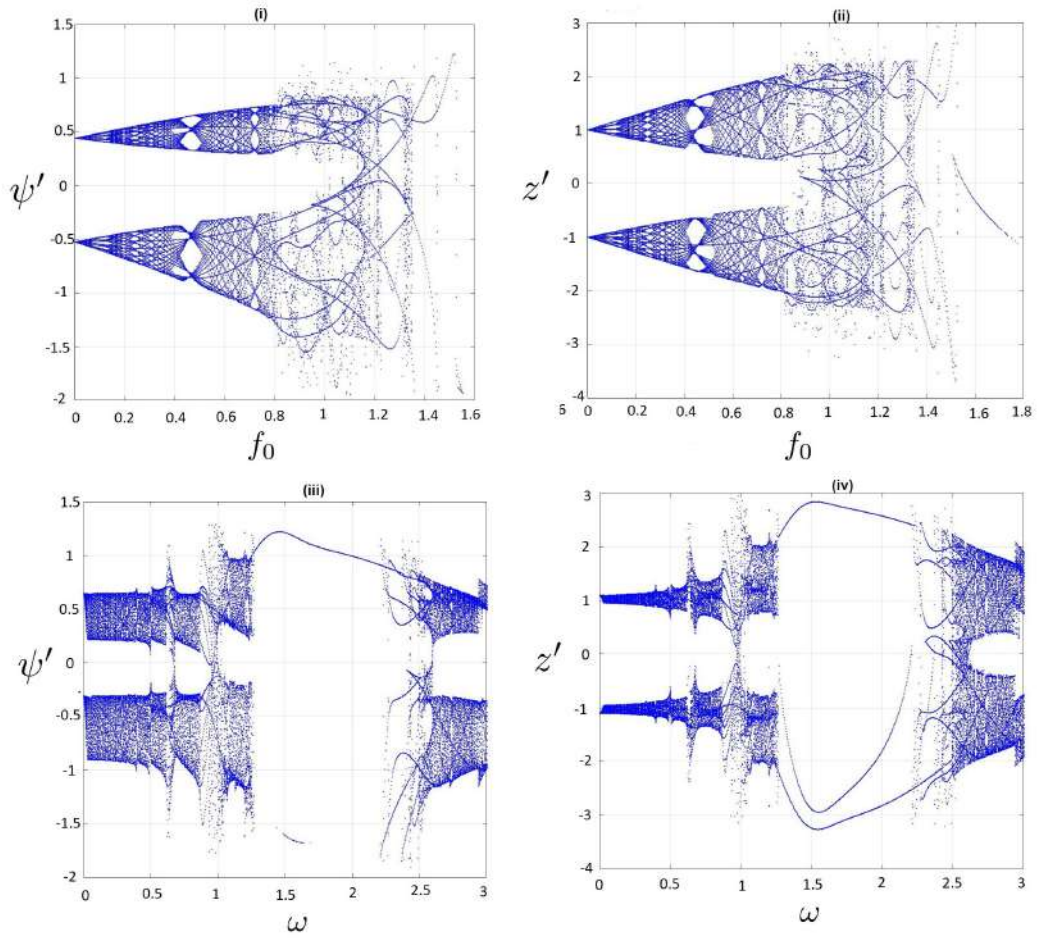


Figure 6.18: Bifurcation plots for ψ' and z for Forced KdV with variation in f_0 and ω for value of different parameters $H=2.2$, $\chi_e=0.8$, $R_{eh0}=8$,

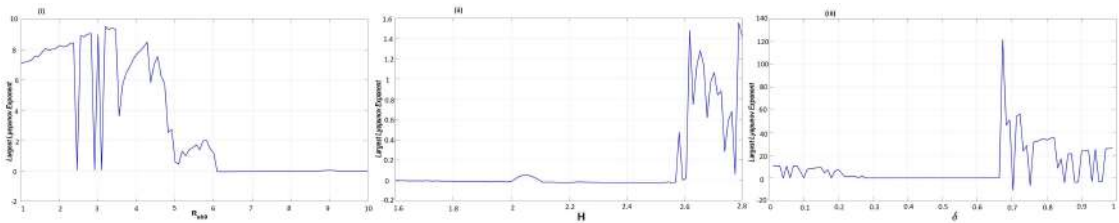


Figure 6.19: Largest Lyapunov exponent for Forced KdV for values of different parameters (i) $H=2.2$, $\chi_e=1$, $R_{eh0}=10$, $f_0=0.8$, $\omega=0.8$, (ii) $H=2.8$, $\chi_e=1$, $R_{eh0}=8$, $f_0=0.8$, $\omega=0.8$, (iii) $H=2.2$, $\chi_e=1$, $R_{eh0}=8$, $f_0=0.8$, $\omega=0.8$

In figure 6.13, for lesser value of χ_e , the thermal energy is greater and hence not enclosed inside the system whereas as χ_e increases, the thermal energy decreases and hence the system is more symmetric which is what stated in second law of thermodynamics. Figure 6.14 demonstrates that increasing the external force leads to period-doubling

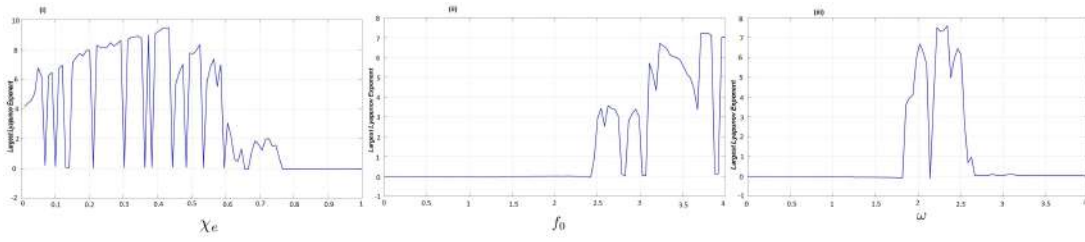


Figure 6.20: Largest Lyapunov exponent for Forced KdV for values of different parameters (i) $H=2.2$, $\chi_e=1$, $R_{eh0}=8$, $f_0=1$, $\omega=0.8$, (ii) $H=2.2$, $\chi_e=1$, $R_{eh0}=8$, $f_0=4$, $\omega=0.8$, (iii) $H=2.2$, $\chi_e=1$, $R_{eh0}=8$, $f_0=1$, $\omega=4$

bifurcation, which occurs when a little change in a system’s properties allows a new periodic trajectory to emerge from an existing periodic trajectory with twice the period of the original. At $\omega=0$ in figure 6.15, there is a constant force being applied to system and hence momentum is linearly increasing with time making the phase lead as the potential energy stored is getting converted into the Kinetic energy. Figures (6.16-6.18) show the range of bifurcation having periods of order and disorder. In fig.6.16, quantum diffraction parameter does not seem to contribute much to either chaotic or ordered pattern from range 1.6 to 2. Higher to this value, the bifurcation is in pure quantum regime. The bifurcation curve converges to a single point in both cases with increase in δ as well as ω .

Figures 6.19 and 6.20 shows the largest Lyapunov exponent that is the value of Lyapunov exponent for given parameter for which the system is chaotic. The influence of parameter R_{eh0} is such that the LLP ceases to determine if the system is chaotic or ordered after value 6. And H begins to determine if the factor is chaotic or ordered after value 2. In case of δ , for lower values of δ , the number density of cold electrons decreases and increases if value of δ is high. In between there is an equilibrium of number density of cold to hot electrons and hence the system is more ordered. Now in figure 6.20, when the value of χ_e is less that (i.e. thermal energy is high, higher than the rest energy), the system is more chaotic. And in case of external force, when the external force applied is higher, the system will be chaotic in nature.

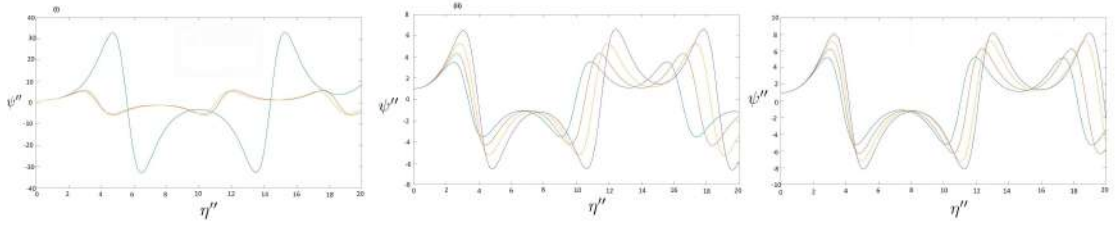


Figure 6.21: Supernonlinear wave solution corresponding to dynamical system for NLSE (i) with different values of parameter $R_{eh0}=4$ (Blue), 6(Pink), 8(Orange), 9(Purple) with value of other parameters $H=2.2$, $\delta=0.3$, $k=0.5$, $\chi_e=0.8$, $R_{ec0}=2$, $F_{ec}=0.35703$, $F_{eh}=2.1333$, (ii) with different values of parameter $H=1.8$ (Blue), 2(Pink), 2.2(Orange), 2.4(Purple) with value of other parameters $\delta=0.3$, $\chi_e=0.8$, $R_{eh0}=8$, $R_{ec0}=2$, $F_{ec}=0.35703$, $F_{eh}=2.1333$ (iii) with different values of parameter $\delta=0.1$ (Blue), 0.2(Pink), 0.3(Orange), 0.4(Purple) with value of other parameters $H=2.2$, $\chi_e=0.8$, $R_{eh0}=8$, $R_{ec0}=2$, $F_{ec}=0.44983$, $F_{eh}=2.1333$

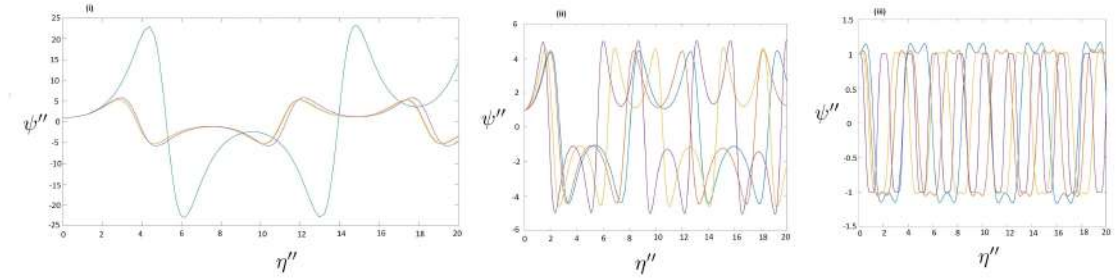


Figure 6.22: Supernonlinear wave solution corresponding to dynamical system for NLSE (i) with different values of parameter $\chi_e=0.4$ (Blue), 0.6(Pink), 0.8(Orange) with value of other parameters $H=2.2$, $\delta=0.3$, $k=0.5$, $R_{eh0}=8$, $R_{ec0}=2$, $F_{ec}=0.35703$, $F_{eh}=2.1333$, (ii)with different values of parameter $k=0.05$ (Blue), 0.1(Pink), 0.12(Orange), 0.125(Purple) with value of other parameters $H=2.2$, $\delta=0.3$, $\chi_e=0.8$, $R_{eh0}=8$, $R_{ec0}=2$, $F_{ec}=0.35703$, $F_{eh}=2.1333$, (iii)with different values of parameter $\omega=2$ (Blue), 3(Pink), 4(Orange), 10(purple) with value of other parameters $H=2.2$, $\chi_e=0.8$, $R_{eh0}=8$, $R_{ec0}=2$, $F_{ec}=0.35703$, $F_{eh}=2.1333$

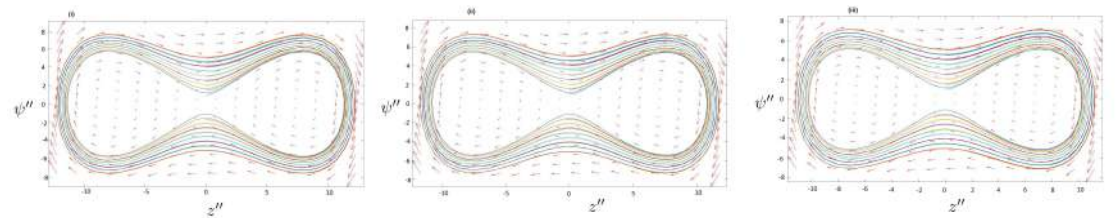


Figure 6.23: Phase portrait of NLSE for different values of (i) $R_{eh0}=6$, (ii) $R_{eh0}=7$, (iii) $R_{eh0}=9$ for different parameters $H=2.2$, $\delta=0.3$, $\chi_e=0.8$, $k=0.5$, $R_{ec0}=2$, $F_{ec}=0.35703$, $F_{eh}=1.6$

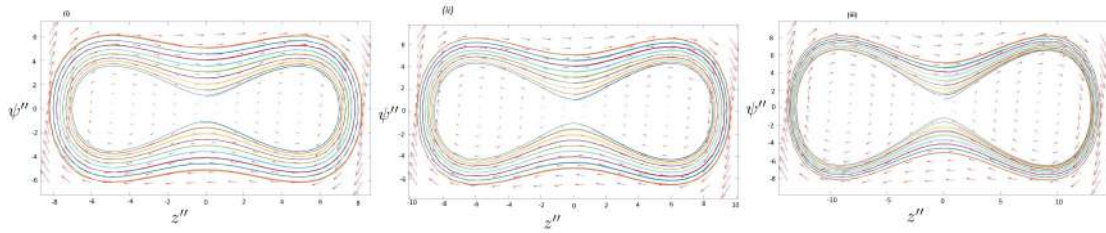


Figure 6.24: Phase portrait of NLSE for different values of (i) $H=1.8$, (ii) $H=2$, (iii) $H=2.4$ for different parameters $R_{eh0}=8$, $\delta=0.3$, $\chi_e=0.8$, $k=0.5$, $R_{ec0}=2$, $F_{ec}=0.35703$, $F_{eh}=2.1333$

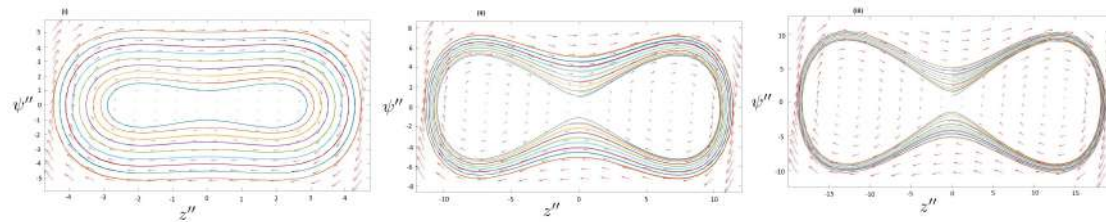


Figure 6.25: Phase portrait of NLSE for different values of (i) $\delta=0.03$, (ii) $\delta=0.3$, (iii) $\delta=0.7$ for different parameters $H=2.2$, $\chi_e=0.8$, $k=0.5$, $R_{eh0}=8$, $R_{ec0}=2$, $F_{ec}=0.35703$, $F_{eh}=2.1333$

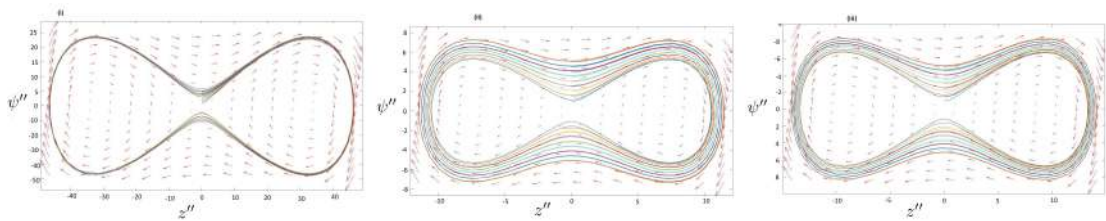


Figure 6.26: Phase portrait of NLSE for different values of (i) $\chi_e=0.4$, (ii) $\chi_e=0.6$ (iii) $\chi_e=1$ for different parameters $H=2.2$, $\delta=0.3$, $k=0.5$, $R_{eh0}=8$, $R_{ec0}=2$, $F_{ec}=0.35703$, $F_{eh}=2.1333$

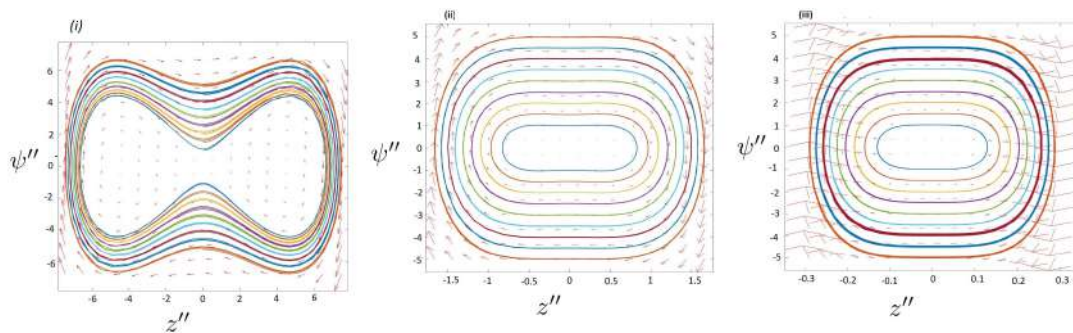


Figure 6.27: Phase portrait of NLSE for different values of (i) $k=0.05$, (ii) $k=2$, (iii) $k=6$ for different parameters $H=2.2$, $\delta=0.3$, $\chi_e=0.8$, $R_{eh0}=8$, $R_{ec0}=8$, $F_{ec}=1.4281$, $F_{eh}=2.1333$

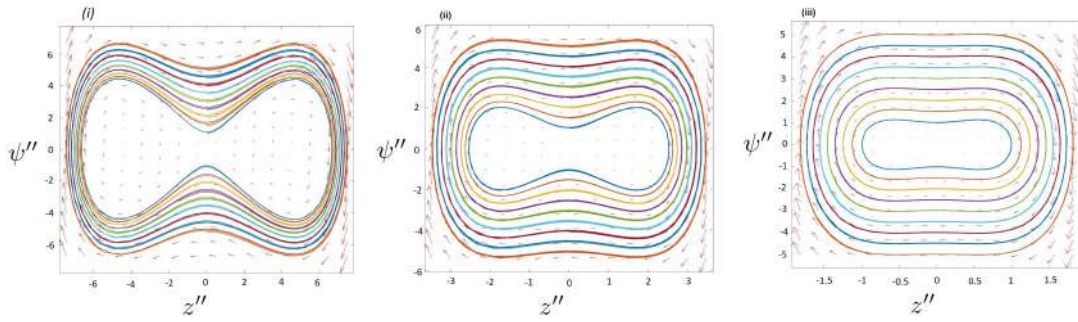


Figure 6.28: Phase portrait of NLSE for different values of (i) $\omega=0.5$, (ii) $\omega=0.9$, (iii) $\omega=2$ for different parameters $H=2.2$, $\chi_e=0.8$, $R_{eh0}=8$, $R_{ec0}=8$, $F_{ec}=1.4281$, $F_{eh}=2.1333$

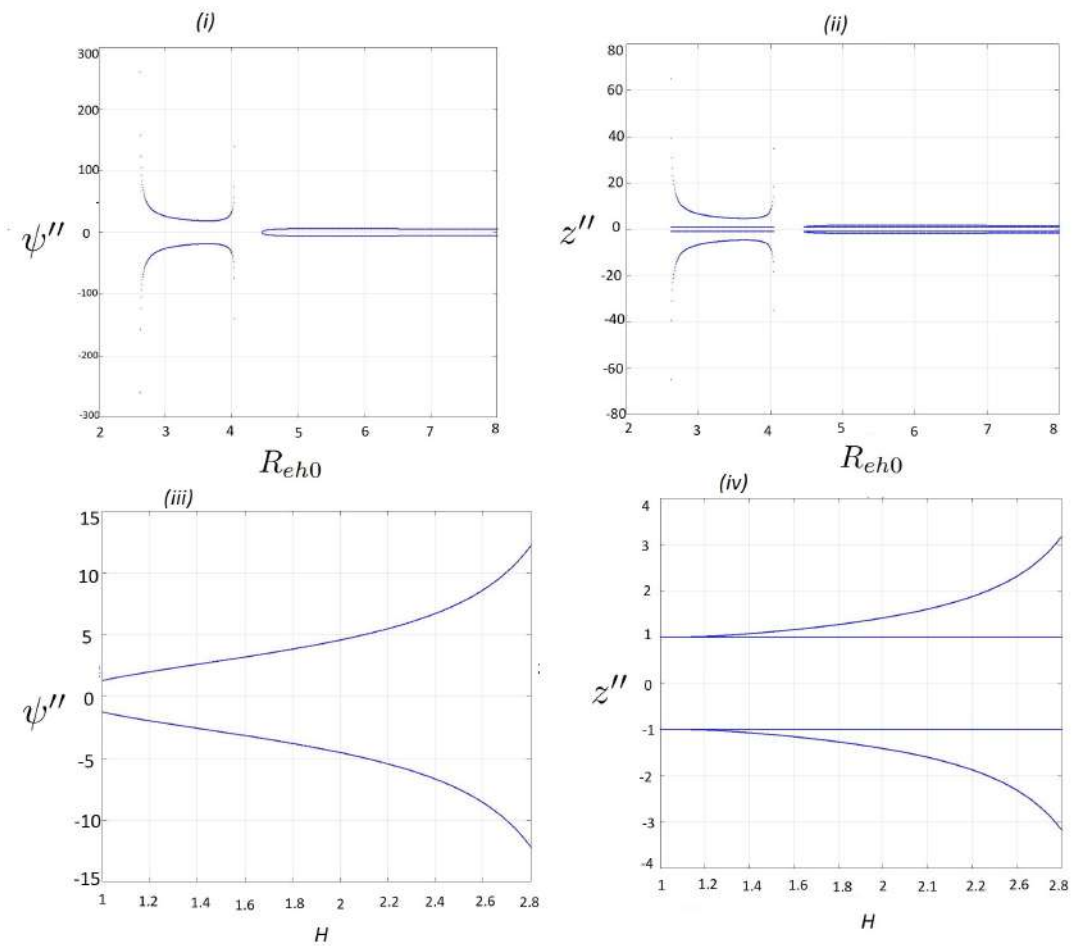


Figure 6.29: Bifurcation plots of NLSE for ψ'' and z for FKdV with variation in R_{eh0} and H for value of different parameters $\chi_e=0.8$, $\delta=0.3$, $k=0.5$, $F_{ec}=0.35703$, $F_{eh}=2.1333$

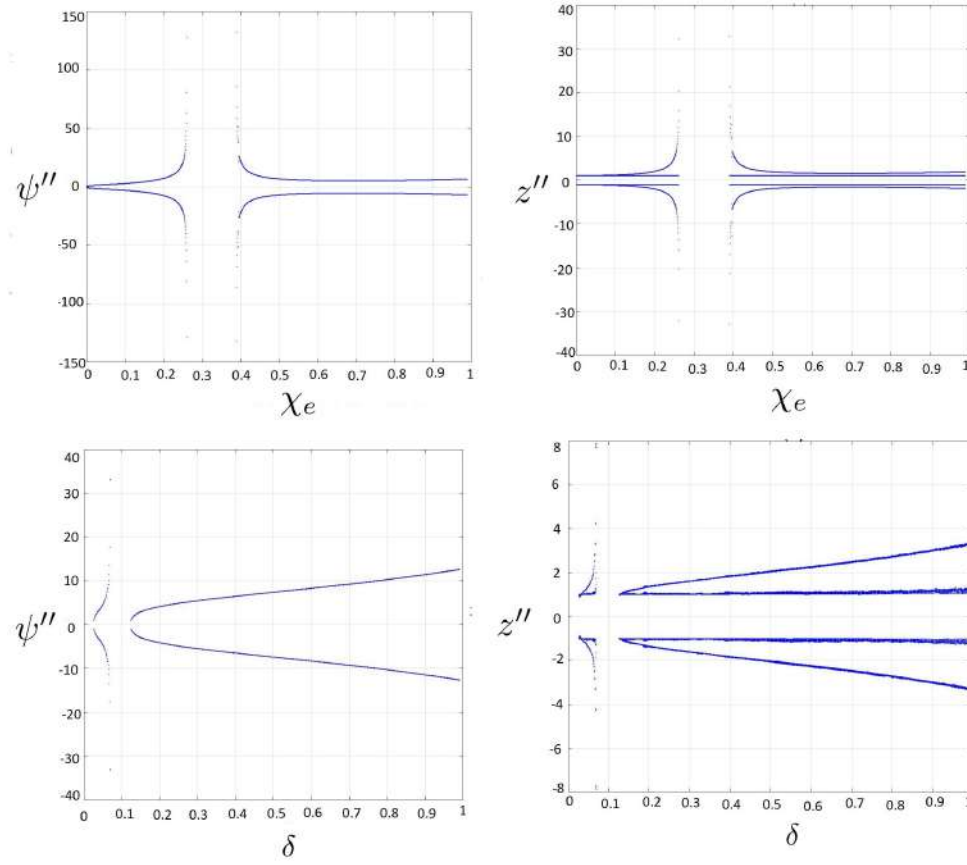


Figure 6.30: Bifurcation plots for ψ'' and z for FKdV with variation in χ_e and δ for value of different parameters $H=2.2$, $k=0.5$, $R_{eh0}=8$, $R_{ec0}=2$, $F_{ec}=0.44183$, $F_{eh}=2.13333$

6.3.3 Analytic derivation of NLSE

We want to look at how an electron acoustic wave evolves non-linearly. Higher harmonic production arises from the carrier wave's nonlinear self-interaction in the background plasma [216, 215]. The field variables are expanded using the Fourier method as follows:

$$\begin{bmatrix} n_j \\ u_j \\ \phi \end{bmatrix} = \begin{bmatrix} 1 \\ 0 \\ 0 \end{bmatrix} + \varepsilon^2 \begin{bmatrix} n_{j0} \\ u_{j0} \\ \phi_0 \end{bmatrix} + \sum_{s=1}^{\infty} \varepsilon^s \left\{ \begin{bmatrix} n_{js} \\ u_{js} \\ \phi_s \end{bmatrix} \exp(is\theta) + \begin{bmatrix} n_{js}^* \\ u_{js}^* \\ \phi_s^* \end{bmatrix} \exp(-is\theta) \right\} \quad (6.37)$$

where $\theta = k_1 x - \omega_1 t$, the field quantities $n_{j0}, u_{j0}, \phi_0, n_{js}, u_{js}$ are expected to change

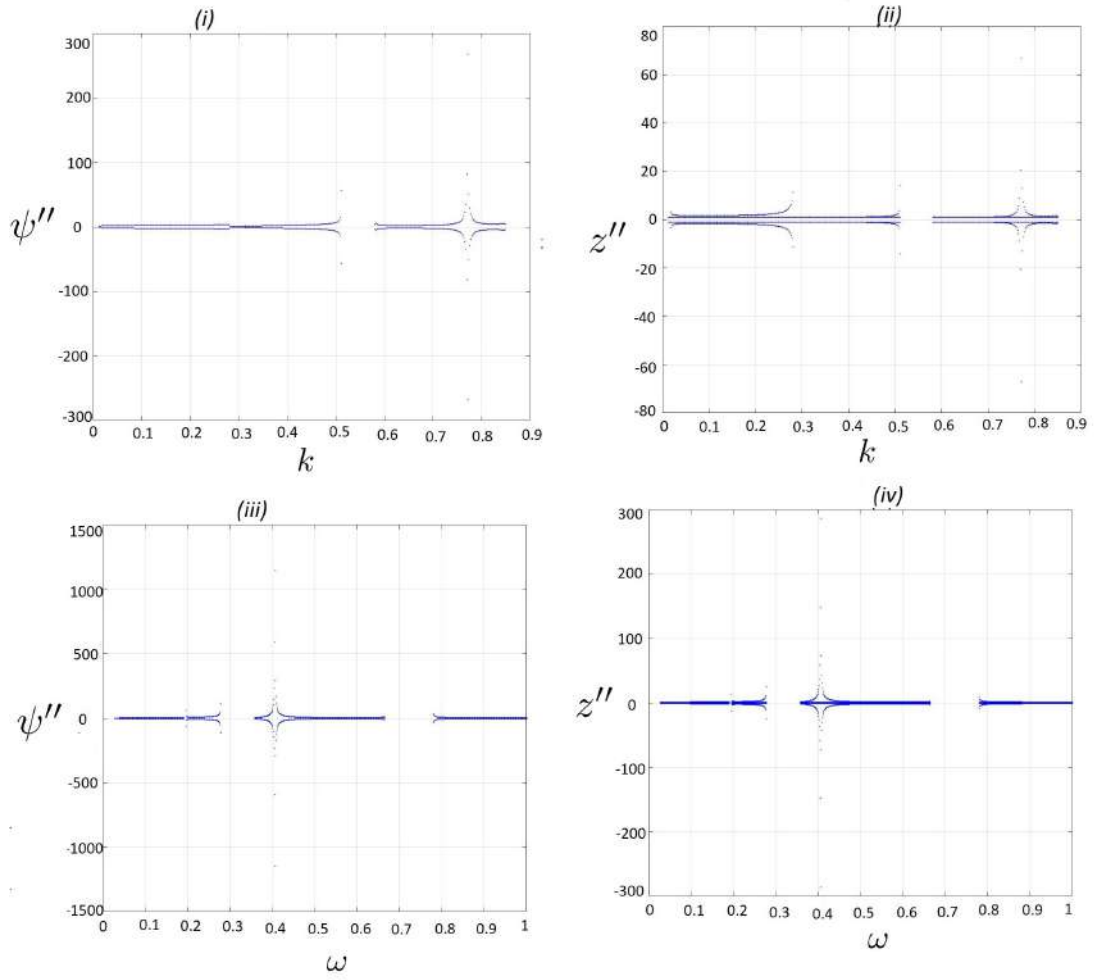


Figure 6.31: Bifurcation plots for ψ'' and z for FKdV with variation in k and ω for value of different parameters $H=2.2$, $\delta=0.3$, $\chi_e=0.8$, $R_{eh0}=8$, $R_{ec0}=2$, $F_{ec}=0.35703$, $F_{eh}=2.13333$

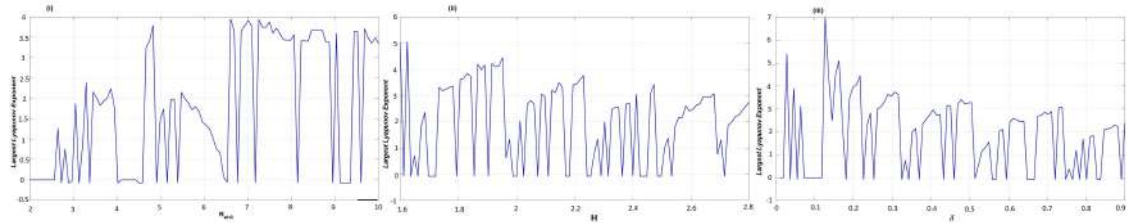


Figure 6.32: Largest Lyapunov exponent for values of different parameters (i) $H=2.2$, $\delta=0.3$, $\chi_e=0.8$, $k=0.5$, $R_{eh0}=10$, $R_{ec0}=2$, $F_{ec}=0.35703$, $F_{eh}=2.6667$, (ii) $H=2.8$, $\delta=0.3$, $\chi_e=0.8$, $k=0.5$, $R_{eh0}=8$, $R_{ec0}=2$, $F_{ec}=0.35703$, $F_{eh}=2.1333$, (iii) $H=2.2$, $\delta=0.9$, $\chi_e=0.9$, $k=0.5$, $R_{eh0}=8$, $R_{ec0}=2$, $F_{ec}=0.51493$, $F_{eh}=2.1333$

slowly when x and t change, i.e. they're supposed to be functions of

$$\xi'' = \varepsilon (x - c_g t) \quad \text{and} \quad \tau_2 = \varepsilon^2 t \quad (6.38)$$

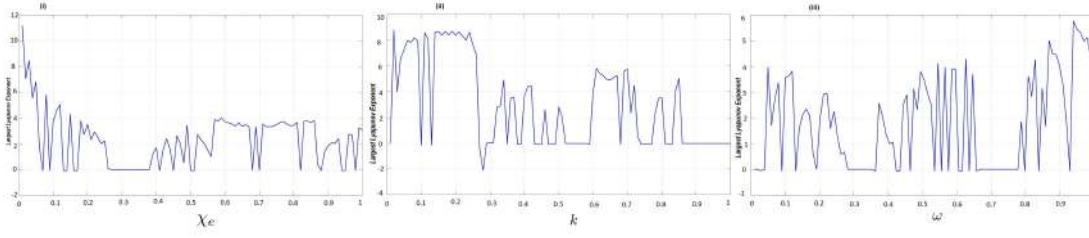


Figure 6.33: Largest Lyapunov exponent for values of different parameters (i) $H=2.2$, $\delta=0.3$, $\chi_e=1$, $k=0.5$, $R_{eh0}=8$, $R_{ec0}=2$, $F_{ec}=0.44629$, $F_{eh}=2.6667$, (ii) $H=2.2$, $\delta=0.3$, $\chi_e=0.8$, $k=1$, $R_{eh0}=8$, $R_{ec0}=2$, $F_{ec}=0.35703$, $F_{eh}=2.1333$, (iii) $H=2.2$, $\delta=0.3$, $\chi_e=0.8$, $k=0.5$, $R_{eh0}=8$, $R_{ec0}=2$, $F_{ec}=0.35703$, $F_{eh}=2.1333$

where ϵ is a smallness parameter and $c_g = \frac{d\omega}{dk}$ is the normalized group velocity. Using standard multiple scale perturbation technique we re-derive the NLSE as [202]

$$i \frac{\partial \phi_2}{\partial \tau_2} + P_2 \frac{\partial^2 \phi_2}{\partial \xi''^2} = Q_2 \phi_2^2 \phi_2^* \quad (6.39)$$

where values of P_2 and Q_2 are

$$P_2 = \frac{1}{2} \frac{dc_g}{dk} = \frac{1 + (A_{ec}/\Omega_{ec}) + (A_{eh}/\delta \cdot \Omega_{eh})}{2\omega [(1/\Omega^2) + (1/\Omega_{ec}^2)]} \quad (6.40)$$

and

$$Q_2 = \frac{(N_{ec}/\Omega_{ec}) + (N_{eh}/\delta \Omega_{ec})}{2\omega [(1/\Omega_{ec}^2) + (1/\Omega_{e\epsilon}^2)]} \quad (6.41)$$

Here, the other functions are provided in the appendix (chapter D) Dey et.al [202] has reported the numerical plots of the NLSE.

6.3.4 Dynamical Systems of Amplitude Modulated EAWs

In the study of dynamical systems with two-dimensional phase space, a limit cycle is a closed trajectory in phase space, with the property that at least one other trajectory spirals into it as time approaches infinity or as time approaches negative infinity. This type of behaviour can be seen in some non-linear systems. To investigate the dynamical properties of EAWs, we consider transformation $\eta'' = l\xi'' - V\tau_2$ and $\phi_2 = \phi(\eta'') = \psi''(\eta'') \exp(i\beta\eta'')$, the NLSE then transforms into:

$$\frac{d^2\psi''}{d\eta''^2} = \left(\beta^2 - \frac{1}{P_2 l^2} \beta V \right) \psi'' + \frac{Q_2}{P_2 l^2} \psi''^3 \quad (6.42)$$

Eqn. (6.42) can be expanded in the dynamical system as

$$\begin{aligned} \frac{\partial \psi''}{\partial \eta''} &= z'' \\ \frac{\partial z''}{\partial \eta''} &= P_2'' \psi'' + Q_2'' \psi''^3 \end{aligned} \quad (6.43)$$

where $P_2'' = \beta^2 - \frac{1}{P_2 l^2} \beta V$ and $Q_2'' = -\frac{Q_2}{P_2 l^2}$

This system will be conservative if the corresponding field is solenoidal, i.e. $\vec{\nabla} \cdot \vec{F}'' = 0$, where $\vec{F}'' = (z'', P_2'' \psi'' + Q_2'' \psi''^3)$. Hence the system is a planar one with Hamiltonian given by $H'' = \frac{z''^2}{2} - \frac{P_2'' \psi''^2}{2} - \frac{Q_2'' \psi''^4}{4}$. The phase plots provide the dynamical properties.

In figure 6.21, the increase in H reduces the modulation and wave number of the waves making plasma more dense and hence giving birth to quantum tunneling. And if figure 6.22, the rise in value of wave number i.e. decreasing frequency made the modulation of envelope soliton cover a larger space.

The phase plots figures, however suggest that there is convergence condition and there are hidden or coexisting attractors that lead to the conclusion of the existence of limit cycle [250]. In figure 6.23, there is no much fluctuation with change in value of R_{eh0} whereas the separation between hidden separators in figure 6.24 increases with rise in value of quantum diffraction parameter (H). In figure 6.25 hidden attractors spread out with increase in value of δ , that is because number density of cold electrons increases and the system becomes more inertial i.e. less mobility and hence the system is more ordered. But in figure 6.26, lesser the value of χ_e , more is the thermal energy and hence more chaotic is the system thus following the second law of thermodynamics. In both figures 6.27 and 6.28, the system becomes more ordered with increase in value of parameter. Further from figure 6.29-6.31, there are some pockets of parametric range in

which dynamical system is highly bifurcated giving bump on tail type distribution. And in figures 6.32 and 6.33, there are certain packets of parametric range within which the distribution is quite similar to other cases.

6.3.5 Applications

This work will find application in theoretically predicting the stable modes in many solar plasma and stellar plasma applications. The current study could also aid in understanding the fundamental properties of electron-acoustic waves in extremely dense astrophysical objects such as white dwarfs and neutron stars [251]. The density of white dwarfs can range between 10^5 to 10^9 . As a result, the relativity parameter R_{j0} in this example can be in the range 0.37 to 8 [220]. These results will also be useful in the future intense laser-solid plasma experiments where the relativistic electron degeneracy effects become important.

6.4 Conclusion

We have shown envelope solitons in relativistic plasma with degenerate hot and cold electrons and perturbed ions as constituents. The fluid quantum hydrodynamic model governs the dynamics of the electron acoustic plasma system. This plasma shows the behaviour of astrophysical plasma where speed of particles approach speed of light. We have taken the relativistic pressure and analyzed behaviour of electron acoustic waves. The solution of Forced-KdV equation explains the dependence of behaviour of these perturbed solitons on various parameters taken. The unperturbed plasma system is studied and then how does the perturbation affects the system is investigated. The dynamical system is studied through non-linear Schrodinger equation (NLSE). The importance of studying dynamical systems is explained through phase portraits. The qualitative change in this system's dynamics with variation in parameters is explained through bifurcation where the characterization of the rate of separation of infinitesimally close trajectories

is done using Lyapunov exponent. And the chaotic behaviour of the system is studied through Largest Lyapunov exponent. This study is applicable to various astrophysical phenomenon like in stellar media, magnetospheres, polar caps etc.

CHAPTER 7

RESONANT INTERACTIONS AND CHAOTIC EXCITATION IN NONLINEAR SURFACE WAVES IN DENSE PLASMA

7.1 Introduction

Plasma in space as well as laboratory are often confined by way of magnetic fields. In most of the cases we have regions rich in ionised gas of finite density and almost vacuum. Thus there appears a boundary between these two regions [252]. The electric and magnetic properties of these regions vary accordingly. For instance a magnetar [253] which has strong magnetic field confines the astrophysical plasma around itself through the magnetic bottling mechanism. Any perturbation of electrical or mechanical in nature at these boundaries can grow up to gigantic proportions or might also die out. There are reports [187, 73] where nonlinear interaction inside plasma can produce harmonics. Such harmonics attribute addition features to the ionised gas. By a judicial study of the data from such harmonics the density and currents of the plasma components may be predicted. The collective behaviour of such plasma is the combined effect of individual particle dynamics. By studying the particle dynamics that might result in such nonlinear phenomena many information can be obtained. Such studies are within the preview of dynamical systems [208, 189] and chaos [190, 254, 177]. The individual particle orbits create a magnetic field that acts as an intermediary to the coupling mechanism. Often space missions [255] report of various wave modes [182, 181] and associated stationary structures like solitary waves [186, 175, 180], shocks [118, 173, 256, 178], double layers [257, 258, 179], vortices [259, 260] etc and associated instabilities [174, 195]. Of the many wave modes, some are extensively studied and are available in the literature. There can be electrostatic modes like Ion acoustic modes (IAW) [168, 167, 117], electron acoustic modes (EAW) [194, 169, 261], dust acoustic modes (DAW) [63]

etc. Some additional electromagnetic modes are the Alfvén mode [262], magnetosonic mode [263, 184] etc.

The plasmas available in the universe may be either dense or dilute. The coupling mechanism in these two categories are very different. Often dense plasma is observed in intense laser plasma interactions [134, 264, 265, 171], neutron stars [266, 64], white dwarfs [267], relativistic streaming plasma [82, 65] etc. The dilute plasma has been extensively studied. Not much works are there which takes into consideration the high density and low temperature effects. These two effects often are beyond the preview of classical plasma and a quantum formulation is necessary. The quantum hydrodynamic model is one such theory which is applicable to these types of plasma. Initially conceptualised by Manfredi [268, 269], Haas [270, 172], Bonitz [271], Shukla [56, 183] and subsequently studied extensively by Chandra [66, 68], Mishra [272], Goswami [176], and others [72, 243, 122]. This theory holds ground in the present days as it takes into consideration many quantum mechanical effects that were otherwise left unexplored. Quantum plasma physics becomes meaningful when the de Broglie wavelength of the plasma particles becomes comparable to the inter-particle distance. Because of this, there is a significant overlap of the corresponding wavefunctions. In such a situation, the study of plasma physics problem is described by quantum statistics, in contrast to the usual classical Maxwell-Boltzmann statistics. The quantum mechanical (Fermionic) character becomes more relevant for sufficiently dense plasma. In a plasma system if the number density of degenerate electrons is of the order of $10^{30}/\text{m}^3$ to $10^{35}/\text{m}^3$ or of closer densities then we need quantum mechanics to support them [191, 207, 185].

The surface wave modes are coupled electrostatic/electromagnetic excitations of electrons near the vacuum-plasma interface and can be excited on a sufficiently dense plasma half-space and can propagate along the interface and decay on either sides of the boundary. Some recent literature can be found in this regard [273, 274, 275] They are characterized by time dependent concentration of surface charge on the surface. These results into the rapid fall of the wave amplitude on the either side of boundary.

The motivation behind this work is the investigation of second harmonic generation and propagation within the bulk of plasma that is bounded by vacuum on one surface. Such a semi bounded plasma shows a transverse propagation of higher harmonics across the interface. The electrical perturbation at the boundary produces additional effects that might directly or indirectly control the conversion efficiency of different harmonics. Here we study the spatial variation of conversion efficiency and the frequency shifts that might have a deep influence on the generation and sustenance of higher harmonics

This chapter is organized in the following ways. In Section §7.2, introduce our governing equations, then (in §7.3), we obtain the linear dispersion relation and the first-order field quantities from which we study the Lagrangian chaos. In Section §7.4, the nonlinear theory of second-harmonic generation is presented. Its parametric influence is also studied. This chapter is concluded with some physical applicabilities of these theoretical findings.

7.2 Model Equations

We have considered a dense plasma whose equation of state is given by degeneracy pressure as:

$$P_e = \frac{\pi m_e^4 c^5}{3h^3} [R_e(2R_e^2 - 3)\sqrt{1 + R_e^2} + 3 \sinh^{-1} R_e] \quad (7.1)$$

Where, $R_e = \left[\frac{3h^3 n_e}{8\pi m_e^3 c^3} \right]^{\frac{1}{3}} = R_{e0} n_e^{\frac{1}{3}}$. For a weak degeneracy the equation can be recast as $P_e = \frac{k_B T_e}{n_{e0}^{2/3}} n_e^{5/3}$. Now as we are interested in the interaction mechanism between the fundamental and higher harmonics of such a plasma separated from the vacuum and waves are being generated at the plasma-vacuum interface are propagated within the bulk of the plasma, the set of governing equations describing the system are given by:

$$\frac{\partial n_e}{\partial t} + \vec{\nabla} \cdot (n_e \vec{u}_e) = 0 \quad (7.2)$$

$$\left[\frac{\partial}{\partial t} + \vec{u}_e \cdot \vec{\nabla} \right] \vec{u}_e = \frac{1}{m_e} \left[e \vec{\nabla} \phi - \frac{1}{n_e} \vec{\nabla} P_e + \frac{\hbar^2}{2m_e} \vec{\nabla} \left[\frac{1}{\sqrt{n_e}} \nabla^2 \sqrt{n_e} \right] \right] \quad (7.3)$$

$$\nabla^2 \phi = (n_e + Z_i n_i) \quad (7.4)$$

and also there is Laplace's equation in vacuum for vacuum field quantity ϕ_v as,

$$\nabla^2 \phi_v = 0. \quad (7.5)$$

Where, $\Lambda = \frac{m_e c^2}{2k_B T_{Fe}}$. And the non-dimensional quantum diffraction parameter H is given as, $H = \frac{\hbar \omega_e}{k_B T_{Fe}}$. T_{Fe} is the Fermi temperature of the electrons, n_{e0} and n_{i0} are equilibrium number densities of electrons and ions respectively and $\omega_e = \sqrt{\frac{4\pi n_{e0} e^2}{m_e}}$ is the electron plasma frequency. Now combining equation ((7.2)-(7.5)) we can write,

$$\left(\frac{\partial^2}{\partial t^2} + 1 - \nabla^2 + \frac{H^2}{4} \nabla^4 \right) \nabla^2 \phi_2 = \frac{\partial \mathcal{L}}{\partial t} + \vec{\nabla} \cdot \vec{T} + \nabla^2 R \quad (7.6)$$

where, $\mathcal{L} = -\vec{\nabla} \cdot (n \vec{u})$, $\vec{N} = (\vec{u} \cdot \vec{\nabla}) \vec{u} + F_e n \vec{\nabla} n$, $\mathcal{R} = \frac{H^2}{4} n \nabla^2 n$

7.3 Linear Theory

7.3.1 Linear Dispersion Characteristic

We can write every field quantity X as [276],

$$X = X_0 + X_1 \quad (7.7)$$

where X can be $\phi, \phi_v, n, u_x, u_z$ and X_0 is equilibrium value and X_1 is a small perturbation and we take X_1 as [276],

$$X_1 = X_1(x) \exp[i(kz - \omega t)] + cc \quad (7.8)$$

Neglecting the non-linear term we can write the linear form of the surface wave, which is associated with the following 1st order perturbation quantities, that decays exponentially in the direction normal to the interface are given in Appendix §C.1.

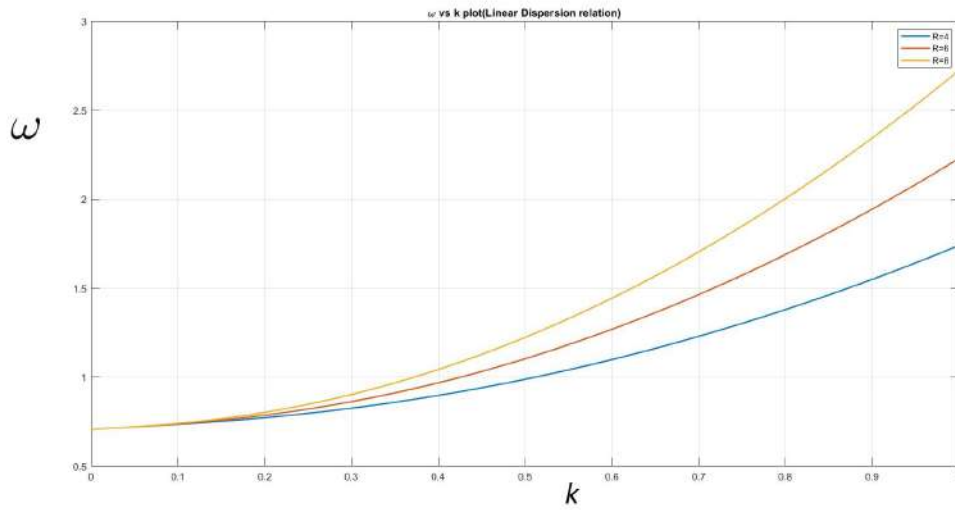


Figure 7.1: Dispersion curve for different quantum diffraction parameter (H)

And the linear dispersion relation is given by:

$$\omega = \frac{1}{\sqrt{2}} \left(1 + \frac{k}{\sqrt{2}} \sqrt{\frac{\Lambda R_e}{3} + \frac{H^2 k^4}{4}} \right) \quad (7.9)$$

The dispersive effects increase with quantum diffraction and the degeneracy effects. From equation (7.9) these effects are clear and to depict the dependence we plot the linear dispersion characterisation for different values of (H) and (Λ) [figure (7.1), (7.2)] respectively.

7.3.2 Linear Surface waves

A linear wave at the surface separating the vacuum and plasma gradually favors the growth of higher harmonics through nonlinear interaction. Such small surface waves on fluids have been well formulated by Airy [277]. A nonlinear interaction of this type is the direct result of particle trajectories mixing within the bulk of the plasma. We restrain ourselves in the linear regime to understand the basic mechanism (chaos) which will induce nonlinear interaction in subsequent stages. In this context of wave mixing it is important to discuss the 'Lagrangian chaos'. The interface which is represented by $x - y$ plane and the wave which is propagating along the surface. We intend to see the

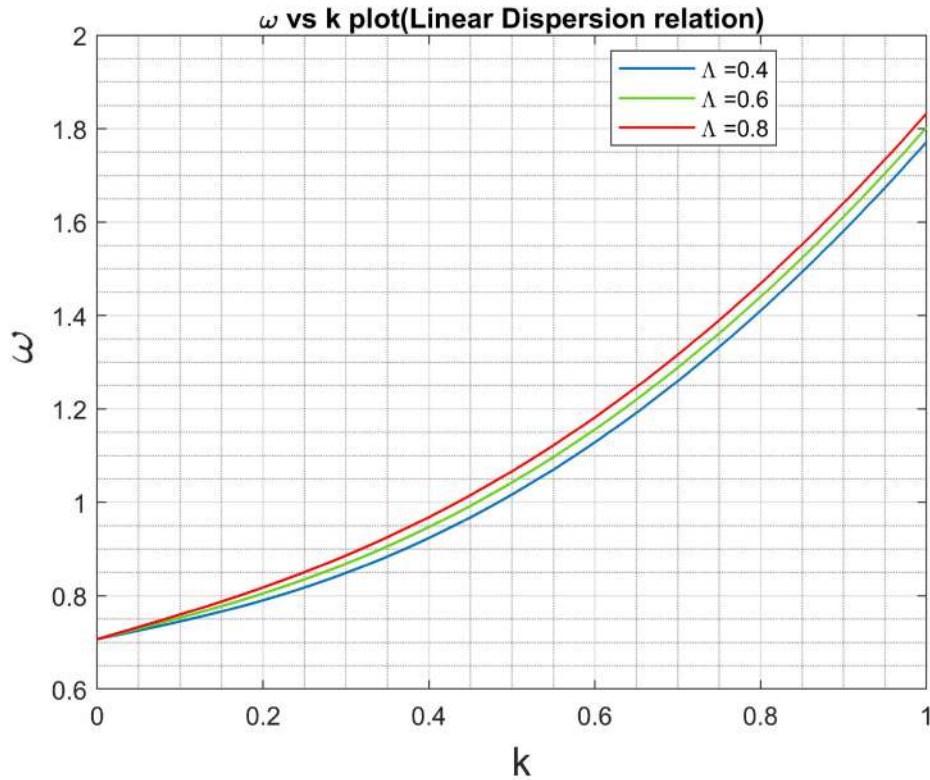


Figure 7.2: Dispersion curve for different degeneracy parameter (Λ)

mechanism in the $x - z$ plane. Assuming the component of the wave under investigation being the x -direction the field quantities of the plasma fluid are given by (7.10)–(7.11). It is to be noted that the amplitude for a harmonic waves travelling on fluid layer at a depth/height of ‘ h ’ from the interface be some function of the surface displacement given by equation (7.10).

$$\xi(x, t) = A \cos(kx - \omega t) \quad (7.10)$$

The velocity field fields in the bulk of plasma of height ‘ h ’ are given by equation (7.11).

$$\left. \begin{aligned} u_x(x, z, t) &= A\omega \frac{\cosh[k(l+z)]}{\sinh(kl)} \cos(kx - \omega t) \\ u_z(x, z, t) &= A\omega \frac{\sinh[k(l+z)]}{\sinh(kl)} \sin(kx - \omega t) \end{aligned} \right\} \quad (7.11)$$

Here, x , u_x , z and u_z are horizontal coordinate, horizontal velocity, vertical coordinate and vertical velocity of the wave respectively. If we get into the bulk of the plasma [i.e. $l \rightarrow \infty$] the fluid velocity components take the form equation (7.12) which can be written as

$$\left. \begin{aligned} u_x(x, z, t) &= A\omega e^{kz} \cos(kx - \omega t) = \dot{x} \\ u_z(x, z, t) &= A\omega e^{kz} \sin(kx - \omega t) = \dot{z} \\ \xi &= A \cos(kx - \omega t) \end{aligned} \right\} \quad (7.12)$$

7.3.3 Particle dynamics under one harmonic wave

In order to study the particle motion under a wave we start from equation (7.12) and change the variable as $\psi = kz - \omega t$. Also, rescaling as, $z_1 = kz$ and $\tau = \omega t$, we get

$$\left. \begin{aligned} \frac{d\psi}{d\tau} = \psi' &= kAe^{z_1} \cos\psi - 1 \\ \frac{dz_1}{d\tau} = z_1' &= kAe^{z_1} \sin\psi \\ kz &= \ln(k) - n\pi, z_1 = \ln(k) - n\pi \end{aligned} \right\} \quad (7.13)$$

Also, these equation can be presented in Hamiltonian form

$$\psi' = \frac{\partial \mathcal{H}}{\partial z_1} \quad \& \quad z_1' = -\frac{\partial \mathcal{H}}{\partial \psi} \quad (7.14)$$

with time independent Hamiltonian given by

$$\mathcal{H} = kAe^{z_1} \cos\psi - z_1 \quad (7.15)$$

To simplify we use, $\zeta = z_1 + \ln(kA)$ then new form of Hamiltonian will be,

$$\left. \begin{aligned} \mathcal{H} &= e^\zeta \cos\psi - \zeta \\ i.e \quad \mathcal{H} &= \mp k^2 A \cos\psi - \ln(k) + n\pi \end{aligned} \right\} \quad (7.16)$$

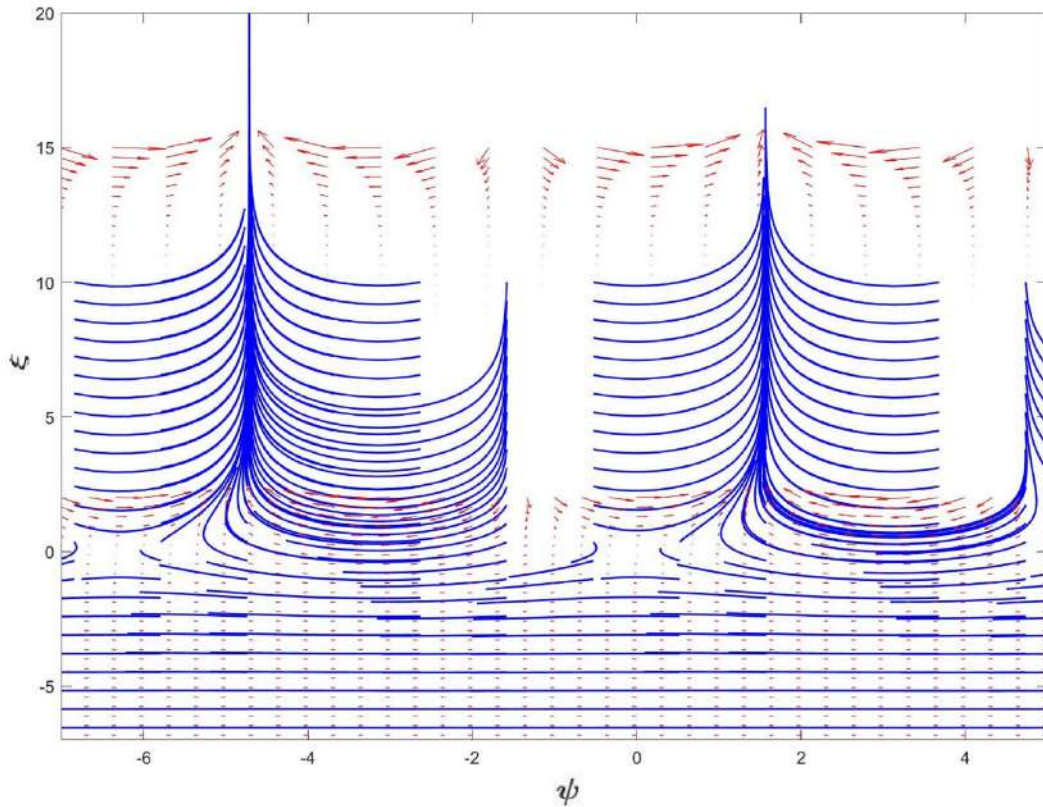


Figure 7.3: Level curves of Hamiltonian (H) defined by (7.17) giving the orbits of a particle under a single harmonic wave

With equations of motion,

$$\psi' = e^\zeta \cos\psi - 1 \quad \& \quad \zeta' = e^\zeta \sin\psi \quad (7.17)$$

Figure (7.3) shows the level curves corresponding to equation (7.17). We find that there are open curves as $\zeta \rightarrow \infty$ and there are periodic shifts at low value of ζ . A level curve of a function (here Hamiltonian) of two variables (ψ and ζ) at a particular values of the function is the set of all particles on the domain of the function which takes up that particular value.

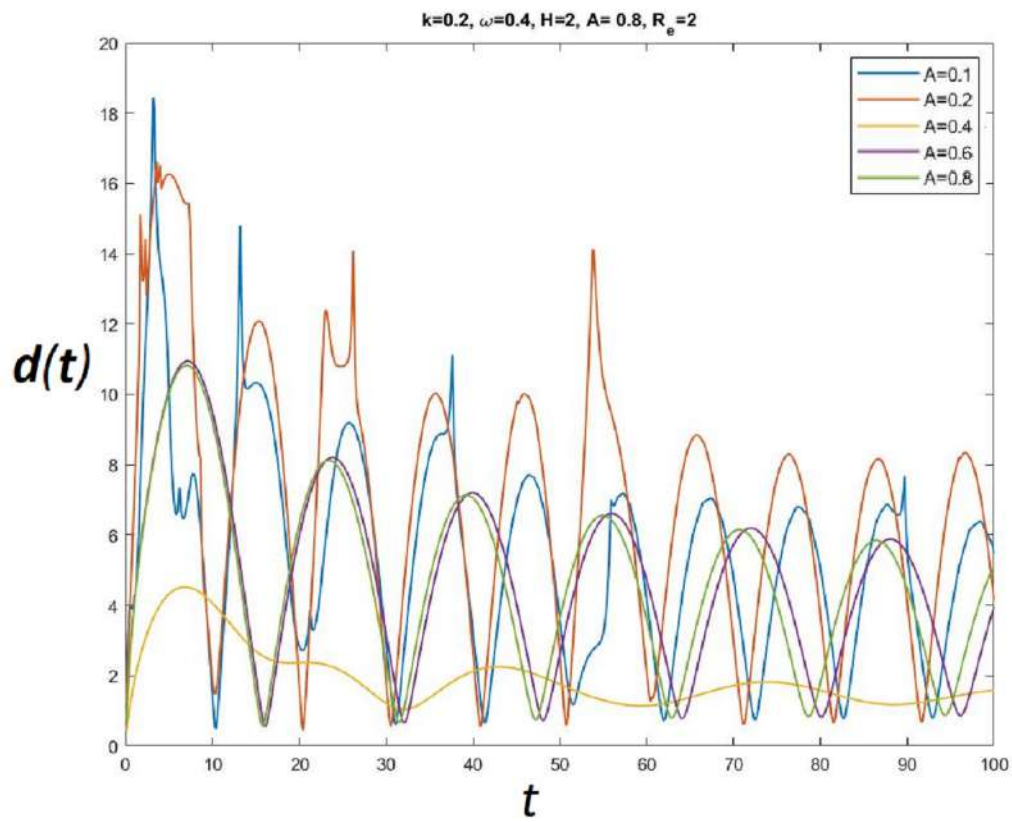


Figure 7.4: The vector length versus time of different amplitude of surface disturbance(A)

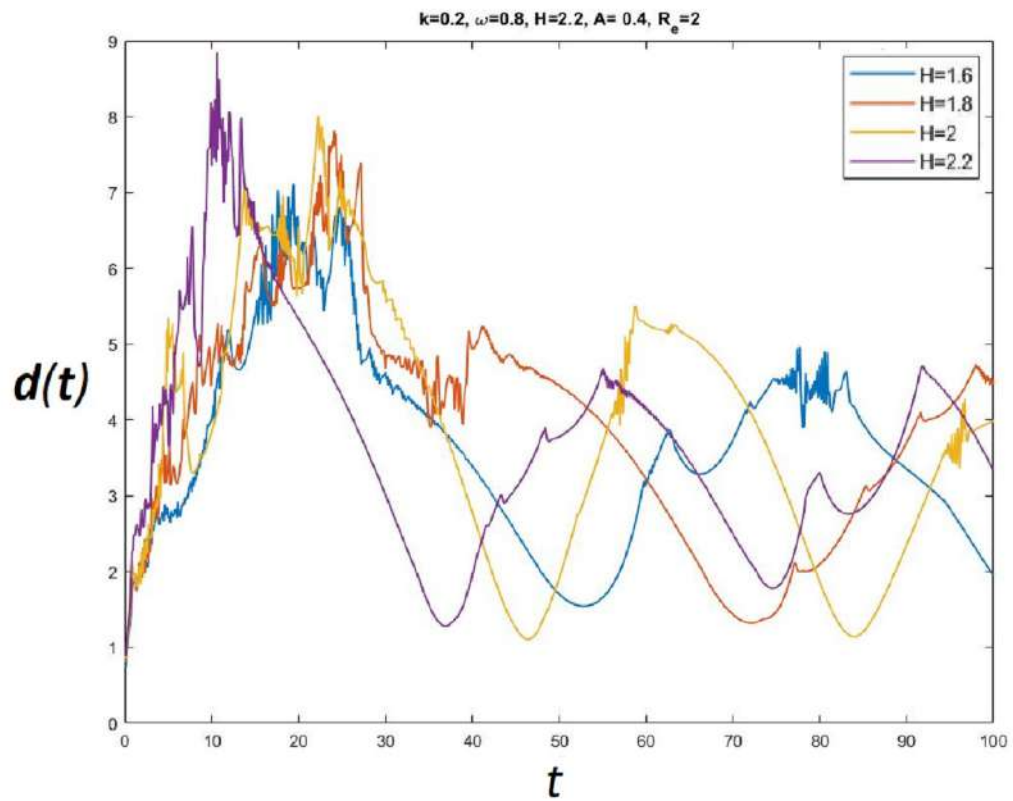


Figure 7.5: The vector length versus time of different quantum diffraction parameters(H)

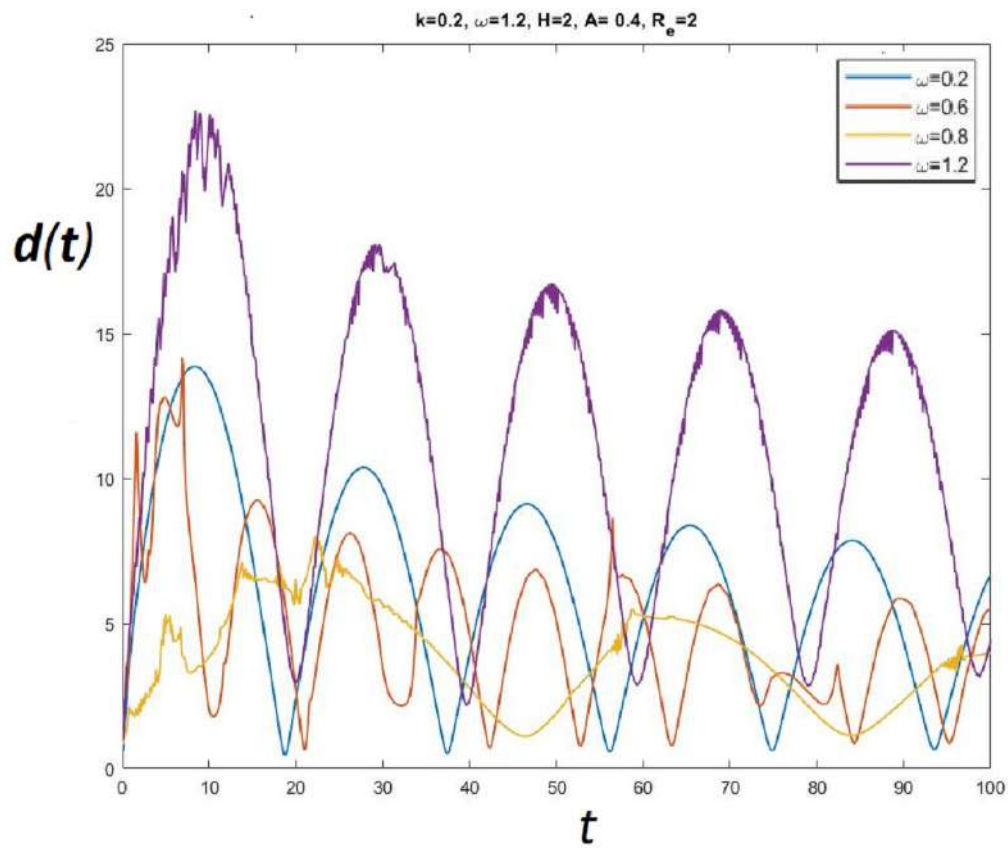


Figure 7.6: The vector length versus time of different values frequency (ω)

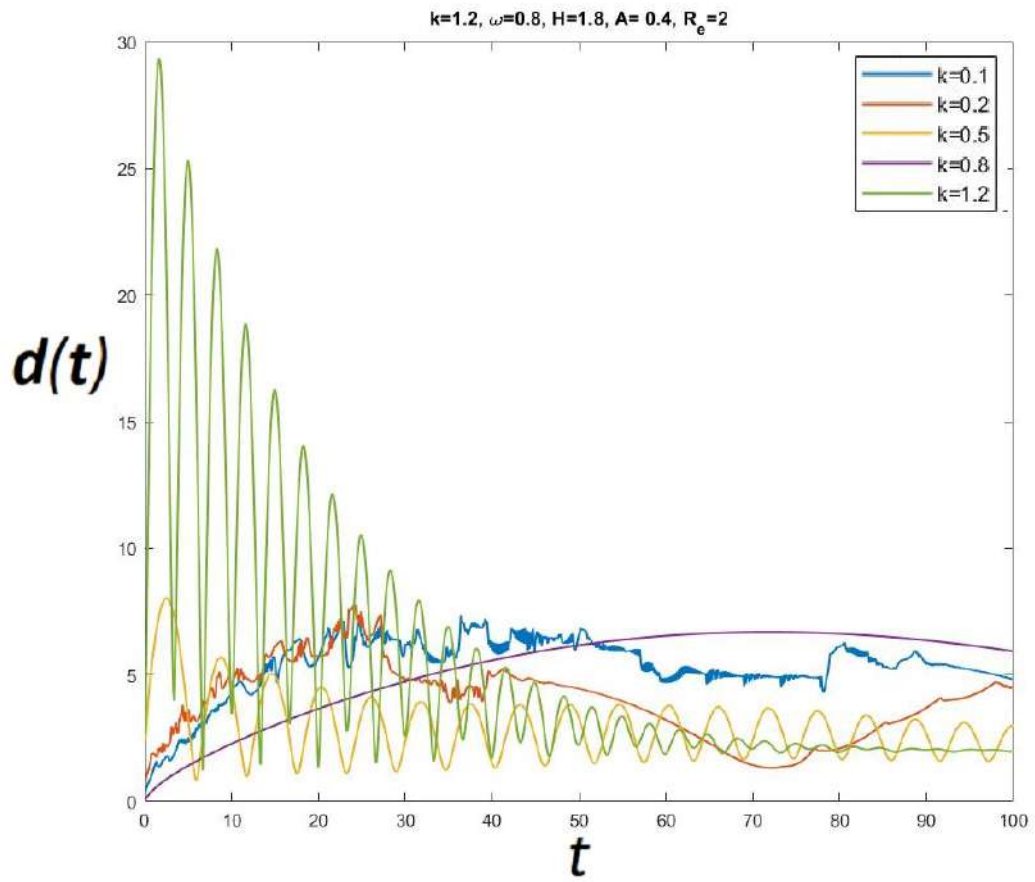


Figure 7.7: The vector length versus time of different values wave vector (k)

7.3.4 Superposition of Waves and Lagrangian Chaos

It is now important to study the dependence of particle motion on various particles. The dynamic system equation are analyzed. To brief about the analytic approach to study the particle advection in a more complicated flow we superpose the harmonics, $\dot{x} = \sum_j u_{x,j}(x, z, t)$ and $\dot{z} = \sum_j u_{z,j}(x, z, t)$ For our case $j = 1$ and 2 .

The surface distortion is therefore given by $\tilde{D}(x, t) = \sum_{j=1}^2 A_j \cos(k_j x - \omega_j t + \theta_j)$, θ_j is the phase difference. Since the fluid is considered incompressible we can use the condition $\frac{\partial u_x}{\partial x} = -\frac{\partial u_z}{\partial z}$. The streamfunction is therefore given by,

$$\Sigma' = \sum_{j=1}^2 A_j \frac{\omega_j}{k_j} e^{k_j z} \cos(k_j x - \omega_j t + \theta_j).$$

These can be a potential given by the complex conjugate of stream function given by,

$$\Pi = \sum_{j=1}^2 A_j \frac{\omega_j}{k_j} e^{k_j z} \sin(k_j x - \omega_j t + \theta_j).$$

Now, these streamline function (Σ') and potential function (Π) can be coupled as real and imaginary part of a single complex function dependent of complex variable ($\rho = x + iz$) given by,

$$F(\rho) = \sum_{j=1}^2 A_j \frac{\omega_j}{k_j} e^{k_j z} [\exp(k_j x - \omega_j t + \theta_j)].$$

The equation of motion accordingly becomes

$$\dot{\rho} = -i \frac{dF}{d\rho}$$

To investigate whether the orbit is chaotic or not we compute the Largest Lyapunov exponent (LLE). This is done by studying the linear perturbation around the flow (7.11). Equation (7.13) is supplemented by the linear dynamical system for deviations ($\delta x, \delta z$)

given by,

$$\left. \begin{aligned} \delta\dot{x} &= \frac{\partial u_x}{\partial x} \delta x + \frac{\partial u_x}{\partial z} \delta z \\ \delta\dot{z} &= \frac{\partial u_z}{\partial x} \delta x + \frac{\partial u_z}{\partial z} \delta z \end{aligned} \right\}. \quad (7.18)$$

The above symmetry is used based on the incompressibility and potentiality of the flow suggesting the Lyapunov exponent is symmetric about the origin.

Chaos requires a positive values of Largest Lyapunov exponent (LLE). This can be interpreted by studying the long time properties of the modulus of the vector $(\delta x, \delta z)$, which is $d(t) = \sqrt{(\delta x)^2 + (\delta z)^2}$. In figures (7.4) to (7.7) we plot the vector length versus time of different parameters. The exponential decay or growth or oscillatory nature of $d(t)$ suggests chaos or order based on the equation $d(t) \sim e^{\lambda_m t}$. Here, λ_m is the LLE. The nature and stability of the orbits are thus predicted for these figures. In figure (7.4) we find that the distance vector gradually oscillates with diminishing magnitude which is more rapid for larger amplitude of surface disturbance (A). This is due to the decrease of skin depth with amplitude of surface distance. Maximum the energy is used for lateral movement, more quickly the motion cease to exists. The effect of quantum diffraction (figure (7.5)) is anisotropic during the waxing and waning phase, when the length of the deviation vector $d(t)$ increases there appears small fluctuations in the crests which is due to quantum mechanical tunneling. As quantum diffraction parameter (H) increases periodically increases resulting in smaller periods.

Figures (7.6) and (7.7) show the dependence of deviation vector on the frequency (ω) and wavenumber (k) of the surface disturbance. We see that a frequency (ω) increases (Figure (7.6)) from 0.2 to 1.2 anomalous behaviour appears. Initially the derivation decreases in amplitude (Blue and Orange). Then the system shows lower periodicity with asymmetric profile depicting lagging behaviour (yellow) or in other sense some kind of energy mismatch. Suddenly the derivation peaks up from which we can infer that some resonance mechanism occurs at $\omega = 1.2$. The effect of wavenumber (k) is more interesting. From figure (7.7) we see that the wavenumber increases from 0.1, 0.2

small magnitude, but at $u = 0.8$ there is no such fluctuations suggesting a total mismatch of energy exchange. Such a phenomena cannot be explained in the linear theory and we have to resort to the nonlinear theory for it. At $k = 1.2$ we find an exponentially decaying periodic fluctuations suggesting heavy damping, but the damping cannot overpower the periodic restoring force that is supplied from the system through the stress created in the system given by the equation of state.

To summarise our findings from the linear theory we conclude that the linear dispersion characteristics depends positively on the quantum diffraction parameter (H) and the degeneracy factor (R_{h0}). We have also studied the dynamical behaviour and the level curves of the Hamiltonian. Further we studied the Lagrangian chaos by studying the Maximal/Largest Lyapunov exponents (LLE). From the linear theory, a suggestive resonant interaction appears for $k = 1.2$ and $\omega = 1.2$. Both wavenumber and frequency are in normalized scales. To study in more detail we have to investigate the nonlinear interactions that are given in the subsequent sections.

7.4 Nonlinear Theory

7.4.1 Harmonics of Field Quantities: Generation and Evolution

Now, let us consider the nonlinear effects to be incorporated in the system equations. Therefore, to obtain the field quantity of higher harmonics through nonlinear interaction, let us write the generalized field variables as [276],

$$X = X_0 + X_1 + X_2 \tag{7.19}$$

where X_0 is the equilibrium value, X_1 is the 1st order perturbed quantities associated with linear effects and X_2 is the some additional effect due to non-linearity. Substituting the expansion (7.19) in (7.7) and keeping in mind that X_1 satisfy the linear equations we

obtain:

$$\left(\frac{\partial^2}{\partial t^2} + 1 - \nabla^2 + \frac{H^2}{4} \nabla^4 \right) \nabla^2 \phi_2 = \frac{\partial Q}{\partial t} + \vec{\nabla} \cdot \vec{T} + \nabla^2 R \quad (7.20)$$

$$\nabla^2 \phi_{\nu 2} = 0 \quad (7.21)$$

We here will assume that non-linear affects are weak so that we can assume $X_2 \ll X_1$; this will allows us to calculate the nonlinear terms on the right-hand side of (7.7) by using the known linear components in Appendix §C.1. Since we are interested only in the oscillatory part of the second order perturbed quantities, the non-oscillatory terms arising on the right hand side of (7.7) will be ignored. Thus we finally obtain the second order oscillatory quantities using the linear components and boundary conditions given by:

$$\phi_2 = \{P_1 e^{-2kx} + P_2 e^{2i\beta x} + P_3\} e^{i(kz-2\omega t)} \quad (7.22a)$$

$$n_2 = \{N_1 e^{-2kx} - N_2 e^{2i\beta x} + N_3\} e^{i(kz-2\omega t)} \quad (7.22b)$$

$$u_{x2} = \frac{i}{2\omega} \{U_1 e^{-2kx} + e^{-2\gamma x} U_2 \quad (7.22c)$$

$$+ e^{-(\gamma+k)x} U_3 - e^{-2i\beta x} U_4 + U_5\} e^{i(kz-2\omega t)} \quad (7.22d)$$

$$u_{z2} = \frac{i}{2\omega} \{e^{-2kx} W_1 + e^{-2\gamma x} W_2 + e^{-2\gamma x} W_3 \quad (7.22e)$$

$$+ e^{-(\gamma+k)x} W_4 - e^{-2i\beta x} W_5 + W_6\} \quad (7.22f)$$

$$e^{i(kz-2\omega t)} \quad (7.22g)$$

where,

$$4\beta^2 = 4\omega^2 - 1 - 4k^3 - 4H^2 k^4 \quad (7.22h)$$

The constants B_2 , D_2 , p_j 's and F_j 's are given in Appendix §C.2.

7.4.2 Parametric Dependence of Field Quantities

Since we have obtained the second harmonic field quantities it is necessary to study the dependence of velocity vectors in different depths of plasma media on various parameters. In the following figures (7.8)-(7.19) the transverse (x - component) and longitudinal (z - component) of velocities and the streamline corresponding to the velocity vector has been depicted for plasma parameters. In figures (7.8)-(7.11) we see that as the amplitude of the surface disturbance increases it dies out quickly across the interface (figure (7.8)). However, the effect of quantum diffraction parameter (H) extends from the interface at around $H = 2.2$ and the amplitude again grows (figure (7.9)). This growth of transverse velocity component is due to the quantum tunneling effect across the boundary. This means after a certain lateral length along the x -axis the velocity of the wave is totally negative suggesting total internal reflection. This reflection is dependent on wavenumber and for a normalised wave number shift from 0.4 to 0.6 (figure (7.10)).

The frequency of surface disturbance (ω) however can propagate along x -direction, the periodicity in velocity propagates within the bulk but any surface modulation is lost. This is due to the high density of the plasma. Such effect is clearly visible in figures (7.11) b,c.

Contrary to the transverse velocity component (u_{x2}), the longitudinal component (u_{z2}) in the second harmonic shows the variation much within the bulk of the plasma. Figures (7.12)-(7.15) show the effects of surface disturbance amplitude (A), quantum diffraction parameter (H), wavenumber (k) and frequency (ω) of periodic surface disturbance. It is clearly seen that the velocity wave propagate with exponentially decaying amplitude in x -direction (7.12) and at the surface the z - component shows progressive wave suggesting the constant supply of energy in longitudinal direction by the external source. This source may be an electrostatic field, or laser beam or any EM radiation with periodicity that matches exactly (or closely) with the resonant frequency of the sys-

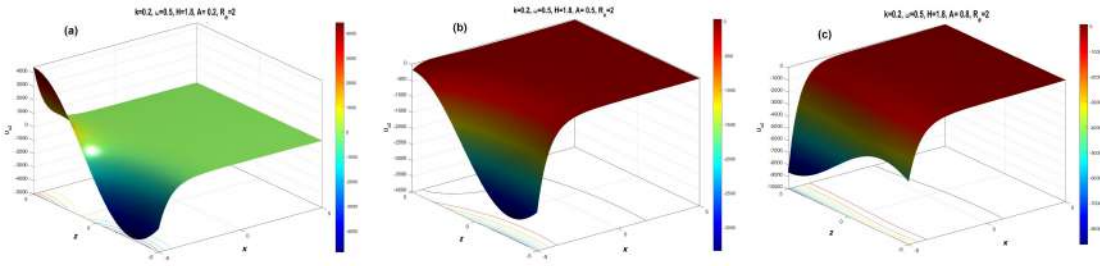


Figure 7.8: x-component of velocity field inside plasma layer for different amplitudes (A) of surface disturbance. (a) $A=0.2$, (b) $A=0.5$ & (c) $A=0.8$. Here $k = 0.2, \omega = 0.5, H = 1.8, R_e = 2$

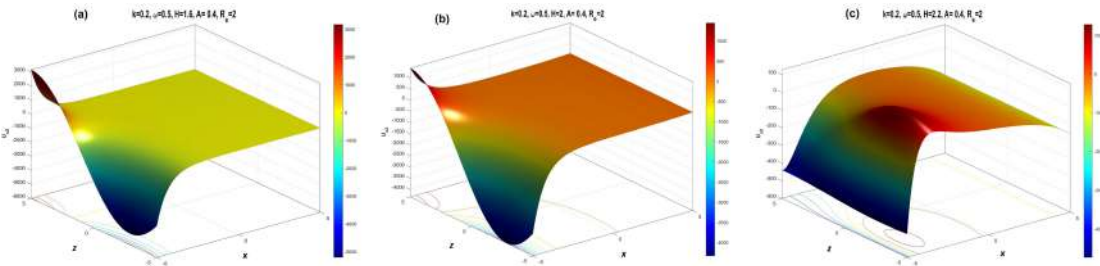


Figure 7.9: x-component of velocity field inside plasma layer for different values of quantum diffraction parameter (H). (a) $H=1.6$, (b) $H=2$ & (c) $H=2.2$. Here $k = 0.2, \omega = 0.5, A = 0.4, R_e = 2$

tem. The quantum diffraction parameter unlike the transverse component does not affect much of the longitudinal velocity component and the velocity field flattens for $x > 0$ (figure (7.13)). The wavenumber however shows a total reflection type mechanism for $u = 0.6$ at a transverse distance of $x = 5$ (figure (7.14)). One interesting effect is seen for frequency of surface disturbance $\omega = 1.2$ (figure (7.15)). From here we can predict a velocity resonance for $\omega = 1.2$ and at a spatial distance $x \rightarrow 5$. The velocity profile takes a solitary structure around $z = 0$ suggesting the excitation of resonant modes close to the resonant frequency ($\omega = 1$).

In figures (7.16)-(7.19) we depict the velocity streamlines and its dependence on various parameters. We see that as the amplitude of surface disturbance increases the obliqueness of velocity streams increases (figure (7.16)). This is due to the energy associated with large amplitude oscillations that enhances the oblique propagation of waves in the lateral direction. As the density increases favoring more tunneling phenomena the

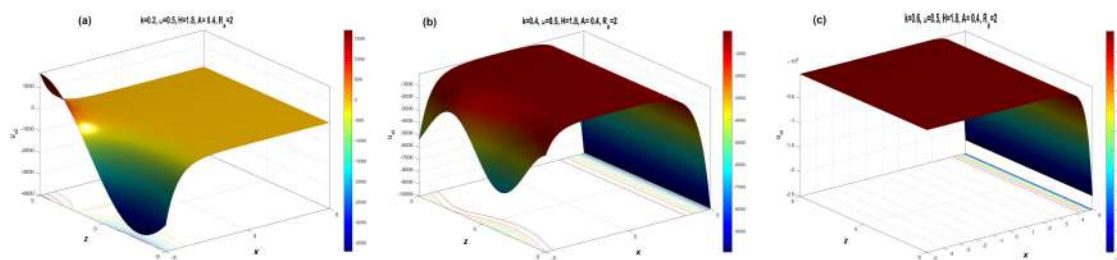


Figure 7.10: x-component of velocity field inside plasma layer for different values wavenumber (k) of surface disturbance.(a) $k=0.2$, (b) $k=0.4$ & (c) $k=0.6$. Here $H = 1.8, \omega = 0.5, A = 0.4, R_e = 2$

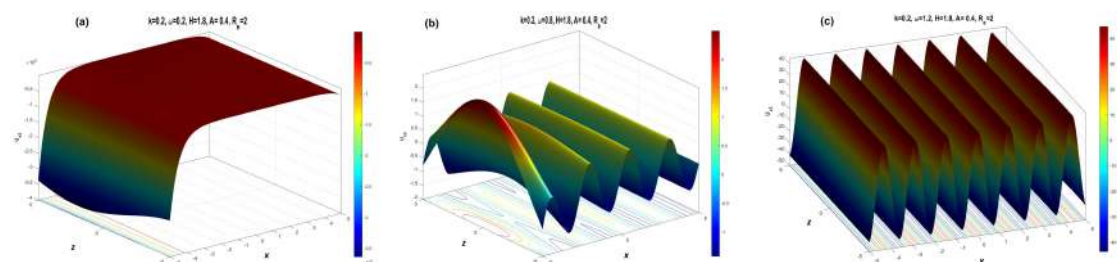


Figure 7.11: x-component of velocity field inside plasma layer for different values frequency (ω) of surface disturbance.(a) $\omega = 0.2$, (b) $\omega = 0.8$ & (c) $\omega = 1.2$. Here $H = 1.8, k = 0.2, A = 0.4, R_e = 2$

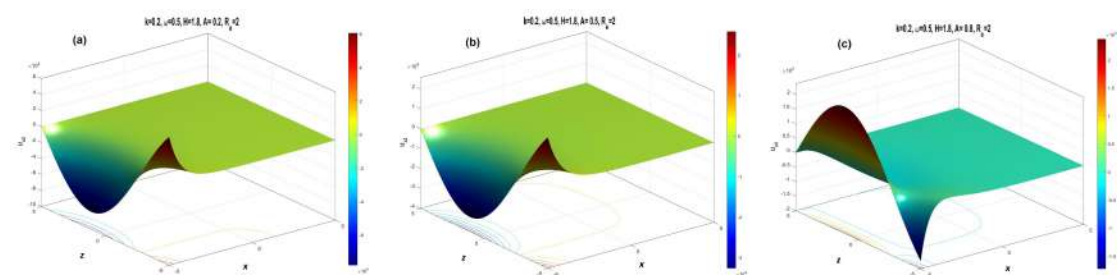


Figure 7.12: z-component of velocity field inside plasma layer for different amplitudes (A) of surface disturbance.(a) $A=0.2$, (b) $A=0.5$ & (c) $A=0.8$. Here $k = 0.2, \omega = 0.5, H = 1.8, R_e = 2$

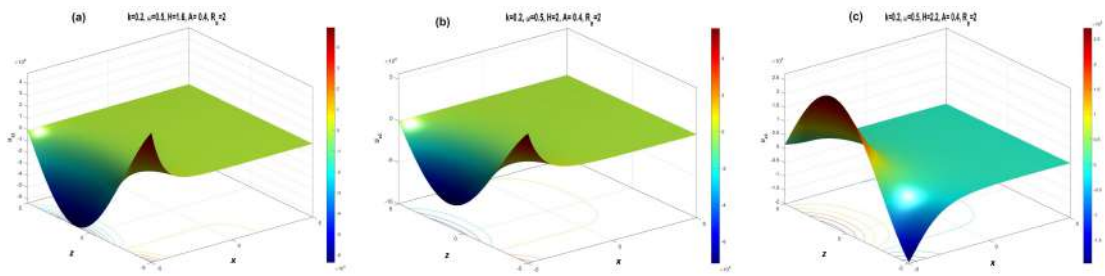


Figure 7.13: z-component of velocity field inside plasma layer for different values of quantum diffraction parameter (H). (a) $H=1.6$, (b) $H=2$ & (c) $H=2.2$. Here $k = 0.2$, $\omega = 0.5$, $A = 0.4$, $R_e = 2$

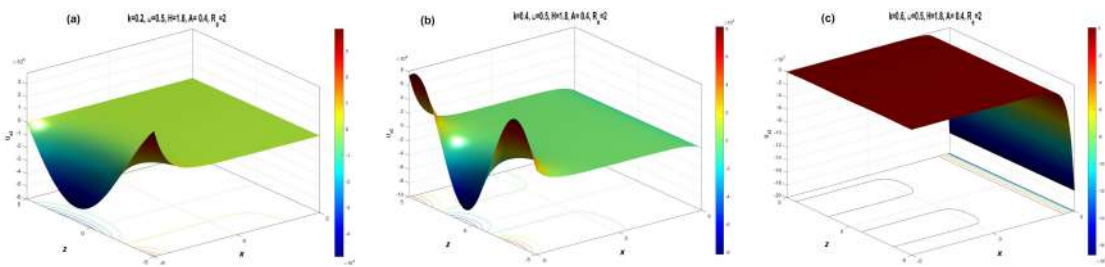


Figure 7.14: z-component of velocity field inside plasma layer for different values wavenumber (k) of surface disturbance. (a) $k=0.2$, (b) $k=0.4$ & (c) $k=0.6$. Here $H = 1.8$, $\omega = 0.5$, $A = 0.4$, $R_e = 2$

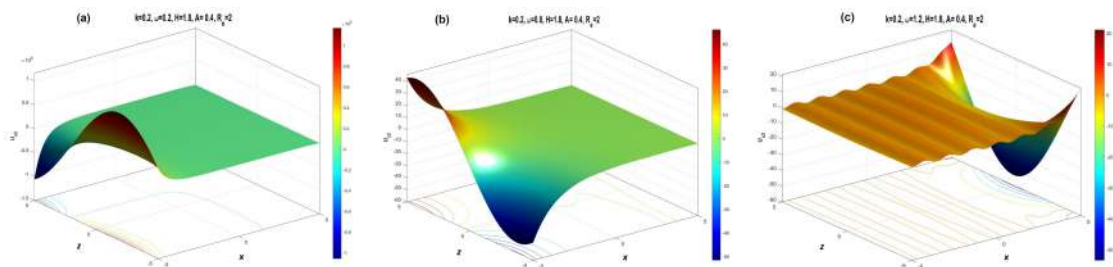


Figure 7.15: x-component of velocity field inside plasma layer for different values frequency (ω) of surface disturbance. (a) $\omega = 0.2$, (b) $\omega = 0.8$ & (c) $\omega = 1.2$. Here $H = 1.8$, $k = 0.2$, $A = 0.4$, $R_e = 2$

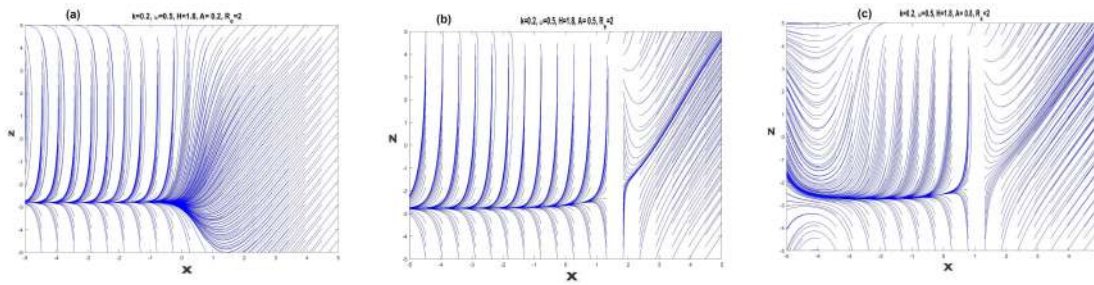


Figure 7.16: Velocity streamline inside plasma layer for different amplitudes (A) of surface disturbance.(a) $A=0.2$, (b) $A=0.5$ & (c) $A=0.8$. Here $k = 0.2, \omega = 0.5, H = 1.8, R_e = 2$

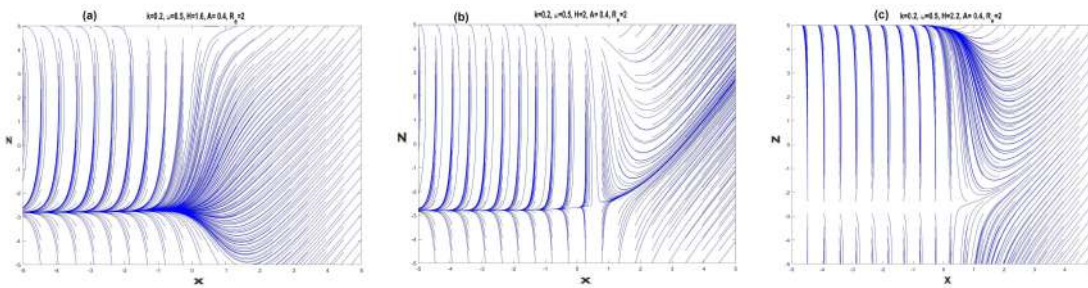


Figure 7.17: Velocity streamline inside plasma layer for different values of quantum diffraction parameter (H). (a) $H=1.6$, (b) $H=2$ & (c) $H=2.2$. Here $k = 0.2, \omega = 0.5, A = 0.4, R_e = 2$

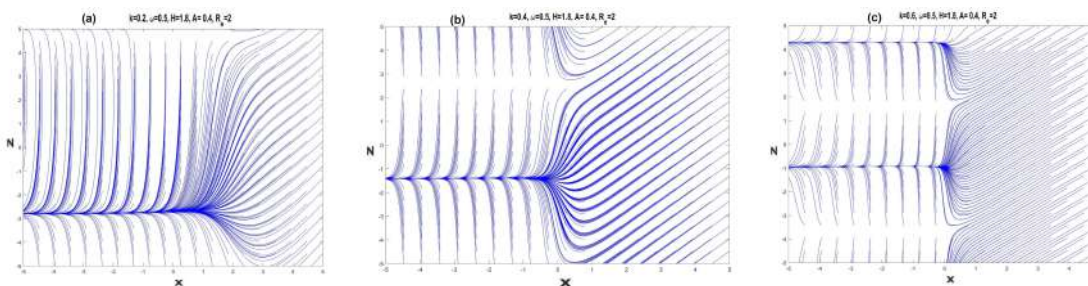


Figure 7.18: Velocity streamline inside plasma layer for different values wavenumber (k) of surface disturbance.(a) $k=0.2$, (b) $k=0.4$ & (c) $k=0.6$. Here $H = 1.8, \omega = 0.5, A = 0.4, R_e = 2$

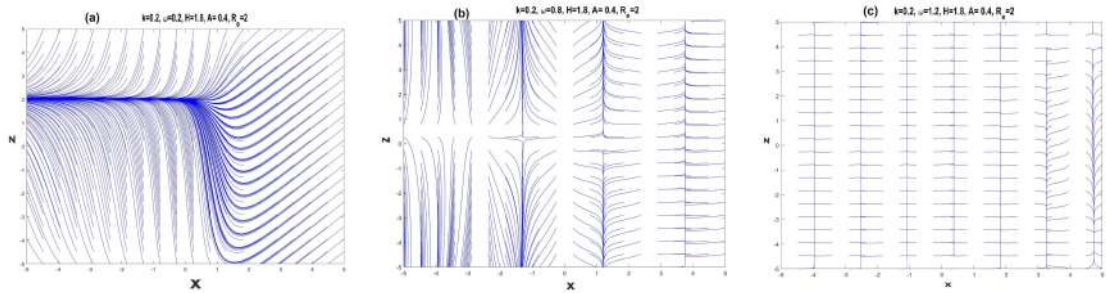


Figure 7.19: Velocity streamline inside plasma layer for different values frequency (ω) of surface disturbance. (a) $\omega = 0.2$, (b) $\omega = 0.8$ & (c) $\omega = 1.2$. Here $H = 1.8$, $k = 0.2$, $A = 0.4$, $R_e = 2$

streamlines deviate from each other due to repulsion of Coloumbic nature as well as due to exclusion principle (figure (7.17)c). Particle flow and localization is visible in figures ((7.18) and (7.19)). As the wavelength (k) and frequency (ω) of surface disturbance increases short range contractions are noticed in the bulk of the plasma. Streamlines are not that closely spaced but it shows a collective response to the external field. We have seen similar resonant behaviour in figures (7.6) and (7.7).

7.5 Conclusions

In this work we have investigated in details the generation and propagation of second harmonics at a plasma vacuum interface and its corresponding field variables inside the bulk of plasma. We also studied Lagrangian chaos and its parametric dependence. The findings will help researchers in Laser-produced plasmas to study the generation and sustenance of higher harmonics and how to make use of them in practical applications.

CHAPTER 8
NONLINEAR WAVE-WAVE INTERACTION IN SEMICONDUCTOR
JUNCTION DIODE

8.1 Introduction

Semiconductors have revolutionized the pursuit of science and engineering in the last century. From miniaturization of instruments to the efficiency of their functioning, semiconductor devices is a necessity for every sphere of S & T. Recently spin effects in memory devices and associated electronics have added more academic and industrial interest [278, 279, 280, 281, 282, 283, 284, 285, 286]. Since then many theoretical models have been used to understand the proper science behind semiconductor physics [287, 288]. The science of semiconductor have received a fresh insight through the experimental modelling by employing plasma fluid theory [288]. The quantum hydrodynamic (QHD) model which was initially developed by Manfredi [268, 269], Haas [172, 289, 290, 291], Shukla [56], Chandra [66, 65, 64, 82, 134, 187, 261, 208] , Bonitz [292], Marklund [184], and others [185, 223, 220, 72, 293, 294, 295, 296, 297, 292, 186, 180] have been widely used to study nonlinear interactions in semiconductor plasma systems. Recently, research groups like Akbari [298, 299] Eliasson [207], Markowich [300] have contributed seriously in the energy transport investigations of heavily doped semiconductors. The Boltzmann equation [301] which is valid for classical system however becomes insufficient to described properly the semiconductor plasma theory [302]. Accordingly, the Fermi Dirac distribution [175, 303] and other similar distribution functions [304] have been used in the theoretical understanding of semiconductor plasma physics. The dynamic equation describing the macroscopic behaviour of semiconductor plasma is based on the microscopic parameters which define the system [305]. The hydrodynamic models [306] and the diffusion models [300] have partially been success-

ful in describing the physical system. However simulation studies [287] have helped to understand the system with more accuracy. This is possible due to the application of super-computing facilities available nowadays [307].

This work is primarily framed on the hydrodynamic model equation governing the holes and electrons in a heavily doped semiconductor device [306]. We can use the same Maxwell equation in semiconductors as we do for electrical charges in plasma physics. Long range interaction [308, 309, 310] like Coulomb force leads to the semi classical Liouville's theorem [311] or Vlasov model [301] whereas short range interaction are studied by the scattering models [312, 313]. The scattering models make use of the Boltzmann equation coupled with the Maxwell's equations [314]. The scattering interactions include short range interactions [315] that encompasses electron interaction [316], electron hole interaction [317], hole-hole interaction [318], electron - neutral interaction [319], neutral hole interaction [320] etc. In diffusion theory [321, 322] for semiconductors Boltzmann equation plays the major role. Semiconductor plasmas can also show many kind of instability [323, 324, 325] like any other plasma [194, 326, 174, 195]. However since we are interested in the study of quantum effects in semiconductors, a quantum statistical equation of state [63, 327, 72, 177, 73] will be more appropriate.

The present work is motivated to carry out a three-pronged investigation on semiconductor diode incorporating an analytical study, numerical analysis, and simulation results that we have recently developed, which uses analytically obtained evolutionary equations (through the extended Poincare-Lighthill-Kuo (PLK) method [328]) initial conditions and different system parameters. This work holds tremendous promise in theoretically investigating actual physical experiments.

This chapter is organized in the following manner. In Section §8.2, we present the fluid equations describing the electron and hole dynamics. We obtain the KdV equation describing the electron and hole flows in the semiconductor by using the extended PLK method (§8.3). In this section, we also plot the numerical results showing the head on collision between the electron and hole solitons (Section §8.3.1). In Section §8.4.1,

we present our simulation algorithm in Section §8.4.1 findings in Section §8.4.2 and conclude this chapter with some application to experimental interpretations in Section §8.5.

8.2 Basic Formulation

There are two species of charge carriers in semiconductors viz. electrons and holes. In our semiconductor plasma model a PN junction diode is considered. When a positive potential is applied across the PN diode, the p-n junction is in forward biased condition, for that the holes of the p-side and the electrons of the n-side is running towards the junction. We consider the length of the semiconductor element some tens of Debye length so that we can consider the electrons and holes flow towards the PN junction. This resembles oppositely propagating solitary structures which in subsequent instants of time will interact in a nonlinear fashion thus giving rise to many interesting mechanisms which we will study in the subsequent sections. The quantum hydrodynamic model equations have been used by many authors [189, 182]

The p-type semiconductor side with hole majority has the basic dynamical equations complying the quantum hydrodynamic (QHD) model given by

$$\frac{\partial n_h}{\partial t} + \frac{\partial}{\partial x}(n_h u_h) = 0 \quad (8.1)$$

$$m_h n_h \left(\frac{\partial u_h}{\partial t} + u_h \frac{\partial u_h}{\partial x} \right) = -e n_h \frac{\partial \phi}{\partial x} - \frac{\partial P_h}{\partial x} - \frac{\hbar^2}{4m_h} \frac{\partial}{\partial x} \left(\frac{\partial^2}{\partial x^2} \sqrt{n_h} \right) - V_{h,xc} \frac{\partial n_h}{\partial x} \quad (8.2)$$

and,

$$\epsilon_L \frac{\partial^2 \phi}{\partial x^2} = e(n_h + n_i - n_e) \quad (8.3)$$

And n-type semiconductor segment with electrons as majority carriers have the follow-

ing dynamical equations given by,

$$\frac{\partial n_e}{\partial t} + \frac{\partial}{\partial x}(n_e u_e) = 0 \quad (8.4)$$

$$m_e n_e \left(\frac{\partial u_e}{\partial t} + u_e \frac{\partial u_e}{\partial x} \right) = e n_e \frac{\partial \phi}{\partial x} - \frac{\partial P_e}{\partial x} - \frac{\hbar^2}{4m_e} \frac{\partial}{\partial x} \left(\frac{\partial^2}{\partial x^2} \sqrt{n_e} \right) - V_{e,xc} \frac{\partial n_e}{\partial x} \quad (8.5)$$

and,

$$\epsilon_L \frac{\partial^2 \phi}{\partial x^2} = e(n_h + n_i - n_e) \quad (8.6)$$

ϵ_L is the linear dielectric constant for the semiconductor. In equations (8.2) and (8.5) there are exchange correlation potential which is given by,

$$V_{j,xc} = -0.985 \frac{n_j^{1/3} e^2}{\epsilon_L} \left[1 + \frac{0.034}{a_{Bj}^* n_j^{1/3}} \ln(1 + 18.37 a_{Bj}^* n_j^{1/3}) \right]. \quad (8.7)$$

Where, ϵ_L is the dielectric constant of semiconductor and $a_{Bj}^* = \frac{\epsilon \hbar^2}{m_j e^2}$ is the effective Bohr atomic radius of the species ($j = h, e$). The ion thermal pressure is given via equation of state i.e., $P_h = k_B T_h n_h$ in which T_h is temperature of holes and k_B is Boltzmann constant. The doping concentrations ratio are given as $n_{e0}/n_{h0} = \alpha$ (for n-side of semiconductor); $n_{h0}/n_{e0} = \rho$ (for p-side of semiconductor). The neutral ions do not take part in the oscillation and are considered to form the uniform neutralising background. We have incorporated the nonlinear Bohm potential [329, 294, 171].

Based on the 3D equilibrium Fermi-Dirac distribution for electrons at an arbitrary temperature Eliasson and Shukla [191] derived a set of fluid equation which are valid both at extremely low temperature as well as finite temperature limits. This model has been used by many authors [190, 183, 66, 208] A plane longitudinal electrostatic wave propagates in quantum plasma without collision and leads to adiabatic compression,

thereby causing temperature anisotropy in the electron distribution. Due to quantum mechanical tunneling the classical compressibility of the electron phase fluid is violated. Further, the non-equilibrium dynamics of the plasma particles is considered with the assumption that the chemical potential (μ) remains constant. Under such assumptions the non-equilibrium particle density is given as,

$$n_0 = \frac{1}{2\pi^2} \left(\frac{2m_e}{\hbar} \right)^{3/2} \int_0^\infty \frac{E^{1/2} dE}{e^{\beta(E-\mu)} + 1} = -\frac{1}{2\pi^2 \beta^{3/2}} \left(\frac{2m_e}{\hbar} \right)^{3/2} \Gamma\left(\frac{3}{2}\right) Li_{3/2}(-e^{\beta\mu})$$

Where, m_e is the electron mass, \hbar is the reduced Planck's constant, n_0 is the equilibrium number density, $\beta = 1/k_B T_{e0}$, T_{e0} is the background temperature of electron, μ is the chemical potential and $Li_\kappa(x)$ is the poly-logarithmic function in x of order κ . When $\beta \rightarrow \infty$ i.e, cold temperature of electron, we have $\mu \rightarrow E_F$, where E_F is the Fermi energy. Accordingly the Fermi energy is given by

$$E_F = (3\pi^2 n_0)^{2/3} \frac{\hbar^2}{2m_e} \quad (8.8)$$

The pressure term for the electron is given as [208]

$$P_e = m_e n_0 v_{Te}^2 F \left(\frac{n_e}{n_0} \right)^3 \quad (8.9)$$

Again, $v_{Te} = \sqrt{\frac{k_B T_{Te}}{m_e}}$ is the thermal speed F is the ratio of two poly-logarithm function given by,

$$F = \frac{Li_{5/2}(-e^{\beta\mu})}{Li_{3/2}(-e^{\beta\mu})} \quad (8.10)$$

The equation of state for holes is given by the Boltzmann distribution. The different plasma parameters for semiconductors are given in table (8.1) [330, 331, 332, 333].

If P_j is the EoS for degenerate matter then it can be presented as, $P_j = (\beta_j/3) \left[\frac{\Gamma^{2/3}}{1+\Gamma^{2/3}} \right]^{1/2}$ for weakly relativistic case where as in ultra-relativistic case it has the form like $P_j =$

Semiconductor	Γ	β	μ_{he}	P_h	P_e	Number Density	Hole mass ratio	Electron mass ratio
Ge	1.03×10^7	1.573×10^7	0.208	2.4×10^8	1.141×10^9	2.02×10^{13}	$0.51m_0$	$0.06m_0$
Si	4.42×10^3	9.7×10^6	0.50	2.653×10^7	5.305×10^7	8.72×10^9	$0.33m_0$	$1.59m_0$
InP	6.6	5.94×10^6	7.50	3.711×10^6	4.95×10^5	1.3×10^7	$0.6m_0$	$0.08m_0$
GaAs	1.03	5.94×10^5	8.50	1.7×10^6	2×10^5	2.03×10^6	$0.51m_0$	$0.06m_0$

Table 8.1: Different plasma parameter for different plasmas

$\frac{\beta_j \Gamma^{1/3}}{3}$. In both the cases $\beta_j = \frac{m_j c^2}{2k_B T_j}$ and Γ is the ratio of the unperturbed densities of holes and electrons; where $j = e, h$. Here μ_{he} stands for the mass ratio between holes and electron. Also, m_0 is the rest mass of electron.

8.3 Derivation of Evolutionary Equations

Now, we solve the normalized form of equations from (8.1) to (8.6) with help of PLK method and use some standard stretching variables. As we consider the wave due to hole plasma flows from left to right thus the stretching variables for the left to right space are given by,

$$\left. \begin{aligned} \xi &= \varepsilon(x - \lambda_h t) + \varepsilon^2 P_0(\xi, \tau) + \dots \\ \tau &= \varepsilon^3 t \end{aligned} \right\} \quad (8.11)$$

Here λ_e & λ_h are the wave group velocities of electrons and holes which is equal to the velocity of waveframes of the corresponding species of carriers. Also, the wave due to electron plasma flows from right to left thus the stretching variables for the left to right space are given by,

$$\left. \begin{aligned} \eta &= \varepsilon(x + \lambda_e t) + \varepsilon^2 Q_0(\eta, \tau) + \dots \\ \tau &= \varepsilon^3 t \end{aligned} \right\} \quad (8.12)$$

Here, ε is smallness parameter measuring the dispersion of the waves. Such stretching and perturbation has been used by many authors [168, 118, 117, 167, 68]. If we assume that both the waves start at a same instant then the wave will interact at a point y -length from the left side of the semiconductor and is given below:

$$y = \frac{2L}{1 + \frac{\lambda_e}{\lambda_h}} \quad (8.13)$$

After some algebraic steps we get the KdV equations for the both sides which are given by,

$$\frac{\partial \phi_h^{(1)}}{\partial \tau} + A_1 \phi_h^{(1)} \frac{\partial \phi_h^{(1)}}{\partial \xi} + B_1 \frac{\partial^3 \phi_h^{(1)}}{\partial \xi^3} \quad (8.14)$$

and,

$$\frac{\partial \phi_e^{(1)}}{\partial \tau} + A_2 \phi_e^{(1)} \frac{\partial \phi_e^{(1)}}{\partial \eta} + B_2 \frac{\partial^3 \phi_e^{(1)}}{\partial \eta^3} \quad (8.15)$$

Here, A_1 and A_2 (equation (8.16)) are the nonlinear coefficients for hole and electron waves respectively and B_1 and B_2 (equation (8.17)) are the dispersive coefficients.

$$A_1 = \left[\frac{(\nu - \delta\sigma^2)(3\lambda_h^2 - \Theta_h - 3)}{18} - \frac{6\lambda_h^3 - 3}{2(3\lambda_h^2 - \Theta_h - 3)^2} \right]$$

$$A_2 = - \left[\left(\frac{9F}{\lambda_e^2} + \lambda_e \right) \left(\delta\sigma_i + \gamma\sigma_h + \frac{3\chi\alpha}{9F + \chi\Theta_e} \right) \right] \quad (8.16)$$

$$B_1 = \left[\frac{\beta_h}{2} - \frac{(3\lambda_h^2 - \Theta_h - 3)}{18} \right]; \quad B_2 = -\frac{\beta_e}{\lambda_e} \quad (8.17)$$

Here $\Theta_j = V_{Fj}^2 \left[3 - (3\pi)^{2/3} H^2 (0.985 + \frac{0.616}{1 + \frac{1.9}{H^2}}) \right]$

and $\beta_j = \frac{\hbar^2}{4m_j^2}$. For details of the derivation one may look in the recent works on degenerate plasma [179, 181]

8.3.1 Numerical Analysis of Solitary waves and Wave-wave Interactions

We start with numerical solutions for the wave interaction in the present system. The electron and hole density solitons propagate towards the junction when a potential bias is applied across the semiconductor. Since we are looking for numerical solutions of the analytical functions we start with a hyperbolic secant squared solution. The bright hole soliton interacts with the negative electron soliton and when they collide to each other at the interface the total potential is negative due to the excess concentration and mobility of electrons. If we had two electrostatic waves propagating toward each other formed

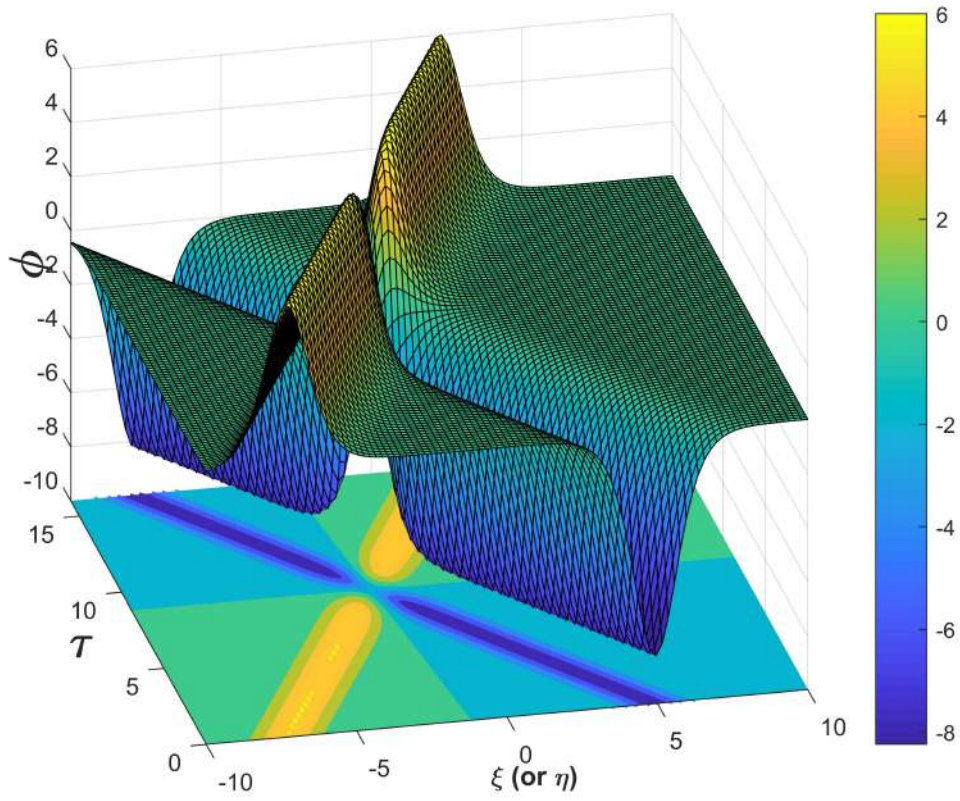


Figure 8.1: Interaction between electron and hole waves

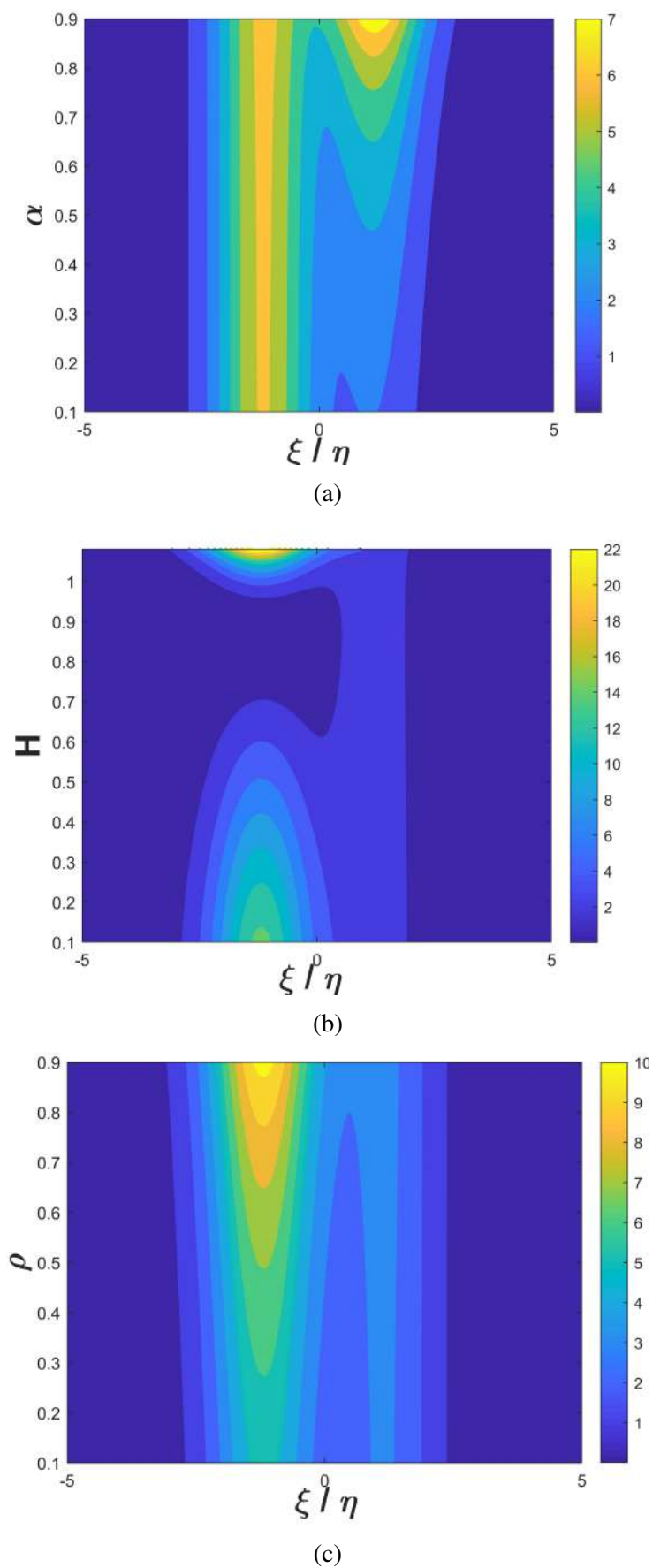


Figure 8.2: Contour plot for different values of (a) doping parameter for n-side of semiconductor α ; (b) quantum diffraction parameter H and (c) doping parameter for p-side of semiconductor ρ

from counter propagating carrier beams equal amplitude then the interaction would have caused a zero potential. However in this numerical analysis the gradual interaction between the electrons and holes are not properly visible. Therefore a real-time simulation will be more appropriate in this study which vein present in the subsequent sections. In figure (8.2) we show the parametric dependence on the soliton interaction. The doping parameter for n-side of semiconductor α (8.2a), quantum diffraction parameter (H) (8.2b), doping parameter for p-side of semiconductor ρ (8.2c) significantly affect the interaction mechanism which is shown through these figures. The simulation results will help in identifying the nonlinear wave wave interaction in a more physical way which is presented in the next section.

8.4 Simulation

8.4.1 Theory

We have carried out a simulation starting with the evolutionary equation and employed our newly developed INSAT-FORK code. We start with the nonlinear partial differential equation obtained from the governing equations (8.1)-(8.6) through the PLK method. In this case the evolution equation is a KdV equation. We transform the equation from real space to Fouriers space and convert the the PDE to ODE and solve by using Runge-Kutta 4th Order (RK4) method and obtained the solution in momentum space which is re-transformed into real space. Alternatively the reductive perturbation technique (RPT) [67, 169, 122, 243, 256, 173, 178, 176, 73, 187] can be used in place of PLK method. This technique is advantageous since we can bypass the numerical viscosity effects in the simulation which is due to the nonlinear terms in the evolution equation. The additional edge in this method is that we can deal with the unnormalised evolutionary equation with different initial and boundary conditions which can acquire gigantic values in similar problems corresponding to numerical viscosity etc.

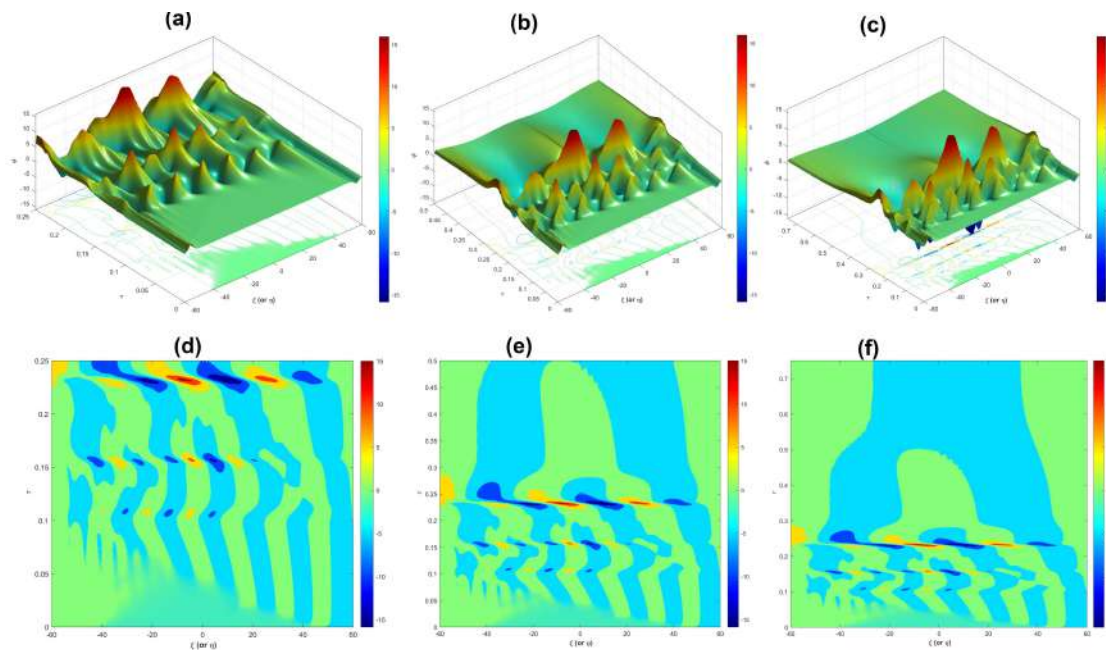


Figure 8.3: Potential evolution for $L=60$ and $\tau = 0.25, 0.5$ and 0.75

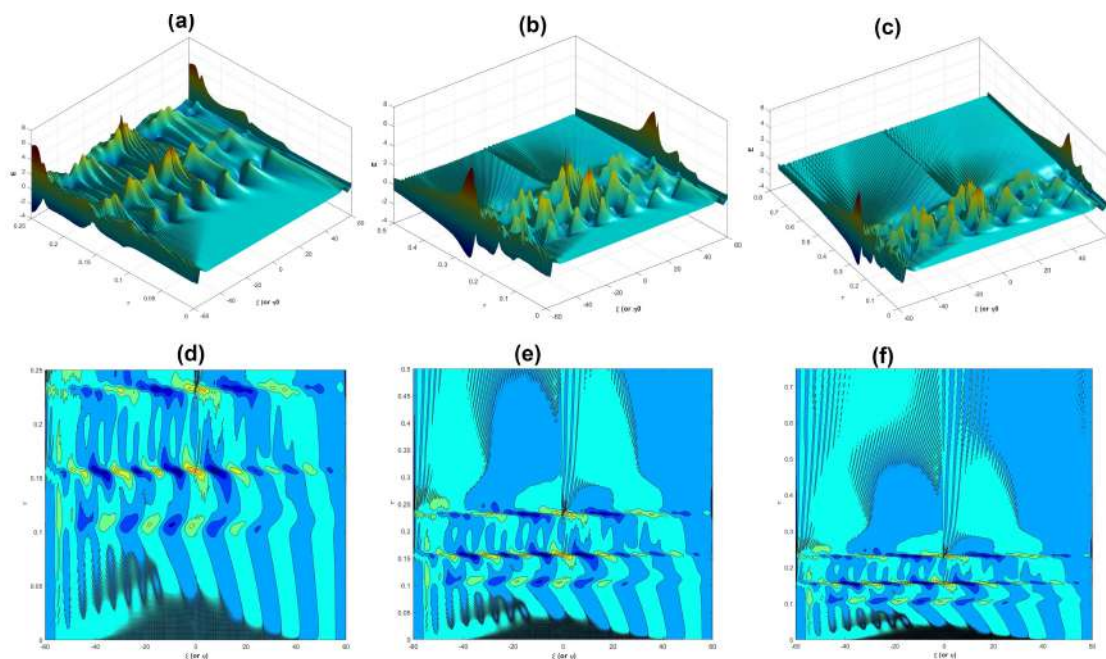


Figure 8.4: Electric field evolution for $L=60$ and $\tau = 0.25, 0.5$ and 0.75

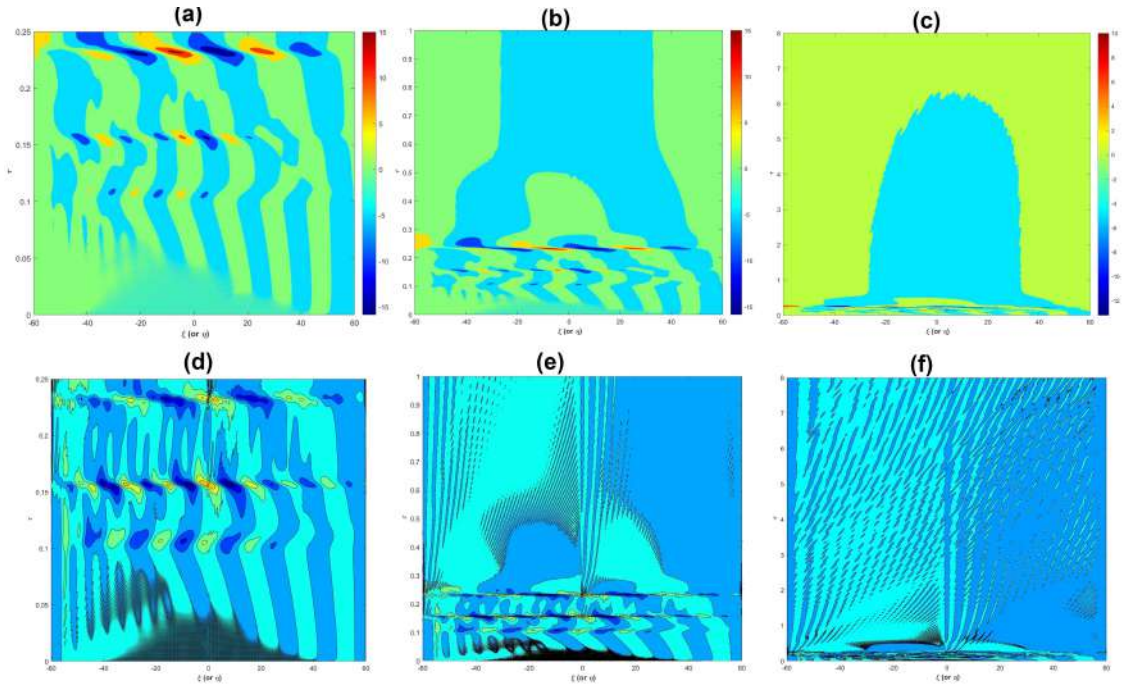


Figure 8.5: Contour plot of long time evolution of potential and field for $L=60$ and $\tau = 0.25, 1$ and 8

8.4.2 Results

In figure (8.3) we plot the potential evolution for different instance of time. During the early phases ($\tau = 0.25, 0.5, 0.75$) of the wave wave interaction, we see that the length of the semiconductor medium is taken as $L=60$ in terms of the the Debye length of the semiconductor plasma. Streams of holes propagate from the left hand side towards the junction and a bunch of electrons propagate from the right hand side towards the junction. At $\tau = 0.25$, both the electron and holes start to move towards the interface. However within the first few instants of time there is no interaction and this time is the response time between which the interaction does not start. As time increases we see that both electrons and holds create secondary potential fluctuations along the length. This is due to the fact that as the pulses propagate along each other, the semiconductor medium starts oscillating in response to the the pulses from the two extremities. This is relatable with the collective behaviour as observed in plasma. As time increases there are zones of interactions visible in figures (8.3)(b, c, e, f). We observe that the region

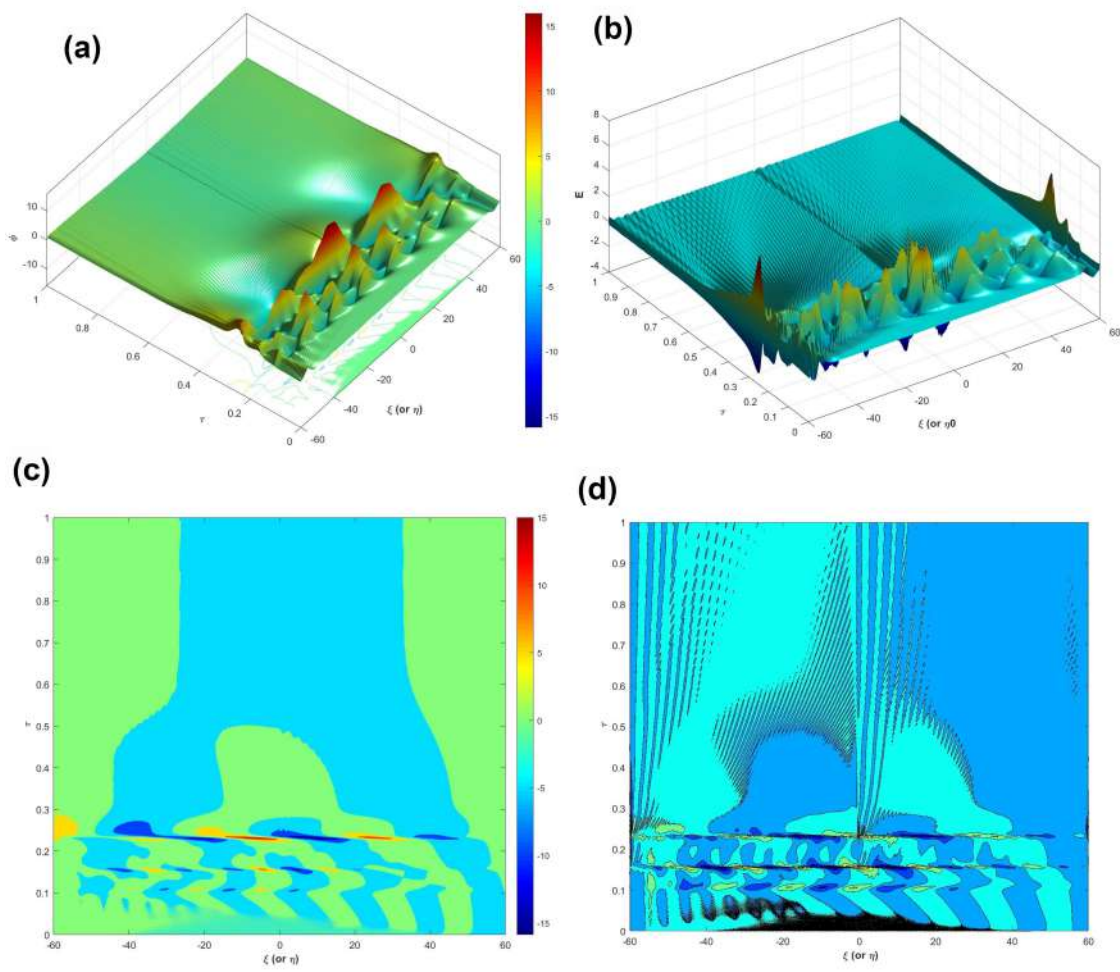


Figure 8.6: Potential and Field for $L=60$ and $\tau = 1$

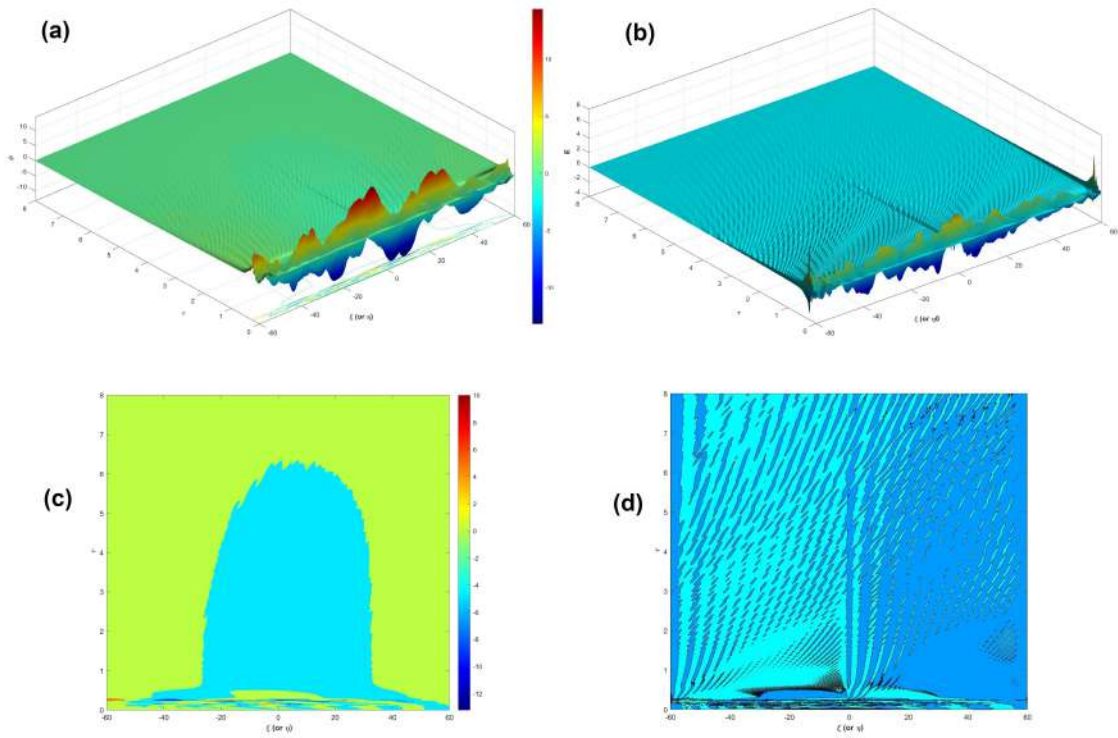


Figure 8.7: Potential and Field for $L=60$ and $\tau = 8$

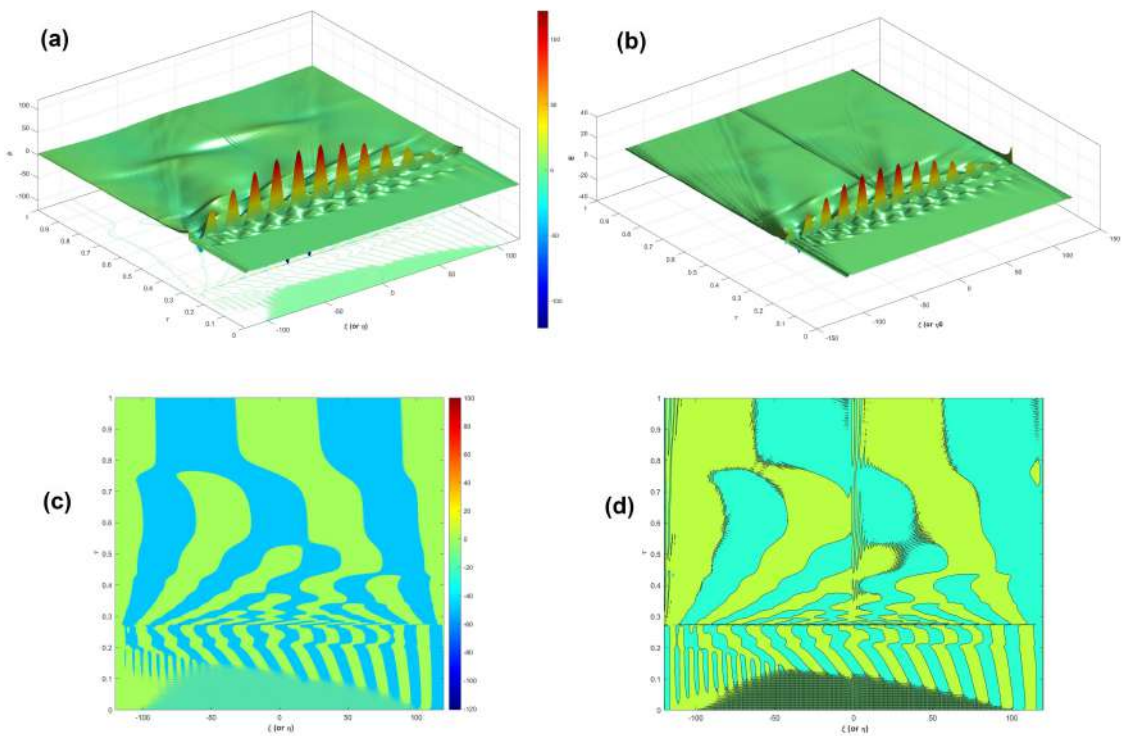


Figure 8.8: Potential and Field for $L=120$ and $\tau = 1$

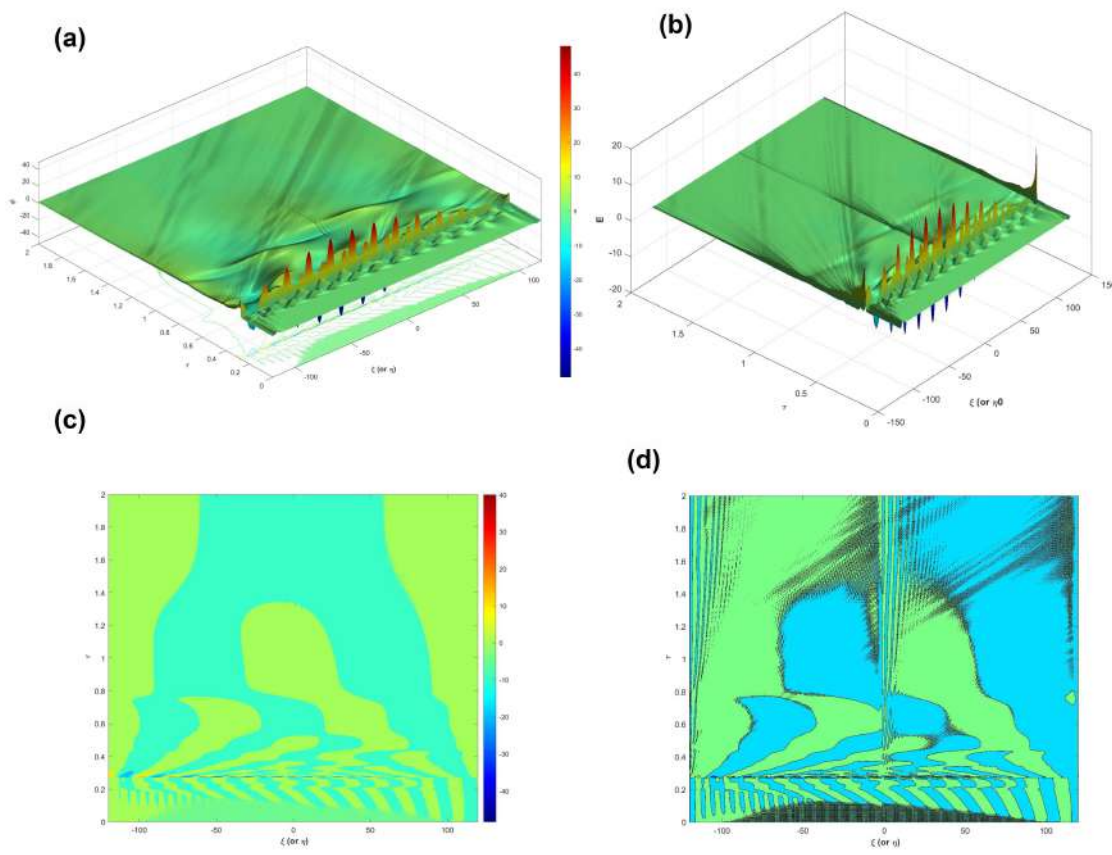


Figure 8.9: Potential and Field for $L=120$ and $\tau = 2$

of interaction gradually increases thus widening the blue and green regions along the τ axis. Nonlinear effects originate in the medium and increases the electron and hole pulses' amplitude and the width as well thereby favouring interactions between electrons and holes. Such interaction may lead into recombination and after a sufficient time the semiconductor medium acquires uniform potential.

In figure (8.4) we show the evolution of electric field which is taken as the gradient of the potential obtained from the simulation and presented in the figure (8.3). We see that there are regions of electron and hole concentration maxima which originate due to the nonlinear interaction of minority charges in the other side of the PN junction. From the contour plots in figures (8.4)(d-f) we conclude that the electrons are creating secondary oscillations in the semiconductor much quickly than the holes. This is due to the fact that electrons are slightly mobile than the holes. In other way we say that the effective mass of the holes being slightly greater than those of electrons show more inertial effect in the medium. At around $\tau = 0.1$ the interaction begins to take place and there are three regions of interaction shown by horizontal modulation along the ξ/η axis. As time increases we notice that there are regions of hole and electron majority on other side of the junction. However there are small short range fields in this regions which are due to the remnant field after interaction. This small scale electric field fluctuations arise from the subsequent acceleration of the minority charges right after the electron and hole solitons collide with each other. One may suggest that such an interaction may lead to recombination phenomenon thereby supplying energy to the semiconductor medium. Electrostatic field die out after sometime and the semiconductor acquires a uniform potential. Figure (8.5) shows the contour plot of long time evolution of potential and field. Our previous claim of potential homogenisation is reflected in figure (8.5)c at sufficient long time ($\tau = 8$). The effect of time of interaction is visible from the comparison of figures (8.6) and (8.7). It is seen that as time increases the solitary structures propagating towards each other from the two extremities of the semiconductor collide and interact in a nonlinear fashion after which they move on either side of the PN junction due to the

applied bias. The effect of length can be compared from figures (8.6) and (8.8). As the length is doubled up from 60 to 120 on either side of the junction we see that the interaction lasts for longer time. This is due to the fact that as the length increases the response time increases as well as the pulses take more time to propagate towards the junction with respective group velocities. The effect of time of neutralisation for longer semiconductor channel can be compared from figures (8.8) and (8.9). All these time series plots hint towards the classical interaction mechanism for a system of quantum particles. An animated version of the evolution of the potential can be checked here [334]. This information can be related with the numerical findings in the previous section when the solitons collide with each other. However the intricate mechanism are clearly visible through the simulation studies. The INSAT FORK code can be applied to multiple component plasma [248], semiconductor diodes [335], Hall systems [336], etc.

8.5 Summary

In this work the interaction between electron and hole waves. In the next part of this work is basically a simulation of colliding electron and hole solitons in a semiconductor plasma. We have successfully shown the interaction mechanism both graphically as well as through animation. The results will help in understanding breakdown mechanism and designing electronic devices accordingly. The analytical approach partly supports the simulation results which has close resemblance with experimental outcome. The newly designed simulation code can be extended to a variety of problems with periodic boundary conditions. A wide range of nonlinear effects can be predicted from such simulation works.

CHAPTER 9

STATIONARY STRUCTURES AND ITS EVOLUTION

9.1 Introduction

Over the past few years there has been a considerable increase in the study of quantum and exotic plasma. Quantum plasma are characterized by high density or low temperature or both such that they might amount to the overlapping of de-Broglie waves so as to give rise to quantum effects. When such a plasma is in motion, i.e the species flow as fluids, there are many hydrodynamic effects that amount to the formation of stationary structures whose stability depends on physical characteristics of the plasma. Many of such structures appear and disappear under different plasma configurations. For instance if we consider the plasma being composed of ions and electrons, where there are statistically differentiated hot and cold electron groups out of which the cold species provide inertia and the warm category provides the restoring force. Such a system allow the propagation of low frequency waves like the electron acoustic waves. The ions being heavier are almost immobile and form an uniform neutralizing background satisfying the quasi-neutrality criteria. The warm electron due to the high mobility provides the pressure that depends upon the equation of state of the system. Now there are small range interactions among the plasma particles, as a result they give rise to viscous effects. Now such a viscous effect slows down the particles' motion and the viscosity greatly affects the structure of the stationary formations. Bernstein, Greene and Kruskal [337] showed that there can be a possibility of an unlimited class of solutions to the Vlasov equations (BGK Solutions). Taking cue from their pioneering works a member of stable and unstable potential structures have been reported. Initially double layers were solved by Langmuir [338] who used the cold particle approximation (delta-function distribution); but with our present knowledge we know that such solutions are unstable. Later

Block(1972) used fluid theory at finite temperature to obtain the solution that was asymptotically self consistent for the potential separation greater than the thermal energy thus creating strong double layers. Later works of Knorr and Goertz [339], Carlqvist [340] and others have enriched the subject knowledge.

Among other stationary structures shocks and solitary waves are often referred to the literature and are obtained in laboratory produce plasma and space plasmas. Such dynamical structure have been extensively studied by M. Akbari-Moghanjoughi [341, 342], Kourakis [343], Shahmansouri [344, 345], Schamel [346], Kim [347], Quon and Wong [348], Chandra [65, 68, 187, 243], Ghosh [82, 64], Bychkov [349], Marklund [184]. Among these works, some are in the classical domain whereas some lie in the quantum range. For instance, in case shock fronts in quantum plasmas the dispersion is due to the Bohm Potential term in contrast to the dissipation effects in classical plasmas. Quantum systems have gathered more prominence due to its applications in nano-structures [350, 351, 352], quantum wells [353, 354, 355], laser fusion plasma [356, 357], ultracold plasmas [358, 359], plasmonic devices [360] and similar other fields. Nonlinear effects in plasma manifest in various forms under various physical situations [187]. Dark and bright soliton [361, 362], vortices, nonlinear interaction with electromagnetic waves [363, 364], turbulence [365], solitary profiles [366, 367] some of which are supported by electron spins [368] are among those effects often observed in plasmas. If viscosity is present shocks are often reported and they are studied by Burgers' equation.

Now it has been reported that quantum effects in dense plasma might not necessarily require ultra cold temperature. Even finite temperature dense Fermi plasma manifest the quantum diffraction effects. In a very novel work carried out by Eliasson and Shukla in 2008 [191], they came up with the evolution of nonlinear fluid equations of in a finite temperature Fermi plasma. The model that they have considered is based on a 3D equilibrium state in which nonlinear electron plasma waves are propagating and have been used by many [73, 72, 169, 167, 134, 171, 176, 122]. In contrast to the classical Vlasov picture where the phase fluid is incompressible; this model incorporates the violations

of incompressibility of phase fluid due to quantum tunneling. To a first order approximation such incompressibility is assumed to hold good. Considering the waves lead to adiabatic compression in the direction of propagation, it leads to temperature anisotropy, the non-equilibrium particle distribution therefore is given by [191]

$$f(x_i, \vec{u}, t) = \frac{F_0}{1 + e^{\beta m/2} ((u_x - u_{av})^2 \alpha + (u_y)^2 + (u_z)^2 - \beta \mu)} \quad (9.1)$$

where u_{av} is the average velocity of the particles, $\alpha(x, t) = \frac{T_{e0}}{T_{au}(x,t)}$ is the temperature anisotropy to be obtained from number density variations. F_0 is a normalizing constant. To a first approximation, we assume the chemical potential to remain constant. Here $F_0 = 2(\frac{m}{h})^3$, α can be written as $\alpha(x, t) = [\frac{n_0}{h_e(x,t)}]^2$.

Space and many other laboratory plasmas have energy and velocity in such a range that often a commonly used distribution function becomes insufficient. Many scientists therefore, attempted to introduce distribution functions that to a great extent successfully describe the physical problem. Tsallis distribution [369, 370, 168], Cairns distribution [371], non thermal distribution [371, 167, 168], Kappa distribution [372, 373, 374, 375, 376, 377], q-non extensive [378, 379] are some of them. Plasmas found in planetary magnetosphere [118, 176] and stellar and solar plasma [380] often display characteristics of Kappa distribution. We have investigated the available literature for a detailed study of Kappa distribution, and designed this problem in the light of such works. Often it is observed that within a plasma various species of particles like electrons [117], ions, positrons [169], dust [63, 381, 181, 182] etc. are present [190]. In dense stellar plasmas [73, 256] where electrons and ions are compactly packed quantum-statistical effects and quantum diffraction effects [188] are additional manifestations. These give rise to several features to existing wave modes.

This chapter is organized in the following manner. In Section §9.2 we introduce the finite temperature Fermi fluid model and the basic governing equation corresponding to

the problem. In Subsection §9.2.2 we obtain the pseudopotential using Sagdeev's method which will help in the study of large amplitude solitary structures. Next we obtain the KdV Burger's equation in Subsection §9.2.3 that provides the differential equation corresponding to small amplitude stationary structures like shocks, double layers and solitary waves. Then in Section §9.3 we study forced KdV and envelope soliton in magnetoplasma with Kappa distributed ions and introduce basic governing equations. In Subsection §9.3.2, we study the symbolic simulation of the forced Korteweg–De Vries (KdV) and its evolution into an envelope soliton. To augment the previous findings, we carry out the linear and nonlinear analysis. Then in Subsection §9.3.3, we obtain the linear dispersion relation and discuss the results therein. Next, we obtained the KdV equation by employing the perturbation technique and obtain the solution for the KdV equation. We plot the solitary profile and discuss the results and finally conclude with some results and application of this problem in real plasma situations. We also utilize the perturbation approach (in §9.3.3) in order to get the Nonlinear Schrodinger equation and analyze the stability and instability criteria of amplitude-modulated envelope solitons. Finally in Section §9.4 we conclude with some remarks on the applicability and the importance of this work in physical scenario.

9.2 Evolution of nonlinear stationary formations in a quantum plasma at finite temperature

Many applications with plasma interactions include the density at which the medium acts primarily as a fluid. The basic movements regarding energy input, force application, and the effects of magnetic and electric fields are continuum fluid movements [382]. Therefore, this explanation and interpretation services as a starting point for understanding the complex behavior of plasmas. It then improves modeling and experimentation to reveal the uniqueness of regimes and interactions and ultimately to an understanding of the plasma, enabling efficient device operation. To create this important explanation, we

will use magnetohydrodynamics (MHD) equations to help us understand and quantify the behavior of plasmas.

The plasma interaction model is an unsteady solver based on the law of conservation of charge. As mentioned earlier [383, 384], the International Space Station is affected by surface differences or deep dielectric charging processes that plague small spacecraft in more demanding charging environments, except for anomalous charging spikes. We sometimes reported very low ionospheric densities during those in the previous section. Active charging of the station's conductive structure powered by the vehicle's electromotive force is the most important charging process for the International Space Station and its security analysis. The stray potential of the plasma interaction model is simulated by computing the equivalent energies associated with capacitively constrained dynamic charges. The lost potential of this approach is unique to the external plasma at any point on the spacecraft. At the same time, the operating voltage and geomagnetic electromotive force of the solar system distribute the potential throughout the structure. The capacitance of the vehicle corresponds to the thin dielectric anodizing material that covers the glued aluminum vehicle structure. The structural metal surrounds one side of the capacitance, and the surrounding conductive plasma surrounding the other side of the capacitance is dominated by the basic material properties of the coating. Charge accumulation is considered according to the positive and negative integrated currents collected in the conductive structure.

It is a matter of fact to have sufficient observational data to support the theory to model / reconstruct the stationary structures in space plasma. To investigate this, we have to define "Stationary structures" first.

A stationary structure encountered by spacecraft in interplanetary plasma, e.g., flux ropes, clouds, reconnection exhaust, etc. One can now use the spacecraft data to reconstruct those sections uniquely. The current method has the problem of data redundancy, but how much data is sufficient for the present scenario. Unfortunately, there is no answer, at least for now. Russian scientist Oleg I. Berngardt, Laboratory Head at the Insti-

tute of Solar-Terrestrial Physics OF SIBERIAN BRANCH OF RUSSIAN ACADEMY OF SCIENCES, can be said that plasma is mainly composed of unsteady and irregular media. Suppose one wants to reconstruct the static structure of the media. Measurement techniques provide temporal and spatial resolution, integration time, detector timing, and more. Therefore, each method offers some smoothed value.

In that case, one needs to look at the theory of metrology, get the model media in the form of a combination of static and dynamic parts, and find the parameters independent of the dynamic characteristics of the model. People usually use different types of statistical analysis to find these parameters: very long (nearly infinite) integrations (like noise in measurement data where the dynamic part of the media is zero on average). (When generating signals), superimposed epoch analysis, correlation techniques (when the dynamic aspects of the media change the temporal or spatial position of the effect of the measured data), and spectral analysis (when the dynamic elements of the media change). When generating a period during which measurement data is missing), etc. The problem is that plasma is usually not a stationary object and its parameters and structure change over time. Therefore, scientists can generally talk very roughly about the steady-state of the plasma. In his opinion, the more data one measures, the better. Even the equipment placed nearby will generate additional information (for example, they may have different noise components and can be used to detect the direction of the effect using interferometry techniques, etc.). This allows one to build more complex models and consider the more complex dynamic parts of the media model when trying to find the static parts of the media model.

9.2.1 Basic equation

The finite temperature Fermi fluid model and the basic governing equations [60, 237, 56, 191, 201] are given as

$$\frac{\partial}{\partial t}(n_h) + \frac{\partial}{\partial x}(n_h u_h) = 0 \quad (9.2)$$

$$\frac{\partial}{\partial t}(n_c) + \frac{\partial}{\partial x}(n_c u_c) = 0 \quad (9.3)$$

$$[\lambda] \left(\frac{\partial}{\partial t} + u_h \frac{\partial}{\partial x} \right) u_h = \frac{\partial}{\partial x} \phi - F_h \left(\frac{\partial}{\partial x} n_h \right) + \frac{H^2}{2} \frac{\partial}{\partial x} \left[\frac{1}{\sqrt{n_h}} \frac{\partial^2}{\partial x^2} \sqrt{n_h} \right] + \eta_h \frac{\partial^2 u_h}{\partial x^2} \quad (9.4)$$

$$\left(\frac{\partial}{\partial t} + u_c \frac{\partial}{\partial x} \right) u_c = \frac{\partial \phi}{\partial x} - F_c \frac{\partial n_c}{\partial x} + \frac{H^2}{2} \frac{\partial}{\partial x} \left[\frac{1}{\sqrt{n_c}} \frac{\partial^2}{\partial x^2} \sqrt{n_c} \right] + \eta_c \frac{\partial^2 u_c}{\partial x^2} \quad (9.5)$$

$$\frac{\partial^2 \phi}{\partial x^2} = (n_c + \frac{n_h}{\delta} - n_i \frac{\delta_1}{\delta}) \quad (9.6)$$

The value of $\lambda = 1, 0$ corresponds to whether or not the inertia effects of hot electrons.

We normalize the above equations as $\bar{n}_j \rightarrow \frac{n_j}{n_{j0}}$, $\bar{u}_j \rightarrow \frac{u_j}{C_{sh}}$, $\bar{x} \rightarrow \frac{x\omega_c}{C_{sh}}$, $\bar{t} \rightarrow \omega_c t$, $\bar{\phi} \rightarrow \frac{e\phi}{k_B T_{Fh}}$, where the subscript j is used to denote hot (h), cold (c) electrons and ion (i), u_j, n_j ($j = c, h$) are the velocity, density, $F_h = (\frac{n_{h0}}{n_0})^{\frac{1}{3}} \frac{m_e c^2}{6k_B T_{Fh}}$, $F_c = (\delta)^{\frac{2}{3}} \frac{m_e c^2}{2k_B T_{Fh}}$, $\delta = \frac{n_{c0}}{n_{h0}}$, $\delta_1 = \frac{n_{i0}}{n_{h0}}$ (subscript 0 stand for equilibrium state) and $H = \frac{\hbar\omega_c}{2k_B T_{Fh}}$, $\omega_c = \sqrt{\frac{n_{c0}e^2}{\epsilon_0 m_e}}$ is the cold electron plasma frequency, $C_{sh} = \sqrt{\frac{2k_B T_{Fh}}{m_e}}$ is the hot electron acoustic speed and T_{Fh} is the hot electron Fermi temperature respectively.

9.2.2 Non-perturbative Analysis

In order to study possibility of formation and nature of such stationary formation (large/arbitrary amplitude solitons) we make use of Sagdeev's pseudopotential method.

Derivation of the Pseudopotential Function:

To obtain the pseudopotential function we apply regular stretched co-ordinate transformation $\rho = x - Mt$, where M is Mach number. Integrating the dynamic equations and employing standard technique we get the field quantities in terms of n_h . Substituting $z = n_h^{1/2} = n^{1/2}$ and perform integration with appropriate boundary conditions i.e; $n(\rho)'' \rightarrow 0, n(\rho)' \rightarrow 0$ and $n \rightarrow 0$ as $\rho \rightarrow |\pm\infty|$, one obtain the energy integral equation as

$$\frac{1}{2} \left(\frac{dn}{d\rho} \right)^2 + U(n) = 0 \quad (9.7)$$

where $U(n)$ can be expressed as

$$\begin{aligned} U(n) = & \frac{1}{2(\eta_e - \eta_h)^2} \left[M^2(\lambda - 1)n(n - 1) \right. \\ & + Mu_0(1 - \lambda)n^2 + \frac{(F_c\delta - F_h)n^2(n-1)}{(\delta+1)} + \frac{u_0(\lambda-1)(u_0-2M)n^2}{2} \\ & \left. + \frac{(1-\lambda)}{2} \left(M^2(n-1)^2 + 2Mn(n-1)u_0 + u_0^2n^2 \right) \right]^2 \end{aligned} \quad (9.8)$$

here $\lambda = 0$ corresponds to hot electrons are inertia less. The pseudopotential is plotted against hot electron density which for brevity we written in figure -9.1 with variation of system parameters and we discuss it in the results section §9.2.2. To yield soliton solution, we use some boundary conditions as follows:

$$\begin{aligned} a) \quad & U(n) = 0 \quad \text{at} \quad n = 0 \quad \text{and} \quad n = n_m \\ b) \quad & \frac{dU}{dn} = 0 \quad \text{at} \quad n = 0 \quad \text{but} \quad \frac{dU}{dn} \neq 0 \quad \text{at} \quad n = n_m \\ c) \quad & \frac{d^2U}{dn^2} < 0 \quad \text{at} \quad n = 0 \end{aligned} \quad (9.9)$$

From Eqn. (9.7), we can say that shape of soliton structure can be decided from the following equation:

$$\rho = \pm \int_{n_m}^n \frac{dn}{\sqrt{-2U(n)}} \quad (9.10)$$

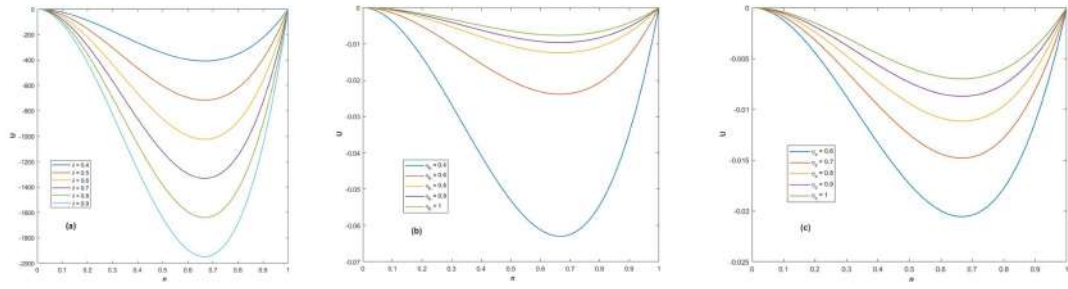


Figure 9.1: U vs n for different values of (a) δ , (b) η_h & (c) η_c with $M = 1.6, H = 2, \lambda = 1, u_0 = 0.5, F_h = 0.05$ & $F_c = 0.0004$. (Individual parameters are in the median range)

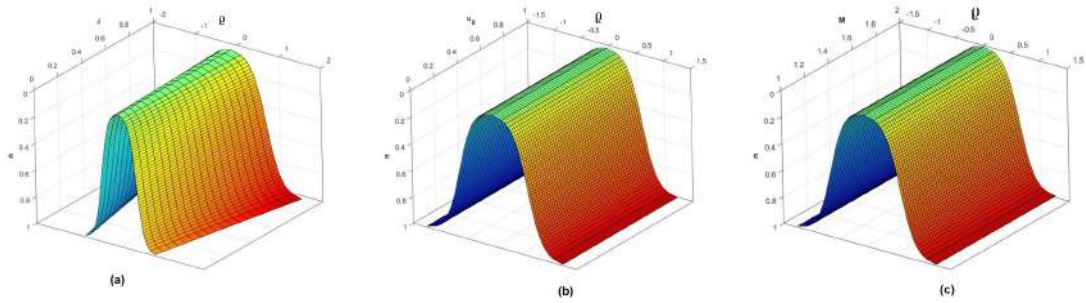


Figure 9.2: Arbitrary amplitude solitary profile vs ρ for different values of (a) δ (b) u_0 , & (c) M with $\delta = 0.5, \eta_h = 0.004, \eta_c = 0.001, H = 2, \lambda = 1, F_h = 0.05$ & $F_c = 0.0004$. (Individual parameters are in the intermediate range)

The corresponding solitary structures with arbitrary amplitude is plotted in figures 9.2,9.3,9.4 for different plasma parameters.

Findings of Non-perturbative Investigation:

For large amplitude solitary structures we need to consider different viscosity parameters for hot and cold electrons. Since the energy associated with such structures are high when compared to small amplitude where both are comparable and few orders lesser. Figure-9.1 show the variation of the pseudo-potential function with δ, η_h & η_c respectively as tuning parameters. The other constants are $F_h = 0.05, F_c = 0.0004, M = 1.6, u_0 = 0.5$. In figures-9.1 (b) and 9.1(c) the effects of hot and cold electron viscosity factors have been shown. From the figures 9.1 (a–c) it is clear that the hot electron density has a positive effect in decreasing the pseudopotential which is due to the increase in mo-

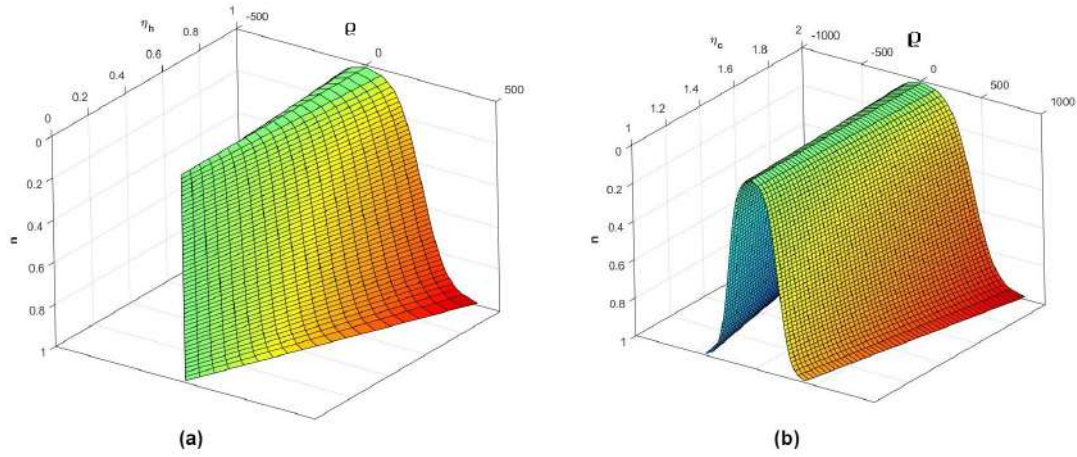


Figure 9.3: Arbitrary amplitude solitary profile vs ρ for different values of (a) η_h & (b) η_c with $\delta = 0.5$, $M = 1.6$, $u_0 = 0.5$, $H = 2$, $\lambda = 1$, $F_h = 0.05$ & $F_c = 0.0004$. (Individual parameters are in the intermediate range)

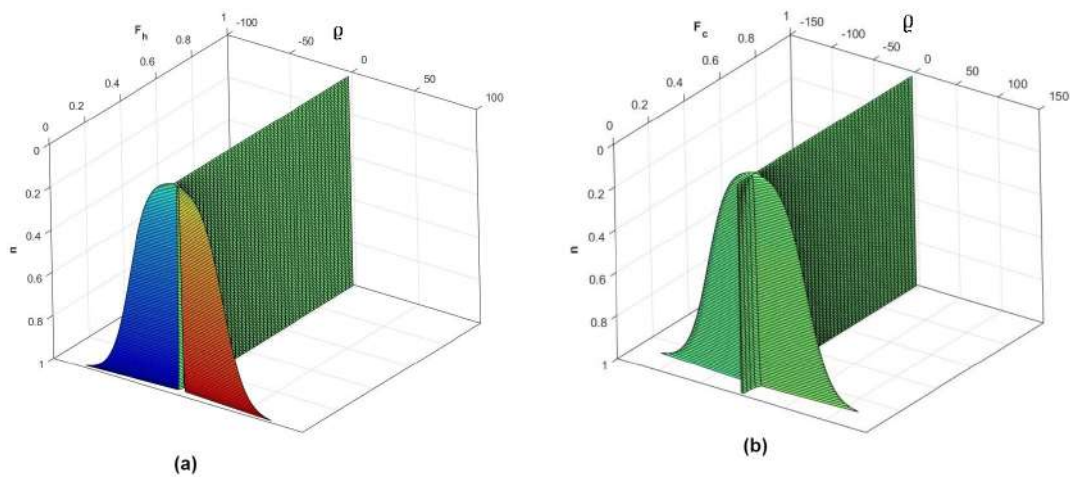


Figure 9.4: Arbitrary amplitude solitary profile vs ρ for different values of (a) F_h & (b) F_c with $M = 1.6$, $u_0 = 0.5$, $\delta = 0.5$, $H = 2$, $\eta_h = 0.004$, $\eta_c = 0.001$ & $\lambda = 1$. (Individual parameters are in the intermediate range)

bility and restoring force terms. The viscosity factors η_c and η_h show opposite effects when compared to the effect of δ . This is relatable as the higher density of cold electrons will provide inertia effect, thus contributing positively to the potential structure and formation of double layers. Apart from δ , Viscosity parameters η_c, η_h other parameters do not have much significant contributions in the pseudopotential. When the large amplitude solitary structures were plotted [figure 9.2] with variations in δ, u_0, M it is clear from 9.2(a) that equilibrium hot-to-cold electron density ratio (δ) has a dispersive effect whereas the streaming or the waveframe motions have no significant changes 9.2 (b–c). The viscous and restoring forces corresponding to hot and cold electron species is shown in figures 9.3 & 9.4. the viscous drag experienced by hot electrons is more compared to cold species. This is a direct consequence of mobility and momentum transfer among particles. There is no dependence of large amplitude structures on $F_h \& F_c$ except for some particular values close to zero. This is clear from figure 9.4(a–b) that the required restoring force term for cold electrons is higher than the hot electrons since the former contribute primarily to inertia. It is to be noted that some parameters were obtained in certain range (η_h, η_c) to obtain this type of conclusions. Some kind of resonant interaction might be instrumental in this phenomena. Relatable works will be available for comparison in some of these papers [134, 358, 345].

9.2.3 Reductive Perturbation Method

In order to study small amplitude stationary formation we make use of reductive perturbation technique (RPT) to obtain the KdV Burger's equation. We have used the same technique previously [118] [169] as used by other authors [167] [341]

Derivation of KdV-Burger's equation:

As done in previous works [68] perturbation expansion of the field quantities have been made. We take ϕ as the amplitude of the electric potential field, χ and τ are the stretched variables corresponding to x and t respectively [68] where $\chi = \varepsilon^{1/2}(x - Mt)$ and $\tau =$

$\varepsilon^{3/2}t$. Accordingly the perturbation series is given by:

$$\begin{bmatrix} n_h \\ n_c \\ u_h \\ u_c \\ \phi \end{bmatrix} = \begin{bmatrix} 1 \\ 1 \\ u_0 \\ u_0 \\ \phi_0 \end{bmatrix} + \varepsilon \begin{bmatrix} n_h^{(1)} \\ n_c^{(1)} \\ u_h^{(1)} \\ u_c^{(1)} \\ \phi^{(1)} \end{bmatrix} + \varepsilon^2 \begin{bmatrix} n_h^{(2)} \\ n_c^{(2)} \\ u_h^{(2)} \\ u_c^{(2)} \\ \phi^{(2)} \end{bmatrix} + \dots \quad (9.11)$$

and the viscosity factor is $\eta_{h,c} = \varepsilon^{\frac{1}{2}}\eta_{h,c}^{(0)}$. Using the standard procedure and equating terms of same power in ε we finally obtain the KdV Burger's equation given by

$$\frac{\partial \phi}{\partial \tau} + A\phi \frac{\partial \phi}{\partial \chi} + B \frac{\partial^3 \phi}{\partial \chi^3} - C \frac{\partial^2 \phi}{\partial \chi^2} = 0 \quad (9.12)$$

where

$$A = \frac{\frac{2(M-u_0)^2}{(F_c-(M-u_0)^2)^3} + \frac{\frac{(M-u_0)^2}{(F_h-(M-u_0)^2)^2} + \frac{(M-u_0)^2}{(F_h-(M-u_0)^2)^2}}{\delta(F_h-(M-u_0)^2)}}{\frac{2(M-u_0)}{(F_c-(M-u_0)^2)^2} + \frac{\frac{M-u_0}{F_h-(M-u_0)^2} + \frac{(M-u_0)}{F_h-(M-u_0)^2}}{\delta(F_h-(M-u_0)^2)}}$$

$$B = -\frac{H^2 \left(\frac{1}{(F_c-(M-u_0)^2)^2} + \frac{1}{\delta(F_h-(M-u_0)^2)(F_h-(M-u_0)^2)} \right)}{4} - 1$$

$$C = \frac{\frac{\eta_c^{(0)}(M-u_0)}{(F_c-(M-u_0)^2)^2} + \frac{\eta_h^{(0)}(M-u_0)}{\delta(F_h-(M-u_0)^2)(F_h-(M-u_0)^2)}}{\frac{2(M-u_0)}{(F_c-(M-u_0)^2)^2} + \frac{\frac{M-u_0}{F_h-(M-u_0)^2} + \frac{(M-u_0)}{F_h-(M-u_0)^2}}{\delta(F_h-(M-u_0)^2)}}$$

Now in equation 9.12 we consider the inertia effects of hot electrons and the pressure degeneracy effect of cold electrons. Comparing with the studies of other researchers the hot electron inertia and the cold electron degeneracy pressure might have negligible effect as we discuss in the following cases

Case-I:

Ignoring the hot electron inertia the KdV-Burger's equation is given by

$$\frac{\partial \phi}{\partial \tau} + A_1 \phi \frac{\partial \phi}{\partial \chi} + B_1 \frac{\partial \phi^3}{\partial \chi^3} - C_1 \frac{\partial^2 \phi}{\partial \chi^2} = 0 \quad (9.13)$$

where

$$A_1 = \frac{\frac{2(M-u_0)^2}{(F_c-(M-u_0)^2)^3} + \frac{(M-u_0)^2}{F_h^2 \delta (F_h-(M-u_0)^2)}}{\frac{2(M-u_0)}{(F_c-(M-u_0)^2)^2} + \frac{M-u_0}{F_h \delta (F_h-(M-u_0)^2)}}$$

$$B_1 = -\frac{H^2 \left(\frac{1}{(F_c-(M-u_0)^2)^2} + \frac{1}{F_h \delta (F_h-(M-u_0)^2)} \right)}{4 \frac{2(M-u_0)}{(F_c-(M-u_0)^2)^2} + \frac{M-u_0}{F_h \delta (F_h-(M-u_0)^2)}} - 1$$

$$C_1 = \frac{\frac{\eta_c^{(0)}(M-u_0)}{(F_c-(M-u_0)^2)^2} + \frac{\eta_h^{(0)}(M-u_0)}{F_h \delta (F_h-(M-u_0)^2)}}{\frac{2(M-u_0)}{(F_c-(M-u_0)^2)^2} + \frac{M-u_0}{F_h \delta (F_h-(M-u_0)^2)}}$$

Case-II:

Ignoring cold electron degeneracy pressure the corresponding equation 9.12 is given as

$$\frac{\partial \phi}{\partial \tau} + A_2 \phi \frac{\partial \phi}{\partial \chi} + B_2 \frac{\partial \phi^3}{\partial \chi^3} - C_2 \frac{\partial^2 \phi}{\partial \chi^2} = 0 \quad (9.14)$$

where

$$A_2 = -\frac{\frac{2}{(M-u_0)^4} - \frac{\frac{(M-u_0)^2}{(F_h-(M-u_0)^2)^2} + \frac{(M-u_0)^2}{(F_h-(M-u_0)^2)^2}}{\delta (F_h-(M-u_0)^2)}}{\frac{2}{(M-u_0)^3} + \frac{\frac{M-u_0}{F_h-(M-u_0)^2} + \frac{(M-u_0)}{F_h-(M-u_0)^2}}{\delta (F_h-(M-u_0)^2)}}$$

$$B_2 = -\frac{H^2 \left(\frac{1}{(M-u_0)^4} + \frac{1}{\delta (F_h-(M-u_0)^2) (F_h-(M-u_0)^2)} \right)}{4 \frac{2}{(M-u_0)^3} + \frac{\frac{M-u_0}{F_h-(M-u_0)^2} + \frac{(M-u_0)}{F_h-(M-u_0)^2}}{\delta (F_h-(M-u_0)^2)}} - 1$$

$$C_2 = \frac{\frac{\eta_c^{(0)}}{(M-u_0)^3} + \frac{\eta_h^{(0)}(M-u_0)}{\delta(F_h-(M-u_0)^2)(F_h-(M-u_0)^2)}}{\frac{2}{(M-u_0)^3} + \frac{\frac{M-u_0}{F_h-(M-u_0)^2} + \frac{(M-u_0)}{F_h-(M-u_0)^2}}{\delta(F_h-(M-u_0)^2)}}$$

Case-III:

Ignoring both hot electron inertia and cold electron degeneracy pressure

$$\frac{\partial \phi}{\partial \tau} + A_3 \phi \frac{\partial \phi}{\partial \chi} + B_3 \frac{\partial \phi^3}{\partial \chi^3} - C_3 \frac{\partial^2 \phi}{\partial \chi^2} = 0 \quad (9.15)$$

where

$$A_3 = -\frac{\frac{2}{(M-u_0)^4} - \frac{(M-u_0)^2}{F_h^2 \delta(F_h-(M-u_0)^2)}}{\frac{2}{(M-u_0)^3} + \frac{M-u_0}{F_h \delta(F_h-(M-u_0)^2)}}$$

$$B_3 = -\frac{H^2 \left(\frac{1}{(M-u_0)^4} + \frac{1}{F_h \delta(F_h-(M-u_0)^2)} \right)}{\frac{2}{(M-u_0)^3} + \frac{M-u_0}{F_h \delta(F_h-(M-u_0)^2)}} - 1$$

$$C_3 = \frac{\frac{\eta_c^{(0)}}{(M-u_0)^3} + \frac{\eta_h^{(0)}(M-u_0)}{F_h \delta(F_h-(M-u_0)^2)}}{\frac{2}{(M-u_0)^3} + \frac{M-u_0}{F_h \delta(F_h-(M-u_0)^2)}}$$

Case-IV:

Ignoring the viscous effects along the hot electron inertia and cold electron degeneracy pressure

$$\frac{\partial \phi}{\partial \tau} + A_4 \phi \frac{\partial \phi}{\partial \chi} + B_4 \frac{\partial \phi^3}{\partial \chi^3} \quad (9.16)$$

where

$$A_4 = \frac{\frac{2(M-u_0)^2}{(F_c-(M-u_0)^2)^3} + \frac{\frac{(M-u_0)^2}{(F_h-(M-u_0)^2)^2} + \frac{(M-u_0)^2}{(F_h-(M-u_0)^2)^2}}{\delta(F_h-(M-u_0)^2)}}{\frac{2(M-u_0)}{(F_c-(M-u_0)^2)^2} + \frac{\frac{M-u_0}{F_h-(M-u_0)^2} + \frac{(M-u_0)}{F_h-(M-u_0)^2}}{\delta(F_h-(M-u_0)^2)}}$$

$$B_4 = - \frac{H^2 \left(\frac{1}{(F_c - (M - u_0)^2)^2} + \frac{1}{\delta (F_h - (M - u_0)^2) (F_h - (M - u_0)^2)} \right)}{\frac{2(M - u_0)}{(F_c - (M - u_0)^2)^2} + \frac{\frac{M - u_0}{F_h - (M - u_0)^2} + \frac{(M - u_0)}{F_h - (M - u_0)^2}}{\delta (F_h - (M - u_0)^2)}} - 1$$

Solution of KdV-Burger's equation:

To solve this equation we employing method of series solutions as suggested by Wazwaz [385]. For this we use tanh transformation and considering the fact the Burgers solution for shocks have 'tanh' type solution and KdV solitary waves have 'sech' type solution one obtain solution for double layers given by

$$\phi_{DL} = \pm \phi_0 [1 + \tanh(\frac{\chi}{2})] \tag{9.17}$$

the \pm sign corresponds to the polarity of double layers. A detailed treatment is provided by Jian-Jun [386]. The KdV-Burger equation incorporate both the term and has a solution of the form

$$\phi_{sh} = \phi_0 [sech^2(\frac{\chi}{2}) \pm (1 + \tanh(\frac{\chi}{2}))] \tag{9.18}$$

equation 9.18 is the solution of the K-dV-Burgers equation describing the shock front coupled with solitary formations. If the stationary formation is stable the nonlinear forces and the dispersive factors balance each other thus give rise to a pure solitary waveform given by

$$\phi_{s0h} = \phi_0 sech^2(\frac{\chi}{2}) \tag{9.19}$$

Here the width has been normalized to a factor of 2 keeping in mind the inter-layer separation and the stationary formations.

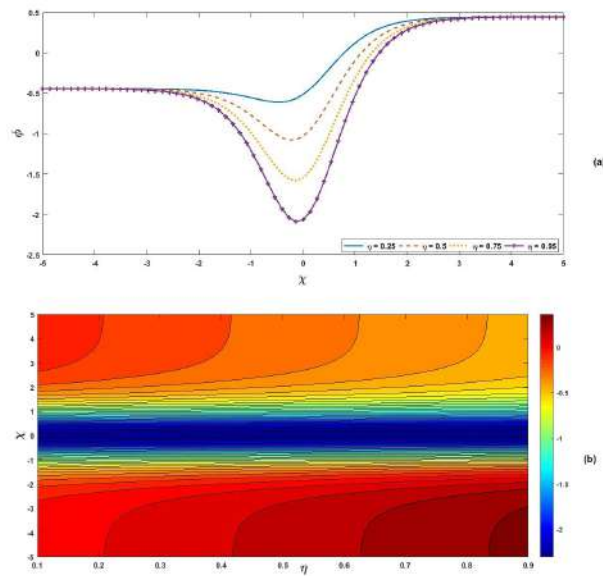


Figure 9.5: (a) Shock profile & (b) Contour plots for different values of viscosity factor (η) with $F_c = 0.48$, $F_h = 1.4$, $M = 1.5$, $u_0 = 0.5$, $H = 2$, $\lambda = 1$ & $\delta = 0.005$.

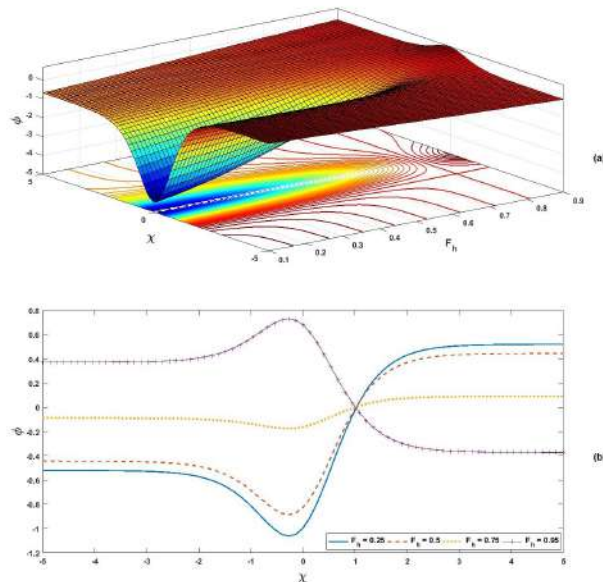


Figure 9.6: (a) Polarity shifting solitary structures with contour plots & (b) Shock profile for different values of F_h with $F_c = 0.48$, $\eta_{h,c} = 1.5$, $M = 1.5$, $H = 2$, $u_0 = 0.5$, $\lambda = 1$ & $\delta = 0.005$.

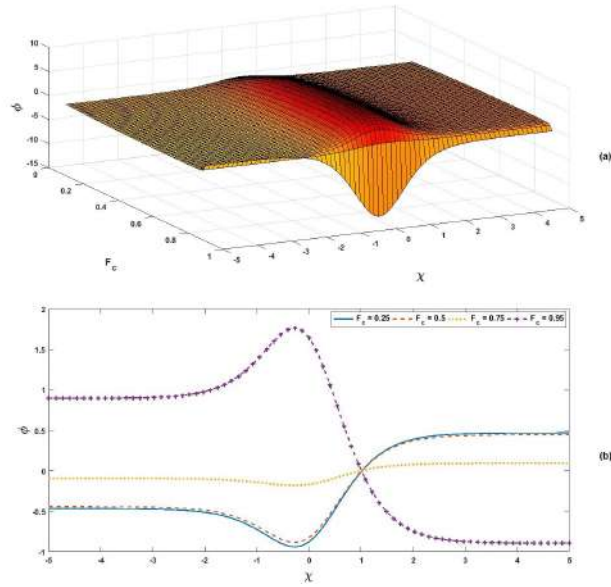


Figure 9.7: (a) Polarity shifting solitary structures with contour plots & (b) Shock profile for different values of F_c with $F_h = 1.4, \eta_{h,c} = 1.5, M = 1.5, H = 2, u_0 = 0.5, \lambda = 1$ & $\delta = 0.005$.

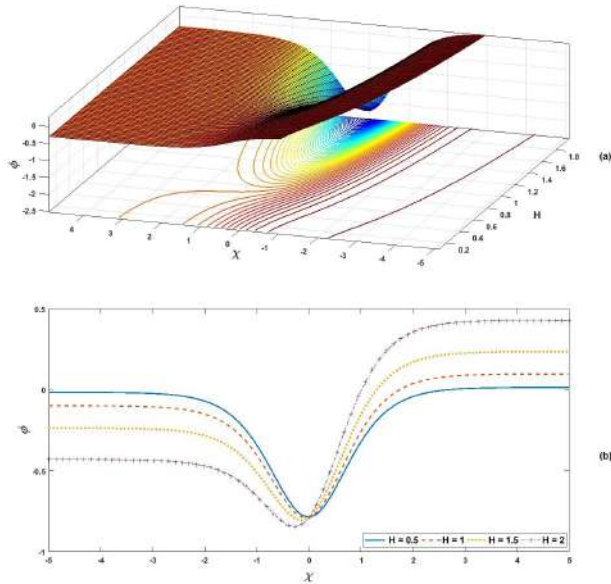


Figure 9.8: (a) Polarity shifting solitary structures with contour plots & (b) Shock profile for different values of quantum diffraction parameter (H) with $F_h = 1.4, F_c = 0.48, \eta_{h,c} = 1.5, M = 1.5, u_0 = 0.5, \lambda = 1$ & $\delta = 0.005$.

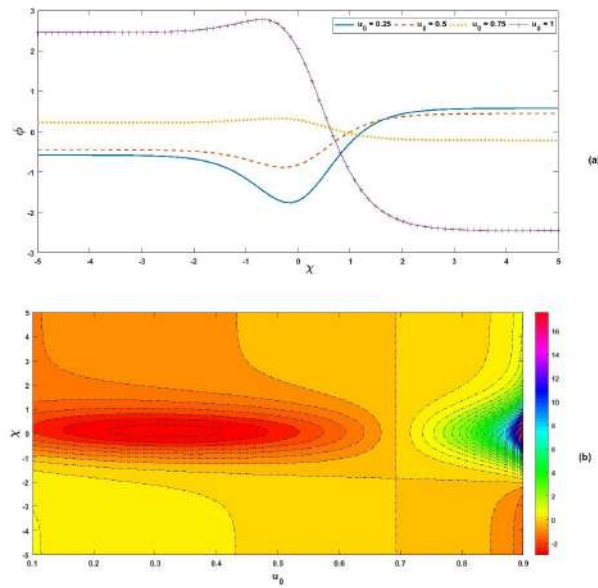


Figure 9.9: (a) Shock profile & (b) Contour plots for different values of streaming velocity (u_0) with $F_h = 1.4$, $F_c = 0.48$, $\eta_{h,c} = 1.5$, $H = 2$, $M = 1.5$, $u_0 = 0.5$, $\lambda = 1$ & $\delta = 0.005$.

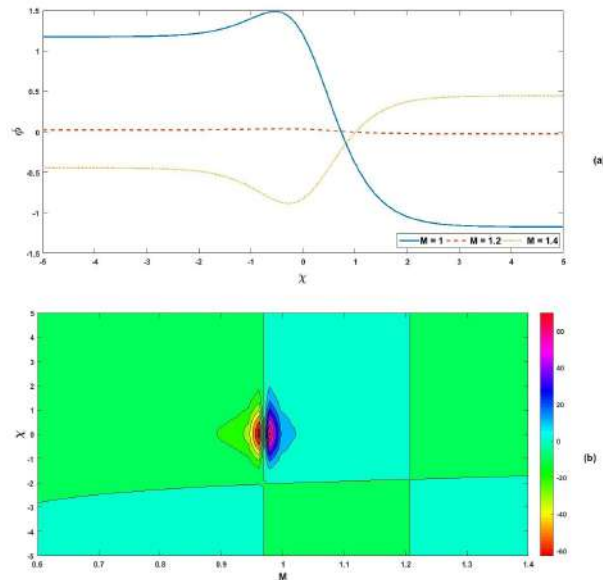


Figure 9.10: (a) Shock profile & (b) Contour plots for different values of wave-frame velocity (M) with $F_h = 1.4$, $F_c = 0.48$, $\eta_{h,c} = 1.5$, $H = 2$, $u_0 = 0.5$, $\lambda = 1$ & $\delta = 0.005$.

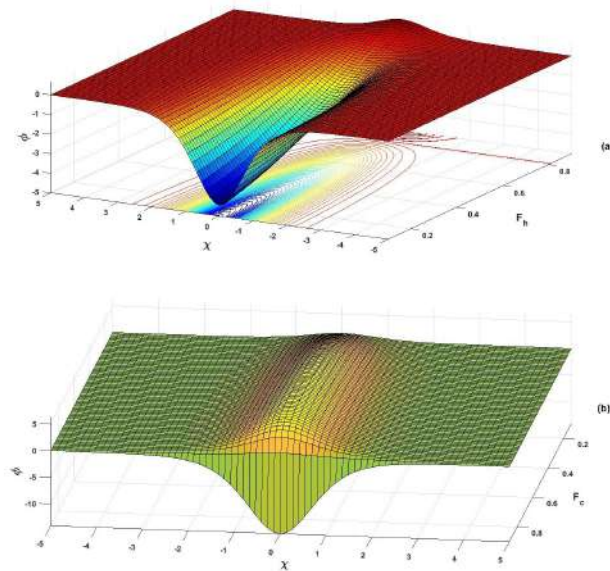


Figure 9.11: Polarity shifting small amplitude solitary structures with contour plots vs χ for different values of (a) F_h & (b) F_c with $M = 1.6, u_0 = 0.5, \delta = 0.5, H = 2, \eta_{h,c} = 1.5$ & $\lambda = 1$.

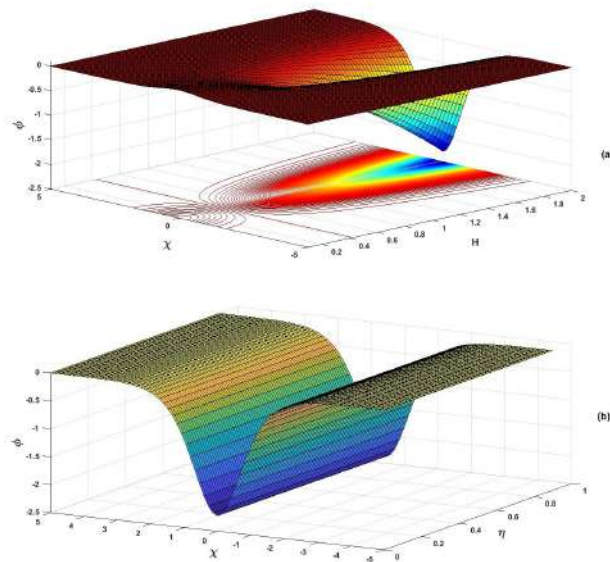


Figure 9.12: Polarity shifting small amplitude solitary profile vs χ for different values of (a) quantum diffraction parameter (H) & (b) unipolar Small amplitude solitary profile with change in viscosity factor (η) with $F_h = 1.4, F_c = 0.48, M = 1.6, u_0 = 0.5, H = 2, \delta = 0.5$ & $\lambda = 1$.

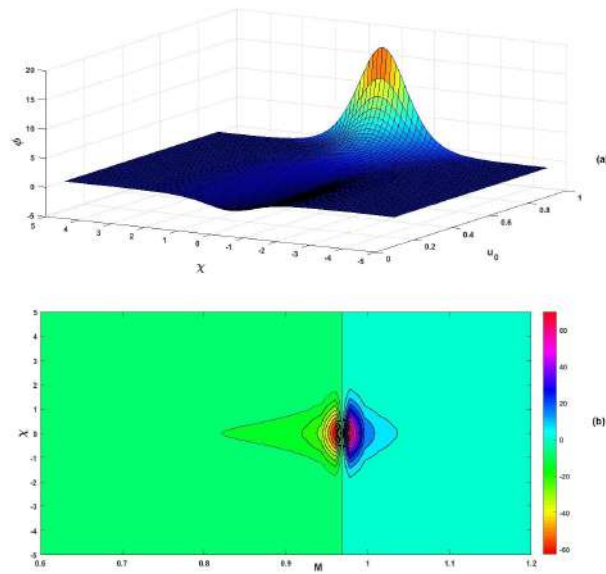


Figure 9.13: Small amplitude solitary profile vs χ for different values of (a) streaming velocity (u_0) & (b) wave-frame velocity (M) with $F_h = 1.4, F_c = 0.48, H = 2, \eta_{h,c} = 1.5, \delta = 0.5$ & $\lambda = 1$.

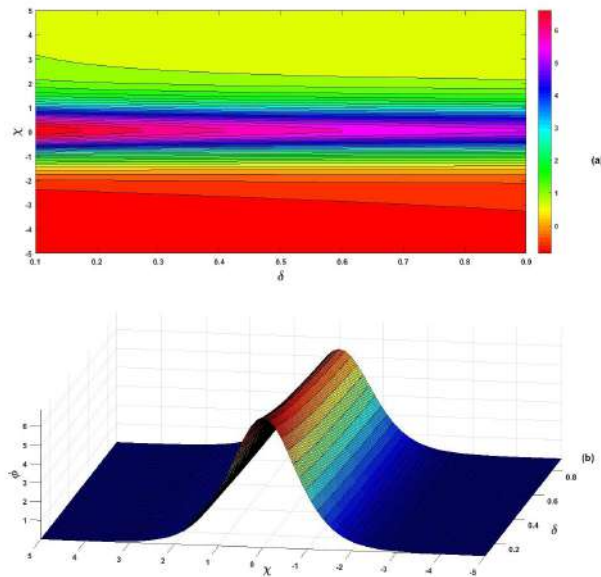


Figure 9.14: Effect of equilibrium hot-to-cold electron concentration ratio (δ) in the formation of small amplitude shocks (a) and solitary structures (b) $\eta_{h,c} = 1.5$ with $F_h = 1.4, F_c = 0.48, M = 1.6, u_0 = 0.5, H = 2$ & $\lambda = 1$.

Findings of the Reductive Perturbation Method:

Now in general plasma being a highly nonlinear media, nonlinear effects start coming into play right from the instance of small amplitude perturbations. To study such phenomena we start with the basic normalised equations (9.2)–(9.6) and with the perturbation expansion (9.11) of field variables in stretched co-ordinates. After obtaining the KdV-Burgers equation and using the standard solutions as used by many [256, 169, 168] we plot the functions. From the figure 9.5 shows the dependence of shocks fronts on various plasma parameters. Figures (9.6–9.7) shows the variation of solitary and shock frontson the degeneracy parameters F_h, F_c . With reference to figure-9.8 we see that H has positive effect in creating the shocks fronts. On other side of $\chi = 0$, H has enhancing effect of shock separation. This is due to the greater diffraction effect associated with high density. Streaming motion has an interesting behavior. It can independently convert positive shocks to negative and vise-versa. This is due to the streaming velocity u_0 (figure9.9). Much similar to streaming velocity, the waveframe speed (M) shows converting feature in shock front (figure-9.10). The only difference in u_0 and M have reciprocal effects. When the nonlinear effect is more pronounced and is also balanced by dispersive effects, the shock front propagates in space and time as a solitary structure. The mathematical expression for such a structure is given by (9.19). It may have a potential base of different magnitude on either side where the solution takes the form (9.18). The following figures explain such a possibility. Figure 9.11 shows similar effect due to F_h and F_c . Both F_h and F_c corresponds to restoring force term. Once the restoring force is in play, it is immaterial what be the source, it can be due to both hot and cold electrons, the total effect is important. Quantum diffraction term (figure-9.12) has deepening effect in enhancing the solitary profiles (relatable with figure 9.8). In the same figure (figure-9.12b) viscosity parameters are found to have almost no effect. In figure 9.13 the effect of streaming and the propagating wave-frame's dependence have been shown. The change in the polarity of the wave changes around $M=0.95$ and $u_0 = 0.65$. Thus

both the fluid velocity and the wave velocity is instrumental in determining the shock's polarity. In the figure 9.14 the relative proportion of hot and cold electron is found to affect in an interesting manner, while they cant alter the polarity they can slightly alter the magnitude. This is absolutely new finding. The saddle-back like profile points to the possibility of energy redistribution and this is clear from shock contours (in $\chi - \delta$ plane) and solitary profiles (in $\chi - \delta$ plane). From the nature of these figures we see that δ and η have reversed effect in delimiting the shock contours. Such an inferences can be also drawn for figure (9.1). The effect of δ is effective in the delimiting the regions of shocks fronts. Figure-9.5(b) shows the corresponding shocks contour in $\chi - \eta$ plane which is quite relatable. In the figures 9.11–9.14 above we find that there is a solitary feature in plasma which gradually takes shape of a wave pulse once the nonlinear and dispersive effects balance each other. It is evident due to fact that ions which have huge inertia has a tendency to enhance the shock separation much opposite the effect of F_h . In figure 9.10 the $\chi - M$ contour for shocks is shown. It beautifully depicts the domains of positive and negative shocks. The contour codes are informative in this aspect. Figure-9.8 very beautifully shows the transition from a negative shock front into a rarefactive soliton. Here H is the tuning parameter. Clearly it is seen that if H value increases the balancing of nonlinear and dispersive forces become more effective. Keeping the anisotropy on either side of χ it is possible to create a solitary features. Figure-9.12 further depicts how a comprehensive soliton converts into a rarefactive one when the parameters favour such a consideration criteria. In contrast to quantum diffraction (H), the streaming velocity (u_0) is also instrumental in such a conversion, we find that a typical value of u_0 figure-9.13 (near to 0.45) no such solitary structure appears. As u_0 increases nonlinearity increase due to the to cope up with the dispersive elements. Because of such a non-responsive dispersion, the nonlinearity gets sufficient time to grow up in the media. Figure-9.13(b) shows the contour plots of dark and bright solitons with M. However M and u_0 have reverse effects as observed in figures (9.13) and (9.2). The figures show almost negligible dependence on δ and η . The fact here is we have considered same value of η_c and

η_h and to be equal to η due to the such a high density plasma. The nature of solitary transition due to values of F_h (figure-9.11) is similar to that of u_0 , but more pronounced. It is because the mobility of hot electron and its ability to provide restoring forces. Interestingly F_c [figure-9.11(b)] has unipolar behavior. Omitting the plot for $F_c = 0$ which would be an ideal case of cold electrons produce some restoring effect it gives positive solitary formations with diminishing amplitude. Works by Shukla [56, 387] and others have seemingly alike results in some of their problems.

9.3 Forced KdV and Envelope Soliton in Magnetoplasma with Kappa Distributed Ions

Magnetic field is often seen in the astrophysical plasma [388, 389, 243, 174, 195, 223, 220, 213, 222, 216] and planetary environment [390, 391, 392, 393, 394, 395]. In artificially produced plasma applications often magnetic modulation or magnetic confinement is used. There too the effect of the magnetic field becomes exceptionally important. Accordingly, we have involved the magnetic field in this section. Solitary structures with large amplitude were observed by FAST [396] and Polar [397, 398] satellites has been reported to give rise to amplitude modulated electron-acoustic solitons [399, 178]. Determining the Kappa Distributions of Space Plasmas from Observations have been carried out by many researchers [400, 401, 402, 168, 403, 404, 169, 73, 72]. Further such quantum plasmas are observed in astrophysical environments and has been the motivation of many early workers on quantum plasma [405, 406, 208]. Recently several studies have drawn attention to the structure and behaviour of the rogue [179, 173, 189, 177, 186]. In this section we confine ourselves to the study of electron acoustic wave (EAW) [194, 407, 408, 409, 410, 411, 215, 412, 413, 414, 415, 416, 417, 68, 180] mode where there are two categories of electrons [175], hot (warm) inertia-less electrons and the cold (inertial) electrons those provide the restoring force.

9.3.1 Basic Equations

Streams of charged particles in space plasma undergo ponderomotive forces [72, 418] owing to the magnetic field and oscillate depending on the arrangement and composition of the plasma components. We assume a plasma with cold electrons and inertialess hot electrons, as well as kappa distributed ions, producing a homogeneous neutralising background. The quantum diffraction term for electrons is considered solely. There is an additional transverse streaming motion. In this light, the following are the dynamic equations,

$$\partial_t n_j + \nabla \cdot (n_j \mathbf{u}_j) = 0 \quad (9.20)$$

$$(\partial_t \mathbf{u}_c + \mathbf{u}_c \cdot \nabla) = (q_e/m_c)[\mathbf{u}_c \times \mathbf{B} + \mathbf{E}] + (\hbar^2/2m_c^2) \nabla (\nabla^2 \sqrt{n_c}/\sqrt{n_c}) \quad (9.21)$$

$$0 = (q_e/m_h)[\mathbf{u}_h \times \mathbf{B} + \mathbf{E}] + 1/n_h \nabla \Pi + (\hbar^2/2m_h^2) \nabla (\nabla^2 \sqrt{n_h}/\sqrt{n_h}) \quad (9.22)$$

$$\nabla^2 \psi = 4\pi e(n_c + n_h - Zn_i) \quad (9.23)$$

where, $\Pi = \frac{1}{8} \left(\frac{3}{\pi}\right)^{\frac{1}{3}} \hbar c n_h^{\frac{4}{3}}$. The electrons are statistically degenerate so the quantum diffraction effects are incorporated in equations (9.21) & (9.22). Further the pressure given by (π) is relativistically degenerate. The supra-thermal ions are governed by the kappa distributions given by

$$\begin{aligned} n_i &= \left[1 + \frac{\psi}{\kappa - (3/2)} \right]^{(\kappa + (1/2))} \\ &= 1 + c_1 \psi + c_2 \psi^{(3/2)} + \dots \end{aligned} \quad (9.24)$$

Where, $c_1 = \frac{2\kappa-1}{2\kappa-3}$, $c_2 = -\frac{2\kappa^2-\frac{1}{2}}{4\kappa^2-12\kappa+9}$

We have assumed $\omega_{cc} = eB_0/mc$ is the gyro-frequency and magnetic field is acting along \hat{z} direction. u_c and u_h are fluid velocity of cold and hot electron species respectively. e is the electronic charge. With reference to quasi-neutrality condition $\delta = \frac{n_{i0}}{n_{h0}}$ and $\rho = \frac{n_{c0}}{n_{h0}}$.

Equations (9.20) - (9.23) are scaled with the time t and space by $1/\omega_j = \sqrt{\left(\frac{m_j}{4\pi n_{j0} Z^2 e^2}\right)}$ and the Debye length $\lambda_{De} = \sqrt{\left(\frac{k_B T_e}{4\pi n_{j0} Z e^2}\right)}$. We altered the number densities of electrons (n_c, n_h) by unperturbed densities n_{c0} & n_{h0} and fluid velocity u_j by the sound speed $c_{sh} = \left(\frac{ZkT_e}{m_h}\right)^{1/2}$, the electrostatic potential ψ by $\frac{kT_e}{e}$ respectively and the equations can be written in normalised and scalar form. For aptness and simplicity of this chapter we omit this trivial section.

9.3.2 Results of HASS Technique

Now in order to investigate the problem in the light of Homotopy, we refer to the following figures (9.15)-(9.21). We see that in the plot of ψ vs τ and ξ' with variations in wavenumber (k) there are significant changes. Here $\delta = 0.5$, $H = 1.8$, $V = 1.2$, $\omega_{cc} = 0.5$, $f_0 = 0.6$ and $\rho = 0.4$ the initial waveform of a KdV soliton under the action of external applied force gradually evolves into different forms with different values of wavenumber (k). Concerning figure 9.15 the gradual increase in wavenumber (k) (a) $k = 1$, (b) $k = 1.7$ and (c) $k = 2$, the waveform evolves in the time domain. Higher the value of wavenumber, higher is the associated energy in the wave. It, therefore, creates a type of instability due to its higher inherent energy. It will be reflected once we study the amplitude modulation in the latter part of this section.

We see that in the plot of ψ vs ξ' and quantum diffraction parameter (H) with variations in wavenumber (k) there are significant changes (9.16). Here $\delta = 0.5$, $\tau = 0.5 = 1.8$, $V = 1.2$, $\omega_{cc} = 0.7$, $f_0 = 0.6$ and $\rho = 0.5$ the initial ($sech^2$) waveform of a KdV soliton gradually evolves into different forms with varying wavenumber (k). With reference to

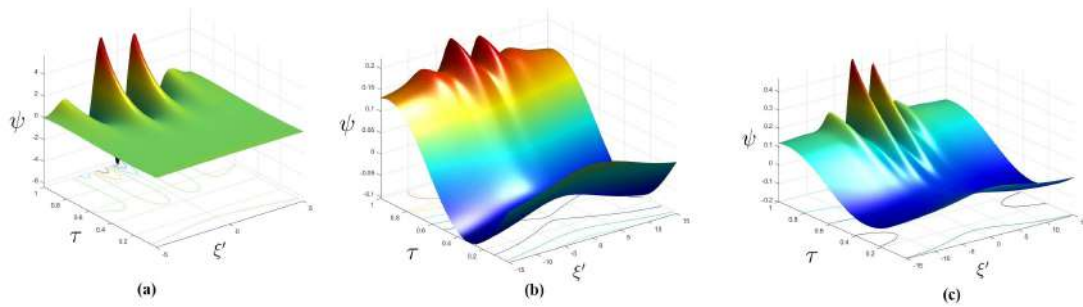


Figure 9.15: HASS plots for F-KdV solitons for different values of k with τ as variable. Here $\delta = 0.5$, $H = 1.8$, $V = 1.2$, $\omega_{cc} = 0.5$, $f_0 = 0.6$ and $\rho = 0.4$ (a) $k = 1$, (b) $k = 1.7$ and (c) $k = 2$.

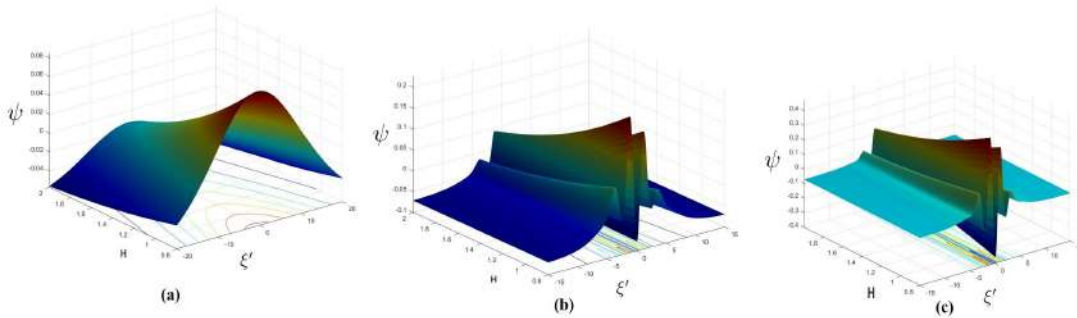


Figure 9.16: HASS plots for F-KdV solitons for different values of k with H as variable. Here $\delta = 0.5$, $\tau = 0.5$, $V = 1.2$, $\omega_{cc} = 0.7$, $f_0 = 0.6$ and $\rho = 0.5$, (a) $k = 1.2$, (b) $k = 1.7$ and (c) $k = 2$.

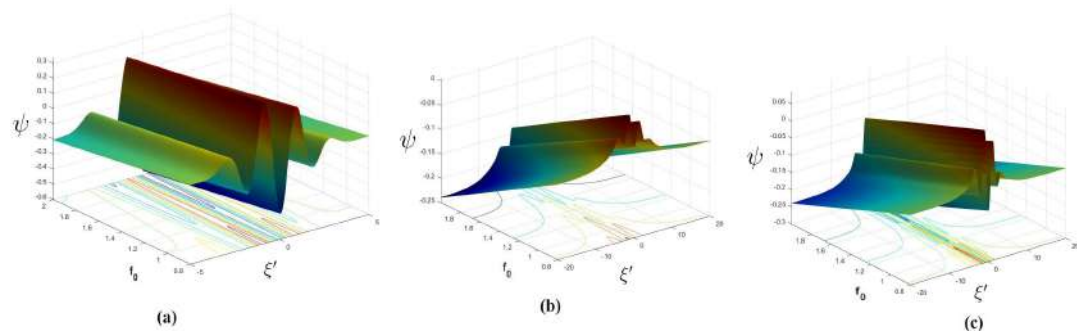


Figure 9.17: HASS plots for F-KdV solitons for different values of k with f_0 as variable. Here $\delta = 0.5$, $\tau = 0.5$, $H = 1.8$, $V = 1.2$, $\omega_{cc} = 0.7$ and $\rho = 0.5$, (a) $k = 0.7$, (b) $k = 2.5$ and (c) $k = 4$.

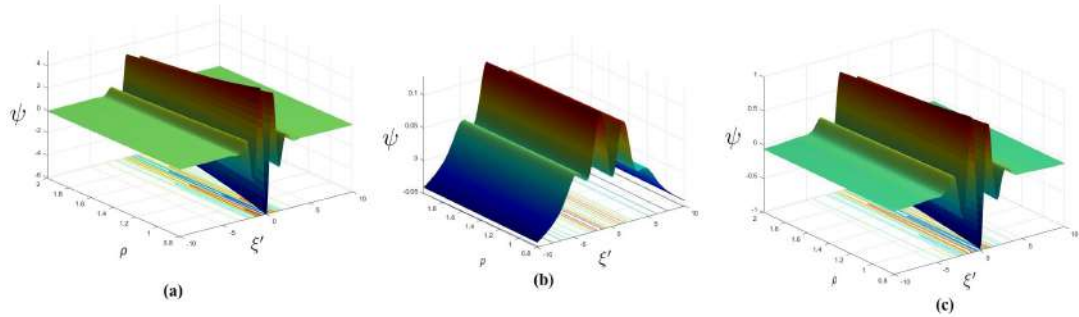


Figure 9.18: HASS plots for F-KdV solitons for different values of k with ρ as variable. Here $\delta = 0.5$, $\tau = 0.5$, $H = 2$, $V = 0.9$, $\omega_{cc} = 0.7$ and $f_0 = 0.6$, (a) $k = 0.7$, (b) $k = 2.5$ and (c) $k = 4$.

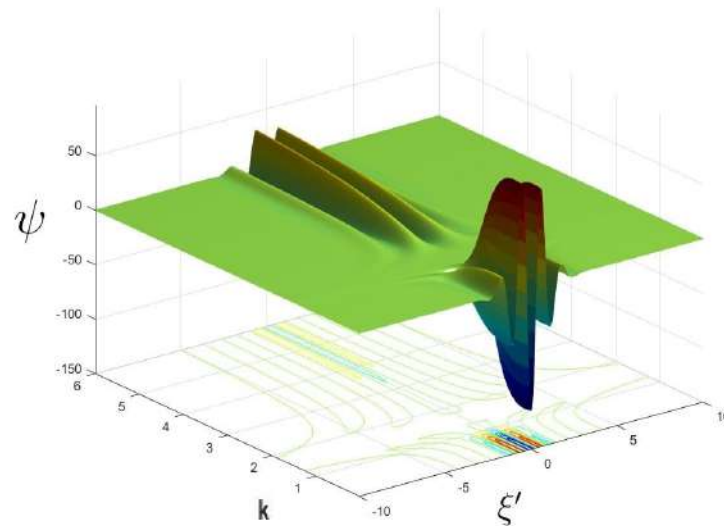


Figure 9.19: HASS plot for F-KdV solitons for different values of ξ' with wavenumber (k) as variable. Here $\delta = 0.5$, $\tau = 0.5$, $H = 2$, $V = 0.9$, $\omega_{cc} = 0.7$ and $f_0 = 0.6$,

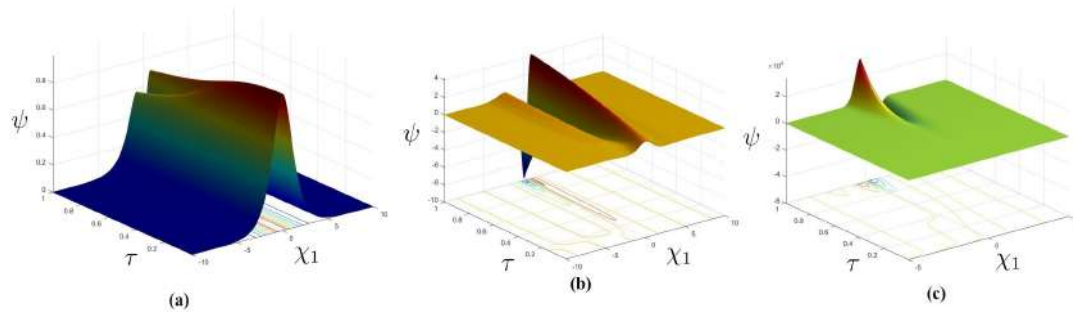


Figure 9.20: HASS plots for envelope solitons for different values of k with τ as variable. (a) $\delta = 0.5$, $H = 1.8$, $V = 0.9$, $\omega_{cc} = 0.5$, $\rho = 0.4$ and $k = 0.1$; (b) $\delta = 0.5$, $H = 1.8$, $V = 1.2$, $\omega_{cc} = 0.5$, $\rho = 0.4$ and $k = 0.8$; (c) $\delta = 0.5$, $H = 2$, $V = 1.2$, $\omega_{cc} = 0.5$, $\rho = 0.4$ and $k = 1.2$.

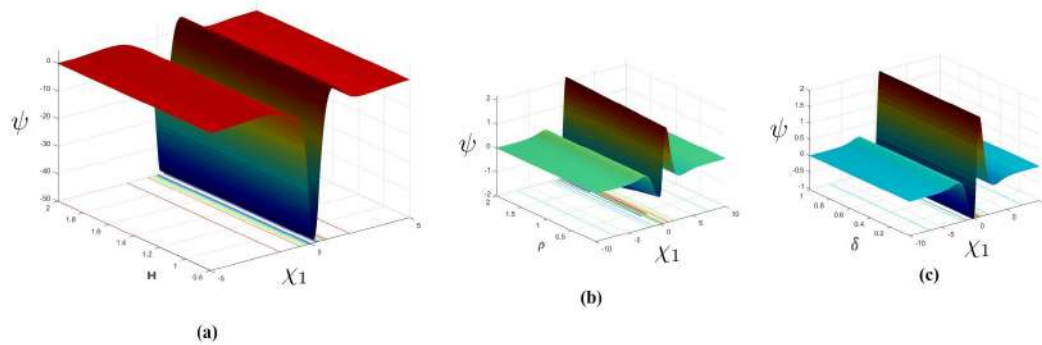


Figure 9.21: HASS plots for envelope solitons for different values of k with (a) Quantum diffraction parameter [H], (b) cold-to-hot electron concentration [ρ] and (c) ions-to-hot electron concentration [δ] as variables. Other parameters are (a) $\delta = 0.5$, $\tau = 0.5$, $V = 1.2$, $\omega_{cc} = 0.7$, $f_0 = 0.6$ and $\rho = 0.5$, (b) $\delta = 0.5$, $\tau = 0.5$, $H = 2$, $V = 0.9$, $\omega_{cc} = 0.7$ and $f_0 = 0.6$, (c) $\rho = 0.4$, $\tau = 0.5$, $H = 2$, $V = 0.9$, $\omega_{cc} = 0.7$ and $f_0 = 0.6$.

figure 9.16 the gradual increase in wavenumber (k); (a) $k = 1.2$, (b) $k = 1.7$ and (c) $k = 2$ the waveform changes. Higher the value of wavenumber, more modulations appear and although it decreases exponentially on either side of space coordinate, its effect is more diminished. In figure 9.17 we find that the amplitude of external force field linearly attenuates the soliton profile. This is more pronounced when the wave energy increases (with increased wavenumber). It means that the external perturbations cause the system more damping effect by inducing it to give up energy. Such an energy shedding causes instability as was evident from figure 9.15. The equilibrium concentration ratio (ρ) however, shows additional resonance like features that might be attributed to the energy sharing between the inertial and non-inertial components of the plasma. In (b) of figure 9.18 it suddenly shows spiking up of solitary profile due to the addition of plasma particles whose energy is in sync with the external system. It is therefore understood that the wavenumber (k) has significant effects in creating and maintaining the waveforms. To study the effect of wavenumber, a $(\psi - \xi' - k)$ plot is presented 9.19. Here, the zones of resonance and dissonance are visible. The intermediate zone in k space where no stationary formations are observed is due to the fact the energy of the soliton dies off completely to reappear again when the wavenumber crosses a certain range. We further study the formation of enveloping solitons and its fluctuations with parameters. In figure 9.20 (a) the parameters are $\delta = 0.5$, $H = 1.8$, $V = 0.9$, $\omega_{cc} = 0.5$, $\rho = 0.4$ and $k = 0.1$ respectively. For (b) in the same figure they are $\delta = 0.5$, $H = 1.8$, $V = 1.2$, $\omega_{cc} = 0.5$, $\rho = 0.4$ and $k = 0.8$; plot (c) have parameter values $\delta = 0.5$, $H = 2$, $V = 1.2$, $\omega_{cc} = 0.5$, $\rho = 0.4$ and $k = 1.2$. In the next figure 9.21 parametric plot is shown distinctively. Here quantum diffraction parameter (H), hot-cold electron concentration ρ and ion to electron concentration δ are the tuning parameters in (a), (b) and (c) respectively. The effects of the quantum diffraction is contrary to the other two. Such an inference can be drawn from the analytical sections as well. The importance of this section is that it gives an exact picture of the problem and can be easily visualised with real time.

9.3.3 Analytical Study

Dispersion characteristics:

Since we anticipated that there is a minor perturbation so that we can linearise the field quantities to a significant degree, we assume the field quantities to fluctuate in this manner, $\exp[i(\vec{k} \cdot \vec{r} - \omega t)]$. We assume the forcing term in the momenta equations to be absent initially and come into play once the particles interact to form stationary formations. We will add the forcing after the first round of nonlinear analysis. Using the standard procedure, one obtains the linear dispersion relation.

$$1 + \left[\frac{1}{((\omega - ku_{x0})^2 + \frac{H^2 k^4}{4})} + \frac{1}{(\omega_{cc}^2 + (\omega - ku_{x0})^2 + \frac{H^2 k^4}{4})} \right] + \frac{1}{\frac{k^2}{3} + \frac{H^2 k^4}{4}} - \frac{\delta(2\kappa - 1)}{k^2(2\kappa - 3)} = 0 \quad (9.25)$$

The quantum diffraction term (H) is derived from the Bohm potential term from the energy due to the oscillating electromagnetic field coupled with moving charged particle. This dispersion relationship conforms to the typical electron acoustic wave dispersion relation, under certain circumstances. And solving equation (9.25) we get four roots of ω ,

$$\omega = ku_{x0} \pm \left\{ \frac{-A \pm \sqrt{A^2 - 4AB}}{2} \right\}^{1/2} \quad (9.26)$$

Where,

$$A = \left\{ \frac{\omega_{cc}^2 + 2H^2 k^4 + C\omega_{cc}^2 + 2CH^2 k^4 + 8}{1+C} \right\},$$

$$B = \left\{ \frac{H^2 k^4 \omega_{cc}^2 + H^4 k^8 + 4\omega_{cc}^2 + 8H^2 k^8 + CH^2 k^4 \omega_{cc}^2 + CH^4 k^8}{1+C} \right\} \text{ and}$$

$$C = \left\{ \frac{1}{\frac{k^2}{3} + \frac{H^2 k^4}{4}} - \frac{\delta(2\kappa-1)}{k^2(2\kappa-3)} \right\}.$$

The slow and fast modes are obtained through the dispersion relation (9.26). The \pm before the braces corresponds to the fast and slow modes.

Features of linear dispersion relation:

In figure 9.22, we plot the contour plots of linear dispersion characteristics with variation in quantum diffraction parameter (H). It shows that as the system moves towards higher quantum diffraction regime the contours are more closely packed showing a positive dependence on (H). Figure 9.23 shows the same for different values of kappa index. It is clear that though kappa indices are important in higher wavenumber (k) region it is less prominent at small wavenumber. Figure 9.24 shows the classical and quantum counterpart of magnetic field dependence. In the classical range, the magnetic field dependence is prominent but it is not so for the quantum case. Figure 9.25 shows the classical and quantum variants of the ionic density distribution (δ). Whereas in classical case such dependence is clear in small wave-numbers, it is reversed for the quantum range. The streaming velocity gives rise to fast and slow modes as evident from equation 9.26. The streaming motion only adds some excess linear term turn in the dispersion curve. As an additional analysis, we showed in the figure how the energy propagates with wave-number. It is reflected in the group velocity curves Figure 9.26. For $\kappa = 2$, there is a gradual shift in the wave group velocity whereas for $\kappa = 4$ there is a discontinuity. This may be accorded to the high energy streaming in a κ distributed plasma. Figure 9.27 depicts the contour plots for comparison with variation of quantum diffraction term (H) for different kappa index. Figure 9.28 shows similar plots in the classical and quantum figures for the dependence of the dispersion curve with the kappa index.

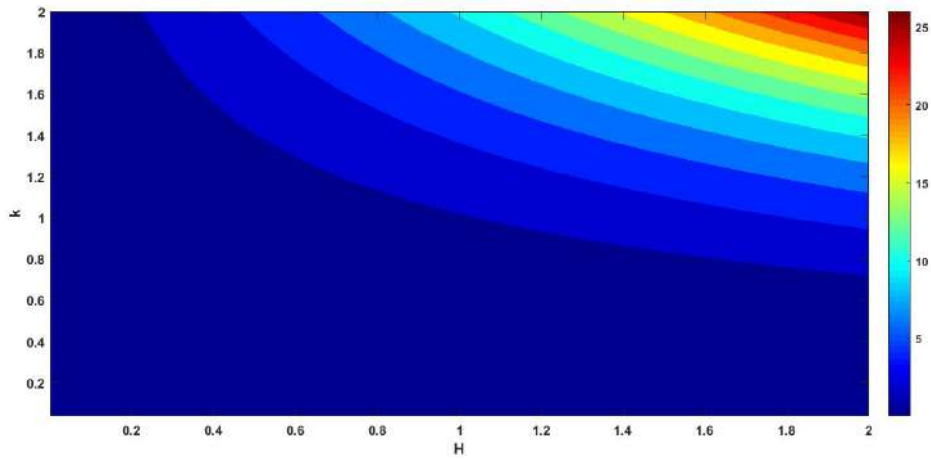


Figure 9.22: A contour plot of angular frequency in $(k - H)$ plane where $\kappa = 4$ and $\delta = 0.5$.

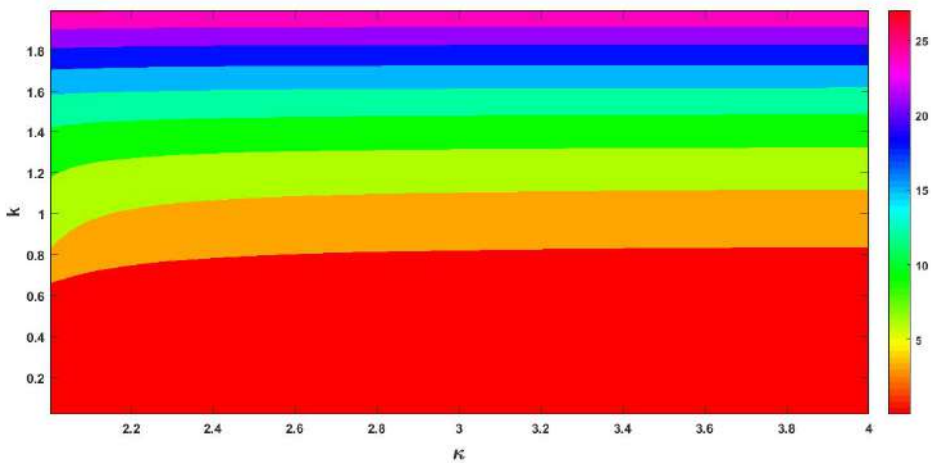


Figure 9.23: A contour plot of angular frequency in $(k - \kappa)$ plane when $H = 2$ and $\delta = 0.5$.

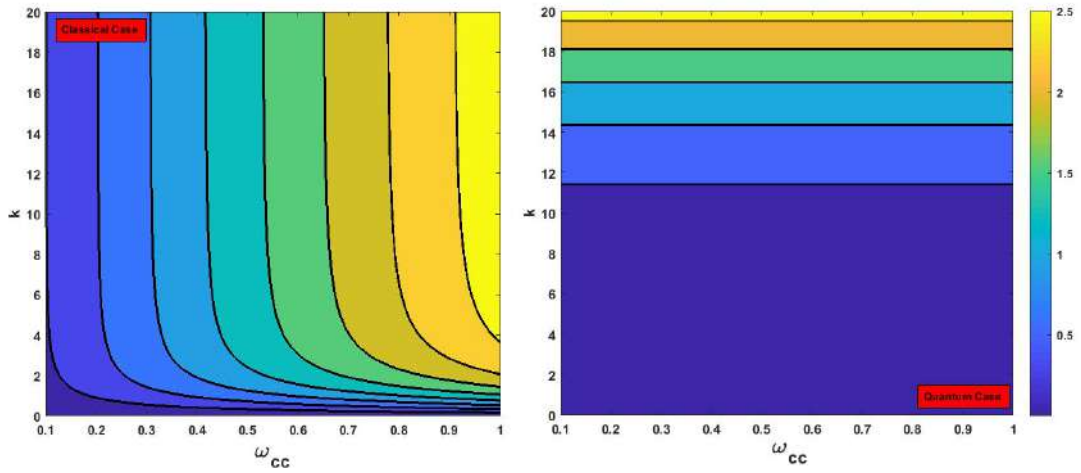


Figure 9.24: A contour plot of angular frequency in $(k - \omega_{cc})$ plane when $\delta = 0.5$ and $\kappa = 3$.

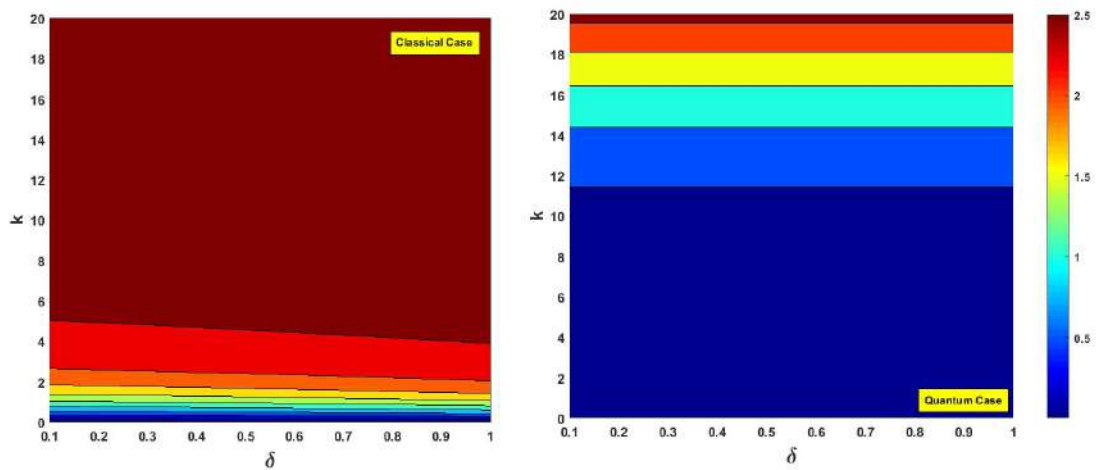
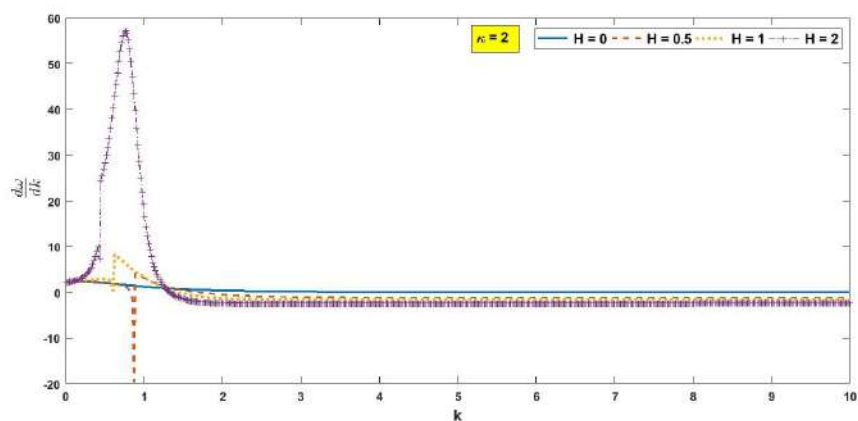
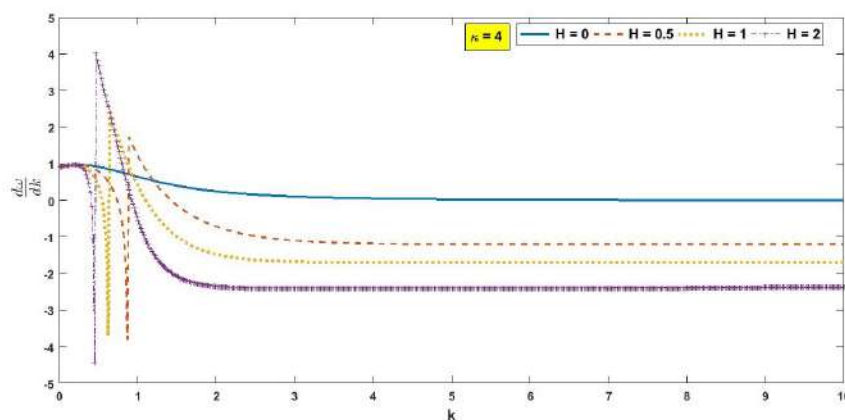


Figure 9.25: A contour presentation of dispersion curve with variation of δ when $H = 2$ and $\kappa = 3$



(a)



(b)

Figure 9.26: A graphical comparison of variation of group velocity versus normalised wave number with different values of quantum diffraction parameter and κ

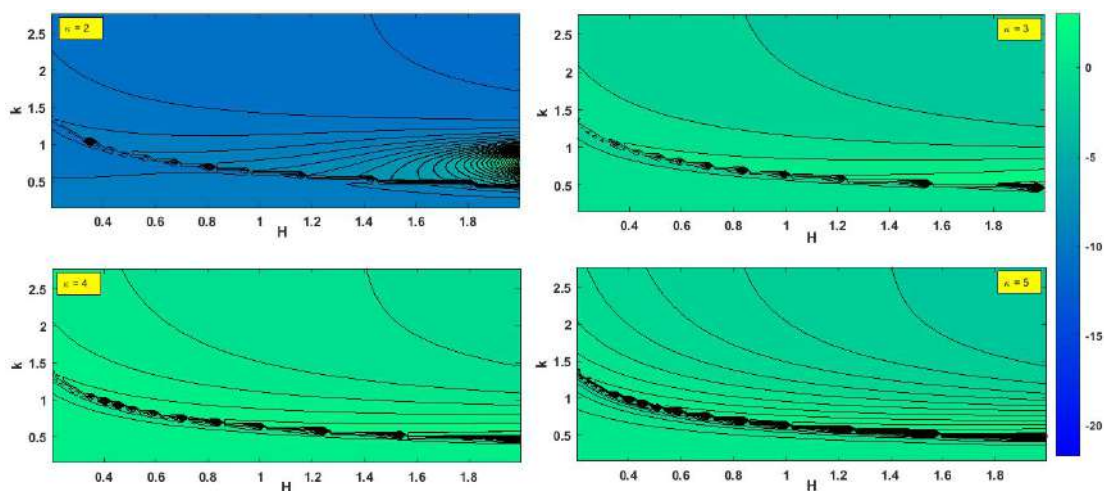


Figure 9.27: A contour plots comparison of group velocity and normalised wave number with variation of H for different values of κ indices

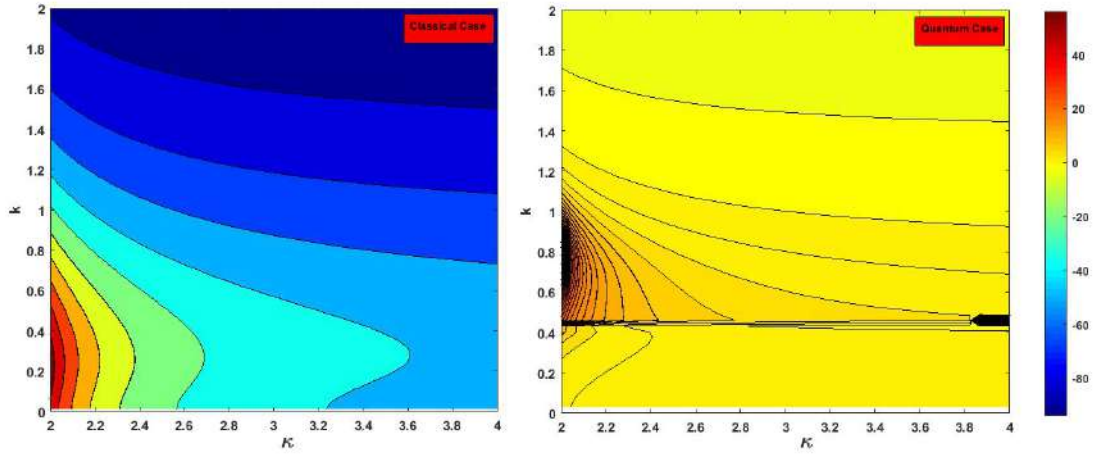


Figure 9.28: A contour plots comparison of group velocity and normalised wave number with variation of κ for classical case and quantum case

Non-linearity and the Korteweg-de Vries equation:

We follow the appropriate perturbation expansion for field quantities to understand the non-linearity of electron acoustic waves,

$$\begin{cases} n_j = 1 + \lambda_1 n_j^{(1)} + \lambda_1^2 n_j^{(2)} + \dots \\ \psi = \lambda_1 \psi^{(1)} + \lambda_1^2 \psi^{(2)} + \dots \\ u_z = \lambda_1 u_z^{(1)} + \lambda_1^2 u_z^{(2)} + \lambda_1^3 u_z^{(3)} + \dots \\ u_{x,y} = u_{x0} + \lambda_1^{3/2} u_{x,y}^{(1)} + \lambda_1^2 u_{x,y}^{(2)} + \lambda_1^{5/2} u_{x,y}^{(3)} + \dots \end{cases} \quad (9.27)$$

λ_1 is the smallness parameter measuring the extent of perturbation in the system. We employ the typical spacial and time variables according to the conventional reductive perturbation technique,

$$\xi' = \lambda_1^{1/2} (l_x + l_y + l_z - Vt), \quad \tau = \lambda_1^{3/2} t \quad (9.28)$$

where V indicates the Mach number, the intensity of non-linearity is λ_1 and $l_x^2 + l_y^2 + l_z^2 =$

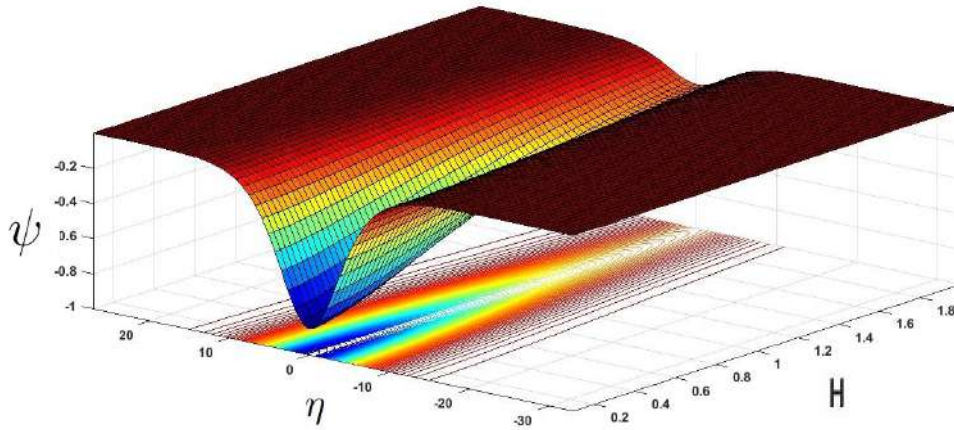


Figure 9.29: A graphical presentation of solitary structure for different values of (H), when $\kappa = 4$, $V = 1.4$, $\omega_{cc} = 0.5$, $\rho = 0.4$, $l_z = 0.3$ and $\delta = 0.5$

1. The KdV equation of the first order is obtained

$$\frac{\partial \psi}{\partial \tau} + P\psi \frac{\partial \psi}{\partial \xi'} + Q \frac{\partial^3 \psi}{\partial \xi'^3} = 0 \quad (9.29)$$

Where, $P = \frac{(V-u_{x0})^3 \left(\frac{H^2 l_z^2}{4(V-u_{x0})^4} + \frac{(V-u_{x0})(l_x^2 + l_y^2)}{\omega_{cc}^2} - \frac{9H^2}{4} l_z + 1 \right)}{2l_z^2}$ and

$$Q = - \frac{(V-u_{x0})^3 \left(\frac{\rho l_z^4}{(V-u_{x0})^4} + 3l_z^2 - \frac{\delta \frac{1-4\kappa^2}{2}}{2(2\kappa-3)^2} \right)}{2l_z^2}$$

By employing the transformation ($\eta = \xi' - V\tau$) and applying the boundary conditions, $\psi \rightarrow 0$, $\frac{d^2 \psi}{d\xi'^2} \rightarrow 0$ as $\xi' \rightarrow \infty$, the solution of equation (9.29) is given by,

$$\psi = \psi_m \sec^2(\eta/\Delta) \quad (9.30)$$

here, $\psi_m = 3V/P$ and $\Delta = \sqrt{\frac{4Q}{V}}$

the development of KdV solitary structure is described by equation (9.30). A stationary system of this type gives a great deal of information on the plasma waves, and their correlation to many plasma parameters.

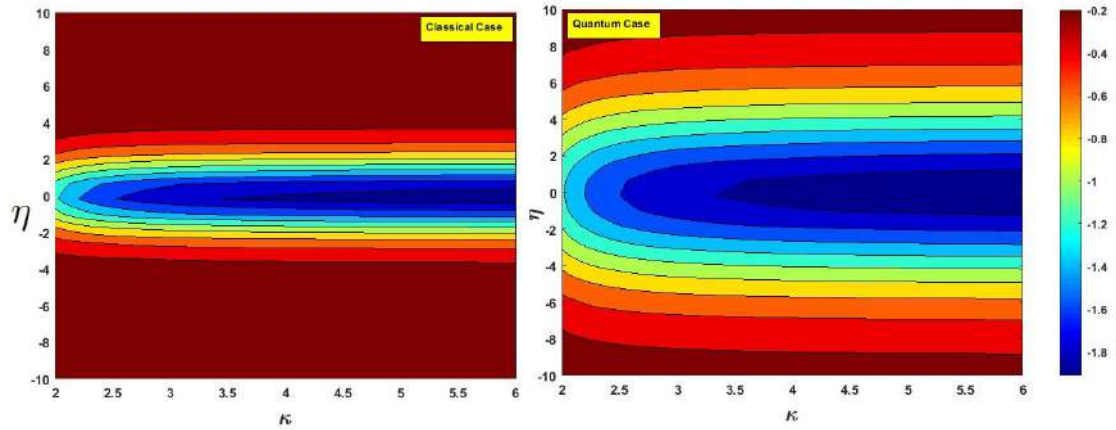


Figure 9.30: A contour plot of solitary profile for different values of (κ), when $H = 2, V = 1.4, \omega_{cc} = 0.5, \rho = 0.4, l_z = 0.3$ and $\delta = 0.5$

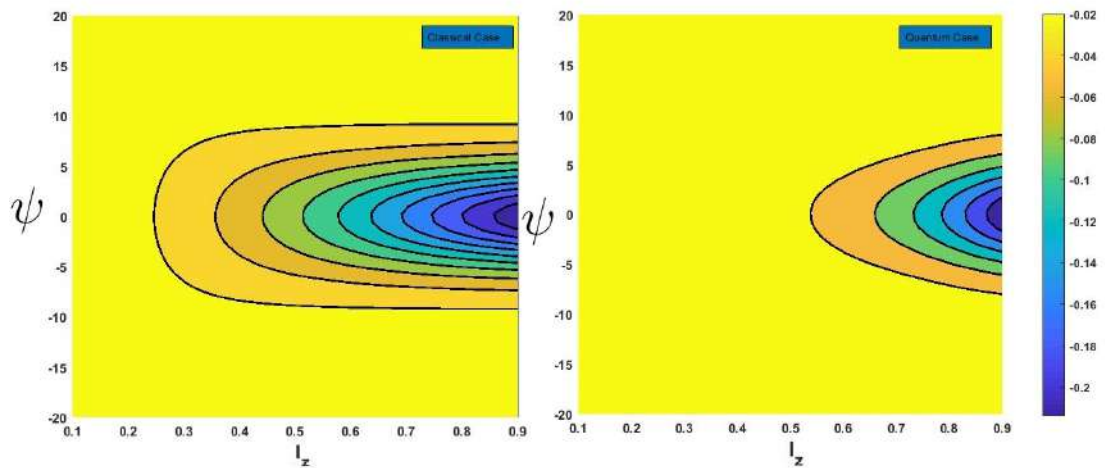


Figure 9.31: A contour plot of solitary profile for different values of (l_z), when $H = 2, \kappa = 6, \omega_{cc} = 0.9, \rho = 0.8, V = 1.4$ and $\delta = 0.7$

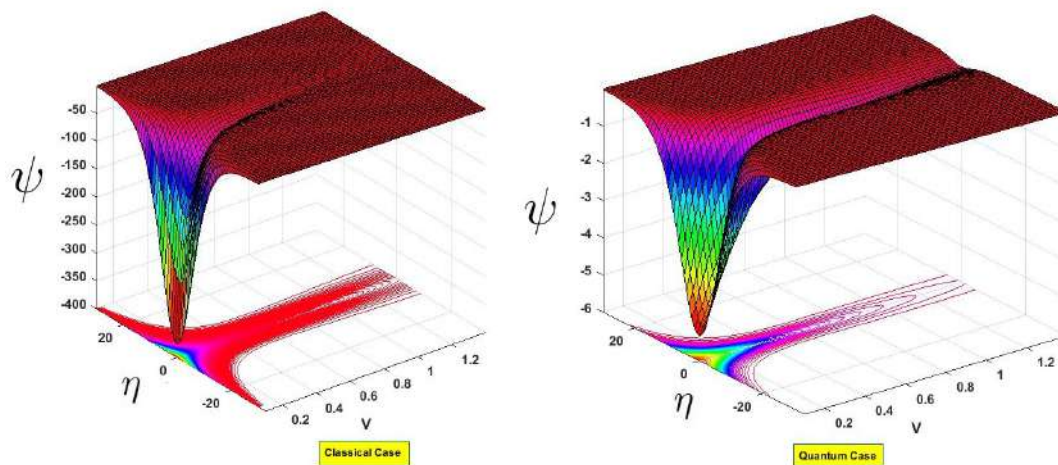


Figure 9.32: A comparison of solitary structure for different values for Mach number (V) between classical and quantum scenario when $\omega_{cc} = 0.5$, $l_z = 0.3$, $\kappa = 3$, $\rho = 0.4$ and $\delta = 0.5$

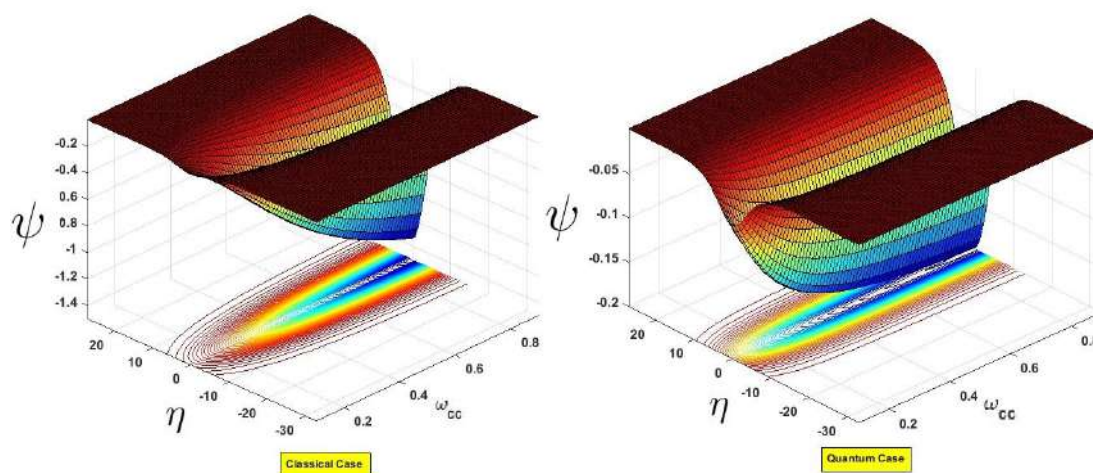


Figure 9.33: A comparison of solitary structure for different values for different values of (ω_{cc}), when $V = 1.4$, $\delta = 0.5$, $\rho = 0.4$, $l_z = 0.3$ and $\kappa = 3$

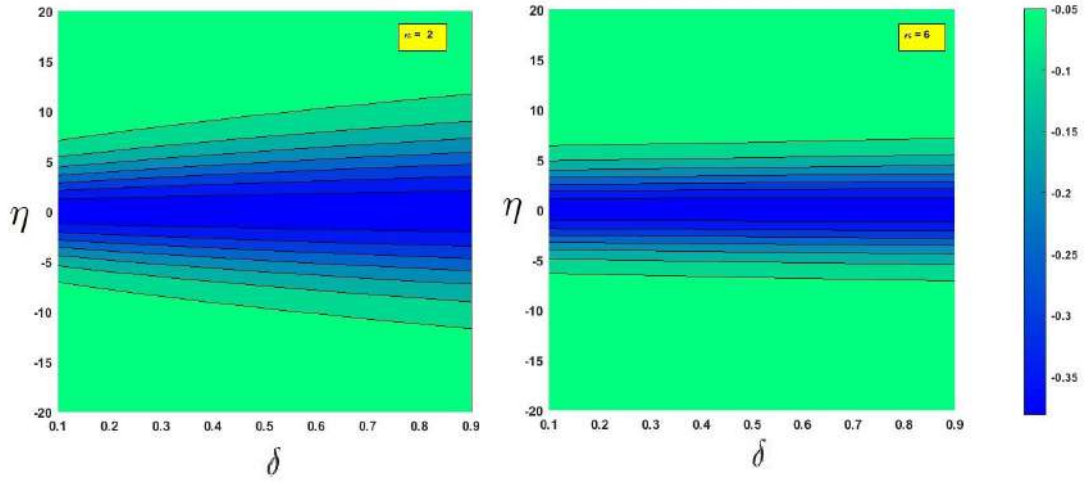


Figure 9.34: Contour plots for different values of (δ), when $V = 1:4$, $\omega_{cc} = 0:5$, $\kappa = 3$ and $\rho = 0:5$

Nature of KdV soliton:

The variation of KdV solitary structures on various plasma parameters are discussed with reference to the following figures. Figure 9.29 - 9.35 provides the plots of KdV solitary structure for various parametric variations. Figure 9.29 depicts the solitary profile for varying values of quantum diffraction parameter (H). As the system moves in the quantum domain the solitary profile is flattened. This may be due to the strong correlation of the particle in such a range. Additionally, it can be said that at such high densities the system has less available states and the degree of non-linearity is overpowered by the dispersive effects. Figure 9.30 shows the contour plots for the Kappa index in the classical and quantum domain. Here in the classical case, the kappa index is prominent in the small η - space whereas it is more spaced in the quantum case. Contour plots for variations in the (l_z) value (i.e; the directional cosine for the z - component) is shown in figure 9.31. It shows that the classical counterpart is short & more closely packed and there are fewer variations at the periphery than the centre. Figure 9.32 makes a comparison for the solitons in quantum and classical domain with the variation of wave frame velocities [or Mach number (V)]. The quantum plots are more extensive at high Mach number (V). The effect of magnetic field (via ω_{cc}) is shown in figure 9.33. In both quantum and clas-

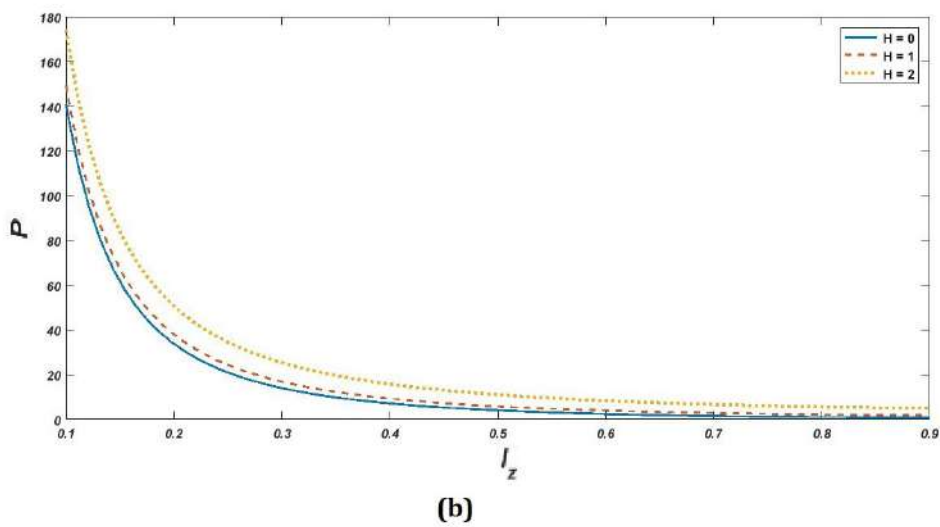
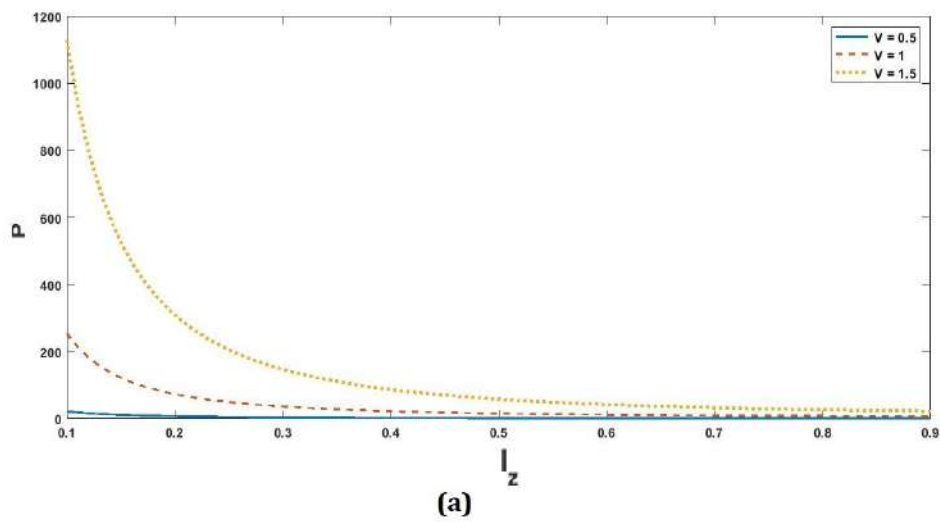


Figure 9.35: Variation of non-linearity with direction cosine for different Mach number (a) and Quantum diffraction parameter (b)

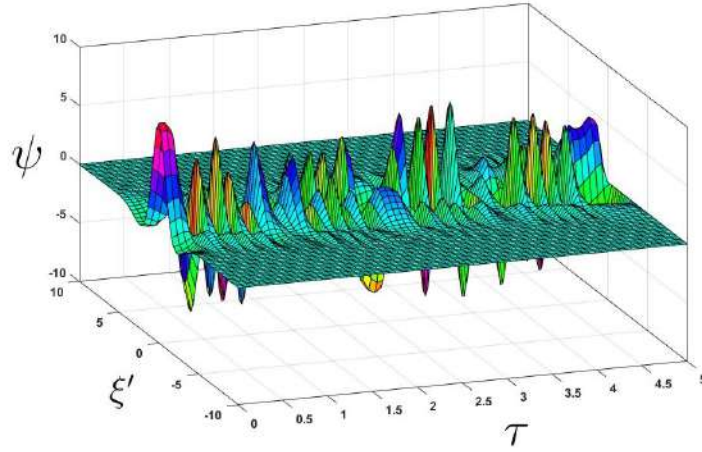


Figure 9.36: Spatio-temporal evolution of the Envelope Solitary structure

sical range the magnetic field increases the depth of rarefactive solitary structures. It is more pronounced in the quantum region. It is because of the high density such that the system particles as a whole respond to the magnetic field without any dispersive action. Figure 9.34 shows the $(\eta - \delta)$ plot for two values of Kappa index. A smaller value of kappa indices the $(\eta - \delta)$ curves have a progression with ion density but for high k value, ion density is almost ineffective in affects the solitary structures. Figure 9.35 shows how the nonlinear coefficient (P) varies with directional cosine (l_z), Mach number (V) and quantum diffraction term (H) as tuning parameters.

Envelope soliton and the non-linear Schrödinger equation:

If non-linearity in the plasma is very high and an initial uniform waveform gets converted into a wave structure so that it further undergoes self-modulation then envelope solitary formations are found to evolve. To study the nature of such envelope solitons and to analyze whether such modulation is stable against dispersion, we calculate a non-linear Schrödinger equation. To derive it, we make use of a simple transformation followed by expansion. For NLSE, We introduced the stretching variables χ_1 and τ as

$$\chi_1 = \epsilon(\xi - \tau); \quad t = \epsilon^2 \tau \quad (9.31)$$

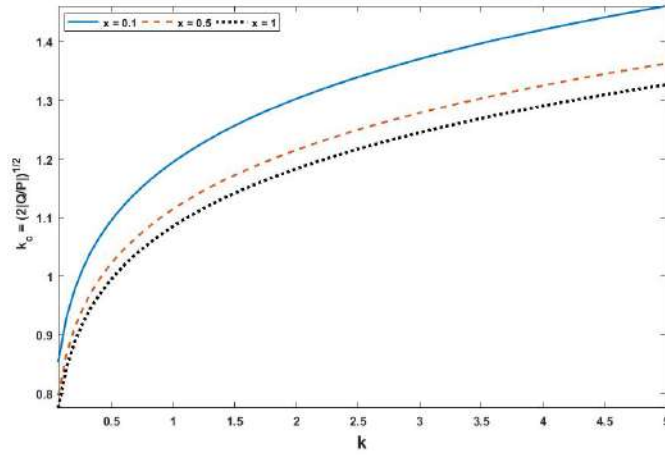


Figure 9.37: The variation of the critical wave number (k_C).

Now we consider that electrons only participate in this linear approximations. Employing Fourier expansion of field quantities such that

$$u_l(\chi_1, t) = u_l^{(0)} + \sum_{n=1}^{\infty} \varepsilon^n \sum_{l=-\infty}^{\infty} u_l^{(n)} e^{il(kx - \omega t)} \quad (9.32)$$

using perturbations of field variables such as

$$\psi = \sum_{n=1}^{\infty} \varepsilon^{(n)} \psi^{(n)}$$

We get the equation of NLS given by

$$i \frac{\partial \psi}{\partial t} + R \frac{\partial^2 \psi}{\partial \chi_1^2} = S \psi^2 \psi^*. \quad (9.33)$$

While studying amplitude modulation and related envelope soliton, the non-linear Schrodinger (NLSE) equation is essential. Here, the balance of nonlinear and dispersive components is maintained. The dispersive (R) and Nonlinear (S) coefficients are

$$R = \frac{3kV^3}{2l_z^2} \left(\frac{\rho l_z^4}{V^4} + 3l_z^2 - \delta \frac{1-4\kappa^2}{4(2\kappa-3)^2} \right);$$

$$S = \frac{V^3 \left(\frac{H^2 l_z^2}{4V^4} + \frac{V(l_x^2 + l_y^2)}{\omega_{2c}^2} - \frac{9H^2}{4} l_z + 1 \right)}{12l_z^2 k \left(\frac{\alpha l_z^4}{V^4} + 3l_z^2 - \delta \frac{1-4\kappa^2}{4(2\kappa-3)^2} \right)} \quad (9.34)$$

We adopt function transformation approach in order to obtain the solution of the equation (9.33), and assume that the solution turns into the form

$$\psi(\chi_1, t) = f(\varsigma) e^{i\theta} \quad (9.35)$$

where ς & θ are related as

$$\varsigma = \chi_1 - (\alpha R + \beta S); \theta = \alpha \chi_1 + \gamma t \quad (9.36)$$

Wherever there is α , β and γ constantly, the real function is $f(\varsigma)$. Now that equation (9.35) is replaced with equation (9.33), we have the usual differential equation

$$R \partial_{(\varsigma)}^2 f - (R\alpha^2 + \gamma) f + S f^3 = 0 \quad (9.37)$$

which can be written as

$$(\partial_{\varsigma} f)^4 = \frac{2R\alpha^2 + \gamma}{R} \left\{ f^2 - \left(\frac{S}{R\alpha^2 + \gamma} \right) \frac{1}{8} f^4 \right\} \quad (9.38)$$

With the equation (9.38) integrated, the NLSE (9.33) solution has been formed,

$$\psi = \sqrt{\left(\frac{\gamma}{R} + \alpha^2 \right) \frac{R}{S}} \cdot \operatorname{sech} \left[\left\{ \sqrt{\frac{\gamma}{R} + \alpha^2} \right\} (\varsigma - 2\alpha R\theta) \right] e^{i(\alpha\varsigma + \gamma\theta)} \quad (9.39)$$

The wavelength (or corresponding energy) due to which the waves will be stable is directly related to the performance of RS and its sign in wave-number (k) space. Figure 9.36 depicts the amplitude modulated envelope soliton or envelope solitary wave. Figure

9.37 illustrates the modifications of the crucial (k_C) wave number, which brings forth the utmost modulation wave number (k_C) value for the wave stability of the condition ($RS > 0$). From the figures one may grasp the parametric dependence easily.

9.4 Conclusion

The findings of this work will help in the understandings of the various parameters in determining the origin and nature of stationary formations like double layers, shocks and solitary structures. The gradual evolution of sheet like charge separations (the double layers) to a shock front and finally as a solitary wave profile is often crucial while carrying out experiments in plasma and interpreting astronomical shocks. A couple of year back the interplanetary shocks observed on 19/04/2018 [118, 256] can be interpreted for and in future measurements can be made to account for any similar astrophysical phenomena. This theoretical work also shows step by step evolution of an electron acoustic rogue wave with huge energy starting from weak plasma oscillations. The model has the potential to identify the parametric range for stable envelop soliton and the minute fluctuations which might cause serious instability. An extension of the theory can employed in studying rogue waves (RW) in optical fibers. However, the basic equations will undergo some changes and the parameters chosen accordingly. Apart from plasma physics, this work can find application in fiber optics, arterial mechanics and similar fields where nonlinear Schrodinger equation describes the evolution process.

CHAPTER 10

SUMMARY AND CONCLUSION

In the present thesis, we have investigate the amplitude modulation and envelop soliton formation in a dense plasma when such a plasma interacts with an intense laser beam. We have used the symbolic simulation technique to find the modulation instability of an electrostatic wave with higher orders of nonlinearity. We identified the range of wavenumber in which such instability can occur. Furthermore, we have analysed the formation of envelope soliton of waves localized in space. The importance of the relativistic contribution of streaming particles is discussed alongside the parametric influences experienced by the plasma particles. The results obtained here will help interpret different phenomena that arise in laser plasma interaction. The findings are presented in the second and third chapters. The employment of homotopy-assisted symbolic simulation has been instrumental in studying the nature and formation of envelope solitons and their dependence on various parameters. The different orders of homotopy perturbation generate a convergent series solution for such nonlinear coupled partial differential equations. Our technique bypasses the rigorous analytical derivation of coupled partial differential equations without a loss of information. The methodology is novel and holds promise for application in models that explain experimental observations. The results will be beneficial in interpreting various dense laser-plasma interactions.

In chapter four the effects of exchange correlation, streaming motion, and quantum diffraction on the nonlinear evolution of modulated electron plasma waves have been investigated. The nonlinear Schrodinger equation (NLSE) is obtained using the standard Fourier technique. The nonlinear evolution of the envelope soliton, its associated modulational instability, and its growth rate are described by the nonlinear Schrodinger equation. We have demonstrated how wave instability is affected by various parameters

and the wave number domain. The dynamical properties of amplitude-modulated electrostatic waves help to understand the physical process occurring in the system.. The dynamical system analysis supports the findings of the perturbative analysis.

In chapter four we employ the semi-Lagrangian method for the kinetic Vlasov equation to study the instabilities in a quantum plasma with one-dimensional temperature anisotropy. Taking the Fermi Dirac type of distribution function and using the semi-Lagrangian Vlasov code, we have investigated the gradual evolution of density and kinetic energy in a degenerate plasma with quantum effects. In this collisionless plasma, adiabatic compression take place along the direction of wave propagation. It lead to temperature anisotropy of the electron distribution that varies along the wave propagation path. The findings will find application for dense plasma at finite temperatures as in laser-produced plasmas, fusion plasma, and solar plasmas. Here we have studied the gradual evolution of stationary formations in electron acoustic waves at a finite temperature quantum plasma. We have used quantum hydrodynamics model equations and obtained the KdV-Burgers equation. From here, we show how the amplitude-modulated solitons evolve from double-layer structures through shock fronts and ultimately converge into solitary structures. The stability of modulation and its propagation in space are crucial in laboratory plasma. The dynamical analysis and the chaotic portraits have helped to understand the system very well. The parametric phase portraits will help the theoretical understanding of the parametric influence of large and small amplitude stationary structures. The findings of chapter six incorporates the dynamical system study and application of chaos theory in plasma physics. Bifurcation analysis and dynamical system studies are carried out to find the stability regime and chaotic scenario in electron-acoustic waves in relativistic degenerate plasma. Using the quantum hydrodynamic model we have derived Korteweg-de Vries equation describing the nature and characteristics of solitary structures. The amplitude modulated envelop soliton formation due to external perturbations has been studied by analysing the nonlinear Schrodinger equation. Further, to explore the stability factors and the parametric range for such sta-

bility, a dynamical system is inspected, and a bifurcation analysis is carried out. The chaotic behavior of the system is studied through the largest Lyapunov exponent. This work will find application in theoretically predicting the stable modes in solar plasma, stellar plasma applications and laser plasma in the future. In subsequent sections the nonlinear self-interaction of an electrostatic surface wave on an otherwise homogeneous semi-bounded plasma with degeneracy effects is examined in a quantum hydrodynamic model with suitable boundary conditions. It has been shown that a portion of the second harmonic produced by self-interaction lacks a proper surface wave feature and instead spreads obliquely into the bulk of the plasma, away from the plasma-vacuum interface. A situation like this occurs during surface etching, plasma processing, and other laser-plasma interactions. We have explored how harmonics are formed when a powerful laser strikes an unmagnetized plasma, as well as the resulting Lagrangian chaos and harmonic conversion rate. The dense plasma exhibits quantum statistical effects as well as quantum diffraction effects. In chapter seven a semiconductor p-n junction diode with heavy doping under consideration is kept in forward biased condition. These are oppositely streams of electrons and holes. These two streams interact among themselves and result in recombination, which supplies additional energy to the system. Such thermal energy creates additional electrical fluctuations, which exist long after the interaction. We have carried out an analytical investigation with numerical techniques and a simulation of the wave-wave interaction in semiconductor junction diodes. We have been successful in graphically and animatedly demonstrating the interaction mechanism. The findings will aid in understanding the breakdown mechanism and assist in designing electronic devices appropriately. The simulation results, which closely resemble the newly developed simulation code (INSAT-FORK) and can be extended to various problems with periodic boundary conditions, are partly supported by the analytical approach. These simulation studies can be used to predict a broad range of nonlinear effects. In subsequent chapters, we have studied the electron acoustic waves in a magnetized plasma containing Kappa distributed ions which are streaming with high velocity within the plasma and under the

action of external force. We have employed the homotopy perturbation method to obtain the graphical plots of solitary structures and their evolution into an envelope soliton. Analytically, we have obtained the linear dispersion relation and studied its characteristics. Further, we have derived the KdV equation using the reductive perturbation technique and studied the parametric dependence on the KdV solitary profile. These findings augment the homotopy results. The analytical and simulation results thus obtained will help interpret and identify electron acoustic wave modes in such a plasma system. To sum up we have seen that in a magnetized plasma with Kappa distributed ions that are streaming at high speeds inside the plasma and under the influence of an external force, show significant new effects. In such a plasma system, the analytical and simulation results will aid in understanding and identifying the electron acoustic wave modes. To obtain the graphical plots of solitary structures and their growth into an envelope soliton, we have used the homotopy perturbation method. We obtained the linear dispersion relation analytically and investigated its properties. Additionally, we investigated the parametric dependence on the KdV solitary profile. These results support the homotopy findings.

The findings in this work will help explore new aspects of nonlinear plasma physics. Introducing some new codes opens the possibility of studying mini-complex phenomena in real-time using simple computation tools and a small desktop computer. We have tried to maintain a correlation between experimental findings and theoretical understanding. Based on the findings of this work, we can extend our research in semiconductor plasma and laser-plasma, as well as the application of bifurcation theory to practical plasma problems. The future investigation will include:

- Upgradation of simulation techniques.
- Regularisation of schemes and conservation laws.
- Simplification of nonlinear partial differential equations' solution techniques.

Since we have used a bit of topology here, we expect to incorporate some advanced mathematical ideas to be used in plasma physics and fluid systems.

Appendices

APPENDIX A

NONLINEAR INTERACTION OF INTENSE LASER BEAM WITH DENSE PLASMA

$$\text{Let } \bar{\mathcal{U}} = (\mathbf{n}_e, \vec{\mathcal{V}}_e, \vec{\mathcal{E}}), \quad \mathcal{D} = \begin{pmatrix} \frac{\partial}{\partial t} + \vec{V}_e \cdot \vec{\nabla} + (\vec{\nabla} \cdot \vec{V}_e) \\ \frac{\partial}{\partial t} + \vec{V}_e \cdot \vec{\nabla} + 0 \cdot (\vec{\nabla} \cdot \vec{V}_e) \\ \frac{\partial}{\partial t} + \vec{V}_e \cdot \vec{\nabla} + 0 \cdot (\vec{\nabla} \cdot \vec{V}_e) \end{pmatrix},$$

$$\mathbf{f}(\mathbf{r}) = \begin{pmatrix} 0 \\ -\frac{e}{m_e} \left(\vec{E} + \frac{\vec{V}_e}{c} \times \vec{B} \right) \\ \frac{1}{\epsilon_0} n_e \vec{V}_e \end{pmatrix} - \frac{\vec{\nabla} p_e}{m_e n_e}, \quad \vec{\mathcal{V}} = (\mathcal{N}_e, \vec{\mathcal{V}}_e, \vec{\mathcal{E}})$$

and $\vec{\mathcal{V}}^{(0)} = \bar{\mathcal{U}}_0$ be the initial approximation.

Using (3.18) and linearizing by the Taylor series $\mathcal{N}(\vec{\mathcal{V}})$ in p , we get the linear form

$$\mathcal{N}(\vec{\mathcal{V}}) = p^0 \mathcal{N}_0(\vec{\mathcal{V}}^{(0)}) + p \mathcal{N}_1(\vec{\mathcal{V}}^{(0)}, \vec{\mathcal{V}}^{(1)}) + p^2 \mathcal{N}_2(\vec{\mathcal{V}}^{(0)}, \vec{\mathcal{V}}^{(1)}, \vec{\mathcal{V}}^{(2)}) + \dots \quad (\text{A.1})$$

Similarly we expand $\mathbf{f}(\mathbf{r})$ by the Taylor series in p , and the coefficients of linearization are obtained by using Matlab R2019 symbolic computation. Putting these expression for $\mathcal{N}(\vec{\mathcal{V}})$ and $\mathbf{f}(\mathbf{r})$ in equation (3.17) and equating like powers of p , we get a set of equations which can solve iteratively. Finally we get the solution as

$$\bar{\mathcal{U}} = \lim_{p \rightarrow 1} \vec{\mathcal{V}} = \vec{\mathcal{V}}^{(0)} + \vec{\mathcal{V}}^{(1)} + \vec{\mathcal{V}}^{(2)} + \dots \quad (\text{A.2})$$

APPENDIX B

EFFECTS OF EXCHANGE SYMMETRY AND QUANTUM DIFFRACTION ON AMPLITUDE MODULATED ELECTROSTATIC WAVES IN QUANTUM MAGNETOPLASMA

B.1 $n=1, l=1$ perturbation relations:

$$\begin{aligned}
 -i\omega\gamma_1 n_{e,1}^{(1)} + ik\gamma_1 v_{e,1}^{(1)} + ik\gamma_1 u_0 n_{e,1}^{(1)} &= 0, \\
 -i\omega n_{i,1}^{(1)} + ikv_{i,1}^{(1)} &= 0, \\
 -ik\varphi_1^{(1)} - \frac{v_{e\perp,1}^{(1)}}{\rho_s} + \frac{ik\lambda_1}{3} n_{e,1}^{(1)} - \frac{2ik\lambda_2}{3} n_{e,1}^{(1)} + i\frac{H^2}{4\gamma_3} k^3 n_{e,1}^{(1)} &= 0, \\
 -i\omega v_{i,1}^{(1)} + ik\varphi_1^{(1)} + ikn_{i,1}^{(1)} &= 0, \\
 -k^2\varphi_1^{(1)} - n_{e,1}^{(1)} + n_{i,1}^{(1)} &= 0. \quad (\text{B.1})
 \end{aligned}$$

B.2 $n=1, l=1$ perturbation coefficients:

$$\begin{aligned}
 A_{11} &= \frac{k^4 + k^2 - \omega^2 k^2}{\omega^2 - k^2}, \\
 B_{11} &= \frac{k^2}{\omega^2 - k^2}, \quad C_{11} = \left(\frac{\omega - ku_0}{k}\right) \left(\frac{k^4 + k^2 - \omega^2 k^2}{\omega^2 - k^2}\right), \\
 D_{11} &= \frac{\omega k}{\omega^2 - k^2}. \quad (\text{B.2})
 \end{aligned}$$

B.3 n=2, l=1 perturbation relations:

$$\begin{aligned}
 & -C_g \gamma_1 \frac{\partial n_{e,1}^{(1)}}{\partial \xi} - i\omega \gamma_2 n_{e,1}^{(2)} + \gamma_1 \frac{\partial v_{e,1}^{(1)}}{\partial \xi} + ik \gamma_2 v_{e,1}^{(2)} + u_0 \gamma_1 \frac{\partial n_{e,1}^{(1)}}{\partial \xi} + ik u_0 \gamma_2 n_{e,1}^{(2)} = 0, \\
 & -C_g \frac{\partial n_{i,1}^{(1)}}{\partial \xi} - i\omega n_{i,1}^{(2)} + \frac{\partial v_{i,1}^{(1)}}{\partial \xi} + ik v_{i,1}^{(2)} = 0, \\
 & -\frac{\partial \varphi_1^{(1)}}{\partial \xi} - ik \varphi_1^{(2)} + \frac{\lambda_1}{3} (ik n_{e,1}^{(2)} + \frac{\partial n_{e,1}^{(1)}}{\partial \xi}) - \frac{2\lambda_2}{3} (ik n_{e,1}^{(2)} + \frac{\partial n_{e,1}^{(1)}}{\partial \xi}) - \frac{H^2}{2\gamma_3} \left(-\frac{ik^3}{2} n_{e,1}^{(2)} - 3k^2 \frac{\partial n_{e,1}^{(1)}}{\partial \xi} \right) = 0, \\
 & -C_g \frac{\partial v_{i,1}^{(1)}}{\partial \xi} - i\omega v_{i,1}^{(2)} + \frac{\partial \varphi_1^{(1)}}{\partial \xi} + ik \varphi_1^{(2)} + \frac{\partial n_{i,1}^{(1)}}{\partial \xi} + ik n_{i,1}^{(2)} = 0, \\
 & 2ik \frac{\partial \varphi_1^{(1)}}{\partial \xi} - k^2 \varphi_1^{(2)} - n_{e,1}^{(2)} + n_{i,1}^{(2)} = 0. \quad (\text{B.3})
 \end{aligned}$$

B.4 n=2, l=1 perturbation coefficients:

$$\begin{aligned}
 A'_{21} &= \frac{12\gamma_3 k}{4\lambda_1 \gamma_3 - 8\lambda_2 \gamma_3 + 3H^2 k^2}, \\
 A''_{21} &= 2iA_{11} \frac{\gamma_3 (-6 + 2\lambda_1 - 4\lambda_2) + 9H^2 k^2}{k(4\gamma_3 \lambda_1 - 8\gamma_3 \lambda_2 + 3H^2 k^2)}, \\
 B'_{21} &= \frac{k^2}{\omega(\omega - k)}, \\
 B''_{21} &= i \frac{k(1 - C_g D_{11} + B_{11}) - (k - \omega)(C_g B_{11} - D_{11})}{\omega(k - \omega)}, \\
 C'_{21} &= \frac{\gamma_1 (\omega - k u_0) A'_{21}}{k \gamma_2}, \\
 C''_{21} &= \frac{k \gamma_2 A''_{21} + i \gamma_1 (-C_g A_{11} + C_{11} + u_0 A_{11})}{k \gamma_2}, \\
 D'_{21} &= \frac{\omega B'_{21}}{k}, \\
 D''_{21} &= \frac{B''_{21} + i(C_g B_{11} - D_{11})}{k}, \\
 E'_{21} &= \frac{2ik - A''_{21} + B''_{21}}{k^2 + A'_{21} - B'_{21}}, \\
 iA_{21} &= A'_{21} E_{21} + A''_{21}, \quad iB_{21} = B'_{21} E_{21} + B''_{21}, \quad iC_{21} = C'_{21} E_{21} + C''_{21}, \\
 iD_{21} &= D'_{21} E_{21} + D''_{21}, \quad iE_{21} = E'_{21}. \quad (\text{B.4})
 \end{aligned}$$

B.5 n=2, l=2 perturbation relations:

$$\begin{aligned}
 -C_g \gamma_1 \frac{\partial n_{e,2}^{(1)}}{\partial \xi} - 2i\omega \gamma_2 n_{e,2}^{(2)} + \gamma_1 \frac{\partial v_{e,2}^{(1)}}{\partial \xi} + 2ik \gamma_2 v_{e,2}^{(2)} + u_0 \gamma_1 \frac{\partial n_{e,2}^{(1)}}{\partial \xi} + 2iku_0 \gamma_2 n_{e,2}^{(2)} + 2ik \gamma_1^2 n_{e,1}^{(1)} v_{e,1}^{(1)} &= 0, \\
 -C_g \frac{\partial n_{i,2}^{(1)}}{\partial \xi} - 2i\omega n_{i,2}^{(2)} + \frac{\partial v_{i,2}^{(1)}}{\partial \xi} + 2ik v_{i,2}^{(2)} + 2ik n_{i,1}^{(1)} v_{i,1}^{(1)} &= 0, \\
 -\frac{\partial \varphi_2^{(1)}}{\partial \xi} - 2ik \varphi_2^{(2)} + \frac{\lambda_1}{3} (2ik n_{e,2}^{(2)} + \frac{\partial n_{e,2}^{(1)}}{\partial \xi}) - \frac{2\lambda_2}{3} (2ik n_{e,2}^{(2)} + \frac{\partial n_{e,2}^{(1)}}{\partial \xi}) - \frac{H^2}{2\gamma_3} (-4ik^3 n_{e,2}^{(2)} - 4k^2 \frac{\partial n_{e,2}^{(1)}}{\partial \xi}) &= 0, \\
 -C_g \frac{\partial v_{i,2}^{(1)}}{\partial \xi} - 2i\omega v_{i,2}^{(2)} + \frac{\partial \varphi_2^{(1)}}{\partial \xi} + 2ik \varphi_2^{(2)} + \frac{\partial n_{i,2}^{(1)}}{\partial \xi} + 2ik n_{i,2}^{(2)} + 2ik v_{i,1}^{(1)} v_{i,1}^{(1)} &= 0, \\
 4ik \frac{\partial \varphi_2^{(1)}}{\partial \xi} - 4k^2 \varphi_2^{(2)} - n_{e,2}^{(2)} + n_{i,2}^{(2)} - \frac{1}{2} \varphi_1^{(1)} \cdot \varphi_1^{(1)} &= 0. \quad (\text{B.5})
 \end{aligned}$$

B.6 n=2, l=2 perturbation coefficients:

$$\begin{aligned}
 E_{22} &= \frac{2kD_{11}(\omega B_{11} + kD_{11}) - 1}{2(\omega^2 - k^2) \left(4k^2 + \frac{3\gamma_3}{\gamma_3(\lambda_1 - 2\lambda_2) + 3H^2 k^2} - \frac{k^2}{\omega^2 - k^2} \right)}, \\
 A_{22} &= \frac{3\gamma_3 E_{22}}{\gamma_3(\lambda_1 - 2\lambda_2) + 3H^2 k^2}, \\
 B_{22} &= \frac{kD_{11}(\omega B_{11} + kD_{11}) + k^2 E_{22}}{\omega^2 - k^2}, \\
 C_{22} &= \frac{A_{22}(\omega - ku_0) + kA_{11}C_{11}}{k}, \\
 D_{22} &= \frac{\omega B_{22}}{k} - B_{11}D_{11}. \quad (\text{B.6})
 \end{aligned}$$

B.7 n=3, l=0 perturbation relations:

$$\begin{aligned}
 \gamma_1 \frac{\partial n_{e,0}^{(1)}}{\partial \tau} - C_g \gamma_2 \frac{\partial n_{e,0}^{(2)}}{\partial \xi} + \gamma_2 \frac{\partial v_{e,0}^{(2)}}{\partial \xi} + u_0 \gamma_2 \frac{\partial n_{e,0}^{(2)}}{\partial \xi} &= 0, \\
 \frac{\partial n_{i,0}^{(1)}}{\partial \tau} - C_g \frac{\partial n_{i,0}^{(2)}}{\partial \xi} + \frac{\partial v_{i,0}^{(2)}}{\partial \xi} &= 0, \\
 -\frac{\partial \varphi_0^{(2)}}{\partial \xi} + \frac{\lambda_1}{3} \left(\frac{\partial n_{e,0}^{(2)}}{\partial \xi} \right) - \frac{2\lambda_2}{3} \left(\frac{\partial n_{e,0}^{(2)}}{\partial \xi} \right) &= 0, \\
 \frac{\partial v_{i,0}^{(1)}}{\partial \tau} - C_g \frac{\partial v_{i,0}^{(2)}}{\partial \xi} + \frac{\partial \varphi_0^{(2)}}{\partial \xi} + \frac{\partial n_{i,0}^{(2)}}{\partial \xi} &= 0, \\
 \frac{\partial^2 \varphi_0^{(1)}}{\partial \xi^2} - n_{e,0}^{(3)} + n_{i,0}^{(3)} - |\varphi_1^{(1)}|^2 &= 0. \quad (\text{B.7})
 \end{aligned}$$

B.8 n=2, l=0 perturbation coefficients:

$$\begin{aligned}
 E_{20} &= \frac{(C_g^2 - 1)(\lambda_1 - 2\lambda_2)}{(\lambda_1 - 2\lambda_2) - 3(C_g^2 - 1)}, \\
 A_{20} &= \frac{3E_{20}}{\lambda_1 - 2\lambda_2}, \\
 B_{20} &= \frac{E_{20}}{C_g^2 - 1}, \\
 C_{20} &= \frac{3(C_g - u_0)E_{20}}{(\lambda_1 - 2\lambda_2)}, \\
 D_{20} &= \frac{C_g E_{20}}{C_g^2 - 1}. \quad (\text{B.8})
 \end{aligned}$$

B.9 n=3, l=1 perturbation relations:

$$\begin{aligned}
 & \gamma_1 \frac{\partial n_{e,1}^{(1)}}{\partial \tau} - C_g \gamma_2 \frac{\partial n_{e,1}^{(2)}}{\partial \xi} - i\omega \gamma_3 n_{e,1}^{(3)} + \gamma_2 \frac{\partial v_{e,1}^{(2)}}{\partial \xi} + ik\gamma_3 v_{e,1}^{(3)} + u_0 \gamma_2 \frac{\partial n_{e,1}^{(2)}}{\partial \xi} + ik u_0 \gamma_3 n_{e,1}^{(3)} \\
 & \quad + ik\gamma_1 \gamma_2 \left[n_{e,1}^{(1)} \cdot v_{e,0}^{(2)} + n_{e,-1}^{(1)} \cdot v_{e,2}^{(2)} + n_{e,0}^{(2)} \cdot v_{e,1}^{(1)} + n_{e,2}^{(2)} \cdot v_{e,-1}^{(1)} \right] = 0, \\
 & \frac{\partial n_{i,1}^{(1)}}{\partial \tau} - C_g \frac{\partial n_{i,1}^{(2)}}{\partial \xi} - i\omega n_{i,1}^{(3)} + \frac{\partial v_{i,1}^{(2)}}{\partial \xi} + ik v_{i,1}^{(3)} + ik \left[n_{i,1}^{(1)} \cdot v_{i,0}^{(2)} + n_{i,-1}^{(1)} \cdot v_{i,2}^{(2)} + n_{i,0}^{(2)} \cdot v_{i,1}^{(1)} + n_{i,2}^{(2)} \cdot v_{i,-1}^{(1)} \right] = 0, \\
 & \quad - \frac{\partial \varphi_1^{(2)}}{\partial \xi} - ik \varphi_1^{(3)} + \frac{\lambda_1}{3} \left(ik n_{e,1}^{(3)} + \frac{\partial n_{e,1}^{(2)}}{\partial \xi} \right) - \frac{2\lambda_2}{3} \left(ik n_{e,1}^{(3)} + \frac{\partial n_{e,1}^{(2)}}{\partial \xi} \right) \\
 & \quad - \frac{H^2}{2\gamma_3} \left(-\frac{ik^3}{2} n_{e,1}^{(3)} - 3k^2 \frac{\partial n_{e,1}^{(2)}}{\partial \xi} + ik \frac{\partial^2 n_{e,1}^{(1)}}{\partial \xi^2} \right) = 0, \\
 & \frac{\partial v_{i,1}^{(1)}}{\partial \tau} - C_g \frac{\partial v_{i,1}^{(2)}}{\partial \xi} - i\omega v_{i,1}^{(3)} + \frac{\partial \varphi_1^{(2)}}{\partial \xi} + ik \varphi_1^{(3)} + \frac{\partial n_{i,1}^{(2)}}{\partial \xi} + ik n_{i,1}^{(3)} \\
 & \quad + ik \left[2v_{i,-1}^{(1)} \cdot v_{i,2}^{(2)} + v_{i,0}^{(2)} \cdot v_{i,1}^{(1)} - v_{i,2}^{(2)} \cdot v_{i,-1}^{(1)} \right] = 0; \\
 & \frac{\partial^2 \varphi_1^{(1)}}{\partial \xi^2} + 2ik \frac{\partial \varphi_1^{(2)}}{\partial \xi} - k^2 \varphi_1^{(3)} - n_{e,1}^{(3)} + n_{i,1}^{(3)} - \left[\varphi_1^{(1)} \cdot \varphi_0^{(2)} + \varphi_{-1}^{(1)} \cdot \varphi_2^{(2)} \right] = 0. \quad (\text{B.9})
 \end{aligned}$$

APPENDIX C

RESONANT INTERACTIONS AND CHAOTIC EXCITATION IN NONLINEAR SURFACE WAVES IN DENSE PLASMA

C.1 First Harmonic Quantities

$$\phi_1 = \frac{A}{\gamma - k} [-2ke^{-\gamma x} + (\gamma + k)e^{-kx}] \quad (\text{C.1})$$

$$\phi_{\nu 1} = Ae^{kx} \quad (\text{C.2})$$

$$n_1 = A(\gamma^2 - k^2)e^{-\gamma x} = \alpha e^{-\gamma x} \quad (\text{C.3})$$

$$(\text{C.4})$$

$$u_{x1} = \frac{iA\gamma}{\omega} \left[(\gamma^2 - k^2) \left(1 - \frac{H^2(\gamma^2 - k^2)}{4} \right) - 1 \right] (e^{-\gamma x} - e^{-kx}) \quad (\text{C.5})$$

$$= i(\psi_x e^{-\gamma x} + \theta_x e^{-kx}) \quad (\text{C.6})$$

$$(\text{C.7})$$

$$u_{z1} = \frac{A}{\omega} \left[(\gamma^2 - k^2) \left(1 - \frac{H^2(\gamma^2 - k^2)}{4} \right) - 1 \right] (\gamma e^{-\gamma x} + k e^{-kx}) \quad (\text{C.8})$$

$$= (\psi_z e^{-\gamma x} + \theta_z e^{-kx}) \quad (\text{C.9})$$

$$(\text{C.10})$$

where,

$$\gamma^2 = 1 + \left(\frac{\Lambda R_e}{3} \right) k^2 + \left(\frac{H^2 k^4}{2} \right) - \omega^2$$

C.2 Second Harmonic Quantities

$$P_1 = \frac{(2i\beta - 2k)M_2}{2i\beta + 2k} \quad (\text{C.11})$$

$$- \sum_{j=1}^3 \frac{(F_j(2i\beta + p_j))}{(2i\beta + 2k)p_j^2 \left(1 - p_j^2 + (H^2 p_j^4/4) - 4\omega^2\right)} \quad (\text{C.12})$$

$$P_2 = \frac{4kM_2}{2i\beta + 2k} - \quad (\text{C.13})$$

$$\sum_{j=1}^3 F_j \frac{(2k - p_j)}{(2i\beta + 2k)p_j^2 \left(1 - p_j^2 + (H^2 p_j^4/4) - 4\omega^2\right)^1} \quad (\text{C.14})$$

$$p_1 = 2k \quad (\text{C.15})$$

$$p_2 = 2\gamma \quad (\text{C.16})$$

$$p_3 = k + \gamma \quad (\text{C.17})$$

$$F_1 = 2k^2(\theta_x^2 - 2\theta_z^2) \quad (\text{C.18})$$

$$F_2 = 2\alpha^2(\gamma^2 - k^2) - 2\omega\alpha(2k\psi_z - 2\gamma\psi_x) \quad (\text{C.19})$$

$$-(2\gamma^2\psi_x^2 + 4k^2\psi_z^2) + H^2\alpha^2(\gamma^2 - k^2)^2/4 \quad (\text{C.20})$$

$$F_3 = 2\omega\alpha\{(\gamma + k)\theta_x - 2k\theta_z\} - \{(\gamma + k)^2\theta_x\psi_x + 8k^2\theta_z\} \quad (\text{C.21})$$

$$P_3 = \sum_{j=1}^3 F_j \frac{e^{-p_j x} p_j^{-2}}{\left(1 - p_j^2 + \frac{H^2 p_j^4}{4} - 4\omega^2\right)} \quad (\text{C.22})$$

$$N_1 = 4k^2 P_1 \quad (\text{C.23})$$

$$N_2 = 4\beta^2 P_2 \quad (\text{C.24})$$

$$N_3 = \sum_{j=1}^3 \frac{F_j e^{-p_j x}}{1 - p_j^2 \left(+ \frac{H^2 p_j^4}{4} - 4\omega^2 \right)} \quad (\text{C.25})$$

$$U_1 = \left[k(\theta_x^2 + 2P_1) + 8k^3 P_1 + \frac{32H^2 k^5 P_1}{4} + 2ik\theta_x \theta_z \right] \quad (\text{C.26})$$

$$U_2 = \left[\gamma(\psi_x^2 + \alpha^2) + 8k^3 P_1 + H^2 \alpha^2 \gamma \frac{\gamma^2 - k^2}{4} + 2ik\psi_x \psi_z \right] \quad (\text{C.27})$$

$$U_3 = ((\gamma + k)\theta_x \psi_x + 2ik(\theta_x \psi_z + \theta_z \psi_x)) \quad (\text{C.28})$$

$$U_4 = (2i\beta P_2 - 8i\beta^3 P_2 + 32\beta^5 P_2) \quad (\text{C.29})$$

$$U_5 = \sum_{j=1}^3 \frac{F_j e^{-p_j x} (1 + p_j^2 + (H^2 p_j^4)/4)}{p_j \left(1 - p_j^2 + (H^2 p_j^4)/4 - 4\omega^2 \right)} \quad (\text{C.30})$$

$$W_1 = \left[k\theta_x \theta_z + 2H^2 k^5 P_1 + 2ik(\theta_z^2 - P_1 - 4k^2 P_1) \right] \quad (\text{C.31})$$

$$W_2 = \left[ik \left(2\psi_z^2 + \alpha^2 k - \frac{H^2 \alpha^2 (\gamma^2 - k^2)}{4} \right) \right] \quad (\text{C.32})$$

$$W_3 = \gamma \psi_x \psi_z \quad (\text{C.33})$$

$$W_4 = (\theta_x \psi_z \gamma + \theta_z \psi_z k + i4k\theta_z \psi_z) \quad (\text{C.34})$$

$$W_5 = P_2(2ik(1 - 4\beta^2) + 8k^3 \beta^2 H^2) \quad (\text{C.35})$$

$$W_6 = \sum_{j=1}^3 \frac{F_j e^{-p_j x} (2ik(1 + p_j^2) - 2H^2 k 63 p_j^2)}{p_j^2 \left(1 - p_j^2 + (H^2 p_j^4)/4 - 4\omega^2 \right)} \quad (\text{C.36})$$

APPENDIX D
BIFURCATION THEORY AND STABILITY ANALYSIS

$$A_j = \frac{\omega (c_g \sigma_j - \gamma_j)}{k^2} + \frac{1}{k} \left[c_g \gamma_j - \frac{\sigma_j (4F_j + 3H^2 k^2)}{4} + \frac{3H^2 k^3}{4\Omega_j} \right] \quad (\text{D.1})$$

$$\gamma_j = \left\{ \omega^2 k c_g + \omega \left[\Omega_j + F_j (\Omega_j - k^2) + (H^2 k^2 / 4) (3\Omega_j - k^2) \right] + c_g k^3 \left[F_j + (H^2 k^2 / 4) \right] \right\} / \Omega_j^2 \quad (\text{D.2})$$

$$\sigma_j = \left[k (\Omega_j - \omega^2) + 2\omega k^2 c_g - k^3 \left\{ F_j + (3H^2 k^2 / 4) \right\} \right] / \Omega_j^2 \quad (\text{D.3})$$

$$N_j = - \left[\omega^2 + (H^2 k^6 / 8) \chi_j + \omega^2 + (H^2 k^6 / 8) l_j / \Omega_j \right] \quad (\text{D.4})$$

where

$$\chi_j = \left[b_0 - \left[\omega^2 k^2 + 2\omega k^3 c_g - H^2 k^6 / 4 \right] / \Omega_j^2 \right] / (F_j - c_g^2) \quad (\text{D.5})$$

and

$$l_j = -b_2 - \left[3(\omega k)^2 - (H^2 k^6 / 4) \right] / 2\Omega_j^2 \quad (\text{D.6})$$

REFERENCES

- [1] R. Dendy and S. Chapman, “Characterization and interpretation of strongly non-linear phenomena in fusion, space and astrophysical plasmas,” *Plasma physics and controlled fusion*, vol. 48, no. 12B, B313, 2006.
- [2] R. F. Post, “Controlled fusion research—an application of the physics of high temperature plasmas,” *Reviews of Modern Physics*, vol. 28, no. 3, p. 338, 1956.
- [3] D. A. Gurnett and A. Bhattacharjee, *Introduction to plasma physics: with space and laboratory applications*. Cambridge university press, 2005.
- [4] P. H. Diamond, S.-I. Itoh, and K. Itoh, *Modern Plasma Physics: Volume 1, Physical Kinetics of Turbulent Plasmas*. Cambridge University Press, 2010.
- [5] A. L. Peratt, *Physics of the plasma universe*. Springer, 1992, vol. 48.
- [6] J. O. Pouzo and M. M. Milanese, “Applications of the dense plasma focus to nuclear fusion and plasma astrophysics,” *IEEE transactions on plasma science*, vol. 31, no. 6, pp. 1237–1242, 2003.
- [7] H. Schamel, “A modified korteweg-de vries equation for ion acoustic waves due to resonant electrons,” *Journal of Plasma Physics*, vol. 9, no. 3, pp. 377–387, 1973.
- [8] W. Jones, A Lee, S. Gleman, and H. Doucet, “Propagation of ion-acoustic waves in a two-electron-temperature plasma,” *Physical Review Letters*, vol. 35, no. 20, p. 1349, 1975.
- [9] S. Tagare and R. V. Reddy, “Effect of higher-order nonlinearity on propagation of nonlinear ion-acoustic waves in a collisionless plasma consisting of negative ions,” *Journal of plasma physics*, vol. 35, no. 2, pp. 219–237, 1986.
- [10] N. Rao, P. Shukla, and M. Y. Yu, “Dust-acoustic waves in dusty plasmas,” *Planetary and space science*, vol. 38, no. 4, pp. 543–546, 1990.
- [11] H. R. Miller and P. J. Wiita, *Active galactic nuclei*. Springer, Berlin, 1988.
- [12] R. Boström, G. Gustafsson, B. Holback, G. Holmgren, H. Koskinen, and P. Kintner, “Characteristics of solitary waves and weak double layers in the magnetospheric plasma,” *Physical review letters*, vol. 61, no. 1, p. 82, 1988.

References

- [13] M Temerin, K Cerny, W Lotko, and F. Mozer, “Observations of double layers and solitary waves in the auroral plasma,” *Physical Review Letters*, vol. 48, no. 17, p. 1175, 1982.
- [14] F. C. Michel, “Theory of pulsar magnetospheres,” *Rev. Mod. Phys.*, vol. 54, pp. 1–66, 1982. DOI: 10.1103/RevModPhys.54.1. [Online]. Available: <https://link.aps.org/doi/10.1103/RevModPhys.54.1>.
- [15] N. Plihon, P. Chabert, and C. Corr, “Experimental investigation of double layers in expanding plasmas,” *Physics of Plasmas*, vol. 14, no. 1, p. 013506, 2007.
- [16] P. Shukla, R Bingham, R Dendy, H Pécseli, and L Stenflo, “Nonlinear structures in space and laboratory plasmas,” *Le Journal de Physique IV*, vol. 5, no. C6, pp. C6–19, 1995.
- [17] H Boehmer, M Adams, and N Rynn, “Positron trapping in a magnetic mirror configuration,” *Physics of Plasmas*, vol. 2, no. 11, pp. 4369–4371, 1995.
- [18] E. P. Liang, S. C. Wilks, and M. Tabak, “Pair production by ultraintense lasers,” *Physical review letters*, vol. 81, no. 22, p. 4887, 1998.
- [19] B. Ghosh and S. Banerjee, “Modulation instability of ion-acoustic waves in plasma with nonthermal electrons,” *Journal of Astrophysics*, vol. 2014, 2014.
- [20] S. I. Popel, S. V. Vladimirov, and P. K. Shukla, “Ion-acoustic solitons in electron–positron–ion plasmas,” *Physics of Plasmas*, vol. 2, no. 3, pp. 716–719, 1995. DOI: 10.1063/1.871422. eprint: <https://doi.org/10.1063/1.871422>. [Online]. Available: <https://doi.org/10.1063/1.871422>.
- [21] Y. Nejoh, “The effect of the ion temperature on large amplitude ion-acoustic waves in an electron–positron–ion plasma,” *Physics of Plasmas*, vol. 3, no. 4, pp. 1447–1451, 1996.
- [22] H. R. Pakzad, “Ion acoustic solitary waves in plasma with nonthermal electron and positron,” *Physics Letters A*, vol. 373, no. 8-9, pp. 847–850, 2009.
- [23] S. Ghosh and R Bharuthram, “Ion acoustic solitons and double layers in electron–positron–ion plasmas with dust particulates,” *Astrophysics and Space Science*, vol. 314, no. 1, pp. 121–127, 2008.
- [24] P. Shukla, R Bingham, R Dendy, H Pécseli, and L Stenflo, “Nonlinear structures in space and laboratory plasmas,” *Le Journal de Physique IV*, vol. 5, no. C6, pp. C6–19, 1995.

References

- [25] E. Pfender, “Thermal plasma technology: Where do we stand and where are we going?” *Plasma chemistry and plasma processing*, vol. 19, no. 1, pp. 1–31, 1999.
- [26] T. Horbury, R. Wicks, and C. Chen, “Anisotropy in space plasma turbulence: Solar wind observations,” *Space Science Reviews*, vol. 172, no. 1, pp. 325–342, 2012.
- [27] C. Ng and A. Bhattacharjee, “Interaction of shear-alfvén wave packets: Implication for weak magnetohydrodynamic turbulence in astrophysical plasmas,” *The Astrophysical Journal*, vol. 465, p. 845, 1996.
- [28] H. Hora, *Plasmas at high temperature and density: applications and implications of laser-plasma interaction*. Springer Science & Business Media, 2008, vol. 1.
- [29] H. E. Koskinen, “Space plasma instabilities,” in *Physics of Space Storms*, Springer, 2011, pp. 191–218.
- [30] B. T. Tsurutani, B. J. Falkowski, J. S. Pickett, O. P. Verkhoglyadova, O. Santolik, and G. S. Lakhina, “Extremely intense elf magnetosonic waves: A survey of polar observations,” *Journal of Geophysical Research: Space Physics*, vol. 119, no. 2, pp. 964–977, 2014.
- [31] E. Yiğit, “Transport processes in plasma,” in *Atmospheric and Space Sciences: Ionospheres and Plasma Environments*, Springer, 2018, pp. 41–66.
- [32] A. V. Usmanov, W. H. Matthaeus, B. A. Breech, and M. L. Goldstein, “Solar wind modeling with turbulence transport and heating,” *The Astrophysical Journal*, vol. 727, no. 2, p. 84, 2011.
- [33] M. Moisan and J. Pelletier, “Individual motion of a charged particle in electric and magnetic fields,” in *Physics of Collisional Plasmas: Introduction to High-Frequency Discharges*. Dordrecht: Springer Netherlands, 2012, pp. 101–202, ISBN: 978-94-007-4558-2. DOI: 10.1007/978-94-007-4558-2_2. [Online]. Available: https://doi.org/10.1007/978-94-007-4558-2_2.
- [34] J. R. Johnson, S. Wing, and P. A. Delamere, “Kelvin helmholtz instability in planetary magnetospheres,” *Space Science Reviews*, vol. 184, no. 1, pp. 1–31, 2014.
- [35] E. Sonnendrucker, J. Roche, P. R. Bertrand, and A. Ghizzo, “The Semi-Lagrangian Method for the Numerical Resolution of the Vlasov Equation,” *Journal of Computational Physics*, vol. 149, no. 2, pp. 201–220, 1999. DOI: 10.1006/jcph.

References

- 1998.6148. [Online]. Available: <https://hal.univ-lorraine.fr/hal-01791851>.
- [36] A. Khan, N. U. Haq, I. R. Chughtai, A. Shah, and K. Sanaullah, "Experimental investigations of the interface between steam and water two phase flows," *International Journal of Heat and mass transfer*, vol. 73, pp. 521–532, 2014.
- [37] R. Kelly, "The stability of an unsteady kelvin–helmholtz flow," *Journal of Fluid Mechanics*, vol. 22, no. 3, pp. 547–560, 1965.
- [38] P. G. Drazin, *Introduction to hydrodynamic stability*. Cambridge university press, 2002, vol. 32.
- [39] S Chandrasekhar, "Hydrodynamic and hydromagnetic stability oxford univ," *Press (Clarendon) London and New York*, 1961.
- [40] V Shankar, "Introduction to hydrodynamic stability,"
- [41] J. Happel and H. Brenner, *Low Reynolds number hydrodynamics: with special applications to particulate media*. Springer Science & Business Media, 2012, vol. 1.
- [42] T. B. Benjamin and J. Feir, "The disintegration of wave trains on deep water part 1. theory," *Journal of Fluid Mechanics*, vol. 27, no. 3, pp. 417–430, 1967.
- [43] T. B. Benjamin, "Instability of periodic wavetrains in nonlinear dispersive systems," *Proceedings of the Royal Society of London. Series A. Mathematical and Physical Sciences*, vol. 299, no. 1456, pp. 59–76, 1967.
- [44] G. Agrawal and P. Liao, *Nonlinear Fiber Optics: Formerly Quantum Electronics* (Optics and Photonics). Elsevier Science, 2013, ISBN: 9781483288031. [Online]. Available: <https://books.google.co.in/books?id=QEhBQAAQBAJ>.
- [45] H. C. Yuen and B. M. Lake, "Instabilities of waves on deep water," *Annual Review of Fluid Mechanics*, vol. 12, no. 1, pp. 303–334, 1980. DOI: 10.1146/annurev.fl.12.010180.001511. eprint: <https://doi.org/10.1146/annurev.fl.12.010180.001511>. [Online]. Available: <https://doi.org/10.1146/annurev.fl.12.010180.001511>.
- [46] P. A. E. M. Janssen, "Nonlinear four-wave interactions and freak waves," *Journal of Physical Oceanography*, vol. 33, no. 4, pp. 863–884, 2003. DOI: 10.1175/1520-0485(2003)33<863:NFIAFW>2.0.CO;2.

References

- [47] K. Dysthe, H. E. Krogstad, and P. Müller, “Oceanic rogue waves,” *Annual Review of Fluid Mechanics*, vol. 40, no. 1, pp. 287–310, 2008. DOI: 10.1146/annurev.fluid.40.111406.102203.
- [48] R. H. Fowler, “On Dense Matter,” *Monthly Notices of the Royal Astronomical Society*, vol. 87, no. 2, pp. 114–122, Dec. 1926, ISSN: 0035-8711. DOI: 10.1093/mnras/87.2.114. eprint: <http://oup.prod.sis.lan/mnras/article-pdf/87/2/114/3623303/mnras87-0114.pdf>. [Online]. Available: <https://doi.org/10.1093/mnras/87.2.114>.
- [49] R. Fowler, *Statistical Mechanics: The Theory of the Properties of Matter in Equilibrium; Based on an Essay Awarded the Adams Prize in the University of Cambridge, 1923-24*. The University Press, 1929. [Online]. Available: <https://books.google.co.in/books?id=IcgsnQAACAAJ>.
- [50] R. H. Fowler, *The Passage of Electrons Through Surfaces and Surface Films: Being the Thirty-first Robert Boyle Lecture, Delivered Before the Oxford University Junior Scientific Club on 18 May, 1929*. H. Milford, Oxford University Press, 1929, vol. 31.
- [51] S. R. H. Fowler and E. A. Guggenheim, *Statistical Thermodynamics. A Version of Statistical Mechanics [by RH Fowler] for Students of Physics and Chemistry*. Cambridge, 1939.
- [52] S Chandrasekhar, “Radiative transfer,” *Dever, New York*, 1950.
- [53] S. Chandrasekhar and S. Chandrasekhar, *An introduction to the study of stellar structure*. Courier Corporation, 1957, vol. 2.
- [54] P. K. Shukla and S. Ali, “Dust acoustic waves in quantum plasmas,” *Physics of Plasmas*, vol. 12, no. 11, p. 114 502, 2005. DOI: 10.1063/1.2136376. eprint: <https://doi.org/10.1063/1.2136376>. [Online]. Available: <https://doi.org/10.1063/1.2136376>.
- [55] P. K. Shukla and B. Eliasson, “Formation and dynamics of dark solitons and vortices in quantum electron plasmas,” *Phys. Rev. Lett.*, vol. 96, p. 245 001, 24 Jun. 2006. DOI: 10.1103/PhysRevLett.96.245001. [Online]. Available: <https://link.aps.org/doi/10.1103/PhysRevLett.96.245001>.
- [56] P. K. Shukla and B Eliasson, “Nonlinear aspects of quantum plasma physics,” *Physics-Uspeski*, vol. 53, no. 1, pp. 51–76, Jan. 2010. DOI: 10.3367/ufne.0180.201001b.0055. [Online]. Available: <https://doi.org/10.3367%2Fufne.0180.201001b.0055>.

References

- [57] G. Manfredi and F. Haas, “Self-consistent fluid model for a quantum electron gas,” *Phys. Rev. B*, vol. 64, p. 075 316, 7 Jul. 2001. DOI: 10.1103/PhysRevB.64.075316. [Online]. Available: <https://link.aps.org/doi/10.1103/PhysRevB.64.075316>.
- [58] G. Manfredi, “How to model quantum plasmas,” *Fields Inst. Commun*, vol. 46, pp. 263–287, 2005.
- [59] F. Haas, L. G. Garcia, J. Goedert, and G. Manfredi, “Quantum ion-acoustic waves,” *Physics of Plasmas*, vol. 10, no. 10, pp. 3858–3866, 2003. DOI: 10.1063/1.1609446. eprint: <https://doi.org/10.1063/1.1609446>. [Online]. Available: <https://doi.org/10.1063/1.1609446>.
- [60] F. Haas, “A magnetohydrodynamic model for quantum plasmas,” *Physics of Plasmas*, vol. 12, no. 6, p. 062 117, 2005. DOI: 10.1063/1.1939947. eprint: <https://doi.org/10.1063/1.1939947>. [Online]. Available: <https://doi.org/10.1063/1.1939947>.
- [61] A. P. Misra and C. Bhowmik, “Nonlinear wave modulation in a quantum magnetoplasma,” *Physics of Plasmas*, vol. 14, no. 1, p. 012 309, 2007. DOI: 10.1063/1.2432052. eprint: <https://doi.org/10.1063/1.2432052>. [Online]. Available: <https://doi.org/10.1063/1.2432052>.
- [62] A. P. Misra and A. Roy Chowdhury, “Modulation of dust acoustic waves with a quantum correction,” *Physics of Plasmas*, vol. 13, no. 7, p. 072 305, 2006. DOI: 10.1063/1.2217933. eprint: <https://doi.org/10.1063/1.2217933>. [Online]. Available: <https://doi.org/10.1063/1.2217933>.
- [63] H Sahoo, S Chandra, and B Ghosh, “Dust acoustic solitary waves in magnetized dusty plasma with trapped ions and q-non-extensive electrons,” *Afr Rev Phys*, vol. 10, pp. 235–41, 2015.
- [64] B. Ghosh, S. Chandra, and S. Paul, “Amplitude modulation of electron plasma waves in a quantum plasma,” *Physics of plasmas*, vol. 18, no. 1, p. 012 106, 2011.
- [65] S. Chandra and B. Ghosh, “Modulational instability of electron-acoustic waves in relativistically degenerate quantum plasma,” *Astrophysics and Space Science*, vol. 342, no. 2, pp. 417–424, 2012.
- [66] S. Chandra, S. N. Paul, and B. Ghosh, “Linear and non-linear propagation of electron plasma waves in quantum plasma,” *IJPAP*, vol. 50, pp. 314–319, 2012. [Online]. Available: <http://nopr.niscair.res.in/handle/123456789/14001>.

References

- [67] S. Chandra and B. Ghosh, “Non-linear propagation of electrostatic waves in relativistic fermi plasma with arbitrary temperature,” *IJPAP*, 2013. [Online]. Available: <http://nopr.niscair.res.in/handle/123456789/20894>.
- [68] S. Chandra, S. N. Paul, and B. Ghosh, “Electron-acoustic solitary waves in a relativistically degenerate quantum plasma with two-temperature electrons,” *Astrophysics and Space Science*, vol. 343, no. 1, pp. 213–219, 2013.
- [69] G. Brodin, “New aspects of wake field generation in plasmas,” *Physica Scripta*, vol. 2001, no. T89, p. 72, 2001.
- [70] M Bonitz, H Kählert, T Ott, and H Löwen, “Magnetized strongly coupled plasmas and how to realize them in a dusty plasma setup,” *Plasma Sources Science and Technology*, vol. 22, no. 1, p. 015 007, 2012.
- [71] M Bonitz, “Impossibility of plasma instabilities in isotropic quantum plasmas,” *Physics of plasmas*, vol. 1, no. 4, pp. 832–833, 1994.
- [72] A. Singh and S Chandra, “Electron acceleration by ponderomotive force in magnetized quantum plasma,” *Laser and Particle Beams*, vol. 35, no. 2, pp. 252–258, 2017.
- [73] A. Singh and S Chandra, “Second harmonic generation in high density plasma,” *The African Review of Physics*, vol. 12, no. 0011, 2017.
- [74] M Akbari-Moghanjoughi, “Propagation of arbitrary-amplitude ion waves in relativistically degenerate electron-ion plasmas,” *Astrophysics and Space Science*, vol. 332, no. 1, pp. 187–192, 2011.
- [75] R. Roozehdar Mogaddam, N. Sepehri Javan, K. Javidan, and H. Mohammadzadeh, “Perturbative approach to the self-focusing of intense x-ray laser beam propagating in thermal quantum plasma,” *Physics of Plasmas*, vol. 25, no. 11, p. 112 104, 2018.
- [76] B. Eliasson and U. Kogelschatz, “Nonequilibrium volume plasma chemical processing,” *Plasma Science, IEEE Transactions on*, vol. 19, pp. 1063 –1077, Jan. 1992. DOI: 10.1109/27.125031.
- [77] R Roozehdar Mogaddam, N Sepehri Javan, K Javidan, and H Mohammadzadeh, “Modulation instability and soliton formation in the interaction of x-ray laser beam with relativistic quantum plasma,” *Physics of Plasmas*, vol. 26, no. 6, p. 062 112, 2019.

References

- [78] M. B. Hassan, I. J. Abd-Ali, and A. O. Soary, “The filamentation instability of nonparaxial laser beam inside magnetized plasma,” *Results in Physics*, vol. 14, 102386, p. 102386, Sep. 2019. DOI: 10.1016/j.rinp.2019.102386.
- [79] B. Vhanmore, A. Valkunde, T. Urunkar, K. Gavade, S. Patil, and M. Takale, “Self-focusing of higher-order asymmetric elegant hermite-cosh-gaussian laser beams in collisionless magnetized plasma,” *The European Physical Journal D*, vol. 73, pp. 1–5, Mar. 2019. DOI: 10.1140/epjd/e2019-90369-8.
- [80] M. R. Edwards, Y. Shi, J. M. Mikhailova, and N. J. Fisch, “Laser amplification in strongly magnetized plasma,” *Phys. Rev. Lett.*, vol. 123, p. 025001, 2 Jul. 2019. DOI: 10.1103/PhysRevLett.123.025001. [Online]. Available: <https://link.aps.org/doi/10.1103/PhysRevLett.123.025001>.
- [81] I. Kostyukov, A. Pukhov, and S. Kiselev, “Phenomenological theory of laser-plasma interaction in “bubble” regime,” *Physics of Plasmas*, vol. 11, no. 11, pp. 5256–5264, Nov. 2004. DOI: 10.1063/1.1799371.
- [82] B. Ghosh, S. Chandra, and S. N. Paul, “Relativistic effects on the modulational instability of electron plasma waves in quantum plasma,” *Pramana*, vol. 78, no. 5, pp. 779–790, 2012.
- [83] J.-H. He, “Homotopy perturbation technique,” *Computer Methods in Applied Mechanics and Engineering*, vol. 178, no. 3, pp. 257–262, 1999, ISSN: 0045-7825. DOI: [https://doi.org/10.1016/S0045-7825\(99\)00018-3](https://doi.org/10.1016/S0045-7825(99)00018-3). [Online]. Available: <http://www.sciencedirect.com/science/article/pii/S0045782599000183>.
- [84] J.-H. He, “Homotopy perturbation method: A new nonlinear analytical technique,” *Applied Mathematics and Computation*, vol. 135, no. 1, pp. 73–79, 2003, ISSN: 0096-3003. DOI: [https://doi.org/10.1016/S0096-3003\(01\)00312-5](https://doi.org/10.1016/S0096-3003(01)00312-5). [Online]. Available: <http://www.sciencedirect.com/science/article/pii/S0096300301003125>.
- [85] M. Borghesi, A. J. Mackinnon, R. Gaillard, O. Willi, A. Pukhov, and J. Meyer-ter Vehn, “Large quasistatic magnetic fields generated by a relativistically intense laser pulse propagating in a preionized plasma,” *Phys. Rev. Lett.*, vol. 80, pp. 5137–5140, 23 Jun. 1998. DOI: 10.1103/PhysRevLett.80.5137. [Online]. Available: <https://link.aps.org/doi/10.1103/PhysRevLett.80.5137>.
- [86] P. E. Young, H. A. Baldis, T. W. Johnston, W. L. Kruer, and K. G. Estabrook, “Filamentation and second-harmonic emission in laser-plasma interactions,” *Phys. Rev. Lett.*, vol. 63, pp. 2812–2815, 26 Dec. 1989. DOI: 10.1103/PhysRevLett.

References

- 63.2812. [Online]. Available: <https://link.aps.org/doi/10.1103/PhysRevLett.63.2812>.
- [87] P. Young, H. Baldis, T. Johnston, W. Kruer, and K. Estabrook, "Filamentation and second-harmonic emission in laser-plasma interactions," *Physical review letters*, vol. 63, no. 26, p. 2812, 1989.
- [88] P. E. Young, "Experimental study of filamentation in laser-plasma interactions," *Physics of Fluids B: Plasma Physics*, vol. 3, no. 8, pp. 2331–2336, 1991. DOI: 10.1063/1.859600. eprint: <https://doi.org/10.1063/1.859600>. [Online]. Available: <https://doi.org/10.1063/1.859600>.
- [89] A. J. Schmitt, "Three-dimensional filamentation of light in laser plasmas," *Physics of Fluids B: Plasma Physics*, vol. 3, no. 1, pp. 186–194, 1991. DOI: 10.1063/1.859936. eprint: <https://doi.org/10.1063/1.859936>. [Online]. Available: <https://doi.org/10.1063/1.859936>.
- [90] M. Hercher, "Laser-induced damage in transparent media," *J. Opt. Soc. America*, vol. 54, p. 563, 1964.
- [91] Y. Song, X. Shi, C. Wu, D. Tang, and H. Zhang, "Recent progress of study on optical solitons in fiber lasers," *Applied Physics Reviews*, vol. 6, no. 2, p. 021 313, 2019.
- [92] N. Zhao *et al.*, "Trapping of soliton molecule in a graphene-based mode-locked ytterbium-doped fiber laser," *IEEE Photonics Technology Letters*, vol. 26, no. 24, pp. 2450–2453, 2014.
- [93] B. Gao, J. Huo, G. Wu, and X. Tian, "Soliton molecules in a fiber laser mode-locked by a graphene-based saturable absorber," *Laser Physics*, vol. 25, no. 7, p. 075 103, 2015.
- [94] X. He, T. Chen, and D. N. Wang, "Ultra-fast solitons in a long cavity multi-mode-fiber-based graphene mode-locked fiber laser with high slope efficiency," *Laser Physics*, vol. 24, no. 8, p. 085 109, 2014.
- [95] W.-J. Liu, H.-N. Han, L. Zhang, R. Wang, and Z.-Y. Wei, "Analytic study on soliton amplification in graphene oxide mode-locked er-doped fiber lasers," *Journal of Modern Optics*, vol. 61, no. 9, pp. 773–777, 2014.
- [96] X. Li *et al.*, "Observation of soliton bound states in a graphene mode locked erbium-doped fiber laser," *Laser Physics*, vol. 22, no. 4, pp. 774–777, 2012.

-
- [97] Y. Cui, X. Liu, and C Zeng, “Conventional and dissipative solitons in a cfbg-based fiber laser mode-locked with a graphene–nanotube mixture,” *Laser Physics Letters*, vol. 11, no. 5, p. 055 106, 2014.
- [98] Y. F. Song, L. Li, D. Y. Tang, *et al.*, “Quasi-periodicity of vector solitons in a graphene mode-locked fiber laser,” *Laser Physics Letters*, vol. 10, no. 12, p. 125 103, 2013.
- [99] J. Guo, Y. Xiang, X. Dai, H. Zhang, and S. Wen, “Formation and energy exchange of vector dark solitons in fiber lasers,” *IEEE Photonics Journal*, vol. 7, no. 1, pp. 1–9, 2015.
- [100] N. Shukla, J Vieira, P. Muggli, G. Sarri, R. Fonseca, and L. Silva, “Conditions for the onset of the current filamentation instability in the laboratory,” *Journal of Plasma Physics*, vol. 84, no. 3, 2018.
- [101] B. M. Kincaid, “A short-period helical wiggler as an improved source of synchrotron radiation,” *Journal of Applied Physics*, vol. 48, no. 7, pp. 2684–2691, 1977.
- [102] E. Adli *et al.*, “Acceleration of electrons in the plasma wakefield of a proton bunch,” *Nature*, vol. 561, no. 7723, pp. 363–367, 2018.
- [103] G. Inchingolo, T. Grismayer, N. Loureiro, R. Fonseca, and L. Silva, “Fully kinetic simulations of 2d mri-induced turbulence in an electron-ion plasma,” in *APS Meeting Abstracts*, 2018.
- [104] J. P. Van Devender and D. L. Cook, “Inertial confinement fusion with light ion beams,” *Science*, vol. 232, no. 4752, pp. 831–836, 1986.
- [105] S. Vinko *et al.*, “Creation and diagnosis of a solid-density plasma with an x-ray free-electron laser,” *Nature*, vol. 482, no. 7383, pp. 59–62, 2012.
- [106] M Borghesi *et al.*, “Proton imaging: A diagnostic for inertial confinement fusion/fast ignitor studies,” *Plasma physics and controlled fusion*, vol. 43, no. 12A, A267, 2001.
- [107] D. Haberberger *et al.*, “Collisionless shocks in laser-produced plasma generate monoenergetic high-energy proton beams,” *Nature Physics*, vol. 8, no. 1, pp. 95–99, 2012.
- [108] W. M. Manheimer and N. K. Winsor, *Tokamak plasma heating with intense, pulsed ion beams*, US Patent 4,548,782, Oct. 1985.

References

- [109] S. Chandra, “Propagation of electrostatic solitary wave structures in dense astrophysical plasma: Effects of relativistic drifts & relativistic degeneracy pressure,” *Advances in Astrophysics*, vol. 1, no. 3, pp. 187–200, Nov. 2012. [Online]. Available: <https://dx.doi.org/10.22606/adap.2016.1300518>.
- [110] M Tatarakis *et al.*, “Propagation instabilities of high-intensity laser-produced electron beams,” *Physical review letters*, vol. 90, no. 17, p. 175 001, 2003.
- [111] P. Jha, R. K. Mishra, G. Raj, and A. K. Upadhyay, “Second harmonic generation in laser magnetized–plasma interaction,” *Physics of plasmas*, vol. 14, no. 5, p. 053 107, 2007.
- [112] L Stenflo, “Acoustic solitary vortices,” *The Physics of fluids*, vol. 30, no. 10, pp. 3297–3299, 1987.
- [113] J. Mendonça, P Norreys, R Bingham, and J. Davies, “Beam instabilities in laser-plasma interaction: Relevance to preferential ion heating,” *Physical review letters*, vol. 94, no. 24, p. 245 002, 2005.
- [114] A. Bret, M.-C. Firpo, and C. Deutsch, “About the most unstable modes encountered in beam plasma interaction physics,” *Laser and Particle Beams*, vol. 25, no. 1, pp. 117–119, 2007.
- [115] A. Litvak, V. Mironov, G. Fraiman, and A. Iunakovskii, “Thermal self-effect of wave beams in a plasma with a nonlocal nonlinearity,” *Fizika Plazmy*, vol. 1, pp. 60–71, 1975.
- [116] H. Hora, *Laser Plasma Physics: forces and the nonlinearity principle*. Spie Press, 2000.
- [117] I Paul, S Chandra, S Chattopadhyay, and S. Paul, “W-type ion-acoustic solitary waves in plasma consisting of cold ions and nonthermal electrons,” *Indian Journal of Physics*, vol. 90, no. 10, pp. 1195–1205, 2016.
- [118] J. Goswami, S. Chandra, and B. Ghosh, “Shock waves and the formation of solitary structures in electron acoustic wave in inner magnetosphere plasma with relativistically degenerate particles,” *Astrophysics and Space Science*, vol. 364, no. 4, p. 65, 2019.
- [119] S. Tailor, S. Chandra, R. Mohanty, and P. Soni, “Energy transport during plasma enhanced surface coating mechanism: A mathematical approach,” *Advanced Materials Letters*, vol. 4, no. 12, pp. 917–920, 2013.
- [120] H. Washimi and T. Taniuti, “Propagation of ion-acoustic solitary waves of small amplitude,” *Physical Review Letters*, vol. 17, no. 19, p. 996, 1966.

References

- [121] P. Kaw, K. Mima, and K. Nishikawa, “Envelope solutions for random-phase plasmons,” *Physical Review Letters*, vol. 34, no. 13, p. 803, 1975.
- [122] S. Chandra, J. Goswami, J. Sarkar, and C. Das, “Analytical and simulation studies of forced kdv solitary structures in a two-component plasma,” *J. Korean Phys. Soc.*, vol. 76, no. 6, 469–478, 2020. DOI: <https://doi.org/10.3938/jkps.76.469>.
- [123] P. K. Shukla and A. Mamun, “Dust-acoustic shocks in a strongly coupled dusty plasma,” *IEEE transactions on plasma science*, vol. 29, no. 2, pp. 221–225, 2001.
- [124] P. Shukla and A. Mamun, “Solitons, shocks and vortices in dusty plasmas,” *New Journal of Physics*, vol. 5, no. 1, p. 17, 2003.
- [125] A. Yıldırım and Y. Gülkanat, “Analytical approach to fractional zakharov–kuznetsov equations by he’s homotopy perturbation method,” *Communications in Theoretical Physics*, vol. 53, no. 6, p. 1005, 2010.
- [126] Z. Ma, “Homotopy perturbation method for the wu-zhang equation in fluid dynamics,” in *Journal of Physics: Conference Series*, IOP Publishing, vol. 96, 2008, p. 012 182.
- [127] M Moini, “Modified homotopy perturbation method for solving linear and non linear schrodinger equations,” *International Journal of Pure and Applied Mathematics*, vol. 49, no. 4, pp. 489–495, 2008.
- [128] M. M. Škorić, M. Jovanović, and M. Rajković, “Transition to turbulence via spatiotemporal intermittency in stimulated raman backscattering,” *Physical Review E*, vol. 53, no. 4, p. 4056, 1996.
- [129] A. I. Akhiezer, *Plasma Electrodynamics: Nonlinear Theory*. Pergamon Press, Oxford, UK, 1975, vol. 2.
- [130] G. Veldes, J Borhanian, M McKerr, V Saxena, D. Frantzeskakis, and I Kourakis, “Electromagnetic rogue waves in beam–plasma interactions,” *Journal of Optics*, vol. 15, no. 6, p. 064 003, 2013.
- [131] F. Baronio, M. Conforti, A. Degasperis, and S. Lombardo, “Rogue waves emerging from the resonant interaction of three waves,” *Physical review letters*, vol. 111, no. 11, p. 114 101, 2013.
- [132] N. Akhmediev, J. M. Dudley, D. R. Solli, and S. Turitsyn, “Recent progress in investigating optical rogue waves,” *Journal of Optics*, vol. 15, no. 6, p. 060 201, 2013.

References

- [133] N. Akhmediev *et al.*, “Roadmap on optical rogue waves and extreme events,” *Journal of Optics*, vol. 18, no. 6, p. 063 001, 2016.
- [134] C. Das, S. Chandra, and B. Ghosh, “Amplitude modulation and soliton formation of an intense laser beam interacting with dense quantum plasma: Symbolic simulation analysis,” *Contributions to Plasma Physics*, vol. 60, no. 8, e202000028, 2020. DOI: 10.1002/ctpp.202000028. eprint: <https://onlinelibrary.wiley.com/doi/pdf/10.1002/ctpp.202000028>. [Online]. Available: <https://onlinelibrary.wiley.com/doi/abs/10.1002/ctpp.202000028>.
- [135] S. Weber *et al.*, “Modeling of laser–plasma interaction on hydrodynamic scales: Physics development and comparison with experiments,” *Laser and Particle Beams*, vol. 22, Jun. 2004. DOI: 10.1017/S0263034604222157.
- [136] D. BATANI *et al.*, “Recent experiments on the hydrodynamics of laser-produced plasmas conducted at the pals laboratory,” *Laser and Particle Beams*, vol. 25, no. 1, 127–141, 2007. DOI: 10.1017/S0263034607070164.
- [137] A. Lifschitz, J. Faure, Y. Glinec, V. Malka, and P. Mora, “Proposed scheme for compact gev laser plasma accelerator,” *Laser and Particle Beams*, vol. 24, no. 2, p. 255, 2006.
- [138] K. Ta Phuoc *et al.*, “X-ray radiation from nonlinear thomson scattering of an intense femtosecond laser on relativistic electrons in a helium plasma,” *Phys. Rev. Lett.*, vol. 91, p. 195 001, 19 Nov. 2003. DOI: 10.1103/PhysRevLett.91.195001. [Online]. Available: <https://link.aps.org/doi/10.1103/PhysRevLett.91.195001>.
- [139] Z. Najmudin *et al.*, “The effect of high intensity laser propagation instabilities on channel formation in underdense plasmas,” *Physics of Plasmas*, vol. 10, no. 2, pp. 438–442, 2003. DOI: 10.1063/1.1534585. eprint: <https://doi.org/10.1063/1.1534585>. [Online]. Available: <https://doi.org/10.1063/1.1534585>.
- [140] E Lefebvre *et al.*, “Electron and photon production from relativistic laser–plasma interactions,” *Nuclear Fusion*, vol. 43, no. 7, pp. 629–633, Jul. 2003. DOI: 10.1088/0029-5515/43/7/317. [Online]. Available: <https://doi.org/10.1088/0029-5515/43/7/317>.
- [141] G. Shaviv, *The Life of Stars: The Controversial Inception and Emergence of the Theory of Stellar Structure*. Springer Science & Business Media, 2009.
- [142] N. Straumann, “The role of the exclusion principle for atoms to stars: A historical account,” *arXiv preprint quant-ph/0403199*, 2004.

References

- [143] A. G. Truscott, K. E. Strecker, W. I. McAlexander, G. B. Partridge, and R. G. Hulet, "Observation of fermi pressure in a gas of trapped atoms," *Science*, vol. 291, no. 5513, pp. 2570–2572, 2001.
- [144] A. S. Eddington, *Stellar Movements and the Structure of the Universe*. Macmillan and Company, limited, 1914.
- [145] A. S. Eddington, *Report on the relativity theory of gravitation*. Minkowski Institute Press, 1920.
- [146] A. S. Eddington, *Space, time and gravitation: An outline of the general relativity theory*. University Press, 1920.
- [147] A. S. Eddington. *Journal of the British Astronomical Society*, 1988, vol. 98, p. 140.
- [148] J. D. Norton, "General covariance and the foundations of general relativity: Eight decades of dispute," *Reports on progress in physics*, vol. 56, no. 7, p. 791, 1993.
- [149] R. W. Smith, *The expanding universe: Astronomy's' great debate', 1900-1931*. Cambridge University Press, 1982.
- [150] E. A. Milne, "Thermodynamics of the stars," in *Handbuch der Astrophysik*, Springer, 1930, pp. 65–255.
- [151] E. A. Milne, *Nature*, vol. 135, pp. 635–636, 1936.
- [152] E. A. Milne, "Kinematic relativity; a sequel to relativity, gravitation and world structure.," *Oxford*, 1948.
- [153] E. A. Milne, *Vectorial mechanics*. Methuen, 1948.
- [154] D. Koester and G. Chanmugam, "Physics of white dwarf stars," *Reports on Progress in Physics*, vol. 53, no. 7, p. 837, 1990.
- [155] S. Chandrasekhar, *Principles of stellar dynamics*. Courier Corporation, 2005.
- [156] S Chandrasekhar. *Plasma Physics*. Chicago: The University of Chicago Press. ISBN 978-0-226-10084-5., 1960.
- [157] S. Chandrasekhar and K. S. Thorne, *The mathematical theory of black holes*, 1985.

References

- [158] P. A. Andreev, “Exchange effects in coulomb quantum plasmas: Dispersion of waves in 2d and 3d quantum plasmas,” *Annals of Physics*, vol. 350, pp. 198–210, 2014.
- [159] E. Kuznetsov, A. Rubenchik, and V. E. Zakharov, “Soliton stability in plasmas and hydrodynamics,” *Physics Reports*, vol. 142, no. 3, pp. 103–165, 1986.
- [160] L. S. Kuz'menkov, S. G. Maksimov, and V. V. Fedoseev, “Microscopic quantum hydrodynamics of systems of fermions: Ii,” *Theoretical and Mathematical Physics*, vol. 126, no. 2, pp. 212–223, 2001.
- [161] A. Fedoseev, M. Isupov, G. Sukhinin, V. Pinaev, N. Demin, and M. Salnikov, “The effect of chlorine addition on ferromagnetic-enhanced inductively coupled plasma,” *Japanese Journal of Applied Physics*, vol. 59, no. SH, SHHC02, 2020.
- [162] A. Fedoseev, G. Sukhinin, T. Ramazanov, S. Kodanova, and N. Bastykova, “Interaction between glow discharge plasma and dust particles,” *Thermophysics and Aeromechanics*, vol. 18, no. 4, pp. 615–627, 2011.
- [163] L. Faddeev and L. Takhtajan, *Hamiltonian methods in the theory of solitons*. Springer Science & Business Media, 2007.
- [164] C. Sulem and P.-L. Sulem, *The nonlinear Schrödinger equation: self-focusing and wave collapse*. Springer Science & Business Media, 2007, vol. 139.
- [165] R. Dodd *et al.*, *Bulletin (New Series) of the American Mathematical Society*, vol. 19, no. 2, pp. 565–568, 1988.
- [166] C Bhowmik, A. Misra, and P. Shukla, “Oblique modulation of electron-acoustic waves in a fermi electron-ion plasma,” *Physics of Plasmas*, vol. 14, no. 12, p. 122 107, 2007.
- [167] J. Goswami, S. Chandra, and B Ghosh, “Study of small amplitude ion-acoustic solitary wave structures and amplitude modulation in e–p–i plasma with streaming ions,” *Laser and Particle Beams*, vol. 36, no. 1, pp. 136–143, 2018.
- [168] J Sarkar, J Goswami, S Chandra, and B Ghosh, “Study of ion-acoustic solitary wave structures in multi-component plasma containing positive and negative ions and q-exponential distributed electron beam,” *Laser and Particle Beams*, vol. 35, no. 4, pp. 641–647, 2017.
- [169] J. Sarkar, S. Chandra, J. Goswami, and B. Ghosh, “Formation of solitary structures and envelope solitons in electron acoustic wave in inner magnetosphere plasma with suprathermal ions,” *Contributions to Plasma Physics*, vol. 60, no. 7, e201900202, 2020.

References

- [170] L Brey, J. Dempsey, N. F. Johnson, and B. Halperin, “Infrared optical absorption in imperfect parabolic quantum wells,” *Physical Review B*, vol. 42, no. 2, p. 1240, 1990.
- [171] C. Das, S. Chandra, and B. Ghosh, “Nonlinear interaction of intense laser beam with dense plasma,” *Plasma Physics and Controlled Fusion*, vol. 63, no. 1, p. 015 011, Nov. 2020. DOI: 10 . 1088 / 1361 – 6587 / abc732. [Online]. Available: <https://doi.org/10.1088/1361-6587/abc732>.
- [172] F Haas, *Quantum Plasmas*. Springer, NY, 2011, ISBN: 978-1-4419-8201-8.
- [173] M. Chatterjee, M. Dasgupta, S. Das, M. Halder, and S. Chandra, “Study of dynamical properties in shock & solitary structures and its evolutionary stages in a degenerate plasma,” *The African Review of Physics*, vol. 15, p. 75, 2021.
- [174] J. Goswami, S. Chandra, J. Sarkar, and B. Ghosh, “Quantum two stream instability in a relativistically degenerate magnetised plasma,” in *AIP Conference Proceedings*, AIP Publishing LLC, vol. 2319, 2021, p. 030 005.
- [175] A Maiti, S Chowdhury, P Singha, S Ray, R Dasgupta, and S Chandra, “Study of small amplitude ion-acoustic bunched solitary waves in a plasma with streaming ions and thermal electrons,” *The African Review of Physics*, vol. 15, p. 97, 2021.
- [176] J. Goswami, S. Chandra, J. Sarkar, and B. Ghosh, “Electron acoustic solitary structures and shocks in dense inner magnetosphere finite temperature plasma,” *Radiation Effects and Defects in Solids*, vol. 175, no. 9-10, pp. 961–973, 2020.
- [177] P Samanta, A De, S Dey, D Maity, A Ghosh, and S Chandra, “Nonlinear excitations in dust-ion acoustic waves and the formation of rogue waves in stable parametric region in a 3-component degenerate plasma,” *The African Review of Physics*, vol. 15, p. 10, 2021.
- [178] A. Majumdar, A. Sen, B. Panda, R. Ghosal, S. Mallick, and S Chandra, “Study of shock fronts and solitary profile in a weakly relativistic plasma and its evolution into an amplitude modulated envelop soliton,” *The African Review of Physics*, vol. 15, p. 18, 2021.
- [179] A. Mukhopadhyay, D. Bagui, and S. Chandra, “Electrostatic shock fronts in two-component plasma and its evolution into rogue wave type solitary structures,” *The African Review of Physics*, vol. 15, p. 25, 2021.
- [180] S Ghosh, S Saha, T Chakraborty, K Sadhkhani, R Bhanja, and S Chandra, “Linear and non-linear properties of electron acoustic waves in a viscous plasma,” *The African Review of Physics*, vol. 15, p. 90, 2021.

References

- [181] A. Roychowdhury, S. Banerjee, and S. Chandra, “Stationary formation of dust-ion acoustic waves in degenerate dusty plasma at critical regime,” *The African Review of Physics*, vol. 15, p. 102, 2021.
- [182] S Ballav, S Kundu, A Das, and S Chandra, “Non-linear behaviour of dust acoustic wave mode in a dynamic dusty plasma containing negative dust particles and positrons,” *The African Review of Physics*, vol. 15, p. 54, 2021.
- [183] P. K. Shukla, L. Stenflo, and R Bingham, “Shielding of a slowly moving test charge in a quantum plasma,” *Physics Letters A*, vol. 359, no. 3, pp. 218–219, 2006.
- [184] M. Marklund, B. Eliasson, and P. K. Shukla, “Magnetosonic solitons in a fermionic quantum plasma,” *Phys. Rev. E*, vol. 76, p. 067 401, 6 2007. DOI: 10 . 1103 / PhysRevE . 76 . 067401. [Online]. Available: <https://link.aps.org/doi/10.1103/PhysRevE.76.067401>.
- [185] A. Misra, P. Shukla, and C Bhowmik, “Electron-acoustic solitary waves in dense quantum electron-ion plasmas,” *Physics of Plasmas*, vol. 14, no. 8, p. 082 309, 2007.
- [186] M. Ghosh, K Sharry, D Dutta, and S Chandra, “Propagation of rogue waves and cnoidal waves formations through low frequency plasma oscillations,” *The African Review of Physics*, vol. 15, p. 63, 2021.
- [187] J. Sarkar, S. Chandra, and B. Ghosh, “Resonant interactions between the fundamental and higher harmonic of positron acoustic waves in quantum plasma,” *Zeitschrift für Naturforschung A*, vol. 75, no. 10, pp. 819–824, 2020.
- [188] C. Das, S. Chandra, and B. Ghosh, “Effects of exchange symmetry and quantum diffraction on amplitude-modulated electrostatic waves in quantum magnetoplasma,” *Pramana*, vol. 95, no. 2, pp. 1–16, 2021. DOI: 10 . 1007 / s12043 - 021 - 02108 - x. [Online]. Available: <https://doi.org/10.1007/s12043-021-02108-x>.
- [189] S Dey, D Maity, A Ghosh, P Samanta, A De, and S Chandra, “Chaotic excitations of rogue waves in stable parametric region for highly-energetic pair plasmas,” *The African Review of Physics*, vol. 15, p. 33, 2021.
- [190] T. Ghosh, S. Pramanick, S. Sarkar, A. Dey, and S. Chandra, “Chaotic scenario in three-component fermi plasma,” *The African Review of Physics*, vol. 15, p. 45, 2021.

References

- [191] B. Eliasson and P. K. Shukla, “Nonlinear quantum fluid equations for a finite temperature fermi plasma,” *Physica Scripta*, vol. 78, no. 2, p. 025 503, 2008. DOI: 10.1088/0031-8949/78/02/025503.
- [192] C. B. Beatty *et al.*, “Creation of large temperature anisotropies in a laboratory plasma,” *Physics of Plasmas*, vol. 27, no. 12, p. 122 101, 2020. DOI: 10.1063/5.0029315. eprint: <https://doi.org/10.1063/5.0029315>. [Online]. Available: <https://doi.org/10.1063/5.0029315>.
- [193] H Abbasi, M. Jenab, and H. H. Pajouh, “Preventing the recurrence effect in the vlasov simulation by randomizing phase-point velocities in phase space,” *Physical Review E*, vol. 84, no. 3, p. 036 702, 2011.
- [194] J. Goswami, S. Chandra, J. Sarkar, and B. Ghosh, “Amplitude modulated electron acoustic waves with bipolar ions and kappa distributed positrons and warm electrons,” *Pramana-Journal of Physics*, vol. 95, p. 54, 2021.
- [195] J. Sarkar, S. Chandra, J Goswami, C Das, and B Ghosh, “Growth of rt instability at the accreting magnetospheric boundary of neutron stars,” in *AIP Conference Proceedings*, AIP Publishing LLC, vol. 2319, 2021, p. 030 006.
- [196] S. Sarkar, A. Dey, S. Pramanick, T. Ghosh, C. Das, and S. Chandra, “Homotopy study of spherical ion-acoustic waves in relativistic degenerate galactic plasma,” *IEEE Transactions on Plasma Science*, pp. 1–11, 2022. DOI: 10.1109/TPS.2022.3146441.
- [197] S. Kapoor, D. Dutta, M. Ghosh, and S. Chandra, “Magnetosonic shocks and solitons in fermi plasma with quasiperiodic perturbation,” *IEEE Transactions on Plasma Science*, 2022.
- [198] Shilpi, Sharry, C. Das, and S. Chandra, “Study of quantum-electron acoustic solitary structures in fermi plasma with two temperature electrons,” in *International Conference on Nonlinear Dynamics and Applications*, 2022.
- [199] J. Sarkar, S. Chandra, J. Goswami, and B. Ghosh, “Heliospheric two stream instability with degenerate electron plasma,” in *International Conference on Nonlinear Dynamics and Applications*, 2022.
- [200] S. Chandra *et al.*, “Multistability studies on electron-acoustic wave in a magnetized plasma with supra-thermal ions,” *Journal of Astrophysics and Astronomy*, 2022.
- [201] M Akbari-Moghanjoughi and B Eliasson, “Quantum faraday excitations in degenerate electron-ion plasma,” *Physica Scripta*, vol. 95, no. 4, p. 045 604, 2020.

References

- [202] A. Dey, S. Chandra, C. Das, S. Mandal, and T. Das, “Rogue wave generation through non-linear self interaction of electrostatic waves in dense plasma,” *IEEE Transactions on Plasma Science*, 2022.
- [203] C. Benedetti, A. Sgattoni, G. Turchetti, and P. Londrillo, “ALaDyn: A high-accuracy pic code for the maxwell–vlasov equations,” *IEEE Transactions on Plasma Science*, vol. 36, no. 4, pp. 1790–1798, 2008. DOI: 10.1109/TPS.2008.927143.
- [204] C. Cheng and G. Knorr, “The integration of the vlasov equation in configuration space,” *Journal of Computational Physics*, vol. 22, no. 3, pp. 330–351, 1976, ISSN: 0021-9991. DOI: [https://doi.org/10.1016/0021-9991\(76\)90053-X](https://doi.org/10.1016/0021-9991(76)90053-X). [Online]. Available: <https://www.sciencedirect.com/science/article/pii/002199917690053X>.
- [205] M. L. Bégué, A. Ghizzo, P. Bertrand, E. Sonnendrücker, and O. Coulaud, “Two-dimensional semi-lagrangian vlasov simulations of laser–plasma interaction in the relativistic regime,” *Journal of Plasma Physics*, vol. 62, no. 4, pp. 367–388, 1999. DOI: 10.1017/S0022377899008065.
- [206] “Study of laser plasma interactions using an eulerian vlasov code,” *Computer Physics Communications*, vol. 164, no. 1, pp. 156–159, 2004, Proceedings of the 18th International Conference on the Numerical Simulation of Plasmas, ISSN: 0010-4655. DOI: <https://doi.org/10.1016/j.cpc.2004.06.024>. [Online]. Available: <https://www.sciencedirect.com/science/article/pii/S0010465504002747>.
- [207] B. Eliasson and M. Akbari-Moghanjoughi, “Finite temperature static charge screening in quantum plasmas,” *Physics Letters A*, vol. 380, no. 33, pp. 2518–2524, 2016, ISSN: 0375-9601. DOI: <https://doi.org/10.1016/j.physleta.2016.05.043>. [Online]. Available: <https://www.sciencedirect.com/science/article/pii/S0375960116302493>.
- [208] S. Chandra, C. Das, and J. Sarkar, “Evolution of nonlinear stationary formations in a quantum plasma at finite temperature,” *Zeitschrift für Naturforschung A*, 2021.
- [209] S. P. Gary, “The mirror and ion cyclotron anisotropy instabilities,” *Journal of Geophysical Research: Space Physics*, vol. 97, no. A6, pp. 8519–8529, 1992.
- [210] G. Parks *et al.*, “Transport of solar wind h⁺ and he⁺⁺ ions across earth’s bow shock,” *The Astrophysical journal letters*, vol. 825, no. 2, p. L27, 2016.

References

- [211] E. Camporeale and D. Burgess, “Electron temperature anisotropy in an expanding plasma: Particle-in-cell simulations,” *The Astrophysical Journal*, vol. 710, no. 2, p. 1848, 2010.
- [212] H. Sahoo, C. Das, S. Chandra, B. Ghosh, and K. K. Mondal, “Quantum and relativistic effects on the kdv and envelope solitons in ion-plasma waves,” *IEEE Transactions on Plasma Science*, no. DOI: 10.1109/TPS.2021.3120077, 2021.
- [213] A. Das, P. Ghosh, S. Chandra, and V. Raj, “Electron acoustic peregrine breathers in a quantum plasma with 1-d temperature anisotropy,” *IEEE Transactions on Plasma Science*, no. DOI: 10.1109/TPS.2021.3113727, pp. 1–12, 2021.
- [214] K. Chaudhary, A. M. Imam, S. Z. H. Rizvi, and J. Ali, “Plasma kinetic theory,” *Kinetic Theory; InTech: Rijeka, Croatia*, pp. 107–127, 2018.
- [215] S. Chandra, J. Goswami, J. Sarkar, C. Das, B. Ghosh, and D. Nandi, “Formation of electron acoustic shock wave in inner magnetospheric plasma,” *Indian Journal of Physics*, no. 10.1007/s12648-021-02276-x, 2021.
- [216] S. Thakur, C. Das, and S. Chandra, “Stationary structures in a four component dense magnetoplasma with lateral perturbations,” *IEEE Transactions on Plasma Science*, 2021. DOI: 10.1109/TPS.2021.3133082.
- [217] J. Wright and N Bertelli, “The effects of finite electron temperature and diffraction on lower hybrid wave propagation,” *Plasma Physics and Controlled Fusion*, vol. 56, no. 3, p. 035 006, 2014.
- [218] F. Huot, A. Ghizzo, P. Bertrand, E. Sonnendrucker, and O. Coulaud, “Instability of the time splitting scheme for the one-dimensional and relativistic Vlasov–Maxwell system,” *Journal of Computational Physics*, vol. 185, no. 2, pp. 512–531, 2003. DOI: 10.1016/S0021-9991(02)00079-7. [Online]. Available: <https://hal.univ-lorraine.fr/hal-01791854>.
- [219] A. Ghizzo, F. Huot, and P. Bertrand, “A non-periodic 2d semi-lagrangian vlasov code for laser-plasma interaction on parallel computer,” *J. Comput. Phys.*, vol. 186, no. 1, 47–69, Mar. 2003, ISSN: 0021-9991. DOI: 10.1016/S0021-9991(03)00010-X. [Online]. Available: [https://doi.org/10.1016/S0021-9991\(03\)00010-X](https://doi.org/10.1016/S0021-9991(03)00010-X).
- [220] S. Ballav, A. Das, S. Pramanick, and S. Chandra, “Plasma shock wave in gamma-ray bursts: Nonlinear phenomena and radiative process,” *IEEE Transactions on Plasma Science*, 2021.

References

- [221] M. Ghorbanalilu and E. Abdollahazadeh, “Extension of temperature anisotropy weibel instability to non-maxwellian plasmas by 2d pic simulation,” *Laser and Particle Beams*, vol. 36, no. 1, pp. 1–7, 2018.
- [222] J. Goswami, S. Chandra, C. Das, and J. Sarkar, “Nonlinear wave-wave interaction in semiconductor junction diode,” *IEEE Transactions on Plasma Science*, no. DOI: 10.1109/TPS.2021.3124454, 2021.
- [223] A. Ghosh, J. Goswami, S. Chandra, C. Das, Y. Arya, and H. Chhibber, “Resonant interactions and chaotic excitation in nonlinear surface waves in dense plasma,” *IEEE Transactions on Plasma Science*, 2021.
- [224] J. Sarkar, S. Chandra, A. Dey, C. Das, A. Marick, and P. Chatterjee, “Forced kdv and envelope soliton in magnetoplasma with kappa distributed ions,” *IEEE Transactions on Plasma Science*, pp. 10–1109, 2021. DOI: 10 . 1109 / TPS . 2022 . 3140318.
- [225] A Inglebert, A Ghizzo, T Reveille, P Bertrand, and F. Califano, “Electron temperature anisotropy instabilities represented by superposition of streams,” *Physics of Plasmas*, vol. 19, no. 12, p. 122 109, 2012.
- [226] P. Verhulst, “La loi d’accroissement de la population,” *Nouveaux Memories de l’Académie Royale des Sciences et Belles-Lettres de Bruxelles*, vol. 18, pp. 14–54, 1845.
- [227] B. P. Rajvaidya, “Study of decay rate of materials using logistic map equation,” *Materials Today: Proceedings*, 2022.
- [228] H. Youness, “Development of a digital image encryption system based on logistics maps,” Ph.D. dissertation, MINISTRY OF HIGHER EDUCATION, 2020.
- [229] S. H. Kellert, *In the wake of chaos: Unpredictable order in dynamical systems*. University of Chicago press, 1993.
- [230] K. J. DeMars, R. H. Bishop, and M. K. Jah, “Entropy-based approach for uncertainty propagation of nonlinear dynamical systems,” *Journal of Guidance, Control, and Dynamics*, vol. 36, no. 4, pp. 1047–1057, 2013.
- [231] C. Werndl, “What are the new implications of chaos for unpredictability?” *The British Journal for the Philosophy of Science*, 2020.
- [232] K. Nishihara and Y. Ueshima, “Lyapunov exponent of dilute gas, liquid and solid plasmas,” *Plasma physics and controlled fusion*, vol. 41, no. 3A, A257, 1999.

- [233] I. Shevchenko and V. Kouprianov, “On the chaotic rotation of planetary satellites: The Lyapunov spectra and the maximum Lyapunov exponents,” *Astronomy & Astrophysics*, vol. 394, no. 2, pp. 663–674, 2002.
- [234] G. Rubino, D. Borgogno, M. Veranda, D. Bonfiglio, S. Cappello, and D. Grasso, “Detection of magnetic barriers in a chaotic domain: First application of finite time Lyapunov exponent method to a magnetic confinement configuration,” *Plasma Physics and Controlled Fusion*, vol. 57, no. 8, p. 085 004, 2015.
- [235] J. Bec, L. Biferale, G. Boffetta, M. Cencini, S. Musacchio, and F. Toschi, “Lyapunov exponents of heavy particles in turbulence,” *Physics of Fluids*, vol. 18, no. 9, p. 091 702, 2006.
- [236] Y. Ueshima, K. Nishihara, D. M. Barnett, T. Tajima, and H. Furukawa, “Relation between Lyapunov exponent and dielectric response function in dilute one component plasmas,” *Phys. Rev. Lett.*, vol. 79, pp. 2249–2252, 12 1997. DOI: 10.1103/PhysRevLett.79.2249. [Online]. Available: <https://link.aps.org/doi/10.1103/PhysRevLett.79.2249>.
- [237] W. Masood, A. Mushtaq, and R. Khan, “Linear and nonlinear dust ion acoustic waves using the two-fluid quantum hydrodynamic model,” *Physics of Plasmas*, vol. 14, no. 12, p. 123 702, 2007.
- [238] J. Tamang *et al.*, “Dynamical properties of ion-acoustic waves in space plasma and its application to image encryption,” *IEEE Access*, vol. 9, pp. 18 762–18 782, 2021.
- [239] P. K. Prasad, A. Gowrisankar, A. Saha, and S. Banerjee, “Dynamical properties and fractal patterns of nonlinear waves in solar wind plasma,” *Physica Scripta*, vol. 95, no. 6, p. 065 603, 2020.
- [240] A. Abdikian, A. Saha, and S. Alimirzaei, “Bifurcation analysis of ion-acoustic waves in an adiabatic trapped electron and warm ion plasma,” *Journal of Taibah University for Science*, vol. 14, no. 1, pp. 1051–1058, 2020.
- [241] N. Kaur, K. Singh, and N. Saini, “Effect of ion beam on the characteristics of ion acoustic Gardner solitons and double layers in a multicomponent superthermal plasma,” *Physics of Plasmas*, vol. 24, no. 9, p. 092 108, 2017.
- [242] F. Andereg, C. F. Driscoll, D. H. Dubin, T. M. O’Neil, and F. Valentini, “Electron acoustic waves in pure ion plasmas,” *Physics of Plasmas*, vol. 16, no. 5, p. 055 705, 2009.

References

- [243] S. Chandra and B. G. Jit Sarkar Chinmay Das, “Self-interacting stationary formations in plasmas under externally controlled fields,” *Plasma Physics Reports*, 2020.
- [244] K. Singh and N. S. Saini, “Breather structures and peregrine solitons in a polarized space dusty plasma,” *Frontiers in Physics*, p. 511, 2020.
- [245] A. Balogh and M. Krstic, “Boundary control of the korteweg-de vries-burgers equation: Further results on stabilization and well-posedness, with numerical demonstration,” *IEEE Transactions on Automatic Control*, vol. 45, no. 9, pp. 1739–1745, 2000.
- [246] R. L. H. G. R. Blanchard P.; Devaney, *Differential Equations*. 2006, p. 828.
- [247] P. Papavaritis and W. Pardo, “Numerical mode and boundary analysis of bifurcation phenomena in plasmas with stationary striations,” in *IEEE 1989 International Conference on Plasma Science*, 1989. DOI: 10.1109/PLASMA.1989.166266.
- [248] N. Saini and K. Singh, “Head-on collision of two dust ion acoustic solitary waves in a weakly relativistic multicomponent superthermal plasma,” *Physics of Plasmas*, vol. 23, no. 10, p. 103701, 2016.
- [249] S. A. Kurkin, N. S. Frolov, V. A. Maximenko, A. E. Hramov, and A. A. Koronovskii, “Method of the calculation of spectrum of lyapunov exponents for the analysis of dynamics of beam-plasma systems,” in *2014 IEEE 41st International Conference on Plasma Sciences (ICOPS) held with 2014 IEEE International Conference on High-Power Particle Beams (BEAMS)*, 2014, pp. 1–1. DOI: 10.1109/PLASMA.2014.7012541.
- [250] J. Tamang and A. Saha, “Dynamical properties of nonlinear ion-acoustic waves based on the nonlinear schrödinger equation in a multi-pair nonextensive plasma,” *Zeitschrift für Naturforschung A*, vol. 75, no. 8, pp. 687–697, 2020.
- [251] R. Kaur, K. Singh, and N. Saini, “Heavy-and light-nuclei acoustic dressed shock waves in white dwarfs,” *Chinese Journal of Physics*, 2021.
- [252] M Keidar, I Beilis, R. Boxman, and S Goldsmith, “2d expansion of the low-density interelectrode vacuum arc plasma jet in an axial magnetic field,” *Journal of Physics D: Applied Physics*, vol. 29, no. 7, p. 1973, 1996.
- [253] Y. N. Istomin and D. Sobyenin, “Electron-positron plasma generation in a magnetar magnetosphere,” *Astronomy Letters*, vol. 33, no. 10, pp. 660–672, 2007.

References

- [254] A Fasoli, F Skiff, R Kleiber, M. Tran, and P. Paris, “Dynamical chaos of plasma ions in electrostatic waves,” *Physical review letters*, vol. 70, no. 3, p. 303, 1993.
- [255] B. D. T. H. G. M. J. R.-S.-W. R. B. S. J. I. H. C. S. A. E. G. A. P. D. E. E. F. P. G. W. Perkins L J and H. D. Pacher, *Iter system studies and design space analysis*, Dec. 1990.
- [256] J Goswami, S Chandra, J Sarkar, S Chaudhuri, and B Ghosh, “Collision-less shocks and solitons in dense laser-produced fermi plasma,” *Laser and Particle Beams*, pp. 1–14, 2020.
- [257] W. Cox, R. Hawkins, C. Charles, and R. Boswell, “Three-dimensional mapping of ion density in a double-layer helicon plasma,” *IEEE transactions on plasma science*, vol. 36, no. 4, pp. 1386–1387, 2008.
- [258] H.-Y. Jung *et al.*, “Realization of high luminous efficacy at low voltages in the plasma display panel with sro–mgo double layer,” *IEEE Electron Device Letters*, vol. 31, no. 7, pp. 686–688, 2010.
- [259] F. O. Thomas, A. Kozlov, and T. C. Corke, “Plasma actuators for cylinder flow control and noise reduction,” *AIAA journal*, vol. 46, no. 8, pp. 1921–1931, 2008.
- [260] C. S. Kalra, A. F. Gutsol, and A. A. Fridman, “Gliding arc discharges as a source of intermediate plasma for methane partial oxidation,” *IEEE transactions on plasma science*, vol. 33, no. 1, pp. 32–41, 2005.
- [261] C. Das, S. Chandra, and B. Ghosh, “Effects of exchange symmetry and quantum diffraction on amplitude-modulated electrostatic waves in quantum magnetoplasma,” *Pramana*, vol. 95, no. 2, pp. 1–16, 2021. DOI: 10.1007/s12043-021-02108-x.
- [262] A. Hasegawa and L. Chen, “Kinetic processes in plasma heating by resonant mode conversion of alfvén wave,” *The Physics of Fluids*, vol. 19, no. 12, pp. 1924–1934, 1976.
- [263] J Jacquinet, B. McVey, and J. Scharer, “Mode conversion of the fast magnetosonic wave in a deuterium-hydrogen tokamak plasma,” *Physical Review Letters*, vol. 39, no. 2, p. 88, 1977.
- [264] J. Steinke S. and van Tilborg, C Benedetti, and et al., “Multistage coupling of independent laser-plasma accelerators,” *Nature*, vol. 530, 190–193, 2016. DOI: <https://doi.org/10.1038/nature16525>.
- [265] A. Colaitis *et al.*, “Coupled hydrodynamic model for laser-plasma interaction and hot electron generation,” *Physical Review E*, vol. 92, no. 4, Oct. 2015. DOI:

References

- 10.1103/physreve.92.041101. [Online]. Available: <https://doi.org/10.1103/physreve.92.041101>.
- [266] J. Rayimbaev, B. Turimov, and B. Ahmedov, “Braneworld effects in plasma magnetosphere of a slowly rotating magnetized neutron star,” *International Journal of Modern Physics D*, vol. 28, no. 10, p. 1950128, 2019.
- [267] D. Fenn and T. Plewa, “Detonability of white dwarf plasma: Turbulence models at low densities,” *Monthly Notices of the Royal Astronomical Society*, vol. 468, no. 2, pp. 1361–1372, 2017.
- [268] G. Brodin, M. Marklund, and G. Manfredi, “Quantum plasma effects in the classical regime,” *Physical review letters*, vol. 100, no. 17, p. 175001, 2008.
- [269] G. Manfredi, “How to model quantum plasmas,” *Fields Institute Communications*, vol. 46, pp. 263–287, 2005.
- [270] F. Haas, G. Manfredi, and M. Feix, “Multistream model for quantum plasmas,” *Physical Review E*, vol. 62, no. 2, p. 2763, 2000.
- [271] P. Ludwig, M. Bonitz, H. Kählert, and J. W. Dufty, “Dynamics of strongly correlated ions in a partially ionized quantum plasma,” in *Journal of Physics: Conference Series*, IOP Publishing, vol. 220, 2010, p. 012003.
- [272] A. P. Misra and C. Bhowmik, “Nonplanar ion-acoustic waves in a quantum plasma,” *Physics Letters A*, vol. 369, no. 1-2, pp. 90–97, 2007.
- [273] G. Kumar and V. K. Tripathi, “Excitation of a surface plasma wave over a plasma cylinder by a relativistic electron beam,” *Physics of Plasmas*, vol. 15, no. 7, p. 073504, 2008. DOI: [10.1063/1.2955769](https://doi.org/10.1063/1.2955769). eprint: <https://doi.org/10.1063/1.2955769>. [Online]. Available: <https://doi.org/10.1063/1.2955769>.
- [274] R. S. Anwar, H. Ning, and L. Mao, “Recent advancements in surface plasmon polaritons-plasmonics in subwavelength structures in microwave and terahertz regimes,” *Digital Communications and Networks*, vol. 4, no. 4, pp. 244–257, 2018, ISSN: 2352-8648. DOI: <https://doi.org/10.1016/j.dcan.2017.08.004>. [Online]. Available: <https://www.sciencedirect.com/science/article/pii/S2352864817301992>.
- [275] P. Kumar and N. Ahmad, “Surface plasma wave in spin-polarized semiconductor quantum plasma,” *Laser and Particle Beams*, vol. 38, no. 2, pp. 159–164, 2020. DOI: [10.1017/S026303462000018X](https://doi.org/10.1017/S026303462000018X).

References

- [276] S. Chandra, P. Maji, and B. Ghosh, “Propagation of nonlinear surface waves in relativistically degenerate quantum plasma half-space,” *International Journal of Nuclear and Quantum Engineering*, vol. 8, no. 5, pp. 842–845, 2014.
- [277] H. Lamb, *Hydrodynamics. 6th Edition*. Cambridge University Press, 1932.
- [278] Y. K. Kato, R. C. Myers, A. C. Gossard, and D. D. Awschalom, “Observation of the spin hall effect in semiconductors,” *science*, vol. 306, no. 5703, pp. 1910–1913, 2004.
- [279] K. Ando and E. Saitoh, “Observation of the inverse spin hall effect in silicon,” *Nature Communications*, vol. 3, no. 1, p. 629, 2012, ISSN: 2041-1723. DOI: 10.1038/ncomms1640. [Online]. Available: <https://doi.org/10.1038/ncomms1640>.
- [280] N. R. Council, *Plasma Processing and Processing Science*. Washington, DC: The National Academies Press, 1995. DOI: 10.17226/9854. [Online]. Available: <https://www.nap.edu/catalog/9854/plasma-processing-and-processing-science>.
- [281] G. Loubriel *et al.*, “Photoconductive semiconductor switches,” *IEEE Transactions on Plasma Science*, vol. 25, no. 2, pp. 124–130, 1997. DOI: 10.1109/27.602482.
- [282] V. P. Georgiev *et al.*, “Simulation of gated gaas-algaas resonant tunneling diodes for tunable terahertz communication applications,” in *2020 International Conference on Simulation of Semiconductor Processes and Devices (SISPAD)*, 2020, pp. 241–244. DOI: 10.23919/SISPAD49475.2020.9241677.
- [283] H. Haus, “Noise in microwave transmission applications of gunn and impatt diodes – theoretical aspects of gunn and impatt diode noise,” in *1975 IEEE-MTT-S International Microwave Symposium*, 1975, pp. 311–312. DOI: 10.1109/MWSYM.1975.1123376.
- [284] A. Kumar, G. C. Ghivela, A. Supriya, S. R. Choudhury, and J. Sengupta, “A steady state analysis of boron nitride ddr impatt diode,” in *2019 IEEE 1st International Conference on Energy, Systems and Information Processing (ICESIP)*, 2019, pp. 1–4. DOI: 10.1109/ICESIP46348.2019.8938381.
- [285] K.-i. Ohue, F. Kuroki, and T. Yoneyama, “Analysis on locking characteristics of band-stop type of self-injection locked nrd guide gunn oscillator at 60 ghz,” in *2009 Asia Pacific Microwave Conference*, 2009, pp. 2292–2295. DOI: 10.1109/APMC.2009.5385440.

References

- [286] R. van Zyl, W. Perold, and R. Botha, “Multi-domain gunn diodes with multiple hot electron launchers: A new approach to mm wave gaas gunn oscillator optimization,” in *1999 IEEE Africon. 5th Africon Conference in Africa (Cat. No.99CH36342)*, vol. 2, 1999, 1193–1196 vol.2. DOI: 10.1109/AFRCON.1999.821949.
- [287] S. Lu, “Simulation of semiconductor manufacturing equipment and processes,” in *Proceedings of the 3rd World Congress on Mechanical, Chemical, and Material Engineering*, Avestia Publishing, Jun. 2017. DOI: 10.11159/htff17.165. [Online]. Available: <https://doi.org/10.11159/htff17.165>.
- [288] D. Maude and J. Portal, “Chapter 1 - parallel transport in low-dimensional semiconductor structures,” in *High Pressure in Semiconductor Physics II*, ser. Semiconductors and Semimetals, T. Suski and W. Paul, Eds., vol. 55, Elsevier, 1998, pp. 1–43. DOI: [https://doi.org/10.1016/S0080-8784\(08\)60079-4](https://doi.org/10.1016/S0080-8784(08)60079-4). [Online]. Available: <https://www.sciencedirect.com/science/article/pii/S0080878408600794>.
- [289] F. Haas, “A fluid model for quantum plasmas,” in *Quantum Plasmas*, Springer New York, 2011, pp. 65–93. DOI: 10.1007/978-1-4419-8201-8_4. [Online]. Available: https://doi.org/10.1007/978-1-4419-8201-8_4.
- [290] F. Haas, “Electromagnetic quantum plasmas,” in *Quantum Plasmas*, Springer New York, 2011, pp. 109–131. DOI: 10.1007/978-1-4419-8201-8_6. [Online]. Available: https://doi.org/10.1007/978-1-4419-8201-8_6.
- [291] F. Haas, “An introduction to quantum plasmas,” *Brazilian Journal of Physics*, vol. 41, no. 4-6, pp. 349–363, Sep. 2011. DOI: 10.1007/s13538-011-0043-0. [Online]. Available: <https://doi.org/10.1007/s13538-011-0043-0>.
- [292] Z. Moldabekov, T. Schoof, P. Ludwig, M. Bonitz, and T. Ramazanov, “Statically screened ion potential and bohm potential in a quantum plasma,” *Physics of Plasmas*, vol. 22, no. 10, p. 102 104, 2015.
- [293] I Hutchinson and J Freidberg, *Fluid Description of Plasma*. MIT open courseware, 2003, pp. 74–77. [Online]. Available: <https://ocw.mit.edu/courses/nuclear-engineering/22-611j-introduction-to-plasma-physics-i-fall-2003/lecture-notes/chap4.pdf>.
- [294] D. Bohm, “A suggested interpretation of the quantum theory in terms of ”hidden” variables. ii,” *Phys. Rev.*, vol. 85, pp. 180–193, 2 Jan. 1952. DOI: 10.

References

- 1103/PhysRev.85.180. [Online]. Available: <https://link.aps.org/doi/10.1103/PhysRev.85.180>.
- [295] S. A. Hojman, F. A. Asenjo, H. M. Moya-Cessa, and F. Soto-Eguibar, *Bohm potential is real and its effects are measurable*, 2021. arXiv: 2101.06738 [quant-ph].
- [296] C. C. Perelman, “Bohm’s potential, classical/quantum duality and repulsive gravity,” *Physics Letters B*, vol. 788, pp. 546–551, 2019, ISSN: 0370-2693. DOI: <https://doi.org/10.1016/j.physletb.2018.11.013>. [Online]. Available: <https://www.sciencedirect.com/science/article/pii/S0370269318308517>.
- [297] Z. A. Moldabekov, M. Bonitz, and T. S. Ramazanov, “Theoretical foundations of quantum hydrodynamics for plasmas,” *Physics of Plasmas*, vol. 25, no. 3, p. 031903, 2018. DOI: 10.1063/1.5003910. eprint: <https://doi.org/10.1063/1.5003910>. [Online]. Available: <https://doi.org/10.1063/1.5003910>.
- [298] M. Akbari-Moghanjoughi, “Hydrodynamic limit of wigner-poisson kinetic theory: Revisited,” *Physics of Plasmas*, vol. 22, no. 2, p. 022103, 2015. DOI: 10.1063/1.4907167. eprint: <https://doi.org/10.1063/1.4907167>. [Online]. Available: <https://doi.org/10.1063/1.4907167>.
- [299] M. Akbari-Moghanjoughi, “Mode coupling and two-stream instabilities in semiconductors,” *IEEE Transactions on Plasma Science*, vol. 45, no. 2, pp. 174–184, 2017.
- [300] S. Wang, Z. Xin, and P. A. Markowich, “Quasi-neutral limit of the drift diffusion models for semiconductors: The case of general sign-changing doping profile,” *SIAM journal on mathematical analysis*, vol. 37, no. 6, pp. 1854–1889, 2006.
- [301] G. Colonna, “Boltzmann and vlasov equations in plasma physics,” in *Plasma Modeling*, ser. 2053-2563, IOP Publishing, 2016, 1–1 to 1–23, ISBN: 978-0-7503-1200-4. DOI: 10.1088/978-0-7503-1200-4ch1. [Online]. Available: <http://dx.doi.org/10.1088/978-0-7503-1200-4ch1>.
- [302] V. Bonch-Bruевич and S. M. Kogan, “The theory of electron plasma in semiconductors,” *Soviet Phys.-Solid State*, vol. 1, 1960.
- [303] D. B. Melrose and A. Mushtaq, “Plasma dispersion function for a fermi–dirac distribution,” *Physics of Plasmas*, vol. 17, no. 12, p. 122103, 2010. DOI: 10.1063/1.3528272. eprint: <https://doi.org/10.1063/1.3528272>. [Online]. Available: <https://doi.org/10.1063/1.3528272>.

References

- [304] V. I. Kolobov, “Fokker–planck modeling of electron kinetics in plasmas and semiconductors,” *Computational materials science*, vol. 28, no. 2, pp. 302–320, 2003.
- [305] G. R. Misium, “Macroscopic modeling of oxygen plasmas,” *Journal of Vacuum Science & Technology A: Vacuum, Surfaces, and Films*, vol. 8, no. 3, pp. 1642–1647, 1990.
- [306] D Svintsov, V Vyurkov, S Yurchenko, T Otsuji, and V Ryzhii, “Hydrodynamic model for electron-hole plasma in graphene,” *Journal of Applied Physics*, vol. 111, no. 8, p. 083 715, 2012.
- [307] N. Sano and T. Fukui, “Fundamental aspects of semiconductor device modeling associated with discrete impurities: Monte carlo simulation scheme,” *IEEE Transactions on Electron Devices*, pp. 1–6, 2021. DOI: 10.1109/TED.2021.3082804.
- [308] A. Bulgakov and O. Shramkova, “Nonlinear interaction of waves in a semiconductor layered periodic structure in electric field,” in *2006 International Conference on Mathematical Methods in Electromagnetic Theory*, 2006, pp. 475–477. DOI: 10.1109/MMET.2006.1689827.
- [309] A. A. Bulgakov and O. V. Shramkova, “Nonlinear interaction of waves in semiconductor plasma,” *Journal of Physics D: Applied Physics*, vol. 40, no. 19, pp. 5896–5901, 2007. DOI: 10.1088/0022-3727/40/19/017. [Online]. Available: <https://doi.org/10.1088/0022-3727/40/19/017>.
- [310] R Sokel and W. A. Harrison, “Long-range interactions in semiconductors,” *Physical Review Letters*, vol. 36, no. 1, p. 61, 1976.
- [311] L. Takhtajan, “Semi-classical liouville theory, complex geometry of moduli spaces, and uniformization of riemann surfaces,” in *New Symmetry Principles in Quantum Field Theory*, J. Fröhlich, G. ’t Hooft, A. Jaffe, G. Mack, P. K. Mitter, and R. Stora, Eds. Boston, MA: Springer US, 1992, pp. 383–406, ISBN: 978-1-4615-3472-3. DOI: 10.1007/978-1-4615-3472-3_15. [Online]. Available: https://doi.org/10.1007/978-1-4615-3472-3_15.
- [312] J Ibáñez, R Cuscó, L Artús, G González-Diéaz, and J Jiménez, “Raman scattering by an inhomogeneous plasma in implanted semiconductors,” *Solid State Communications*, vol. 121, no. 11, pp. 609–613, 2002, ISSN: 0038-1098. DOI: [https://doi.org/10.1016/S0038-1098\(02\)00058-3](https://doi.org/10.1016/S0038-1098(02)00058-3). [Online]. Available: <https://www.sciencedirect.com/science/article/pii/S0038109802000583>.

- [313] A. Agrawal, N. Yadav, and S. Ghosh, “Study of quantum effect in stimulated brillouin scattering magnetized semiconductor plasma with high dielectric constant,” *AIP Conference Proceedings*, vol. 2224, no. 1, p. 040014, 2020. DOI: 10.1063/5.0000855. eprint: <https://aip.scitation.org/doi/pdf/10.1063/5.0000855>. [Online]. Available: <https://aip.scitation.org/doi/abs/10.1063/5.0000855>.
- [314] N. B. Abdallah, “On a multidimensional schrödinger–poisson scattering model for semiconductors,” *Journal of Mathematical Physics*, vol. 41, no. 7, pp. 4241–4261, 2000.
- [315] A. Franceschetti, L. Wang, H Fu, and A. Zunger, “Short-range versus long-range electron-hole exchange interactions in semiconductor quantum dots,” *Physical Review B*, vol. 58, no. 20, R13367, 1998.
- [316] L. G. Christophorou and J. K. Olthoff, “Electron collision data for plasma-processing gases,” in ser. *Advances In Atomic, Molecular, and Optical Physics*, M. Kimura and Y. Itikawa, Eds., vol. 44, Academic Press, 2001, pp. 59–98. DOI: [https://doi.org/10.1016/S1049-250X\(01\)80029-X](https://doi.org/10.1016/S1049-250X(01)80029-X). [Online]. Available: <https://www.sciencedirect.com/science/article/pii/S1049250X0180029X>.
- [317] F. Zutavern *et al.*, “Electron-hole plasmas in semiconductors,” in *IEEE Conference Record - Abstracts. PPS-2001 Pulsed Power Plasma Science 2001. 28th IEEE International Conference on Plasma Science and 13th IEEE International Pulsed Power Conference (Cat. No.01CH37, 2001*, pp. 352–. DOI: 10.1109/PPPS.2001.961051.
- [318] A. Dörnen *et al.*, “Bound-to-bound transitions at neutral zinc in silicon: Effective-mass-like states and hole-hole interaction,” *Phys. Rev. B*, vol. 40, pp. 12005–12008, 17 1989. DOI: 10.1103/PhysRevB.40.12005. [Online]. Available: <https://link.aps.org/doi/10.1103/PhysRevB.40.12005>.
- [319] W. L. Quan, X. W. Sun, and Q. F. Chen, “Elastic scattering of electron in neutral plasma: Interaction model and plasma environment effects,” *Physics of Plasmas*, vol. 27, no. 11, p. 112701, 2020. DOI: 10.1063/5.0017977. eprint: <https://doi.org/10.1063/5.0017977>. [Online]. Available: <https://doi.org/10.1063/5.0017977>.
- [320] C. Erginsoy, “Neutral impurity scattering in semiconductors,” *Physical Review*, vol. 79, no. 6, p. 1013, 1950.
- [321] Y. F. Chang, “The conduction-diffusion theory of semiconductor junctions,” *Journal of Applied Physics*, vol. 38, no. 2, pp. 534–544, 1967. DOI: 10.1063/1.

References

1709370. eprint: <https://doi.org/10.1063/1.1709370>. [Online]. Available: <https://doi.org/10.1063/1.1709370>.
- [322] P. Kleinert, “Theory of hot-electron quantum diffusion in semiconductors,” *Physics Reports*, vol. 485, no. 1, pp. 1–42, 2010, ISSN: 0370-1573. DOI: <https://doi.org/10.1016/j.physrep.2009.10.003>. [Online]. Available: <https://www.sciencedirect.com/science/article/pii/S0370157309002506>.
- [323] V. I. Gaman, P. N. Drobot, and G. F. Karlova, “Kink instability of the semiconductor plasma in silicon parallelepipeds,” *Russian Physics Journal*, vol. 35, no. 5, pp. 481–486, May 1992. DOI: [10.1007/bf00558864](https://doi.org/10.1007/bf00558864). [Online]. Available: <https://doi.org/10.1007/bf00558864>.
- [324] A. Rasheed, M. Jamil, Siddique, F. Huda, and Y. D. Jung, “Beam excited acoustic instability in semiconductor quantum plasmas,” *Physics of Plasmas*, vol. 21, p. 062 107, Jun. 2014. DOI: [10.1063/1.4883224](https://doi.org/10.1063/1.4883224).
- [325] I. Zeba, M. Yahia, P. Shukla, and W. Moslem, “Electron–hole two-stream instability in a quantum semiconductor plasma with exchange-correlation effects,” *Physics Letters A*, vol. 376, no. 34, pp. 2309–2313, 2012, ISSN: 0375-9601. DOI: <https://doi.org/10.1016/j.physleta.2012.05.049>. [Online]. Available: <https://www.sciencedirect.com/science/article/pii/S0375960112006743>.
- [326] V. V. MITIN and N. Z. VAGIDOV, “Instabilities and fluctuations in semiconductor solid-state plasma,” in *Noise in Physical Systems and 1/F Fluctuations*. World Scientific Publishing Co Pte Ltd, 1997, pp. 293–296. DOI: [10.1142/9789812811165_0066](https://doi.org/10.1142/9789812811165_0066). eprint: https://www.worldscientific.com/doi/pdf/10.1142/9789812811165_0066.
- [327] A. A. Khan, M Jamil, and A Hussain, “Wake potential with exchange-correlation effects in semiconductor quantum plasmas,” *Physics of Plasmas*, vol. 22, no. 9, p. 092 103, 2015.
- [328] K. Singh, N. Kaur, and N. S. Saini, “Head-on collision between two dust acoustic solitary waves and study of rogue waves in multicomponent dusty plasma,” *Physics of Plasmas*, vol. 24, no. 6, p. 063 703, 2017. DOI: [10.1063/1.4984996](https://doi.org/10.1063/1.4984996). eprint: <https://doi.org/10.1063/1.4984996>. [Online]. Available: <https://doi.org/10.1063/1.4984996>.
- [329] D. Bohm, “A suggested interpretation of the quantum theory in terms of ”hidden” variables. i,” *Phys. Rev.*, vol. 85, pp. 166–179, 2 1952. DOI: [10.1103/PhysRev.85.166](https://doi.org/10.1103/PhysRev.85.166). [Online]. Available: <https://link.aps.org/doi/10.1103/PhysRev.85.166>.

References

- [330] G. Ottaviani, L. Reggiani, C. Canali, F. Nava, and A. Alberigi-Quaranta, “Hole drift velocity in silicon,” *Phys. Rev. B*, vol. 12, pp. 3318–3329, 8 1975. DOI: 10.1103/PhysRevB.12.3318. [Online]. Available: <https://link.aps.org/doi/10.1103/PhysRevB.12.3318>.
- [331] C. Canali, G. Majni, R. Minder, and G. Ottaviani, “Electron and hole drift velocity measurements in silicon and their empirical relation to electric field and temperature,” *IEEE Transactions on Electron Devices*, vol. 22, no. 11, pp. 1045–1047, 1975. DOI: 10.1109/T-ED.1975.18267.
- [332] S. Banerjee, “Amplitude modulation of weakly nonlinear electrostatic solitary waves in ultrarelativistic degenerated semiconductor quantum plasma,” *IEEE Transactions on Plasma Science*, vol. 47, no. 1, pp. 121–127, 2019. DOI: 10.1109/TPS.2018.2871954.
- [333] S. Choudhury, T. Das, M. K. Ghorui, and P. Chatterjee, “The effect of exchange-correlation coefficient in quantum semiconductor plasma in presence of electron-phonon collision frequency,” *Physics of Plasmas*, vol. 23, p. 062110, 2016.
- [334] C. Das. “Nonlinear wave-wave interaction in semiconductor junction diode.” (), [Online]. Available: <https://github.com/cdas8016/cdas8016/blob/9739edb233214ffeaba9f82da16239f166af7614/kdv.mp4>.
- [335] R. J. E. Hueting, B. Rajasekharan, C. Salm, and J. Schmitz, “The charge plasma p-n diode,” *IEEE Electron Device Letters*, vol. 29, no. 12, pp. 1367–1369, 2008. DOI: 10.1109/LED.2008.2006864.
- [336] B. Liu *et al.*, “Low-power and high-sensitivity system-on-chip hall effect sensor,” in *2017 IEEE SENSORS*, 2017, pp. 1–3. DOI: 10.1109/ICSENS.2017.8234272.
- [337] I. B. Bernstein, J. M. Greene, and M. D. Kruskal, “Exact nonlinear plasma oscillations,” *Physical Review*, vol. 108, no. 3, p. 546, 1957.
- [338] L. Tonks and I. Langmuir, “A general theory of the plasma of an arc,” *Physical review*, vol. 34, no. 6, p. 876, 1929.
- [339] G. Knorr and C. K. Goertz, “Existence and stability of strong potential double layers,” *Astrophysics and Space Science*, vol. 31, no. 1, pp. 209–223, 1974.
- [340] P. Carlqvist, “On the physics of relativistic double layers,” *Astrophysics and Space Science*, vol. 87, no. 1-2, pp. 21–39, 1982.

References

- [341] M Akbari-Moghanjoughi, “Propagation and oblique collision of electrostatic solitary waves in quantum pair-plasmas,” *Physics of Plasmas*, vol. 17, no. 8, p. 082 317, 2010.
- [342] M Akbari-Moghanjoughi, “Comment on “the effects of bohm potential on ion-acoustic solitary waves interaction in a nonplanar quantum plasma”[phys. plasmas 17, 082307 (2010)],” *Physics of Plasmas*, vol. 17, no. 11, p. 114 701, 2010.
- [343] I Kourakis, S Sultana, and M. Hellberg, “Dynamical characteristics of solitary waves, shocks and envelope modes in kappa-distributed non-thermal plasmas: An overview,” *Plasma Physics and Controlled Fusion*, vol. 54, no. 12, p. 124 001, 2012.
- [344] M Shahmansouri, B Shahmansouri, and D Darabi, “Ion acoustic solitary waves in nonplanar plasma with two-temperature kappa distributed electrons,” *Indian Journal of Physics*, vol. 87, no. 7, pp. 711–716, 2013.
- [345] M Shahmansouri and H Alinejad, “Dust acoustic solitary waves in a magnetized electron depleted superthermal dusty plasma,” *Physics of Plasmas*, vol. 20, no. 3, p. 033 704, 2013.
- [346] H. Schamel, “Stationary solitary, snoidal and sinusoidal ion acoustic waves,” *Plasma Physics*, vol. 14, no. 10, p. 905, 1972.
- [347] T.-H. Kim and K.-Y. Kim, “Modified k-dv theory of non-monotonic double layer in a weak relativistic plasma,” *Physics Letters A*, vol. 286, no. 2-3, pp. 180–184, 2001.
- [348] B. Quon and A. Wong, “Formation of potential double layers in plasmas,” *Physical Review Letters*, vol. 37, no. 21, p. 1393, 1976.
- [349] V. Bychkov, M. Modestov, and M. Marklund, “The structure of weak shocks in quantum plasmas,” *Physics of Plasmas*, vol. 15, no. 3, p. 032 309, 2008.
- [350] M. Gondal, Q. Drmosh, Z. Yamani, and T. Saleh, “Synthesis of zno2 nanoparticles by laser ablation in liquid and their annealing transformation into zno nanoparticles,” *Applied surface science*, vol. 256, no. 1, pp. 298–304, 2009.
- [351] M Sackmann, S Bom, T Balster, and A Materny, “Nanostructured gold surfaces as reproducible substrates for surface-enhanced raman spectroscopy,” *Journal of Raman Spectroscopy: An International Journal for Original Work in all Aspects of Raman Spectroscopy, Including Higher Order Processes, and also Brillouin and Rayleigh Scattering*, vol. 38, no. 3, pp. 277–282, 2007.

- [352] S. Ahmed *et al.*, “Solvent assisted tuning of morphology of a peptide-perylenediimide conjugate: Helical fibers to nano-rings and their differential semiconductivity,” *Scientific reports*, vol. 7, no. 1, pp. 1–13, 2017.
- [353] Z Pan, L. Li, W Zhang, Y. Lin, R. Wu, and W Ge, “Effect of rapid thermal annealing on gainnas/gaas quantum wells grown by plasma-assisted molecular-beam epitaxy,” *Applied Physics Letters*, vol. 77, no. 9, pp. 1280–1282, 2000.
- [354] H. v. Känel, M. Kummer, G. Isella, E. Müller, and T. Hackbarth, “Very high hole mobilities in modulation-doped ge quantum wells grown by low-energy plasma enhanced chemical vapor deposition,” *Applied physics letters*, vol. 80, no. 16, pp. 2922–2924, 2002.
- [355] S. Chandra, S. Das, A. Chandra, B. Ghosh, and A. Jash, “Nonplanar ion-acoustic waves in a relativistically degenerate quantum plasma,” *International Journal of Nuclear and Quantum Engineering*, vol. 9, no. 5, pp. 305–311, 2015.
- [356] R Kodama *et al.*, “Fast heating of ultrahigh-density plasma as a step towards laser fusion ignition,” *Nature*, vol. 412, no. 6849, pp. 798–802, 2001.
- [357] H. Hora, “Physics of laser driven plasmas,” *New York, Wiley-Interscience, 1981. 329 p.*, 1981.
- [358] R. Fletcher, X. Zhang, and S. Rolston, “Observation of collective modes of ultracold plasmas,” *Physical review letters*, vol. 96, no. 10, p. 105 003, 2006.
- [359] J. Roberts, C. Fertig, M. Lim, and S. Rolston, “Electron temperature of ultracold plasmas,” *Physical review letters*, vol. 92, no. 25, p. 253 003, 2004.
- [360] H. Yan *et al.*, “Tunable infrared plasmonic devices using graphene/insulator stacks,” *Nature nanotechnology*, vol. 7, no. 5, pp. 330–334, 2012.
- [361] D Farina and S. Bulanov, “Dark solitons in electron-positron plasmas,” *Physical Review E*, vol. 64, no. 6, p. 066 401, 2001.
- [362] S Poornakala *et al.*, “Weakly relativistic one-dimensional laser pulse envelope solitons in a warm plasma,” *Physics of Plasmas*, vol. 9, no. 9, pp. 3802–3810, 2002.
- [363] P. Shukla, A. Mamun, and L Stenflo, “Vortices in a strongly magnetized electron-positron-ion plasma,” *Physica Scripta*, vol. 68, no. 4, p. 295, 2003.
- [364] L Stenflo, “Acoustic solitary vortices,” *The Physics of fluids*, vol. 30, no. 10, pp. 3297–3299, 1987.

References

- [365] W Daughton *et al.*, “Role of electron physics in the development of turbulent magnetic reconnection in collisionless plasmas,” *Nature Physics*, vol. 7, no. 7, pp. 539–542, 2011.
- [366] I Zeba, W. Moslem, and P. Shukla, “Ion solitary pulses in warm plasmas with ultrarelativistic degenerate electrons and positrons,” *The Astrophysical Journal*, vol. 750, no. 1, p. 72, 2012.
- [367] A. Mamun and P. Shukla, “Solitary waves in an ultrarelativistic degenerate dense plasma,” *Physics of Plasmas*, vol. 17, no. 10, p. 104 504, 2010.
- [368] P. K. Shukla, “A new spin on quantum plasmas,” *Nature Physics*, vol. 5, no. 2, pp. 92–93, 2009.
- [369] R. amour, M. Tribeche, and P. K. Shukla, “Electron acoustic solitary waves in a plasma with nonthermal electrons featuring tsallis distribution.,” *Astrophysics and Space Science*, vol. 338(2), pp. 287–294, 2012.
- [370] G Wilk and Z Włodarczyk, “Tsallis distribution with complex non-extensivity parameter q ,” *Physica A: Statistical Mechanics and its Applications*, vol. 413, pp. 53–58, 2014.
- [371] R. A. Cairns *et al.*, “Electrostatic solitary structures in non-thermal plasmas.,” *Geophysical Research Letters*, vol. 22(20), pp. 2709–2712, 1995.
- [372] M Maksimovic, V Pierrard, and J F. Lemaire, “A kinetic model of the solar wind with kappa distribution functions in the corona,” *Astronomy and Astrophysics*, vol. 324, pp. 725–734, 1997.
- [373] G. Lakhina and S Singh, “Solitary waves in plasmas described by kappa distributions,” in *Kappa Distributions*, Elsevier, 2017, pp. 399–418.
- [374] G. Livadiotis, *Kappa distributions: Theory and applications in plasmas*. Elsevier, 2017.
- [375] G Livadiotis, “Derivation of the entropic formula for the statistical mechanics of space plasmas,” *Nonlinear Processes in Geophysics*, vol. 25(1), p. 77, 2001.
- [376] M. Hellberg, R. Mace, T. Baluku, I Kourakis, and N. Saini, ““mathematical and physical aspects of kappa velocity distribution”[phys. plasmas 14, 110702 (2007)].,” *Physics of Plasmas*, vol. 16(9), p. 094 701, 2009.
- [377] A. V. Milovanov and L. M. Zelenyi, “Functional background of the tsallis entropy: ‘coarse-grained’ systems and ‘kappa’ distribution functions.,” 2000.

References

- [378] M Sharifian, H R. Sharifinejad, M B. Zarandi, and A R. Niknam, “Effect of q-non-extensive distribution of electrons on the plasma sheath floating potential,” *Journal of Plasma Physics*, vol. 80(4), pp. 607–618, 2014.
- [379] M. P. Leubner, “A nonextensive entropy approach to kappa-distributions,” *Astrophysics and space science*, vol. 282(3), pp. 573–579, 2002.
- [380] A. ieee 5, “The plasma universe,” in *IEEE 1989 International Conference on Plasma Science*, 1989, p. 85. DOI: 10.1109/PLASMA.1989.166084.
- [381] O. Petrov, A. Gavrikov, I. Shakhova, O. Vaulina, P. Levashov, and V. Fortov, “Hydrodynamics and structure of dusty plasma fluid,” in *The 31st IEEE International Conference on Plasma Science, 2004. ICOPS 2004. IEEE Conference Record - Abstracts.*, 2004, p. 432. DOI: 10.1109/PLASMA.2004.1340233.
- [382] J. A. Shercliff, “Textbook of magnetohydrodynamics,” 1965.
- [383] H. B. Garrett and A. C. Whittlesey, “Spacecraft charging, an update,” *IEEE transactions on plasma science*, vol. 28, no. 6, pp. 2017–2028, 2000.
- [384] D. E. Hastings and J. Wang, “Induced emission of radiation from a large space-station-like structure in the ionosphere,” *AIAA Journal*, vol. 27, no. 4, pp. 438–445, 1989. DOI: 10.2514/3.10131. eprint: <https://doi.org/10.2514/3.10131>. [Online]. Available: <https://doi.org/10.2514/3.10131>.
- [385] A.-M. Wazwaz, “The extended tanh method for new solitons solutions for many forms of the fifth-order kdv equations,” *Applied Mathematics and Computation*, vol. 184, no. 2, pp. 1002–1014, 2007, ISSN: 0096-3003. DOI: <https://doi.org/10.1016/j.amc.2006.07.002>. [Online]. Available: <http://www.sciencedirect.com/science/article/pii/S0096300306007892>.
- [386] S. Jian-Jun, “The proper analytical solution of the korteweg-de vries-burgers equation,” *J. Phys. A: Math. Gen*, vol. 20, pp. 49–56, 1987.
- [387] P. K. Shukla and B. Eliasson, “Screening and wake potentials of a test charge in quantum plasmas,” *Physics Letters A*, vol. 372, no. 16, pp. 2897–2899, 2008.
- [388] G. Brodin, M. Marklund, and G. Manfredi, “Quantum plasma effects in the classical regime,” *Physical review letters*, vol. 100(17), p. 175 001, 2008.
- [389] Y. Wang, “Nonlinear dusty magnetosonic waves in a strongly coupled dusty plasma,” *AIP Advances*, vol. 9(12), p. 125 216, 2019.

References

- [390] R. A Treumann, "Theory of super-diffusion for the magnetopause.," *Geophysical research letters*, vol. 24(14), pp. 1727–1730, 1997.
- [391] C. Beck and E. GD Cohen, "Superstatistics," *Physica A: Statistical mechanics and its applications*, vol. 322, pp. 267–275, 2003.
- [392] G. S. Lakhina, S. Singh, R. Rubia, and T. Sreeraj, "Existence domains of electrostatic solitary structures in the solar wind plasma," *Phys. Plasmas*, vol. 23(6), 062902 (2016), DOI: 10.1063/1.4953892.
- [393] R. Rubia, S. Singh, and G. S. Lakhina, "Existence domain of electrostatic solitary waves in the lunar wake," *Phys. Plasmas*, vol. 25(3), 032302(2018), DOI: 10.1063/1.5033498.
- [394] G. Lakhina, S. Singh, R Rubia, and T Sreeraj, "A review of nonlinear fluid models for ion-and electron-acoustic solitons and double layers: Application to weak double layers and electrostatic solitary waves in the solar wind and the lunar wake," *Physics of Plasmas*, vol. 25, no. 8, p. 080501, 2018.
- [395] R Rubia, S. Singh, and G. Lakhina, "Occurrence of electrostatic solitary waves in the lunar wake," *Journal of Geophysical Research: Space Physics*, vol. 122, no. 9, pp. 9134–9147, 2017.
- [396] R. E. Ergun *et al.*, "Fast satellite observations of large-amplitude solitary structures," *Geophysical Research Letters*, vol. 25(12), pp. 2041–2044, 1998.
- [397] C Cattell *et al.*, "Polar observations of solitary waves at high and low altitudes and comparison to theory," *Advances in Space Research*, vol. 28(11), pp. 1631–1641, 2001.
- [398] C. Cattell *et al.*, "Large amplitude solitary waves in and near the earth's magnetosphere, magnetopause and bow shock: Polar and cluster observations," *Nonlinear Processes in Geophysics*, vol. 10(1/2), pp. 13–26, 2003.
- [399] T. Akter, F. Deeba, and M. Kamal-Al-Hassan, "Electron-acoustic solitary waves in a two-temperature plasma having electrons with kappa distribution," *IEEE Transactions on Plasma Science*, vol. 44, no. 8, pp. 1449–1459, 2016. DOI: 10.1109/TPS.2016.2582832.
- [400] M. J. Lee and Y. D. Jung, "Astronomical data of atomic shannon entropies in astrophysical lorentzian plasmas.," *The Astrophysical Journal*, vol. 871(1), p. 111, 2019.

- [401] H. Aravindakshan, A. Kakad, and B. Kakad, “Effects of wave potential on electron holes in thermal and superthermal space plasmas,” *Physics of Plasmas*, vol. 25(12), p. 122 901, 2018.
- [402] G. Nicolaou, G. Livadiotis, C Owen, D. Verscharen, and R Wicks, “Determining the kappa distributions of space plasmas from observations in a limited energy range,” *The Astrophysical Journal*, vol. 864(1), p. 3, 2018.
- [403] J. Pickett *et al.*, “Furthering our understanding of electrostatic solitary waves through cluster multispacecraft observations and theory,” *Advances in Space Research*, vol. 41, no. 10, pp. 1666–1676, 2008.
- [404] S. Maharaj, R Bharuthram, S. Singh, and G. Lakhina, “Existence domains of arbitrary amplitude nonlinear structures in two-electron temperature space plasmas. ii. high-frequency electron-acoustic solitons,” *Physics of Plasmas*, vol. 19, no. 12, p. 122 301, 2012.
- [405] Y. D. Jung, “Quantum-mechanical effects on electron–electron scattering in dense high-temperature plasmas,” *Physics of Plasmas*, vol. 8(8), pp. 3842–3844, 2001.
- [406] M. Opher, L. O Silva, D. E Dager, V. K Decyk, and J. M Dawson, “Nuclear reaction rates and energy in stellar plasmas: The effect of highly damped modes,” *Physics of Plasmas*, vol. 8(5), pp. 2454–2460, 2001.
- [407] S. Singh, S Devanandhan, G. Lakhina, and R Bharuthram, “Electron acoustic solitary waves in a magnetized plasma with nonthermal electrons and an electron beam,” *Physics of Plasmas*, vol. 23, no. 8, p. 082 310, 2016.
- [408] S Devanandhan, S. Singh, G. Lakhina, and R Bharuthram, “Small amplitude electron acoustic solitary waves in a magnetized superthermal plasma,” *Communications in Nonlinear Science and Numerical Simulation*, vol. 22, no. 1-3, pp. 1322–1330, 2015.
- [409] S Devanandhan, S. Singh, G. Lakhina, and R Bharuthram, “Electron acoustic waves in a magnetized plasma with kappa distributed ions,” *Physics of Plasmas*, vol. 19, no. 8, p. 082 314, 2012.
- [410] S. Singh, G. Lakhina, R Bharuthram, and S. Pillay, “Electrostatic solitary structures in presence of non-thermal electrons and a warm electron beam on the auroral field lines,” *Physics of Plasmas*, vol. 18, no. 12, p. 122 306, 2011.
- [411] L. Mbuli, S. Maharaj, R Bharuthram, S. Singh, and G. Lakhina, “Arbitrary amplitude fast electron-acoustic solitons in three-electron component space plasmas,” *Physics of Plasmas*, vol. 23, no. 6, p. 062 302, 2016.

References

- [412] G. Lakhina, S. Singh, A. Kakad, F. Verheest, and R. Bharuthram, "Study of nonlinear ion-and electron-acoustic waves in multi-component space plasmas," *Nonlinear Processes in Geophysics*, vol. 15, no. 6, pp. 903–913, 2008.
- [413] S. Singh and G. Lakhina, "Electron acoustic solitary waves with non-thermal distribution of electrons," *Nonlinear Processes in Geophysics*, vol. 11, no. 2, pp. 275–279, 2004.
- [414] S. Tagare, S. Singh, R. Reddy, and G. Lakhina, "Electron acoustic solitons in the earth's magnetotail," *Nonlinear Processes in Geophysics*, vol. 11, no. 2, pp. 215–218, 2004.
- [415] S. Singh and G. Lakhina, "Generation of electron-acoustic waves in the magnetosphere," *Planetary and Space Science*, vol. 49, no. 1, pp. 107–114, 2001.
- [416] S. Devanandhan, S. Singh, G. Lakhina, and R. Bharuthram, "Electron acoustic solitons in the presence of an electron beam and superthermal electrons," *Nonlinear Processes in Geophysics*, vol. 18, no. 5, pp. 627–634, 2011.
- [417] J. Goswami and J. Sarkar, "Kbm approach to electron acoustic envelope soliton in viscous astrophysical plasma," *Physica Scripta*, 2021.
- [418] S. Vladimirov, "Ponderomotive forces in a time-dependent plasma," in *IEEE Conference Record - Abstracts. 1997 IEEE International Conference on Plasma Science*, 1997, p. 208. DOI: 10.1109/PLASMA.1997.604881.